AD-A058 267 MISSION RESEARCH CORP ALBUQUERQUE N MEX F/G 17/2
AIRCRAFT CABLE PARAMETER STUDY.(U)
OCT 77 H M FOWLES, L D SCOTT, A K AGRAWAL F29601-76-C-0091
UNCLASSIFIED AMRC-R-92 AFWL-TR-77-107 NL

1 OF 2
AD A058267

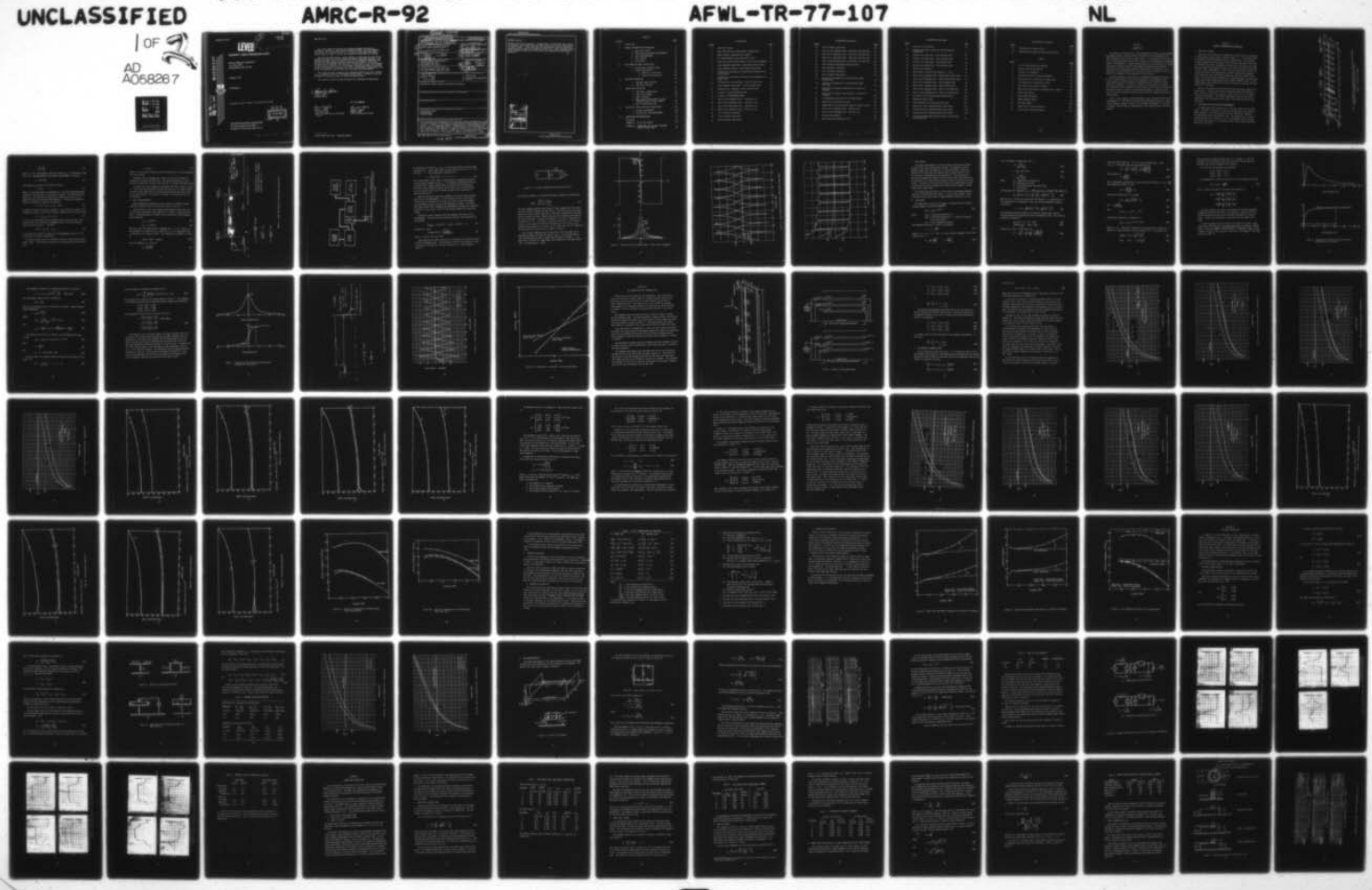

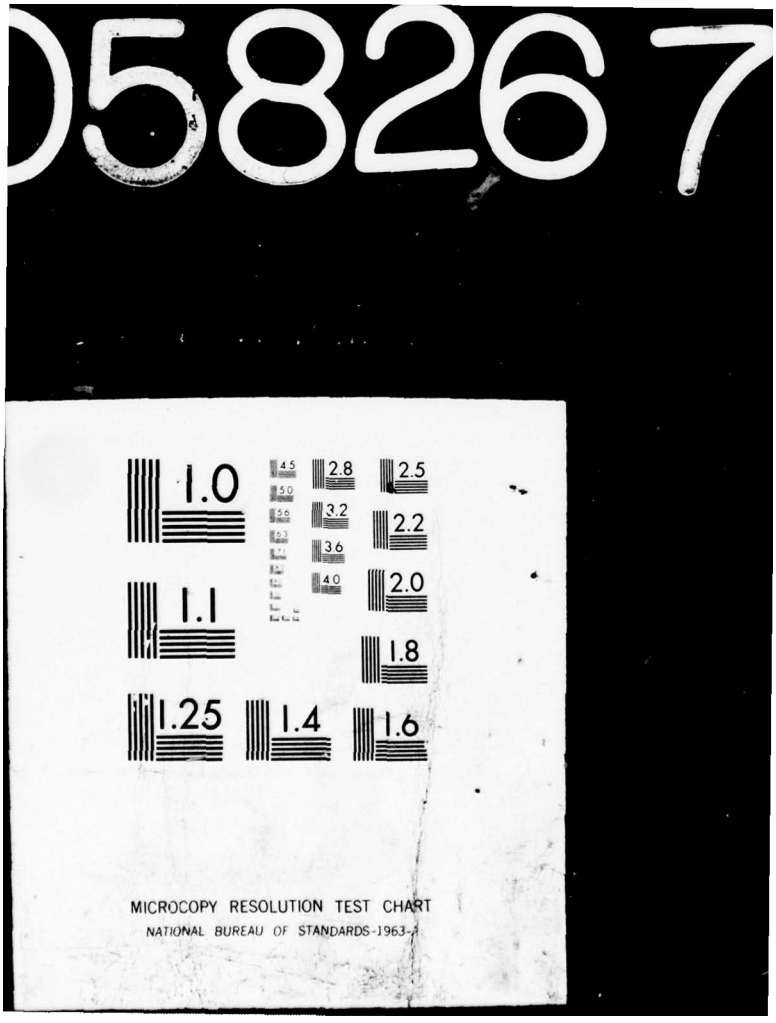
05826 7
1.0
1.1
1.25
1.4
1.6
2.8
2.5
3.2
2.2
3.6
2.0
4.0
1.8
MICROCOPY RESOLUTION TEST CHART
NATIONAL BUREAU OF STANDARDS-1963-A

AFWL-TR-77-107

DDC

AFWL-TR-
77-107

LEVEL II

ADE200096

AIRCRAFT CABLE PARAMETER STUDY

Mission Research Corporation
P. O. Box 8693
Albuquerque, NM 87108

October 1977

Final Report

AIR FORCE WEAPONS LABORATORY
Air Force Systems Command
Kirtland Air Force Base, NM 87117

AFWL-TR-77-107

This final report was prepared by the Mission Research Corporation, Albuquerque, New Mexico, under Contract F29601-76-C-0091, Job Order 12090513 with the Air Force Weapons Laboratory, Kirtland Air Force Base, New Mexico. Captain Howard G. Hudson (ELP) was the Laboratory Project Officer-in-Charge.

When US Government drawings, specifications, or other data are used for any purpose other than a definitely related Government procurement operation, the Government thereby incurs no responsibility nor any obligation whatsoever, and the fact that the Government may have formulated, furnished, or in any way supplied the said drawings, specifications, or other data, is not to be regarded by implication or otherwise, as in any manner licensing the holder or any other person or corporation, or conveying any rights or permission to manufacture, use, or sell any patented invention that may in any way be related thereto.

This report has been reviewed by the Information Office (OI) and is releasable to the National Technical Information Service (NTIS). At NTIS, it will be available to the general public, including foreign nations.

This technical report has been reviewed and is approved for publication.

HOWARD G. HUDSON
Captain, USAF
Project Officer

FOR THE COMMANDER

AARON B. LOGGINS
Lt Colonel, USAF
Chief, Phenomenology and Technology Branch

DONALD A. DOWLER
Colonel, USAF
Chief, Electronics Division

DO NOT RETURN THIS COPY. RETAIN OR DESTROY.

(18) AFWL, SBIE

UNCLASSIFIED

SECURITY CLASSIFICATION OF THIS PAGE *(When Data Entered)*

(19) **REPORT DOCUMENTATION PAGE**

READ INSTRUCTIONS BEFORE COMPLETING FORM

1. REPORT NUMBER: ~~AFWL~~-TR-77-107 ✓
2. GOVT ACCESSION NO.: AD-E 200 896
3. RECIPIENT'S CATALOG NUMBER:

(6) 4. TITLE (and Subtitle): AIRCRAFT CABLE PARAMETER STUDY •

(9) 5. TYPE OF REPORT & PERIOD COVERED: Final report •

(14) 6. PERFORMING ORG. REPORT NUMBER: AMRC-R-92

(10) 7. AUTHOR(s): H. M. Fowles, K. M. Lee, L. D. Scott, A. K. Agrawal

(15) 8. CONTRACT OR GRANT NUMBER(s): F29601-76-C-0091

9. PERFORMING ORGANIZATION NAME AND ADDRESS:
Mission Research Corporation ✓
5601 Domingo Rd, N.E.
Albuquerque, NM 87108

(16) (17) 10. PROGRAM ELEMENT, PROJECT, TASK AREA & WORK UNIT NUMBERS: 64747F, 12090524, 05

(11) 11. CONTROLLING OFFICE NAME AND ADDRESS:
Air Force Weapons Laboratory (ELP)
Kirtland Air Force Base, NM 87117

12. REPORT DATE: October 1977

13. NUMBER OF PAGES: 174

(12) 176 p.

14. MONITORING AGENCY NAME & ADDRESS *(if different from Controlling Office)*

15. SECURITY CLASS. *(of this report)*: Unclassified

15a. DECLASSIFICATION/DOWNGRADING SCHEDULE

16. DISTRIBUTION STATEMENT *(of this Report)*

Approved for public release; distribution unlimited.

17. DISTRIBUTION STATEMENT *(of the abstract entered in Block 20, if different from Report)*

18. SUPPLEMENTARY NOTES

19. KEY WORDS *(Continue on reverse side if necessary and identify by block number)*

Transmission lines
Multiconductor
Aircraft cable

20. ABSTRACT *(Continue on reverse side if necessary and identify by block number)*

This report describes experimental and analytical results obtained from a study of the transmission line properties of multiconductor cables commonly found on aircraft. A method for the complete characterization of multiconductor transmission lines in inhomgeneous media is presented and verified experimentally. Bulk transmission line properties of bundles containing up to 20 closely spaced wires were measured for cases of a bundle near a flat ground plane, near a corner, and in conduit. The results are compared with single wire →(over)

DD FORM 1 JAN 73 1473 A EDITION OF 1 NOV 65 IS OBSOLETE

UNCLASSIFIED

SECURITY CLASSIFICATION OF THIS PAGE *(When Data Entered)*

390 748

ABSTRACT (cont'd)

handbook formulas and discussed. Perturbations on transmission lines caused by bulkheads, cable clamps, and the ribbed interior of aircraft were measured for several cases. It was found that the perturbations could be treated as lumped capacitive loads on an otherwise uniform line. Cable parameter measurements conducted on board an EC-135 aircraft are presented and discussed in Appendix A.

1473B

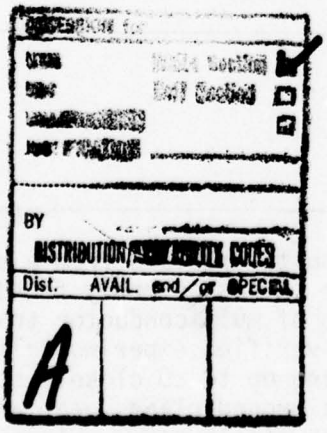

CONTENTS

ILLUSTRATIONS

ILLUSTRATIONS (continued)

ILLUSTRATIONS (continued)

ILLUSTRATIONS (continued)

TABLES

SECTION I

INTRODUCTION

The analysis of multiconductor coupling problems has lead to sophisticated and complex network simulation codes to determine the electromagnetic pulse (EMP) response of cables used in large systems. This approach has the potential of providing accurate results for a large class of multiconductor problems; however, the potential is seldom realized because of the uncertainty with which the physical properties of must multiconductor systems can be specified. A need exists for simple models capable of describing the transmission line properties of cable networks with sufficient accuracy to provide useful estimates of the response of cable networks to EMP excitation.

The work described in this report was undertaken to determine the feasibility of characterizing aircraft cable parameters by experimental means using commonly available laboratory instrumentation and relatively simple analytical procedures. The overall objective of the program is to reduce the complexity of multiconductor coupling problems and to provide information that can be used as a guide by the assessment engineer in determining the scope of the work required to properly evaluate the EMP response of aircraft cable systems.

Early in this program, limited measurements were conducted on the EC-135 (see Appendix A). The results and experience gained were valuable in recognizing inherent problems of making cable parameter measurements *in situ* and influenced certain areas of investigation in the remaining part of the test program.

SECTION II

GENERAL INSTRUMENTATION METHODOLOGY

1. CABLE TEST FIXTURE

The basic test fixture used to measure the transmission line properties of cables above a ground plane is shown in figure 1 . A continuous sheet of 22 gauge (0.6mm) aluminum was used as a ground plane. Sixteen gauge (1.3mm) aluminum plates were used at the driven and load ends of the cable to minimize the residual inductance of the fixture. The plate at the load end was hinged (using conducting tape) to the ground plane and folded down for open circuit measurements. In this case, the cable under test was continued horizontally with monofilament in order to preserve the geometry and minimize the stray capacitance between the cable end and the ground plane. The driven end was connected to the source through a low-capacitance adaptor (part #601A) supplied with the HP 11655A Impedance Probe. A probe-to-BNC adaptor (part #10207A) was modified to provide an optional BNC input connection to the cable.

Aircraft rib mockups were constructed by covering wooden supports with aluminum foil. The ribs were taped to the ground plane with conducting tape. The 50 cm spacing was the same as that of the ribs in the interior of the EC-135 fuselage. "Free space" measurements were carried out by removing the ribs and supporting the cable at the same height with styrofoam blocks.

2. TIME DOMAIN REFLECTOMETER (TDR) MEASUREMENTS

TDR measurements were performed with a Tektronix model 1502 TDR cable tester. The TDR is essentially a step function generator and a sampling scope arranged to record the successive pulses reflected by impedance discontinuities along a transmission line. The output pulse is a 225 mV voltage step with a rise time of 0.1 ns at an impedance level of 50 ohms. The oscilloscope display is calibrated in terms of the voltage reflection coefficient ρ given by

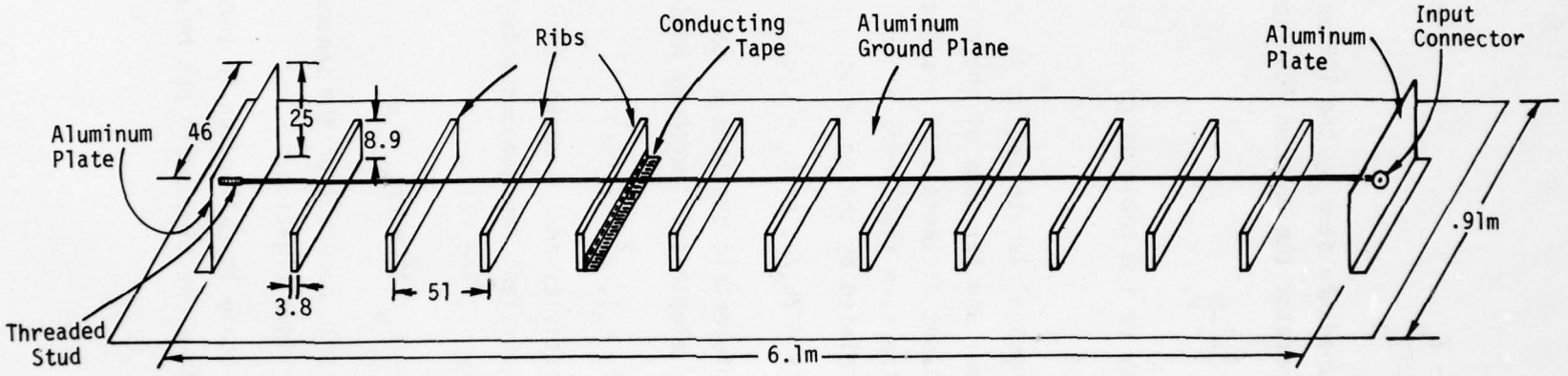

Note: Ribs replaced with stvrofoam blocks for "free space" measurements.
Dimensions in centimeters unless oterwise noted.

Figure 1. Cable Test Fixture

$$\rho = \frac{Z_L - Z_g}{Z_L + Z_g} \tag{1}$$

where Z_L is the load impedance seen by the TDR and Z_g is the generator impedance. For a 50 ohm generator the unknown load impedance is given by

$$Z_L = 50 \frac{1 + \rho}{1 - \rho} \tag{2}$$

The propagation velocity on the cable is given by

$$v = 2L/\Delta t \tag{3}$$

where L is the cable physical length and Δt is the time difference between reflections from the near and far ends of the cable. The cable electrical length L_e is the equivalent distance that a signal would travel at the speed of light during the same time interval Δt. The physical length and electrical length are related by the equation

$$\Delta t = 2L/v = 2L_e/c, \text{ or } L_e = L(c/v) \tag{4}$$

An effective relative dielectric constant ε' can be defined in terms of the propagation velocity or electrical length by making use of the relationships

$$c^2 = 1/(\mu_o \varepsilon_o), \; v^2 = 1/(\mu\varepsilon) \tag{5}$$

ε_o and μ_o are the permittivity and permeability of free space and ε and μ are the values of an equivalent homogeneous medium in which propagation would be at the velocity v. The ratio

$$(c/v)^2 = (L_e/L)^2 = \varepsilon/\varepsilon_o = \varepsilon' \tag{6}$$

is the effective dielectric constant of the inhomogeneous material of the transmission line under investigation.

The TDR horizontal scale is calibrated in terms of the one-way distance along a cable. The equivalent time scale can be obtained from the relationship

$$t = (2/c)x \tag{7}$$

where x is the distance variable on the TDR record and t is the corresponding time variable.

The model 1502 is equipped with a plug in strip chart recorder for permanently recording the TDR traces. The specified accuracy is $\pm 3\%$ in reflection coefficient (vertical axis) and $\pm 2\%$ in distance (horizontal axis).

A typical TDR trace recorded with the model 1502 TDR is shown in figure 2 . This record was obtained by driving the shield of a 6.1 meter length of RG/213 cable supported 9.4 cm above the ground plane with the far end of the cable shorted. The record is included to illustrate the form of the TDR data.

3. SWEPT CW MEASUREMENTS

Swept impedance measurements over the 0.15 MHz to 100 MHz frequency range were performed using the test set-up shown in figure 3 .

Short and open circuit input impedance measurements (the latter with the end plate folded down) were obtained for a number of cable configurations. The measurements are related to the transmission line parameters by the equations

$$Z_{oc} = Z_o \, \mathrm{Coth}(\gamma L) \tag{8}$$

$$Z_{sc} = Z_o \tanh(\gamma L) \tag{9}$$

where Z_o is the line characteristic impedance and $\gamma = \alpha + i\beta$, where α is the attenuation in nepers per unit length and $\beta = \omega/v$ is the phase angle in radians per unit length of cable. The attenuation in decibels is given by

$$\alpha(\mathrm{dB}) = 8.686 \times \alpha(\mathrm{nepers}) \tag{10}$$

The line impedance Z_o is given by

$$Z_o = \sqrt{Z_{sc} Z_{oc}} \tag{11}$$

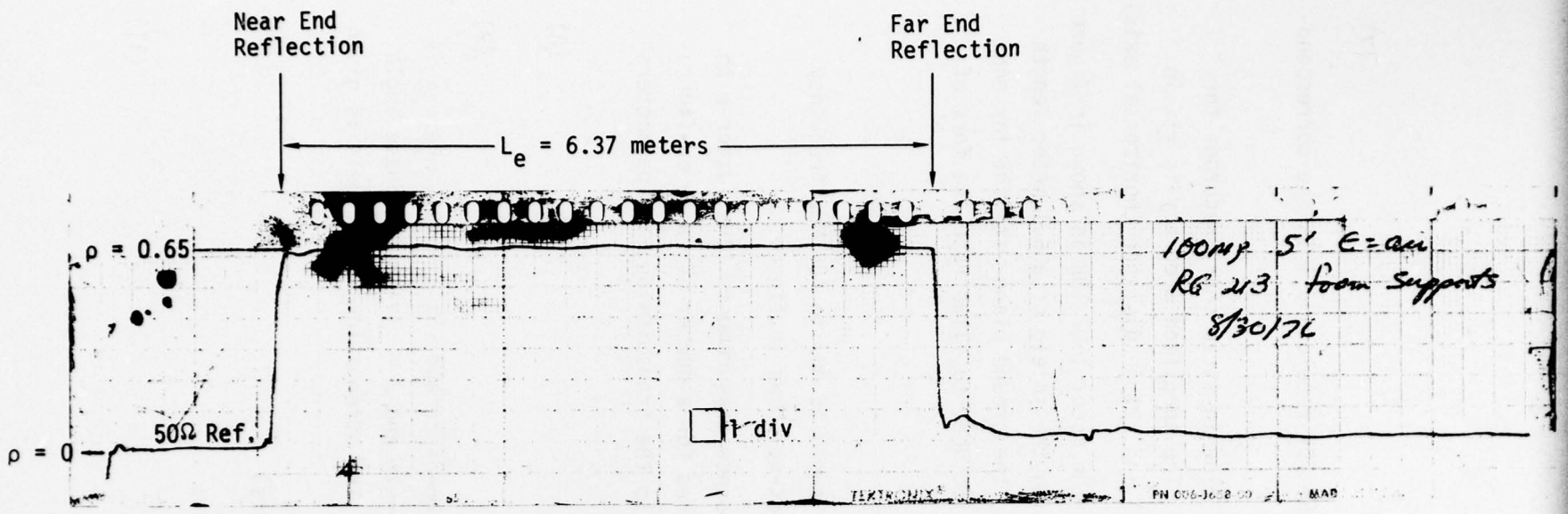

$$Z_c = (50)\,\frac{1 + 0.65}{1 - 0.65} = 236 \text{ ohms}$$

$$\varepsilon' = \left(\frac{6.37}{6.1}\right)^2 = 1.09$$

$$v/c = \left(\frac{6.1}{6.37}\right) = 0.96$$

Vertical Sensitivity: 100 mρ/div
Horizontal Sensitivity: 0.305m/div
Physical Length: 6.1m

Figure 2. Model 1502 TDR Trace, RG/213 Above a Ground Plane

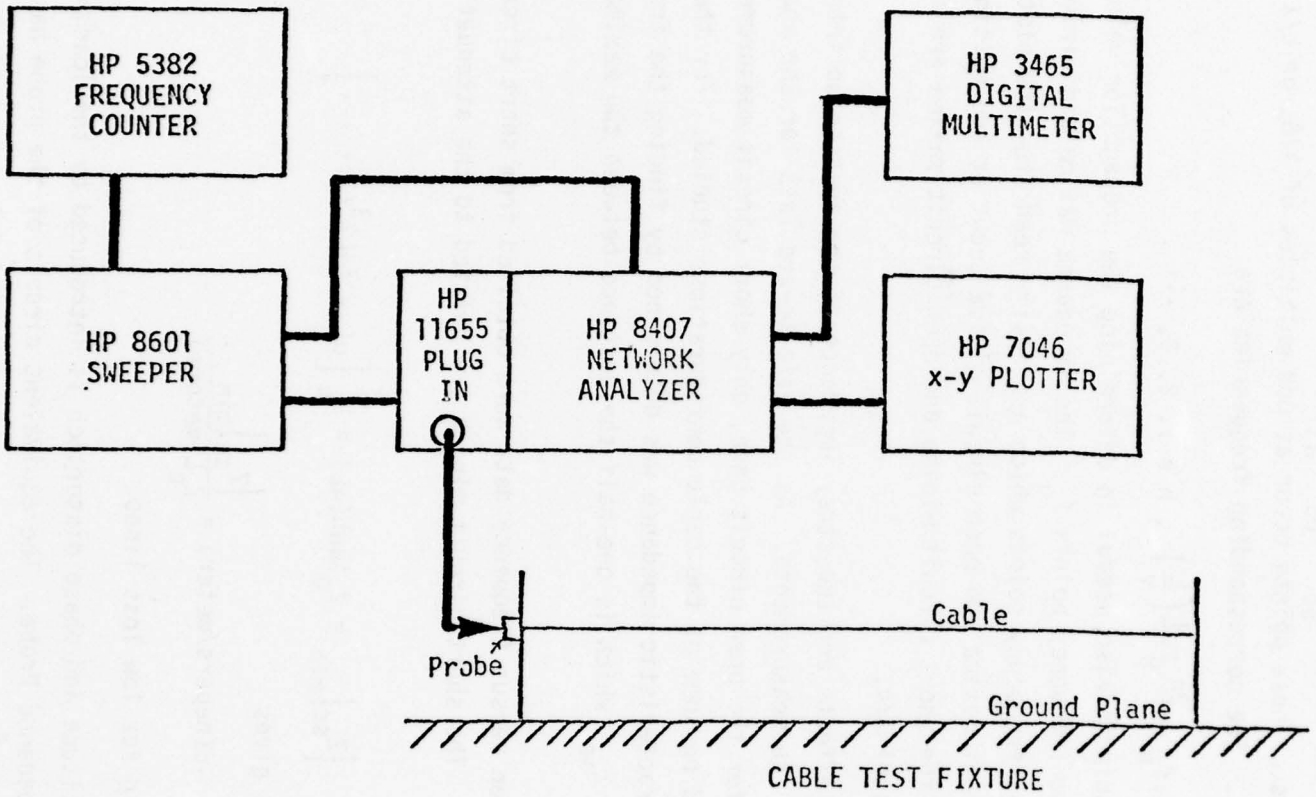

Figure 3. Swept Frequency Impedance Block Diagram

At frequencies for which $Z_{sc} = Z_{oc}$, Z_o can be read directly from the swept frequency plots. These points occur at odd multiples of $\lambda/8$, or $L/\lambda = 1/8$, $3/8$, $5/8$, $\cdots$. The corresponding frequencies are

$$f_n = \frac{2n - 1}{8}\left(\frac{L}{v}\right) \quad , n = 1, 2. 3, \cdots . \tag{12}$$

This relationship is also useful in determining the propagation velocity at the discrete frequency points f_n. The impedance maxima and minima provide additional frequency points which are easily read from the plots. The short circuit maxima and open circuit minima occur at odd multiples of $\lambda/4$, while the short circuit minima and open circuit maxima are at even multiples of $\lambda/4$.

Cable end effects and the stray impedance of the test setup introduce some error in the measurements. As the effects are less for the short circuit than for the open circuit case, only short circuit measurements were performed on some of the cable configurations studied. For these cases the characteristic impedance was determined by finding the frequencies at which $Z_o = Z_{sc}$, which is one-half the distance between the maxima and minima.

Attenuation versus frequency data were obtained from short circuit measurements. The short circuit minima are related to the attenuation by the equation

$$\left|Z_{sc}\right|_{min} = Z_o \tanh(\alpha L) = Z_o\left[\alpha L - (\alpha L)^3/3 + \cdots\right] \tag{13}$$

Solving for α gives

$$\alpha(\text{nepers/meter}) = \frac{\left|Z_{sc}\right|_{min}}{Z_o L(\text{meters})} \tag{14}$$

which is valid for low loss lines.

Some amplitude and phase distortion is introduced by the loading effects of the HP Impedance Probe. The equivalent circuit of the probe has a shunt resistance of 10^4 ohms and a series resistance of 0.1 ohm as shown in figure 4.

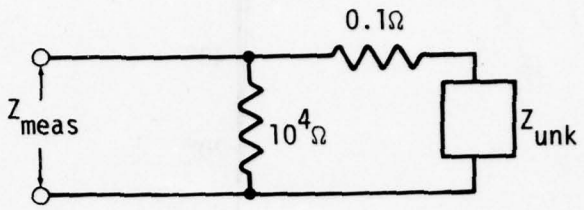

Figure 4. HP 11655A Impedance Probe Equivalent Circuit

The measured impedance is related to the unknown impedance by the equation

$$Z_{meas} = \frac{10^4(0.1 + Z_{unk})}{10^4 + 0.1 + Z_{unk}} \tag{15}$$

The swept impedance maxima often exceed 10^4 ohms, depending on the losses, and are seriously affected by probe loading. The minima can be accurately measured as long as they exceed the 0.1 ohm series resistance of the probe, which is usually the case. Phase errors are also caused by probe loading. The phase distortion is maximum at frequencies for which βL approaches an odd multiple of $\pi/2$. The nature of the phase distortion is illustrated in figure 5a, which shows one period of the phase plot for a short circuit impedance measurement on a lossless line for three values of line impedance. The magnitude of the phase error is shown in figure 5b.

Typical swept impedance plots of the short circuit and open circuit amplitude and phase are shown in figures 6 and 7 for the same RG/213 cable configuration as used to obtain the TDR record of figure 2. The amplitude is plotted on a logarithmic scale relative to a 100 ohm calibration. The phase plot is linear.

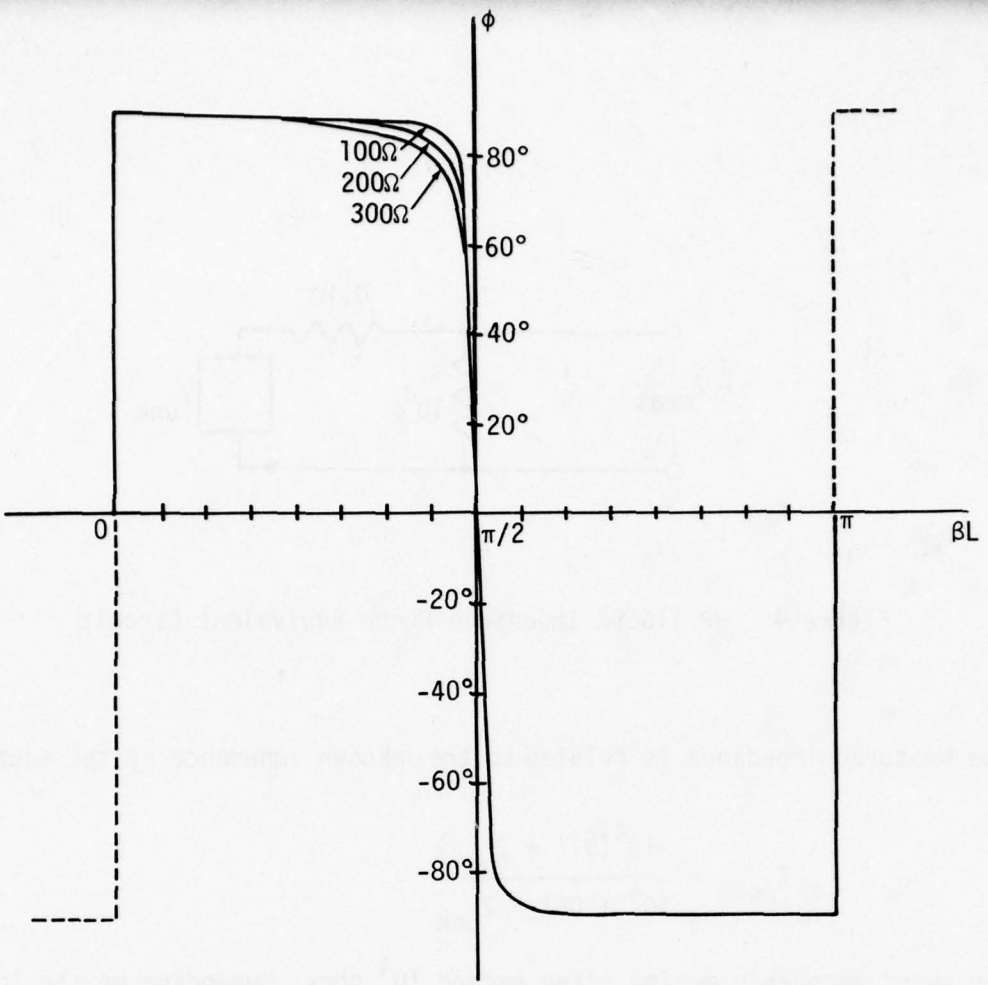

(a)

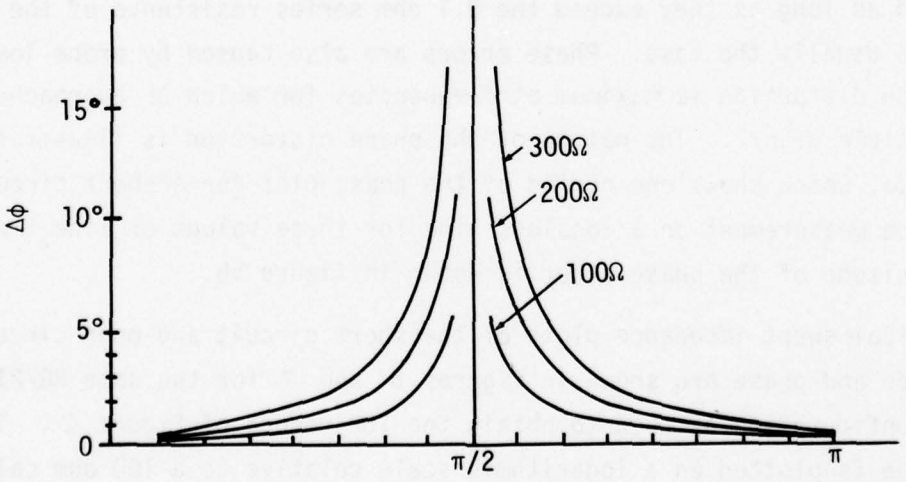

(b)

Figure 5. Phase Error Due to Probe Loading - Short Circuit Impedance

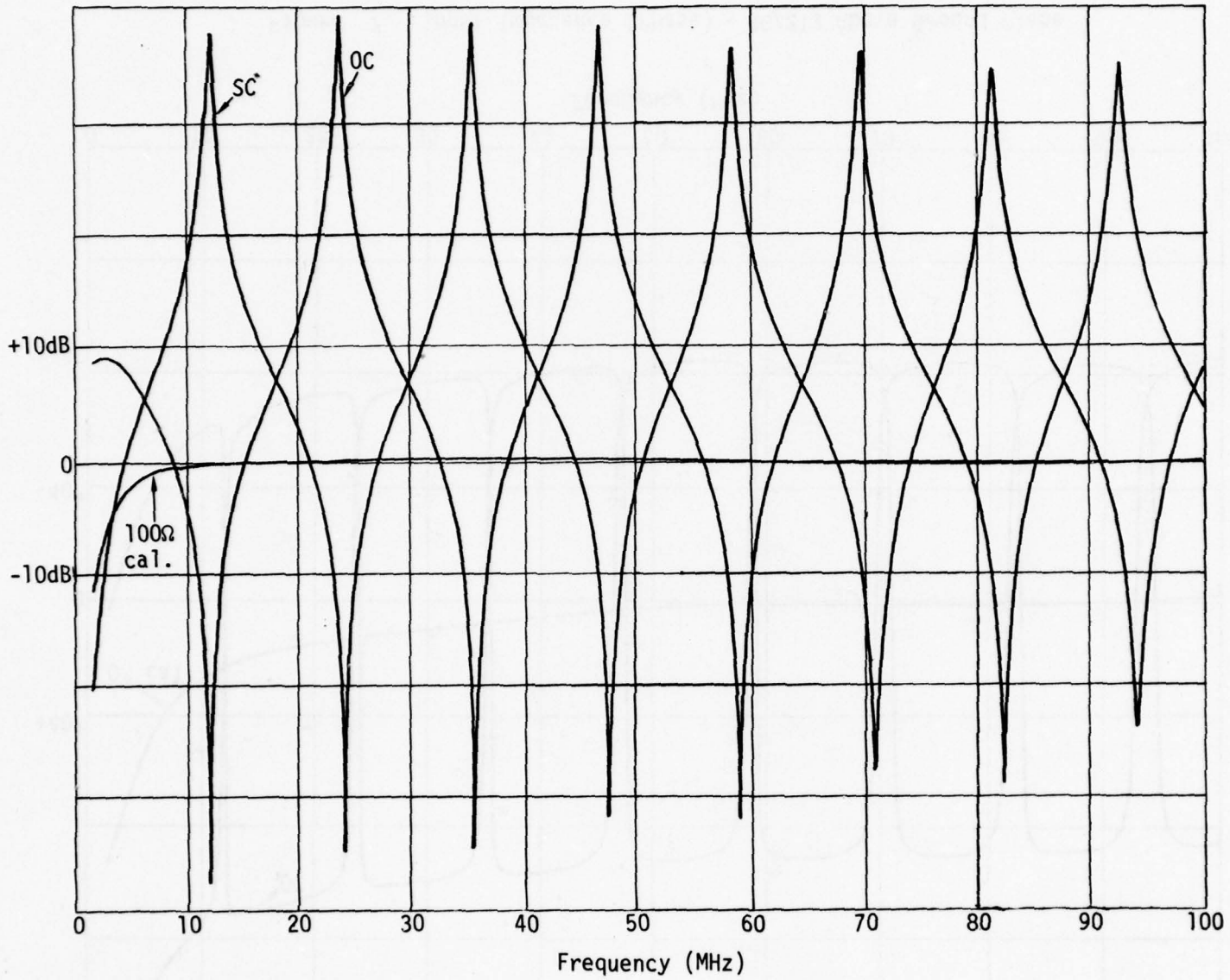

Figure 6. Input Impedance (Magnitude) - RG/213 Above Ground Plane

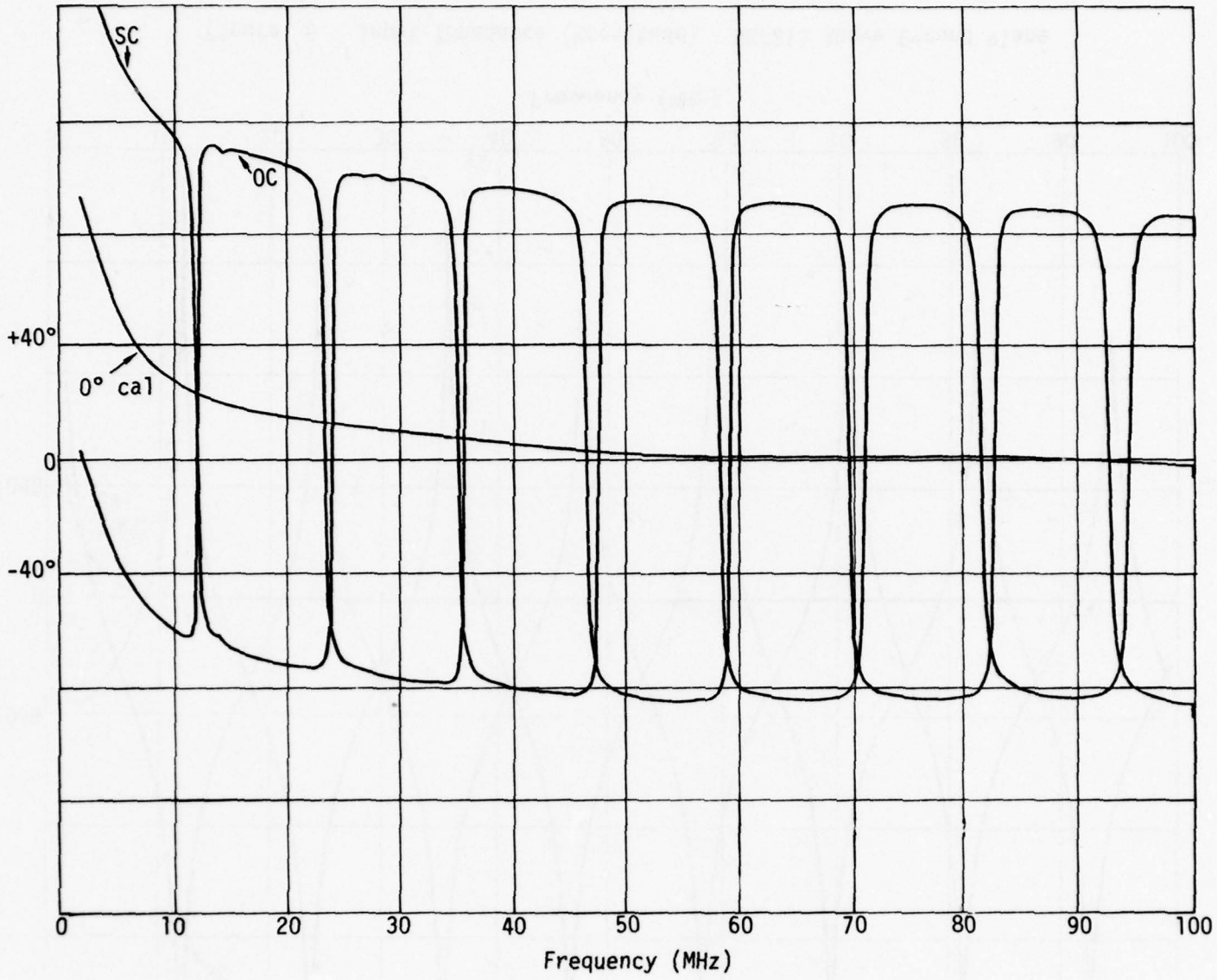

Figure 7. Input Impedance (Phase) - RG/213 Above Ground Plane

4. PULSE TRACING

Time domain measurements of input and output pulses were performed on some of the cable configurations studied. This method utilized a Tektronix Model 109 Pulse Generator for cable excitation. Both short duration (2 ns width) and long duration (40 ns width) pulses of up to 50 volts were used depending on the application. The long duration pulse width exceeded the round trip travel time on the cables tested and was equivalent to a step function insofar as the first reflection was concerned. The pulses at the near and far ends of the cables were recorded on polaroid film using a Tektronix 485 scope and high impedance voltage probes across known loads.

This method was used primarily in the study of multimode propagation discussed in Section IV of this report. It also proved valuable in the investigation and verification of lumped parameter equivalent circuits.

5. LINE LOSSES

The spectrum of a pulse at a distance x from the input on a line of infinite length is given by the equation

$$E_x(\omega) = E_o(\omega)\, e^{-\gamma(\omega)x} \tag{16}$$

where $E_x(\omega)$ is the pulse spectrum at x
$E_o(\omega)$ is the pulse spectrum at x = 0 (Fourier transform of the input pulse)
$\gamma(\omega)$ is the propagation constant.

The propagation constant is given by the equation

$$\gamma = \alpha + i\beta = \sqrt{ZY} \tag{17}$$

where $Z = Z_i + i\omega L$, $Y = G + i\omega C$. Z_i is the internal impedance of the line given by (ref. 1)

$$Z_i = \frac{1}{2\pi a}\sqrt{\frac{i\omega\mu}{\sigma_w}}\ , \qquad a >> \sqrt{\frac{2}{\mu\omega\sigma_w}} \tag{18}$$

For a line above a ground plane (ref. 1)

$$G = \frac{2\pi\sigma_d}{\cosh^{-1}(h/a)} \tag{19}$$

$$L = \frac{\mu}{2\pi} \cosh^{-1}(h/a) \tag{20}$$

$$C = \frac{2\pi\varepsilon}{\cosh^{-1}(h/a)} \tag{21}$$

where σ_d = conductivity of dielectric

σ_w = conductivity of wire

h = wire height above the ground plane

a = wire radius.

The characteristic impedance is $Z_o = \sqrt{Z/Y}$, which for a lossless line reduces to

$$Z_o = \frac{60}{\sqrt{\varepsilon}} \cosh^{-1}(h/a) = \frac{60}{\sqrt{\varepsilon}} \ln\left[h/a + \sqrt{(h/a)^2 - 1}\right] \tag{22}$$

When the wire is above the ground plane the dielectric is predominantly air. The conductance G is negligible in this case and the propagation constant is given by

$$\gamma = (\alpha + i\beta) \simeq \sqrt{(i\omega C)(Z_i + i\omega L)} = \sqrt{i\omega C Z_i - \omega^2 LC} \tag{23}$$

The attenuation and phase angle can be found by squaring both sides of the above equation and equating the real and imaginary terms. The following equations are obtained:

$$\text{Real part:} \quad \alpha^2 - \beta^2 = -\omega^2 LC \tag{24}$$

$$\text{Imaginary part:} \quad i2\alpha\beta = i\omega C Z_i \tag{25}$$

Solving for α with $\beta = \frac{\omega C Z_i}{2\alpha}$ leads to

$$2\alpha^2 = -\left(\frac{\omega}{v}\right)^2 \pm \left(\frac{\omega}{v}\right)^2 \sqrt{1 + \left(\frac{v}{\omega}\right)^2 \left(\frac{Z_i}{Z_o}\right)^2} \tag{26}$$

where the substitutions $LC \simeq 1/v^2$, $Cv \simeq 1/Z_o$ have been made. Since $Z_i/Z_o << 1$, the square root can be expanded to give

$$2\alpha^2 = -\left(\frac{\omega}{v}\right)^2 + \left(\frac{\omega}{v}\right)^2 \left[1 + \frac{1}{2}\left(\frac{v}{\omega}\right)^2\left(\frac{Z_i}{Z_o}\right)^2\right] \tag{27}$$

which reduces to

$$\alpha = \frac{1}{2}\left(\frac{Z_i}{Z_o}\right) \tag{28}$$

With α determined, the equation for β can be solved and gives $\beta = \omega C Z_o = \left(\frac{\omega}{v}\right)$. The propagation constant is then

$$\gamma(\omega) = \frac{1}{2}\left(\frac{Z_i}{Z_o}\right) + i\,\frac{\omega}{v} \tag{29}$$

which upon substitution for Z_i becomes

$$\gamma(\omega) = \frac{1}{4\pi a Z_o}\left(\frac{i\mu\omega}{\sigma}\right)^{\frac{1}{2}} + i\,\frac{\omega}{v} \tag{30}$$

Let $\tau = \dfrac{\mu x^2}{16\pi^2 a^2 Z_o^2 \sigma}$ (31)

then

$$e^{-\gamma(\omega)x} = e^{-(i\omega\tau)^{\frac{1}{2}}} \times e^{-i\frac{\omega x}{v}} \tag{32}$$

and the pulse spectrum at a distance x is

$$E_x(\omega) = E_o(\omega)\, e^{-(i\omega\tau)^{\frac{1}{2}}}\, e^{-i\omega t_x} \tag{33}$$

where $t_x = x/v$. The Fourier transform of $E_x(\omega)$ when $E_o(\omega)$ is equal to an impulse or a step function is given by Sunde (ref. 2). The results are

$$\text{Impulse:} \quad h(t) = \left(\frac{\tau}{\pi t}\right)^{\frac{1}{2}} \frac{e^{-\tau/4t}}{2t} \tag{34}$$

$$\text{Step:} \quad g(t) = 1 - \operatorname{erf}\left(\frac{\tau}{4t}\right)^{\frac{1}{2}} \tag{35}$$

These functions are shown plotted versus t/τ in figure 8. The step function rise time defined in terms of a percent of the maximum pulse amplitude can be used to determine the constant τ.

The following relationships are equivalent:

$$t_r(10\% - 90\%) \doteq 31.31\ \tau$$
$$t_r(10\% - 80\%) = 7.63\ \tau$$
$$t_r(20\% - 80\%) = 7.51\ \tau$$

The attenuation is given by the real part of the propagation constant

$$\alpha(\omega) = R_e(\gamma) = \frac{1}{x}\sqrt{\frac{\omega\tau}{2}} \tag{36}$$

which in terms of the above rise times can be written as:

$$\alpha(f) = \frac{0.3168}{x}\sqrt{f\ t_r(10\% - 90\%)}$$
$$= \frac{0.6147}{x}\sqrt{f\ t_r(10\% - 80\%)} \tag{37}$$
$$= \frac{0.6468}{x}\sqrt{f\ t_r(20\% - 80\%)}$$

The above formulas are useful in estimating the frequency dependent attenuation from the risetime of a step function. They are applicable to TDR records with the far end of the cable terminated in a perfect short. In this case the distance x would be twice the length of the cable.

A similar analysis can be carried out for dielectric losses. These losses can be significant on insulated wires which are lying on a ground plane, if the loss tangent of the dielectric is relatively large. A case in point is vinyl or PVC insulation, which has a loss tangent in the range 0.06 to 0.1 (ref. 3).

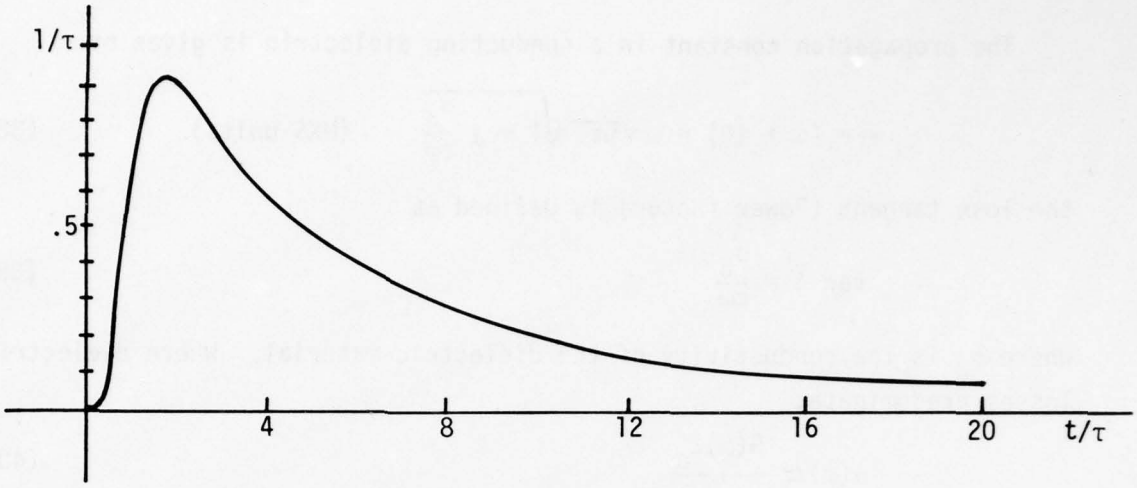

Impulse Response h(t)

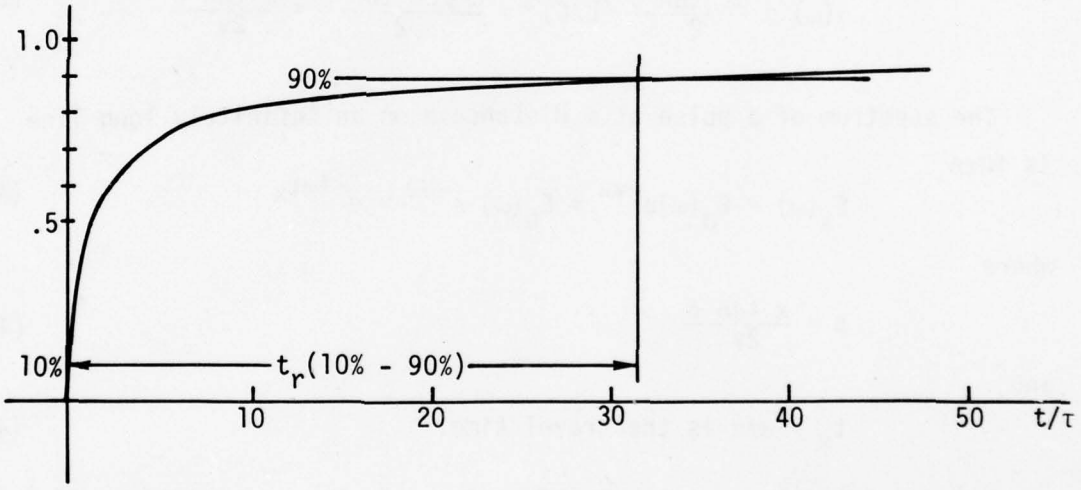

Step Response g(t)

Figure 8. Transmission Line Impulse and Step Function Responses for Series Losses.

The propagation constant in a conducting dielectric is given by

$$\gamma = (\alpha + i\beta) = \omega\sqrt{\mu\varepsilon}\sqrt{1 + j\frac{\sigma_d}{\varepsilon\omega}} \qquad \text{(MKS units)} \tag{38}$$

the loss tangent (Power factor) is defined as

$$\tan\delta = \frac{\sigma_d}{\varepsilon\omega} \tag{39}$$

where σ_d is the conductivity of the dielectric material. Where dielectric losses predominate,

$$\alpha(\omega) \simeq \frac{G(\omega)Z_o}{2} \tag{40}$$

where

$$G(\omega) = \frac{2\pi\sigma_d}{\cosh^{-1}(h/a)} = \frac{\sigma_d C}{\varepsilon} = \omega C \tan\delta \tag{41}$$

Thus

$$\alpha(\omega) = \frac{\omega C \tan\delta}{2}(L/C)^{\frac{1}{2}} = \frac{\omega\sqrt{LC}\tan\delta}{2} = \frac{\omega\tan\delta}{2v} \tag{42}$$

The spectrum of a pulse at a distance x on an infinitely long line is then

$$E_x(\omega) = E_o(\omega)e^{-\gamma x} = E_o(\omega)\, e^{-a\omega} \times e^{-i\omega t_x} \tag{43}$$

where

$$a = \frac{x\tan\delta}{2v} \tag{44}$$

and

$$t_x = x/v \text{ is the travel time.} \tag{45}$$

For $E_o(\omega)$ equal to an impulse function, the Fourier transform of $E_x(\omega)$ is (ref. 4):

$$h(t') = \frac{a/\pi}{a^2 + t'^2} \quad , \quad t' = t - t_x \tag{46}$$

The step response is obtained by integrating $h(t')$

$$g(t') = \int_{-\infty}^{t'} \frac{(a/\pi)d\tau}{a^2 + \tau^2} = \frac{1}{\pi}\left[\tan^{-1}(t'/a) + \pi/2\right] \qquad (47)$$

The functions $h(t')$ and $g(t')$ are shown plotted in figure 9. The parameter a is related to the rise time of the step function response by the formulas

$$t_r(10\% - 90\%) = 6.156a$$
$$t_r(10\% - 80\%) = 4.454a$$
$$t_r(20\% - 80\%) = 2.752a.$$

The attenuation in terms of the rise time is given by

$$\alpha = \frac{1.021\ ft_r(10\% - 90\%)}{x}, \text{ repers/meter}$$
$$= \frac{1.411\ ft_r(10\% - 80\%)}{x} \qquad (48)$$
$$= \frac{2.283\ ft_r(20\% - 80\%)}{x}$$

The attenuation on a 5.94 meter length of 20 gauge insulated (PVC) wire in contact with a ground plane was measured from swept frequency input impedance data. The results were compared with estimates based on the rise time of the TDR step function reflected from the shorted end of the wire. The swept frequency and TDR data are shown in figures 10 and 11 respectively. The 10% to 90% rise time is 5.9 nanoseconds and the propagation velocity is $v = 2.151 \times 10^8$ meters/second. The attenuation versus frequency data are presented in figure 12. The measured high frequency attenuation is seen to be in good agreement with the values estimated by the reflected pulse rise time method, assuming only dielectric losses were present.

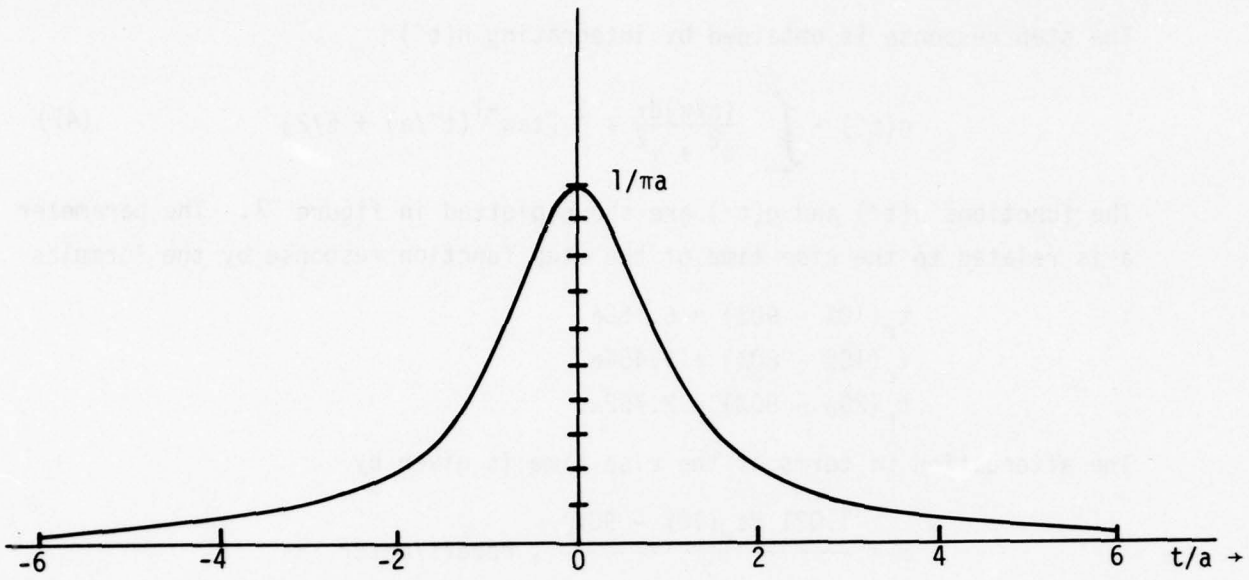

Impulse Response h(t)

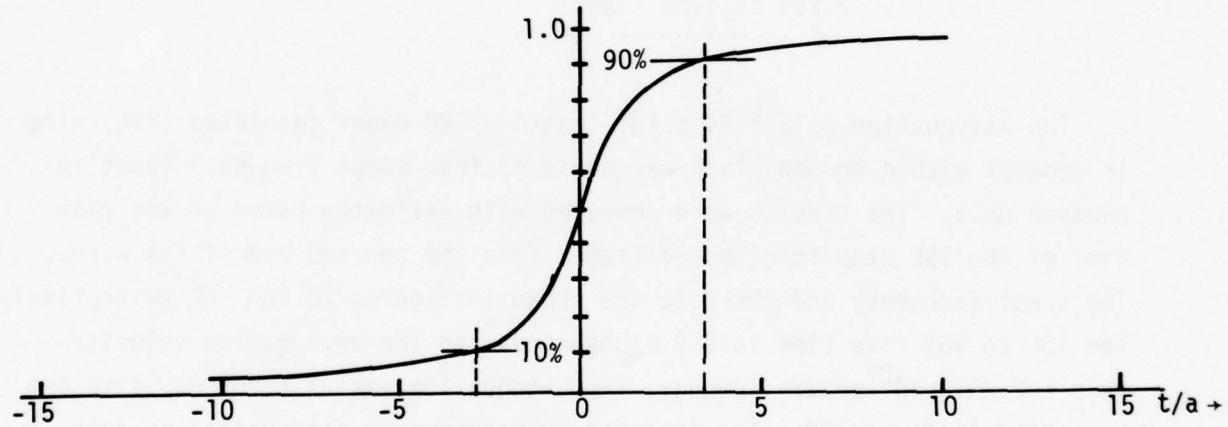

Step Response g(t)

Figure 9. Transmission Line Impulse and Step Function Responses for Shunt Losses

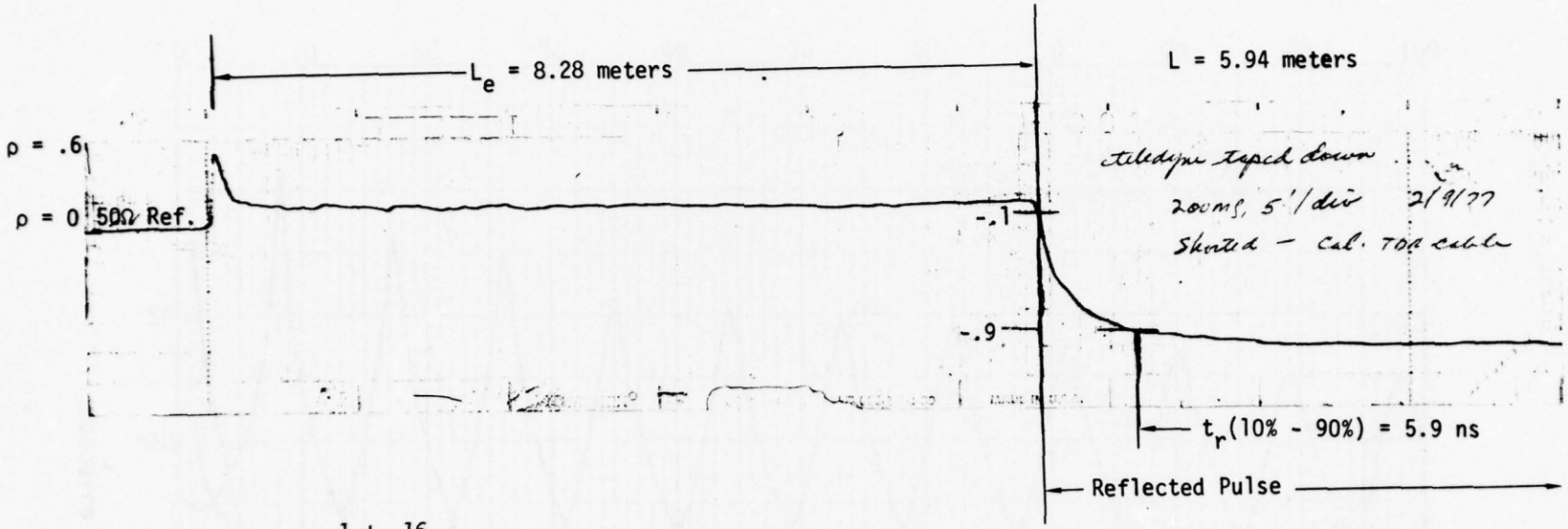

$$Z_c = 50 \frac{1 + .16}{1 - .16} = 69 \text{ ohms}$$

$$v/c = \frac{5.94}{8.28} = 0.717$$

Figure 10. TDR Record for Loss Estimates - Wire on Ground Plane

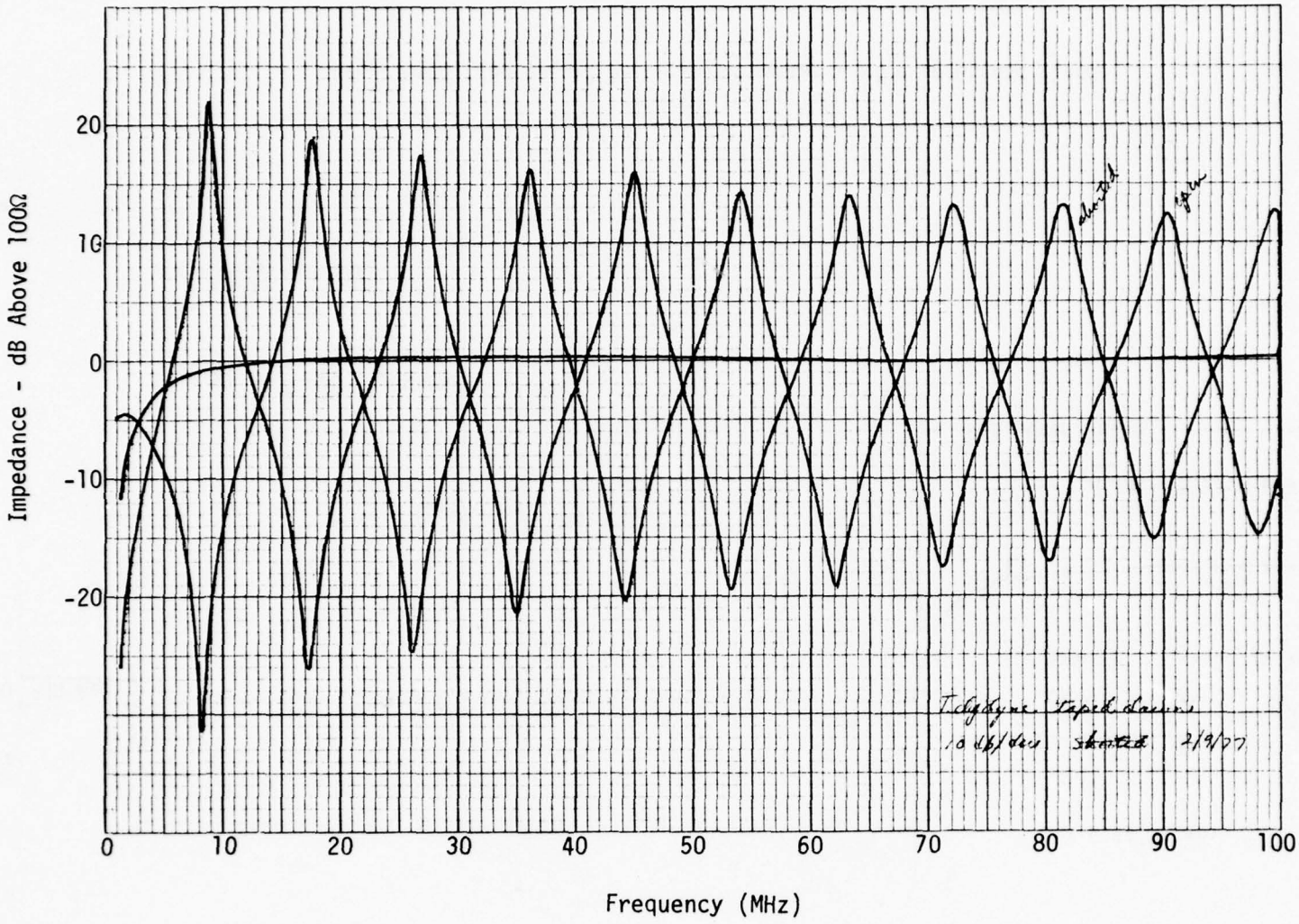

Figure 11. Input Impedance (Magnitude) - Wire on Ground Plane

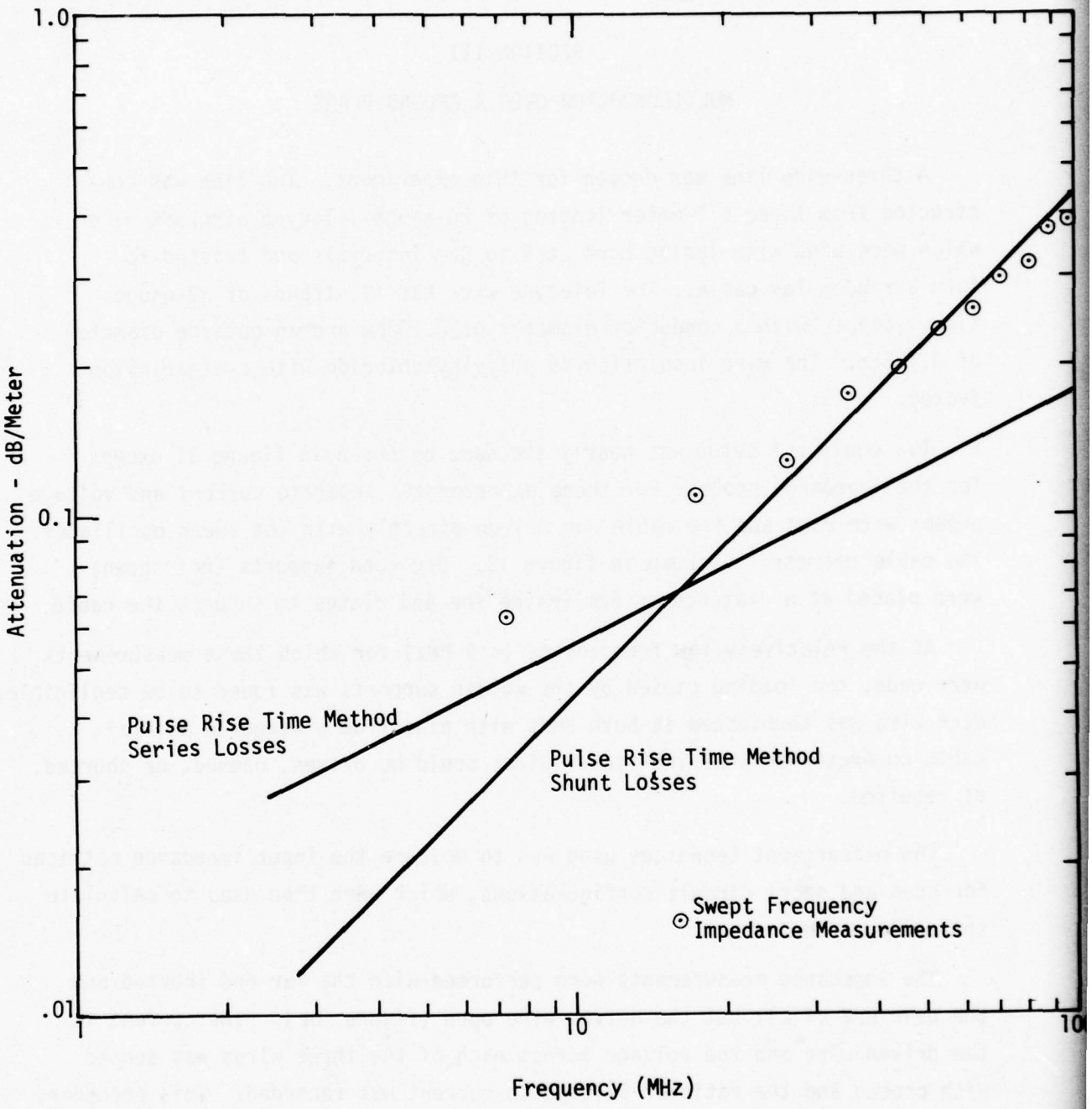

Figure 12. Attenuation vs. Frequency - Wire on Ground Plane

SECTION III

MULTICONDUCTOR OVER A GROUND PLANE

A three-wire line was chosen for this experiment. The line was constructed from three 6.1-meter lengths of 20-gauge Teledyne aircraft wire which were tied with lacing cord at 5 to 8cm intervals and twisted to form a random-lay cable. The Teledyne wire has 19 strands of 32-gauge tinned copper with a conductor diameter of 0.102cm and an outside diameter of 0.198cm. The wire insulation is polyvinylchloride with a clear nylon jacket.

The equipment setup was nearly the same as shown in figure 3, except for the impedance probe. For these experiments, separate current and voltage probes were used and the cable was driven directly with the sweep oscillator. The cable geometry is shown in figure 13. Dry wood supports (not shown) were placed at a distance of 5cm inside the end plates to support the cable.

At the relatively low frequencies (< 5 MHz) for which these measurements were made, the loading caused by the wooden supports was found to be negligible. Each wire was terminated at both ends with pins from a standard aircraft cable connector so that individual wires could be driven, opened, or shorted, as required.

The measurement technique used was to measure the input impedance matrices for open and short circuit configurations, which were then used to calculate the cable parameters.

The impedance measurements were performed with the far end shorted and the near end of all but the driven wire open (figure 14). The current in the driven wire and the voltage across each of the three wires was sensed with probes and the ratio of voltage to current was recorded. This procedure was repeated for each wire in order to isolate the self and mutual impedance terms in the circuit equations (at the near end)

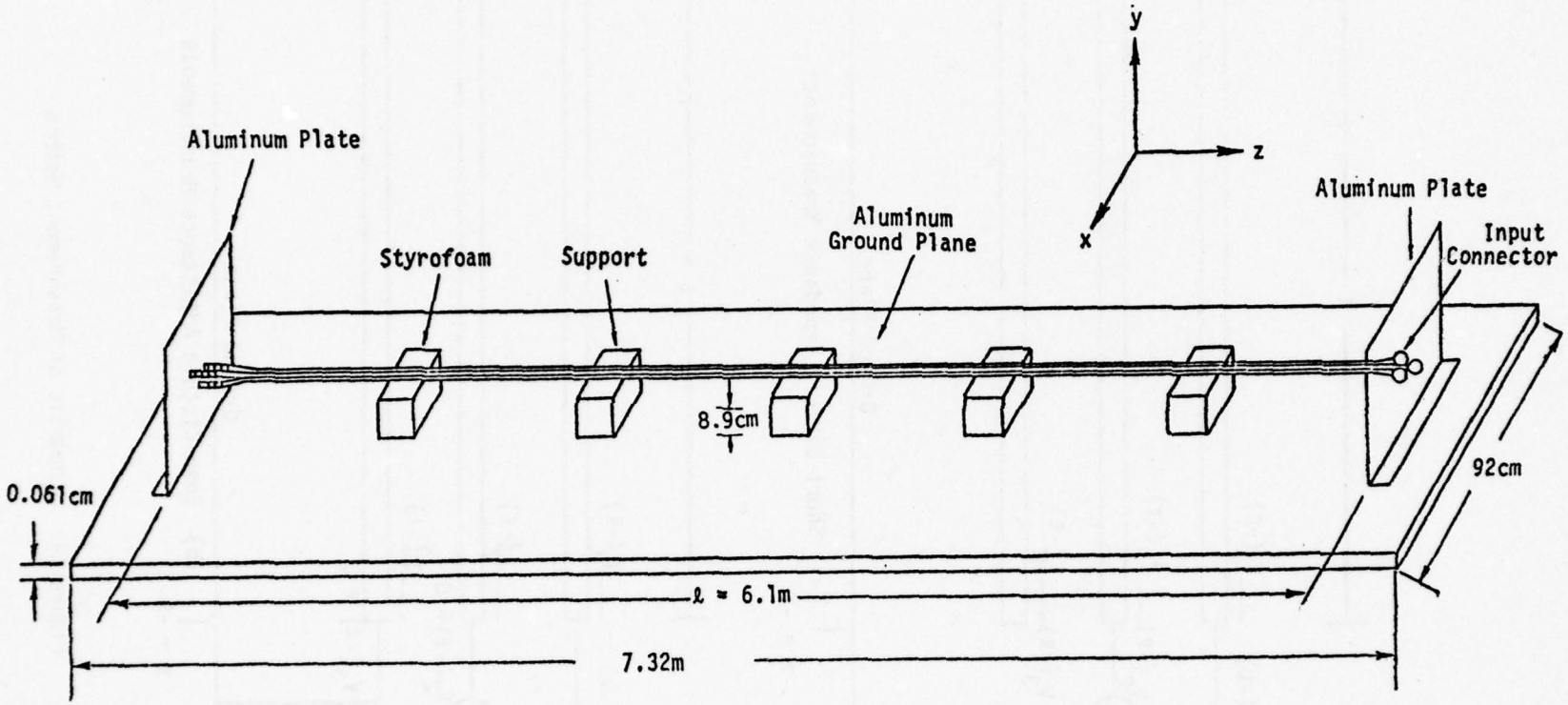

Figure 13. A Sketch of the Experimental Setup

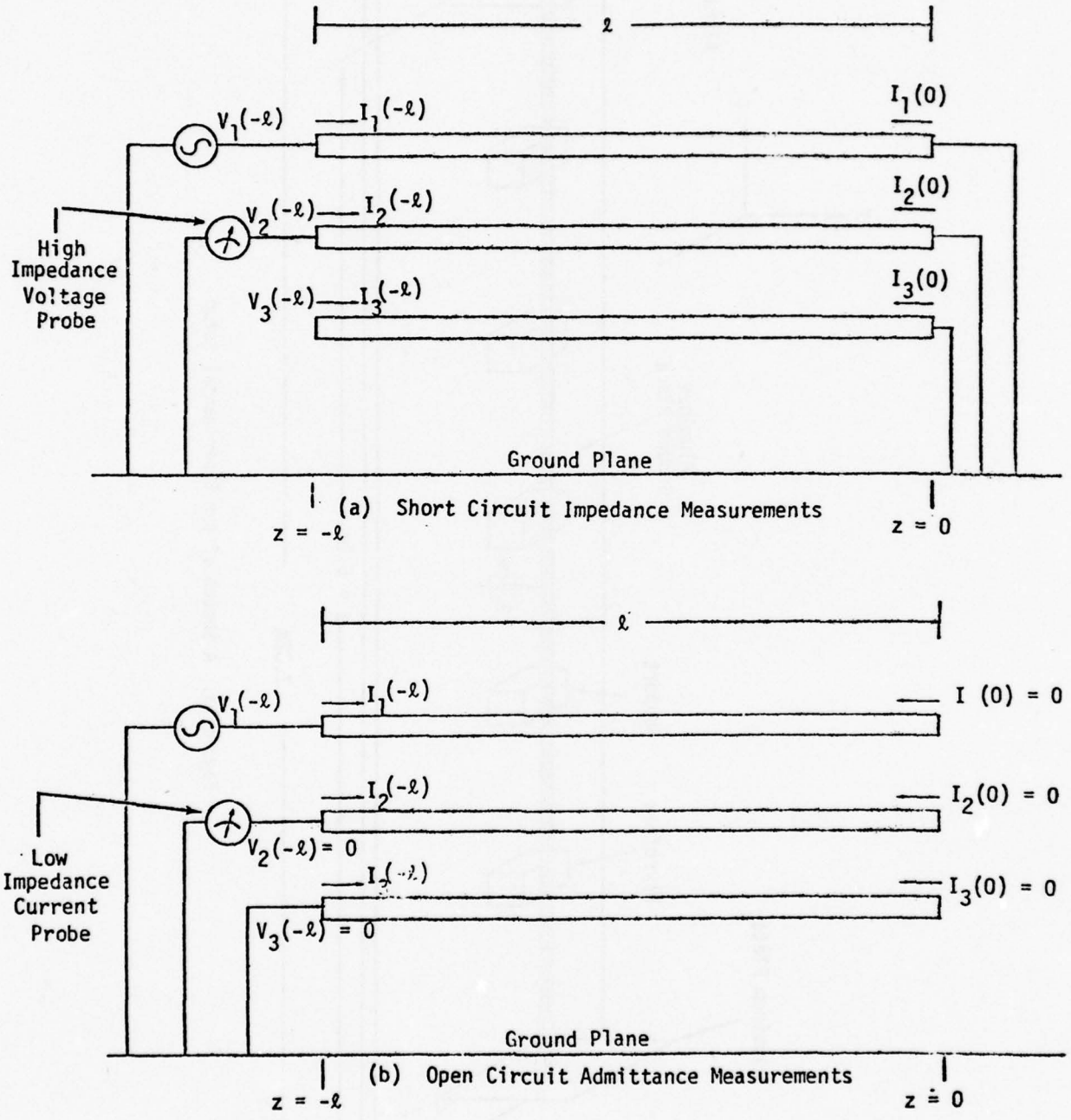

Figure 14. Schematic of Measurement Method

$$V_1 = Z_{11}I_1 + Z_{12}I_2 + Z_{13}I_3 \tag{49}$$

$$V_2 = Z_{21}I_1 + Z_{22}I_2 + Z_{23}I_3 \tag{50}$$

$$V_3 = Z_{31}I_1 + Z_{32}I_2 + Z_{33}I_3 \tag{51}$$

or

$$Z_{ij}^{sc} = \frac{V_i}{I_j} \quad \begin{matrix} \text{for} \quad i = 1,2,3 \\ \qquad\quad j = 1,2,3 \end{matrix} \tag{52}$$

The admittance measurements were made with the far end open and all but the driven wire shorted at the near end. The ratio of current to voltage was recorded in this case to isolate the self and mutual admittances in the equations

$$I_1 = Y_{11}V_1 + Y_{12}V_2 + Y_{13}V_3 \tag{53}$$

$$I_2 = Y_{21}V_1 + Y_{22}V_2 + Y_{23}V_3 \tag{54}$$

$$I_3 = Y_{31}V_1 + Y_{23}V_2 + Y_{23}V_3 \tag{55}$$

in a manner similar to that described for the impedance measurements. In this case,

$$Y_{ij}^{oc} = \frac{I_i}{V_j} \quad \begin{matrix} \text{for } i = 1,2,3 \\ \qquad j = 1,2,3. \end{matrix} \tag{56}$$

1. LOW FREQUENCY PARAMETER STUDY

For an electrically short cable ($k_o \ell << 1$), the open and short circuit measurements lead directly to the capacitance and inductance-per-unit-length matrices [C] and [L] when the resistance [R] and the conductance [G] per unit length are neglected as follows:

$$Z_{ij}^{sc} = R + j\omega L_{ij}, \; L_{ij} \simeq Z_{ij}^{sc}/(j\omega) \tag{57}$$

$$Y_{ij}^{oc} = G + j\omega C_{ij}, \; C_{ij} \simeq Y_{ij}^{oc}/(j\omega) \tag{58}$$

in matrix form

$$[Z] \simeq j\omega\,[L]\ ;\ [Y] = j\omega\,[C]; \tag{59}$$

where [Z] is the series-impedance-per-unit length matrix, and [Y] is the shunt-admittance-per-unit length matrix.

In the above calculations, the lumped parameter model of the multiconductor line is used, and the above relations are only true in the frequency region where the line can be considered as electrically short. At higher frequencies the transmission line equations have to be used in order to calculate the cable parameters from the impedance measurements. This formulation is discussed later in this section.

The data for the 0.15 to 5 MHz frequency are shown in figures 15 through 18. Only small differences are seen among the three self terms (diagonal) or the six mutual terms (off-diagonal) as would be expected for a random-lay cable of three identical wires.

The inductance and capacitance matrices (per-unit-length parameters) were calculated from measurements of $|Z_{ij}^{sc}|$ and $|Y_{ij}^{oc}|$. The self and mutual inductance and capacitance per unit length are plotted versus frequency (0.2 to 5 MHz) in figures 19 through 22. These curves show that beyond 2 MHz, the inductance and capacitance values increase with frequency and the variations are quite large, which are not expected. Up to 2 MHz, the variations in inductance and capacitances are small and are nearly constant. Variations in the values of inductance and capacitance at higher frequencies show that the lumped parameter model is no longer valid in this range. The calculations for higher frequencies are discussed in Section III.2 of this report.

In the following section, the measured values are compared to the theoretical values and the use of [L] and [C] matrices in calculating the propagation velocities of different modes is discussed.

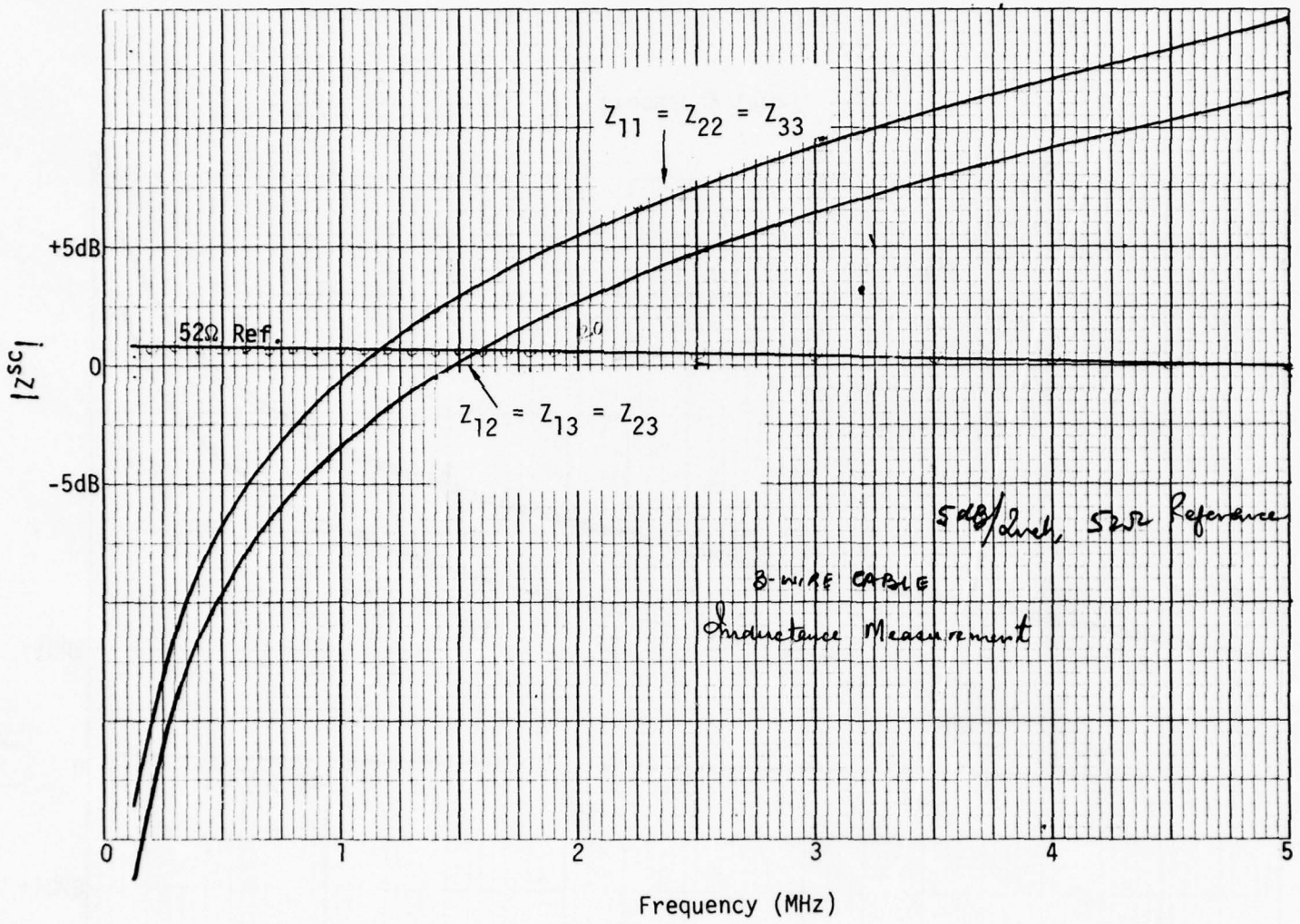

Figure 15. Short Circuit Impedance Data - Three-Wire Line

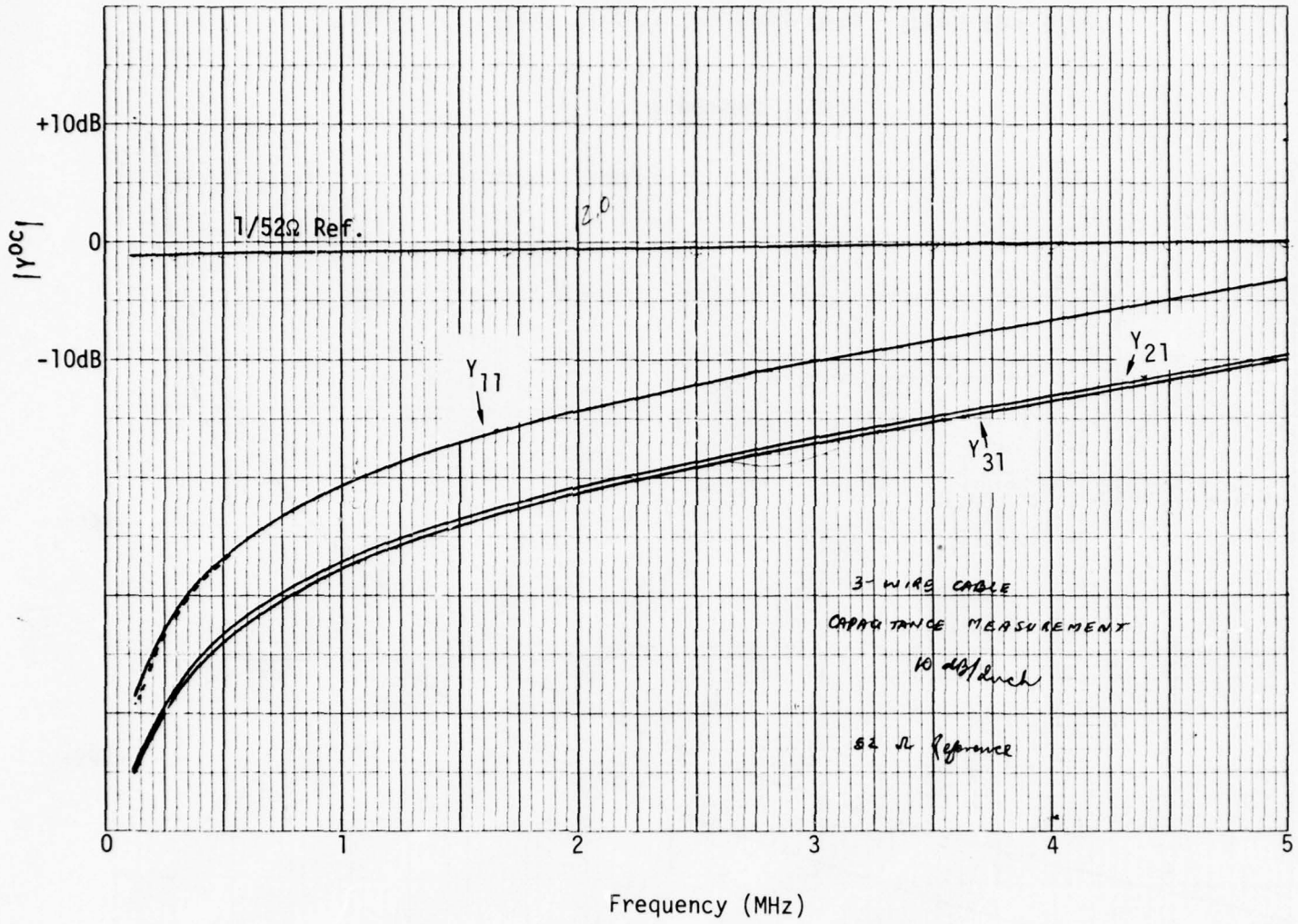

Figure 16. Open Circuit Admittance Data - Three-Wire Line

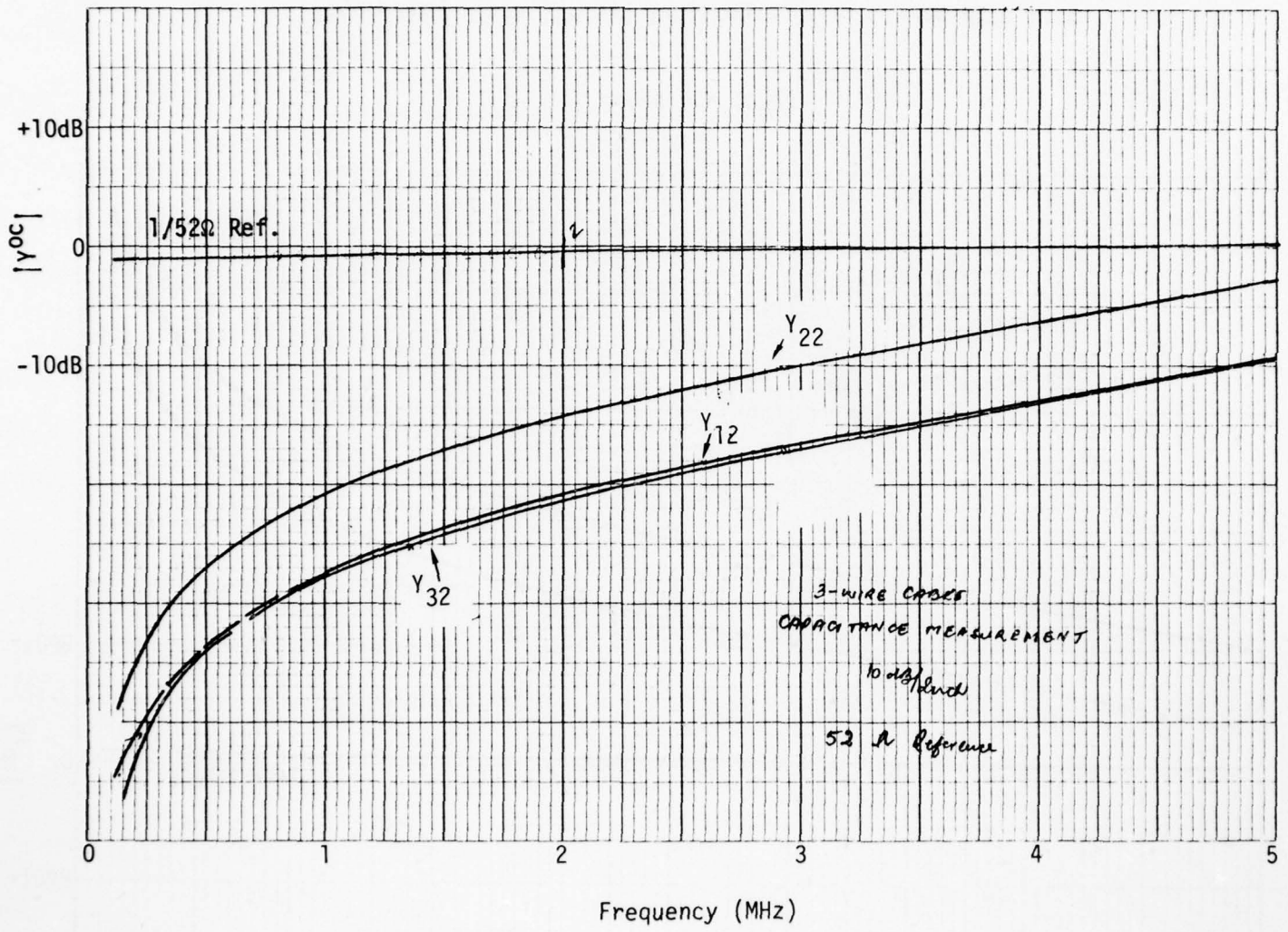

Figure 17. Open Circuit Admittance Data - Three-Wire Line

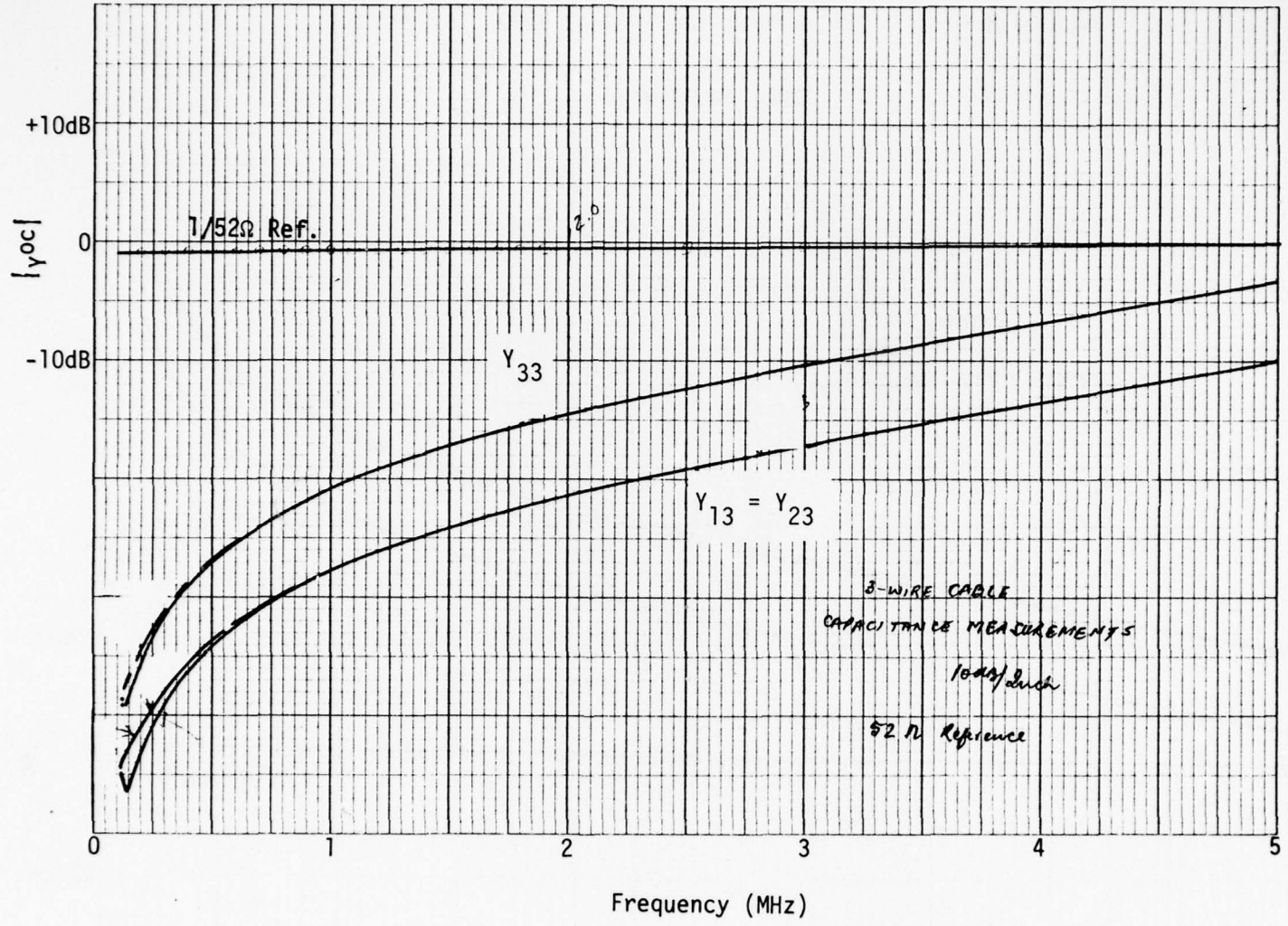

Figure 18. Open Circuit Admittance Data - Three-Wire Line

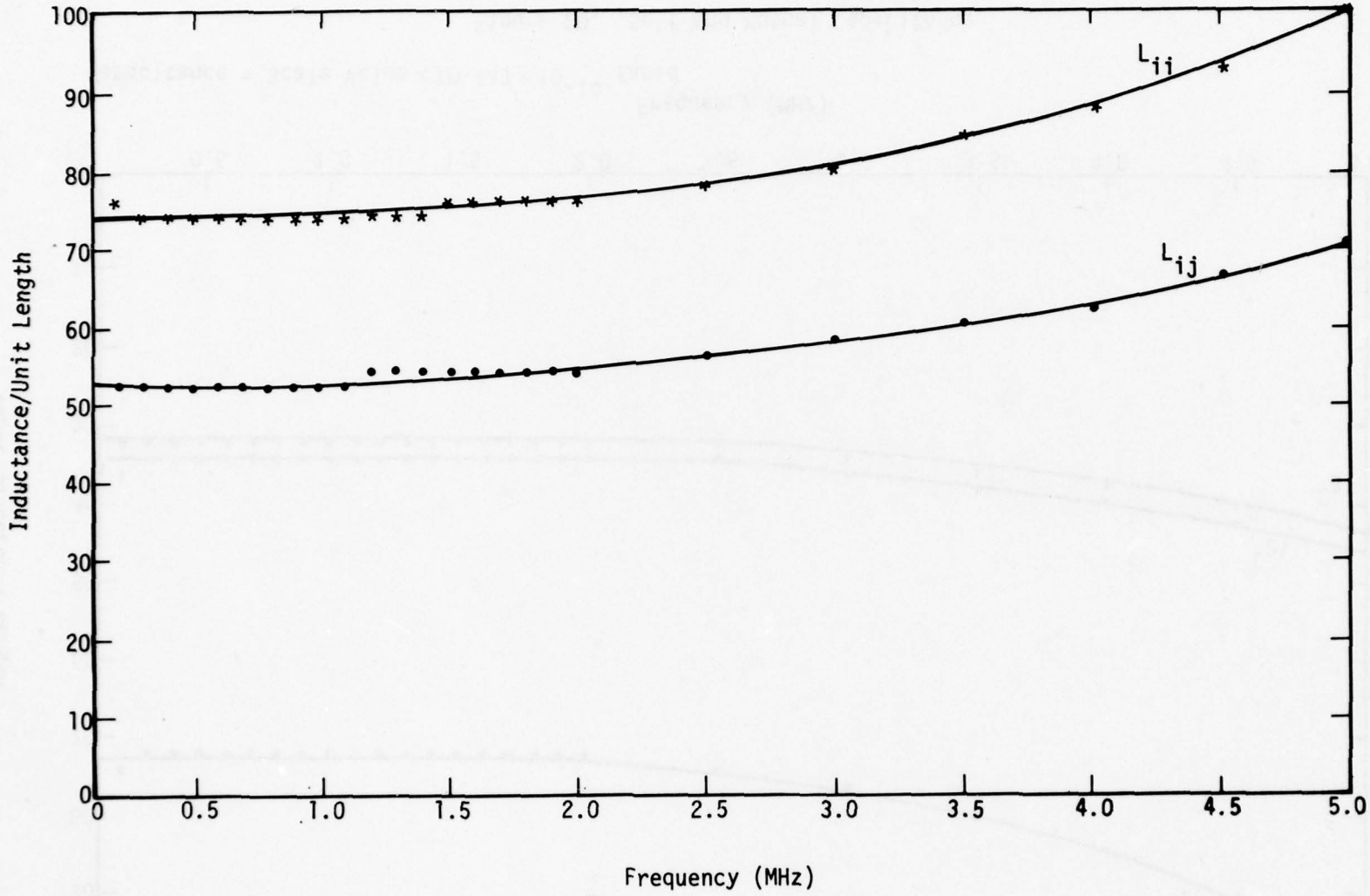

Inductance = Scale Value × 1.51404×10^{-8} henry

Figure 19. Self and Mutual Inductance

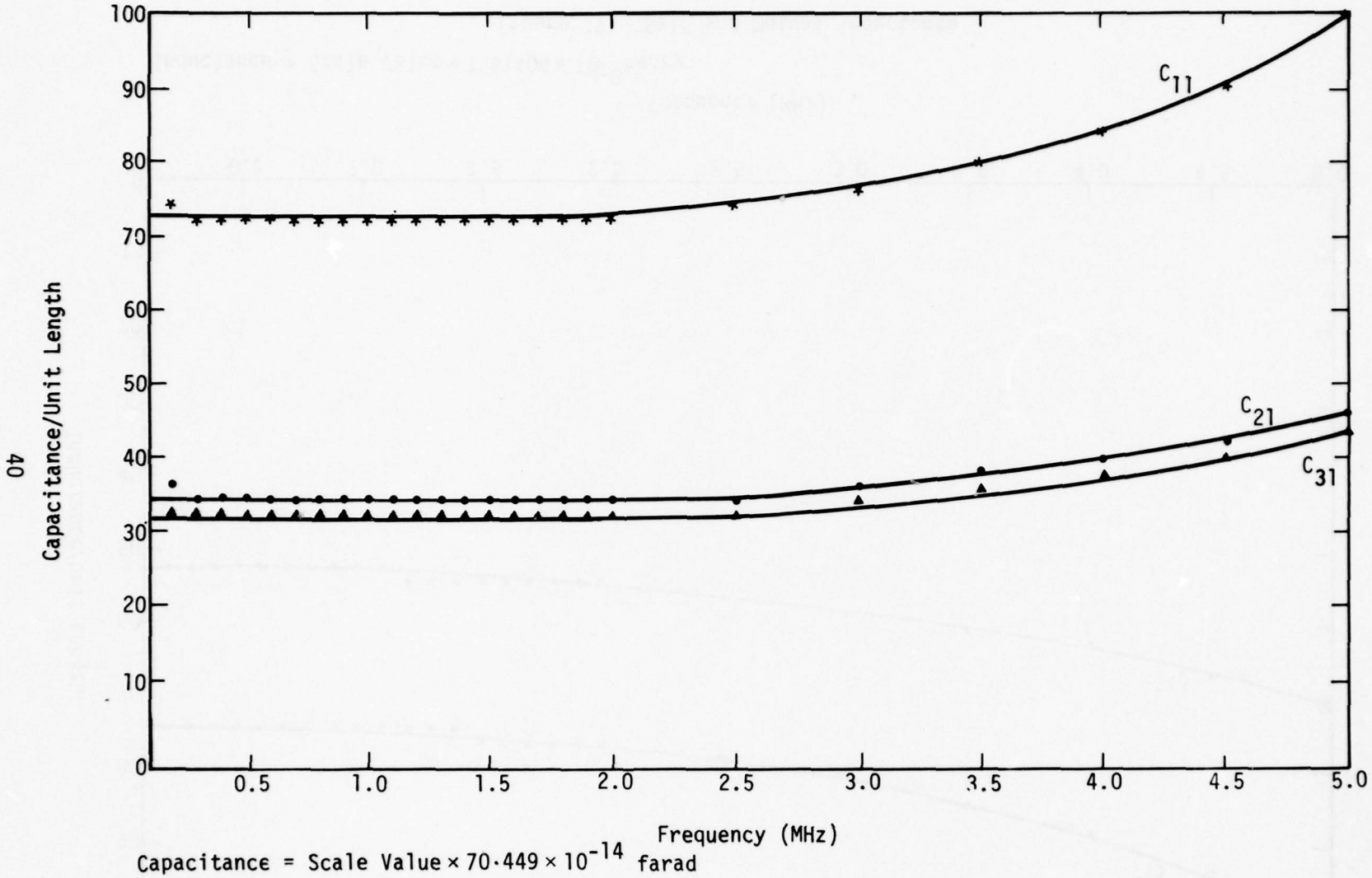

Capacitance = Scale Value $\times 70{\cdot}449 \times 10^{-14}$ farad

Figure 20. Self and Mutual Capacitance

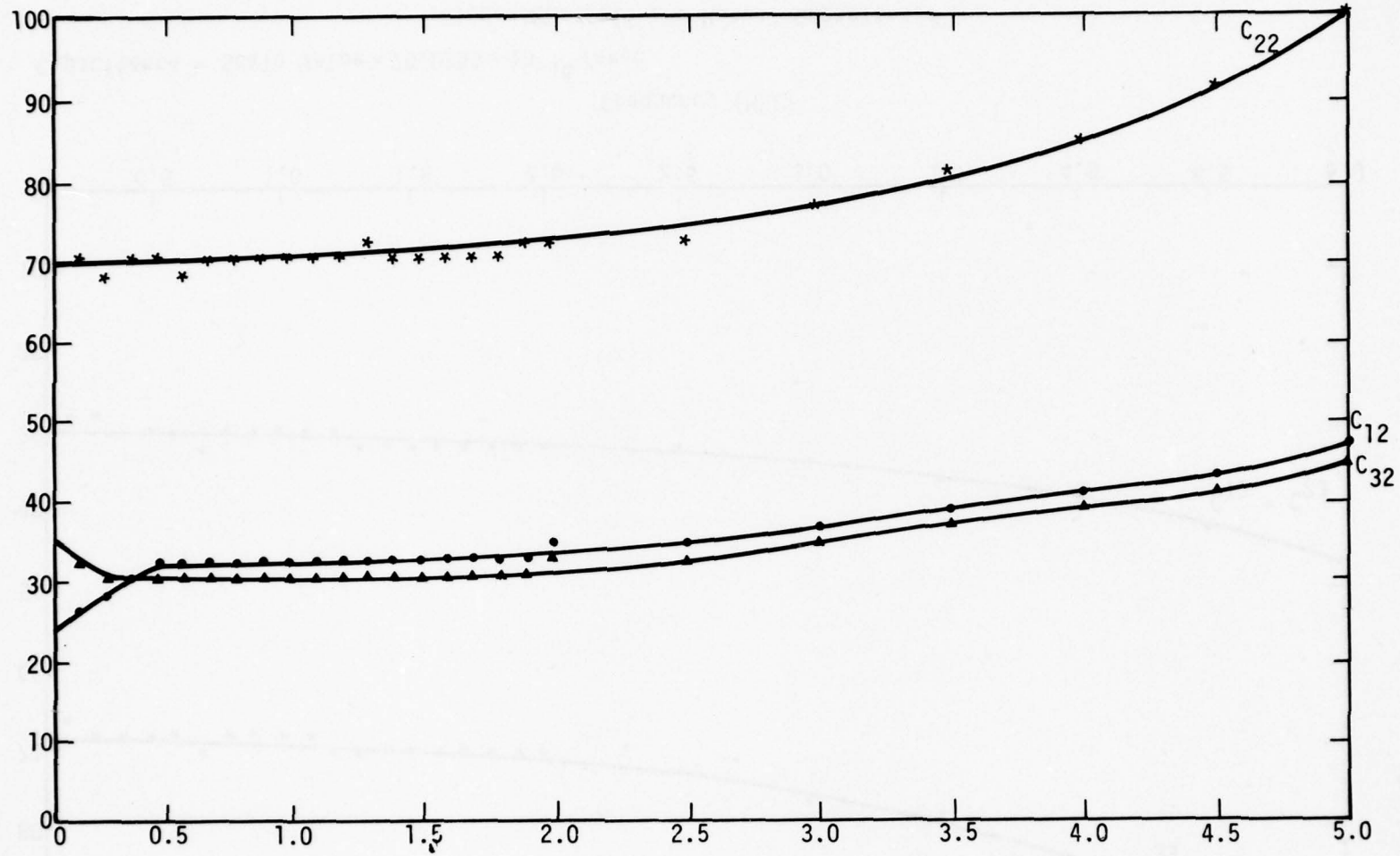

Capacitance = Scale Value $\times 71{\cdot}2838 \times 10^{-14}$ farad

Figure 21. Self and Mutual Capacitance

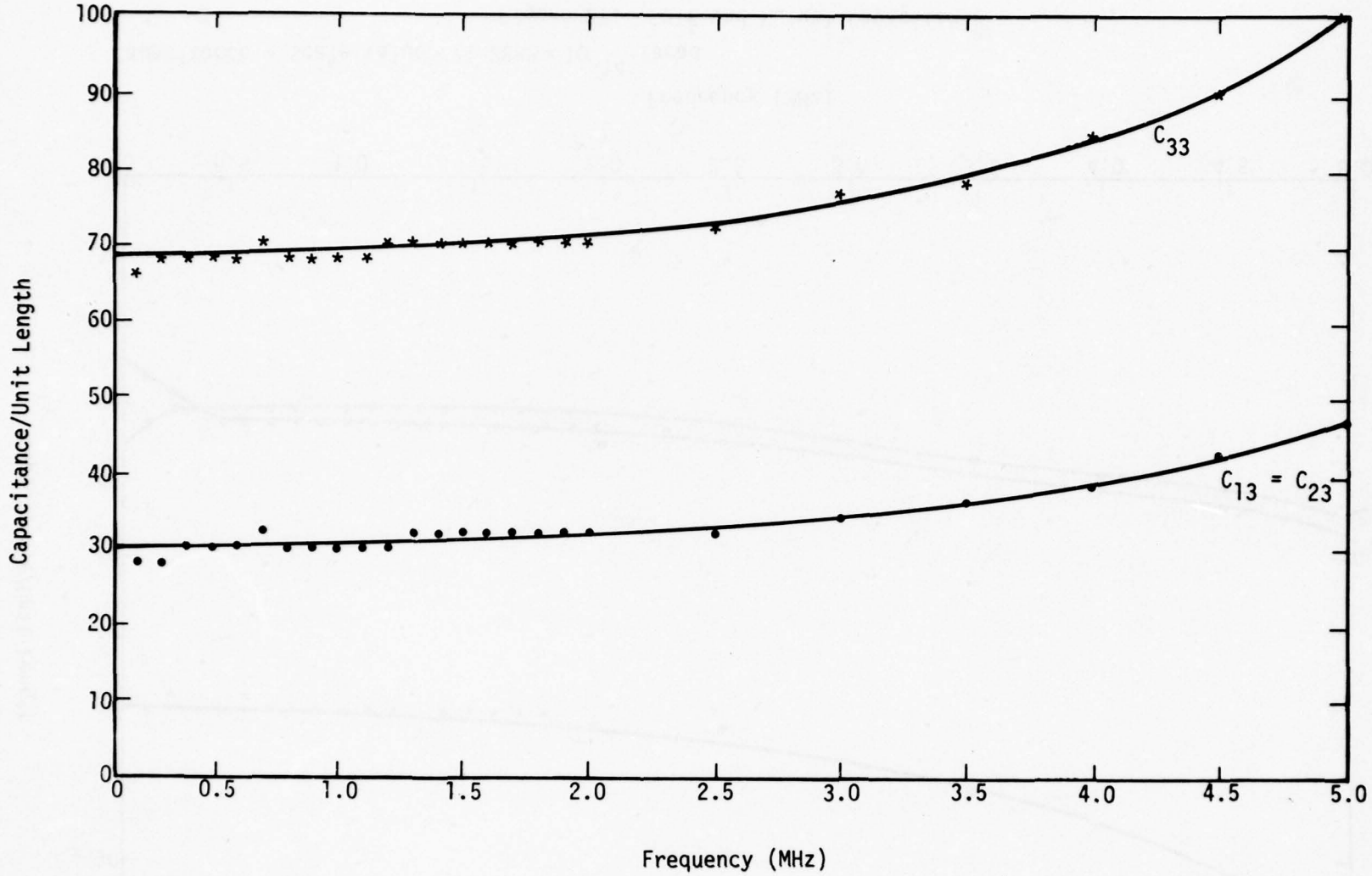

Capacitance = Scale Value $\times$ 70.0355 $\times$ 10^{-14} farad

Figure 22. Self and Mutual Capacitance

The measured results at a frequency of 1 MHz are given in matrix form as:

$$[C] = \begin{bmatrix} 52.16 & -24.34 & -22.87 \\ -24.40 & 51.80 & -23.25 \\ -22.82 & -23.25 & 50.27 \end{bmatrix} \times 10^{-12} \text{ F/m}$$

$$[L] = \begin{bmatrix} 1.209 & 0.874 & 0.868 \\ 0.888 & 1.209 & 0.868 \\ 0.872 & 0.866 & 1.206 \end{bmatrix} \times 10^{-6} \text{ H/m}$$

The propagation velocity for a single line is given by the equation $v_p = (LC)^{-\frac{1}{2}}$. For a multiconductor the relationship is the same except L and C are matrices and the v_p's are found by computing the square root of the reciprocal of the eigenvalues of the [L][C] product. For the case studied the propagation velocities were found to be $v_1 = 0.664c$, $v_2 = 0.666c$, $v_3 = 0.922c$. The first two nearly identical values are identified with the differential modes of the cable. The third corresponds to common mode propagation.

A comparison of the measured coefficients of inductance with theory was carried out using the formulas (ref. 5)

$$L_{ii} = 0.2 \log_e \left[\frac{4H_i}{d_i}\right]$$

$$L_{ij} = 0.2 \log_e [S_{ij}/D_{ij}]$$

where L_{ii} is the self inductance term of the i^{th} conductor, L_{ij} is the mutual inductance term between i^{th} and j^{th} conductors. The other parameters are defined as:

d = the diameter of a conductor
H = the distance from a conductor to ground
D = the distance between two conductors
S = the distance from the conductor to the "image" of a second

The L matrix calculated using the above formulas and the geometry for the three-wire cable above the ground plane was found to be

$$L = \begin{bmatrix} 1.17758 & 0.903483 & 0.903482 \\ 0.903493 & 1.1738 & 0.901628 \\ 0.903682 & 0.901628 & 1.1738 \end{bmatrix} \mu H/m.$$

These values are seen to be within 4% of the measured coefficients.

Comparison of the calculated and measured capacitance is complicated by the nonuniform dielectric material separating the wires. An estimate of the effective dielectric constant was obtained by computing the coefficients of capacitance in the absence of any dielectric material with the MRC CAP code. The result is given by the capacitance matrix

$$C' = \begin{bmatrix} 30.73 & -13.51 & -13.51 \\ -13.51 & 30.73 & -13.49 \\ -13.51 & -13.49 & 30.73 \end{bmatrix} pF/m.$$

The calculated C'_{ij} and measured C_{ij} coefficients are related by the equations

$$C_{ij} = \varepsilon' C'_{ij} \quad , \quad i \neq j \tag{60}$$

$$C_{ii} = C_{io} + \sum_{j=1}^{3} \varepsilon' C'_{ij}, \quad i \neq j, \; i = 1,2,3 \tag{61}$$

where ε' is the effective homogeneous dielectric constant and C_{io} is the capacitance to ground of the i^{th} conductor. The average effective dielectric constant for the case studied is 1.74 determined by comparing the off-diagonal terms of the calculated and measured capacitance matrices. Solid PVC insulation has a dielectric constant of 2.8.

An investigation was carried out of the problems encountered in calculating the [L] or [C] matrix by inversion when one or the other is known either from theory or from measurements. Two main problems are encountered:

(1) The effective dielectric constant of the material between the conductors is not known; (2) the propagation of error in the matrix transformation process can be significant. In certain cases, these errors are very large and the procedure can not be used. This will be shown in following paragraphs. Before presenting the actual numbers we should first define an ill-conditioned matrix.

Assume A is a nonsingular matrix with elements a_{ij} normalized to the largest element. If the matrix A^{-1} contains some very large elements (compared to those of A), then we say the matrix is ill-conditioned. (Conversely, if the largest element in magnitude of A^{-1} is of the same order as the largest element in A, the matrix may be said to be well-conditioned.)

As an example, the C matrix obtained from the calculated L matrix using the relation $[C] = 1/c^2[L]^{-1}$ is

$$[C] = \begin{bmatrix} 28.4197 & -12.3718 & -12.3717 \\ -12.3718 & 28.4745 & 12.3494 \\ -12.3717 & -12.3494 & 28.4744 \end{bmatrix} \text{ pF/m.}$$

The diagonal elements of this matrix are in error by about 8% and off-diagonal elements are in error by about 9% compared to the C matrix obtained from CAP code. Since the normalized elements of the C matrix are large compared to those of L, and the formulas for 'L' are not exact, the errors propagate in the inversion process. The L matrix obtained by inverting the CAP code C matrix using the relation $[L] = 1/c^2[C]^{-1}$ is

$$[L] = \begin{bmatrix} 1.16274 & 0.911173 & 0.911173 \\ 0.911173 & 1.16192 & 0.911173 \\ 0.911173 & 0.911173 & 1.16192 \end{bmatrix} \mu\text{H/m.}$$

When compared to the L matrix obtained from formulas, the diagonal elements are only off by about 1.3% and off-diagonal elements are off about 0.8%.

As another example, the measured L matrix was inverted to give the free space capacitance matrix

$$[C]' = \begin{bmatrix} 23.6941 & -10.1207 & -9.7332 \\ -10.5115 & 23.4697 & -9.3264 \\ -9.5478 & -9.5353 & 22.9479 \end{bmatrix} \text{ pF/m.}$$

Although the measured and calculated coefficients of inductance were in agreement to within 4%, comparison of the elements of C′ above with the CAP code results shows that the diagonal elements differ by about 34% to 44%. The above comparison shows that a small error in the values of L matrix elements results in a large error in the C matrix elements. The large error propagation does not occur if the L matrix is obtained from the C matrix. In this case the L matrix is ill-conditioned while the C matrix is well-conditioned.

Similar data for the evaluation of L and C matrices were taken for the same three-wire cable supported over metallic ribs. The configuration of ribs is identical to that shown in figure 1. The data for the 0.15 to 5 MHz frequency range are shown in figures 23 through 26. The inductance and capacitance matrices are calculated using the method described earlier for a cable without ribs. The self and mutual inductance and capacitance per unit length are plotted versus frequency (0.2 to 5 MHz) in figures 27 through 30. It is noted that the self capacitances-per-unit-length are higher than those for the cable without ribs. This increase in the self-capacitance terms is caused by the periodic capacitive loading by the metallic ribs. A similar effect was observed for a single wire over a ground plane. The capacitive loading by the ribs affects only the self capacitance terms. This increase in the self capacitance values results in a decreased velocity of propagation for the common mode. In figures 31a and 31b, the velocity of propagation for the different modes is plotted versus frequency. It is seen that the propagation velocity of the differential modes is nearly equal for the two cases, cable with and without ribs.

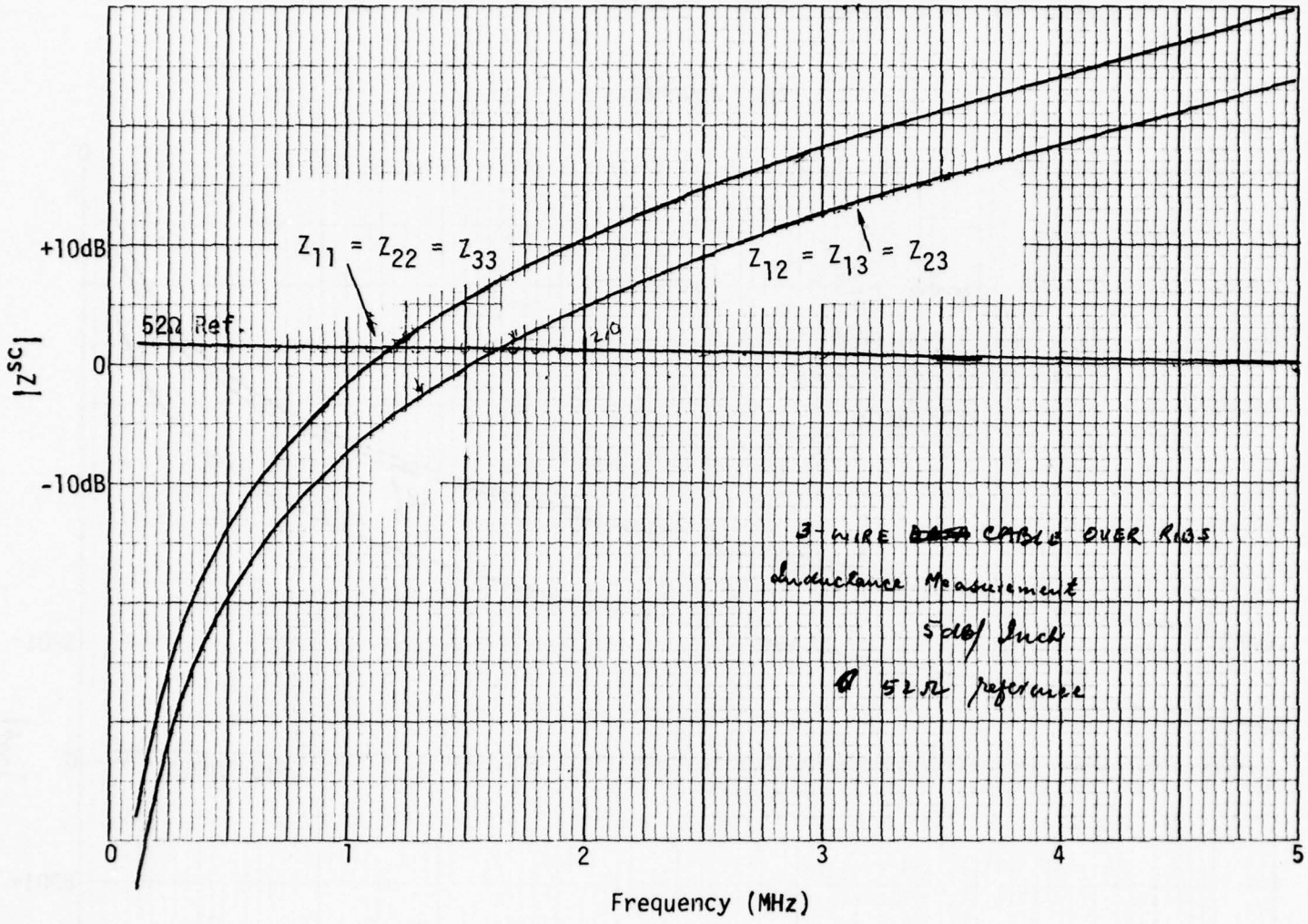

Figure 23. Short Circuit Impedance Data - Three-Wire Line Over Ribs

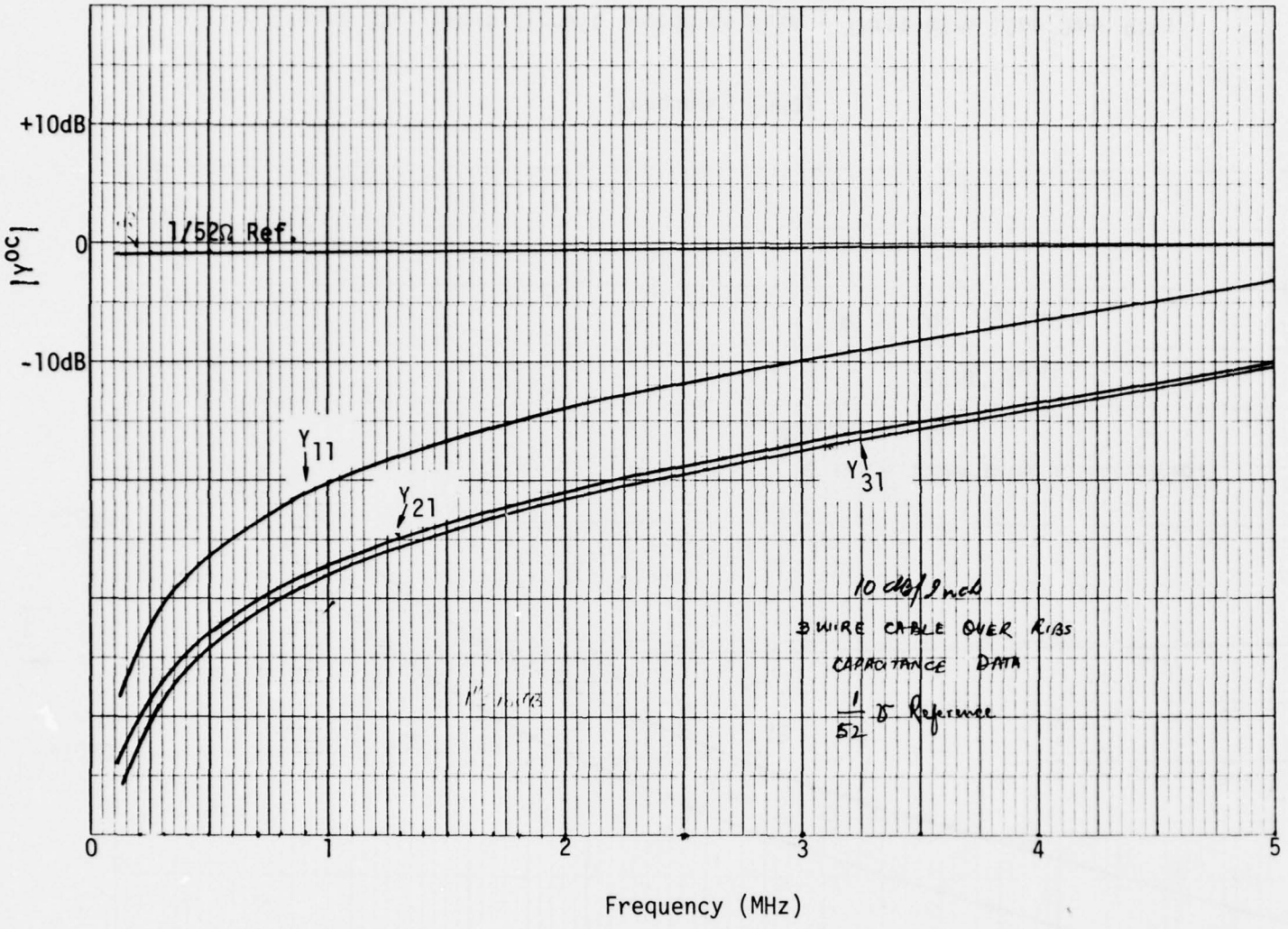

Figure 24. Open Circuit Admittance Data - Three-Wire Line Over Ribs

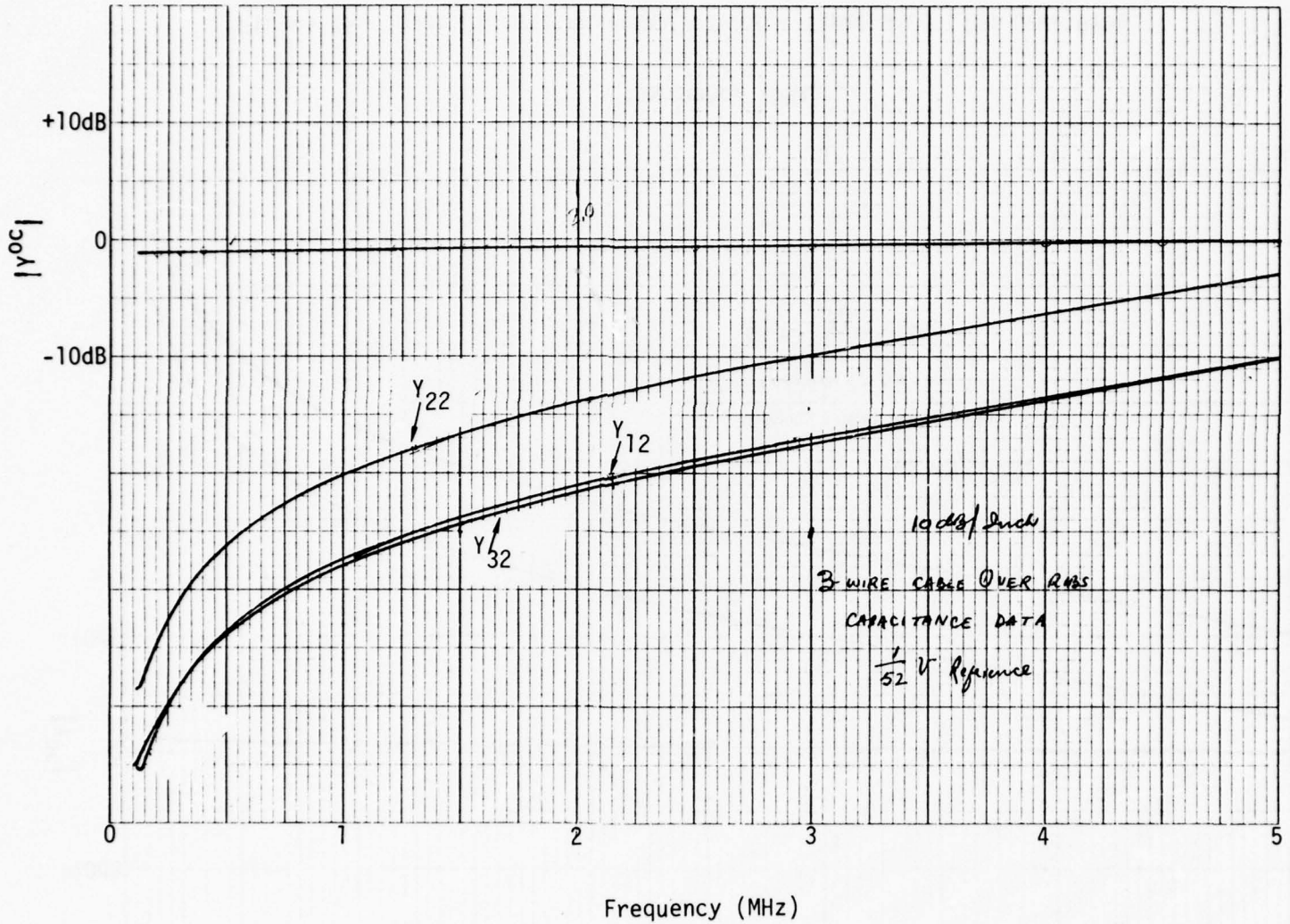

Figure 25. Open Circuit Admittance Data - Three-Wire Line Over Ribs

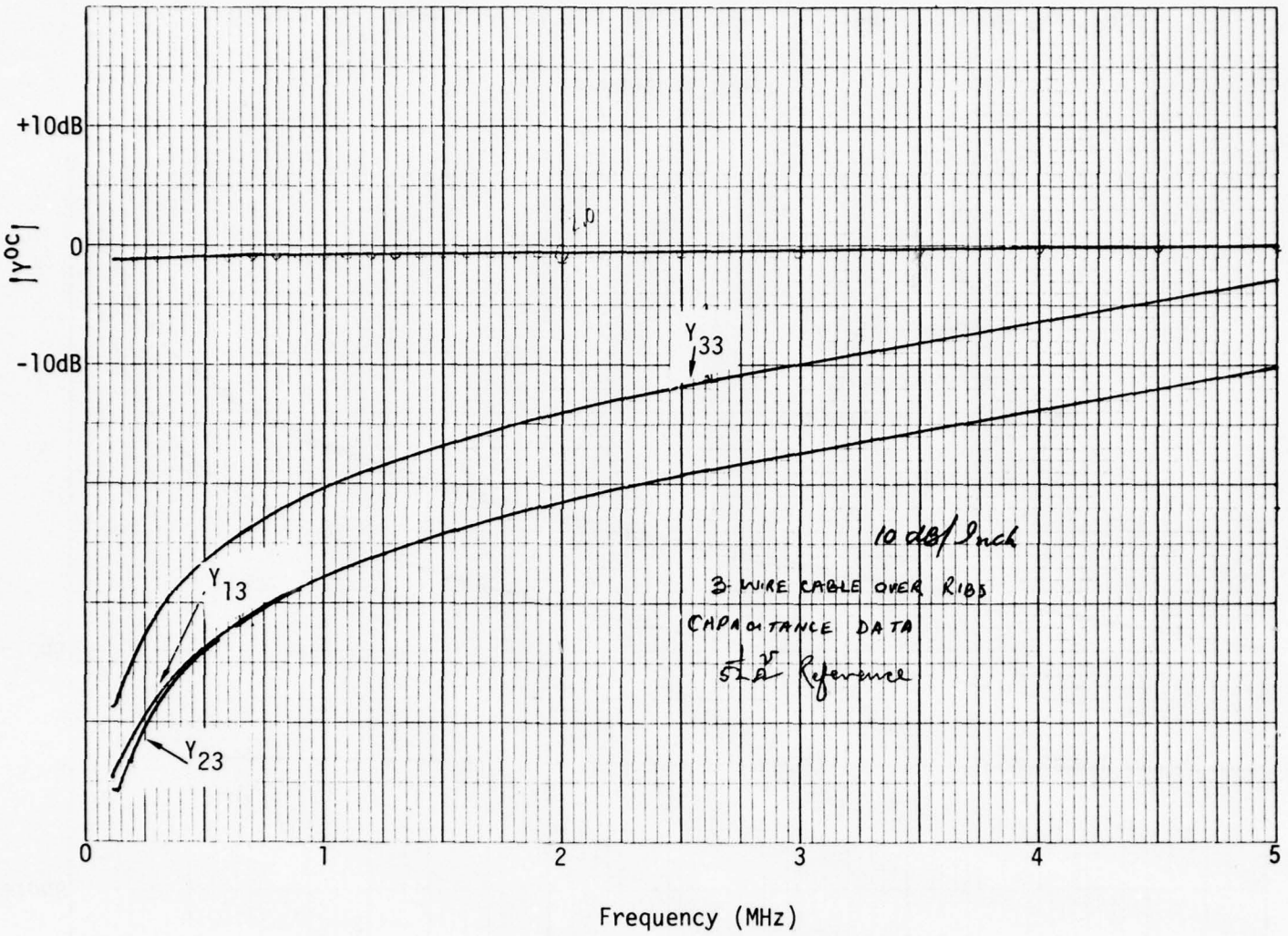

Figure 26. Open Circuit Admittance Data - Three-Wire Line Over Ribs

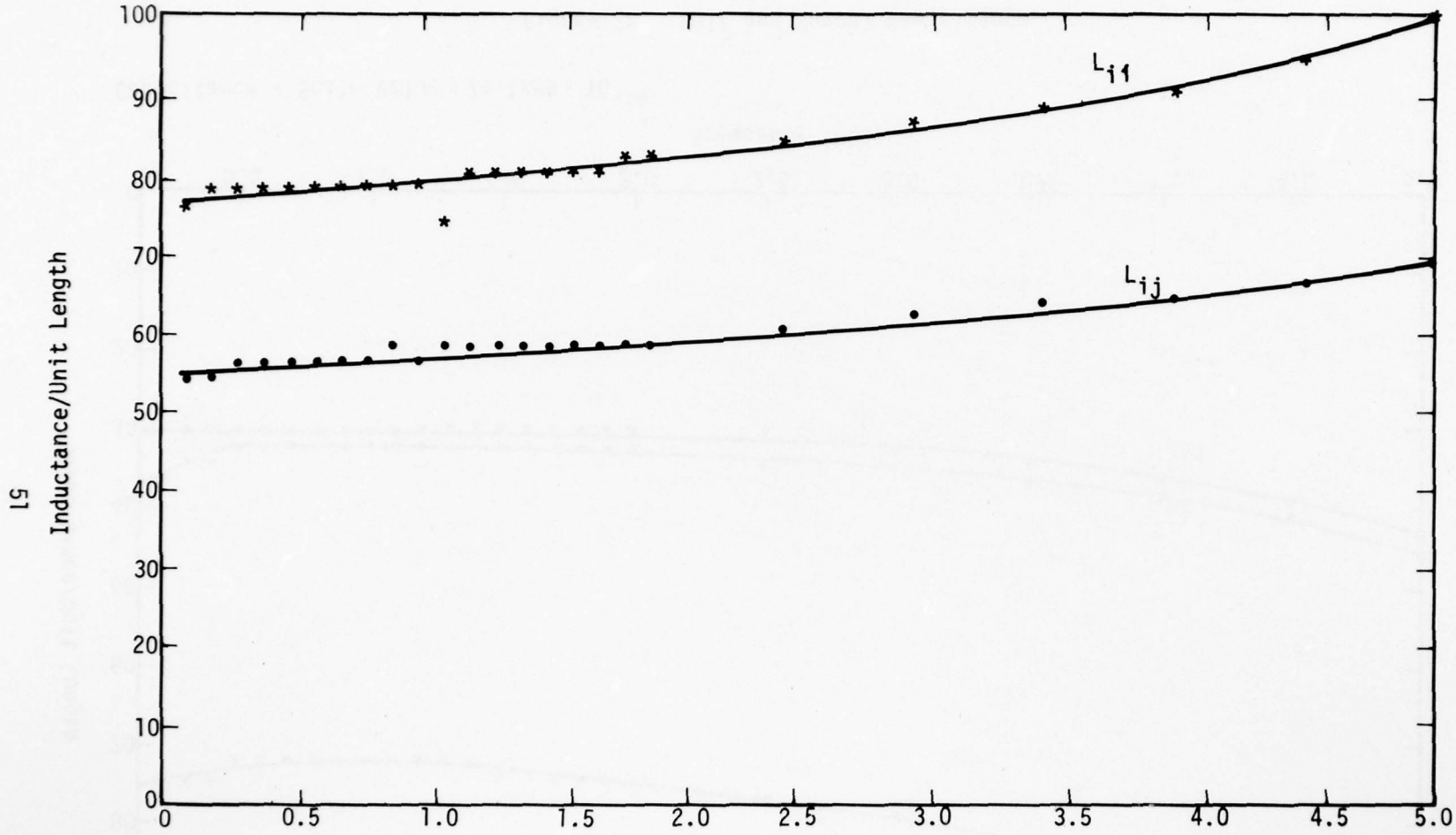

Inductance = Scale Value $\times$ 1.45933×10^{-8} henry

Figure 27. Self and Mutual Inductance (Cable over Rib)

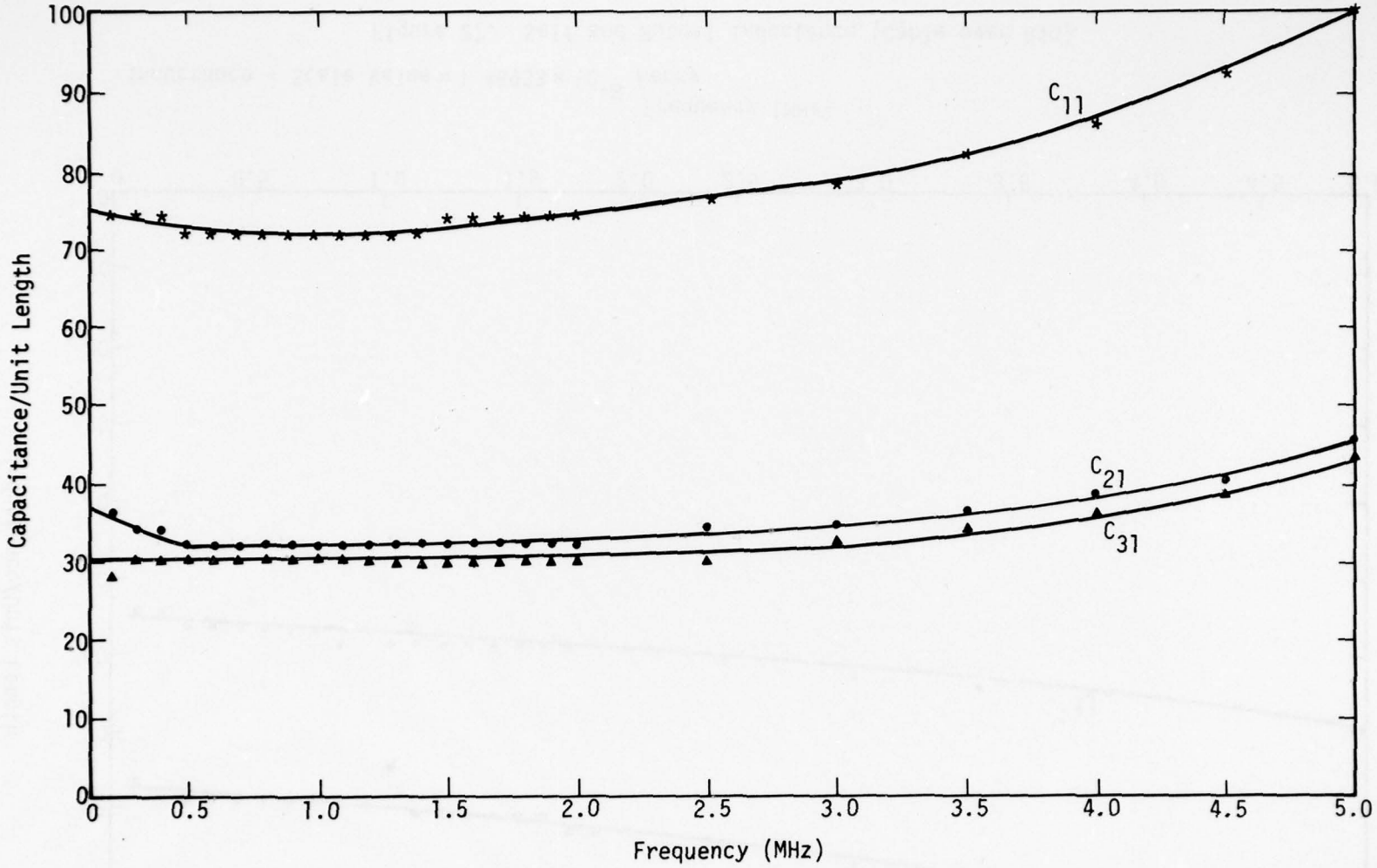

Capacitance - Scale Value $\times 71.1789 \times 10^{-14}$

Figure 28. Self and Mutual Capacitance

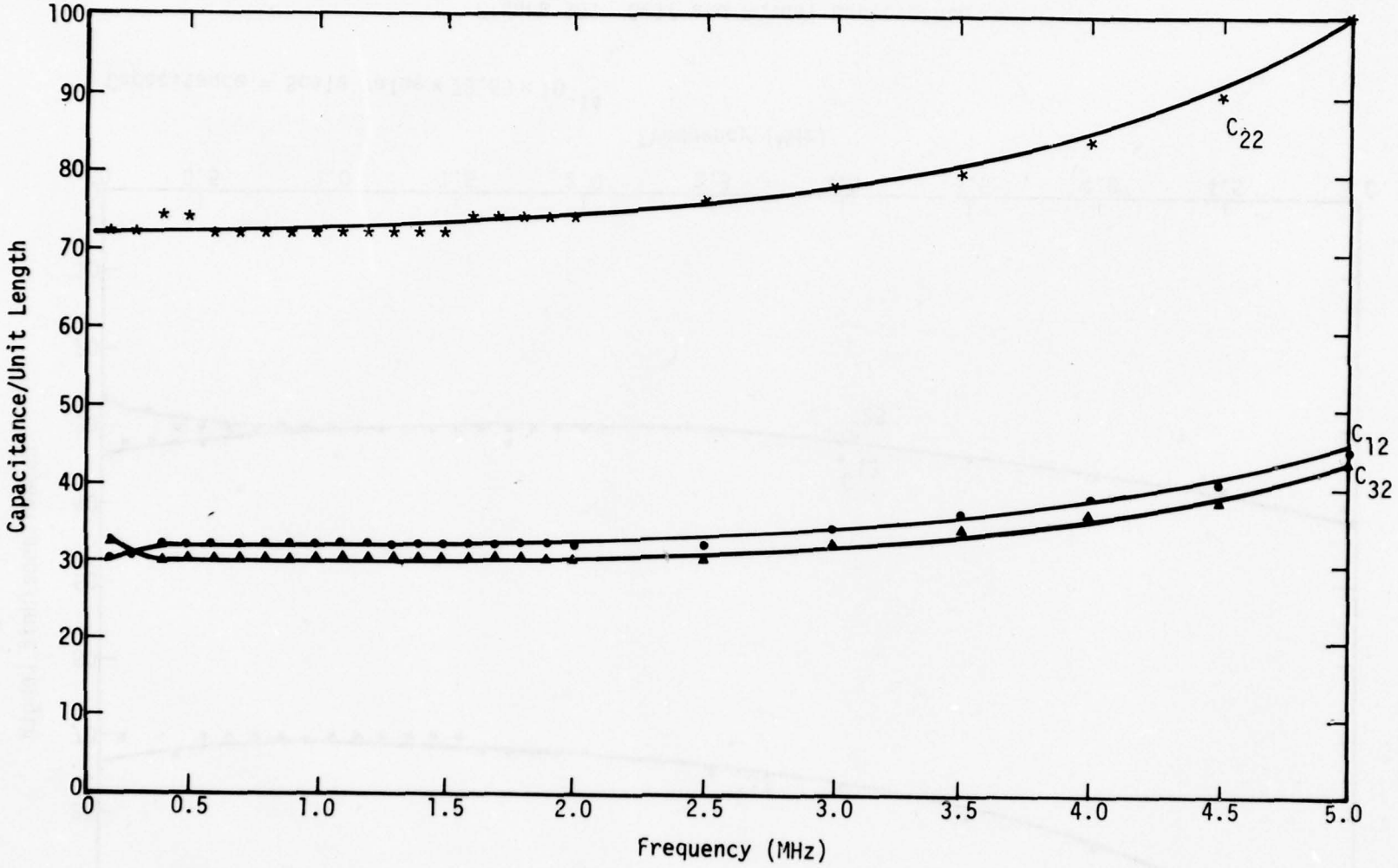

Capacitance = Scale Value $\times 73.198 \times 10^{-14}$

Figure 29. Self and Mutual Capacitance

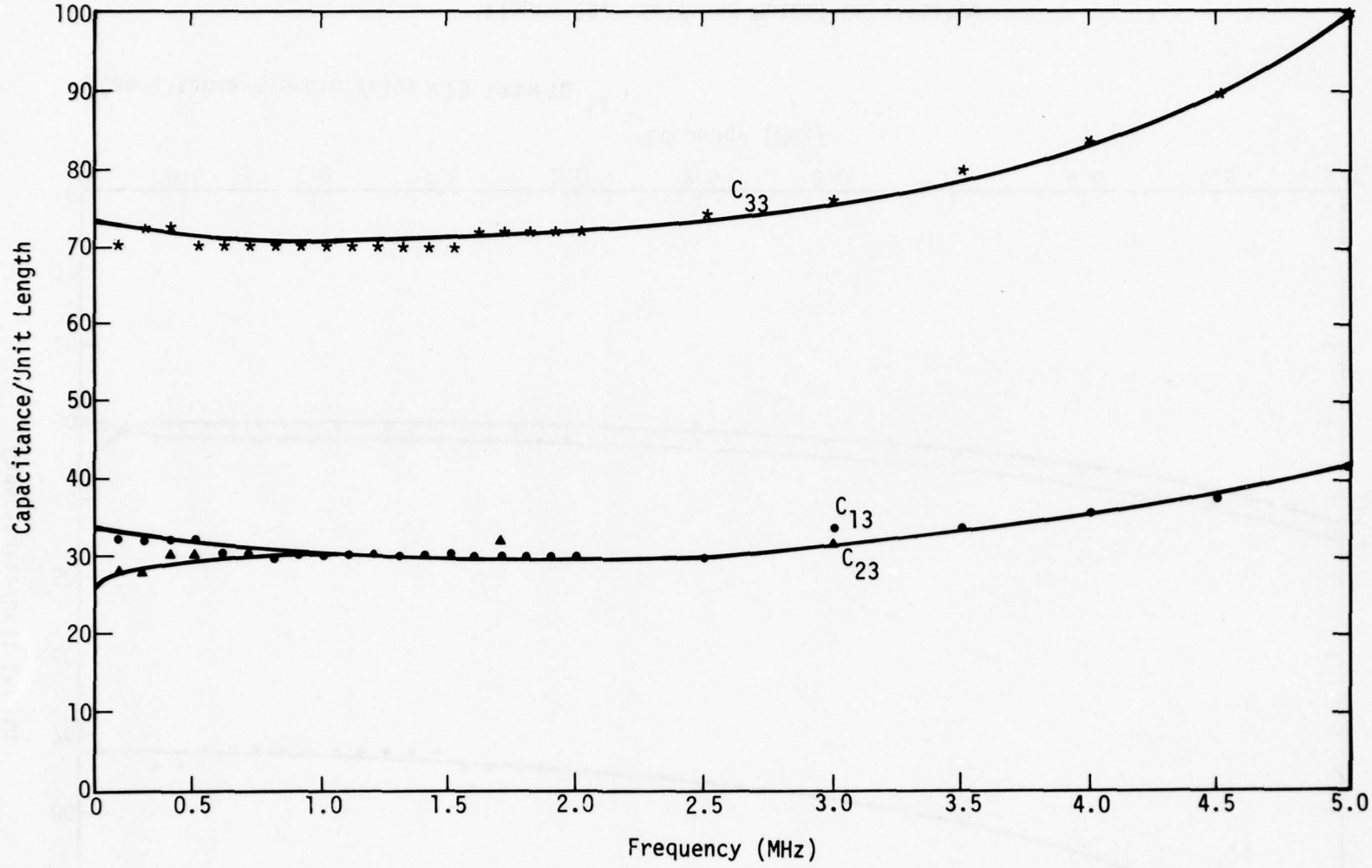

Capacitance = Scale Value $\times 73.63 \times 10^{-14}$

Figure 30. Self and Mutual Capacitance

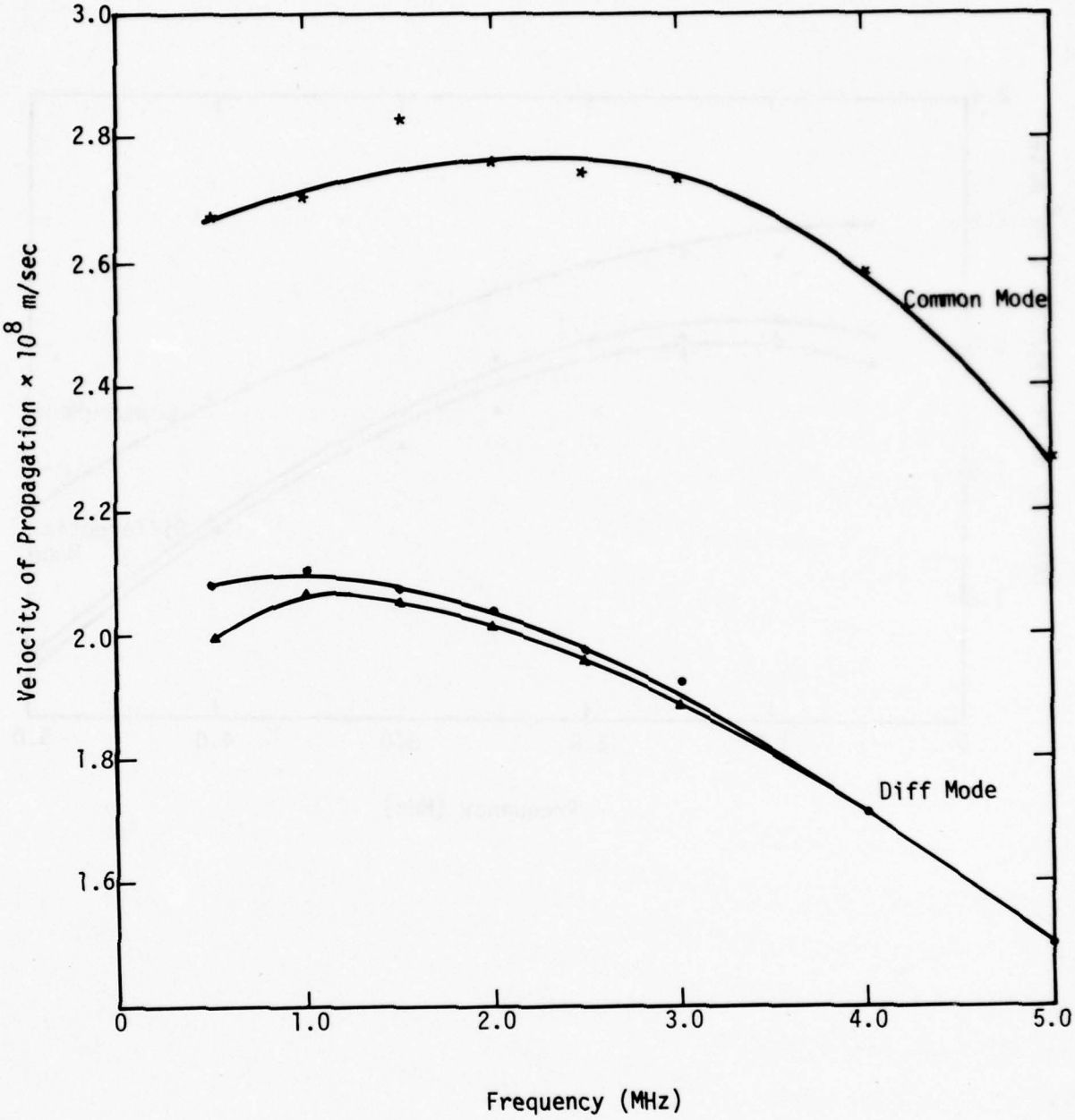

Figure 31a. Velocity of Propagation of Different Modes (Cable without Ribs)

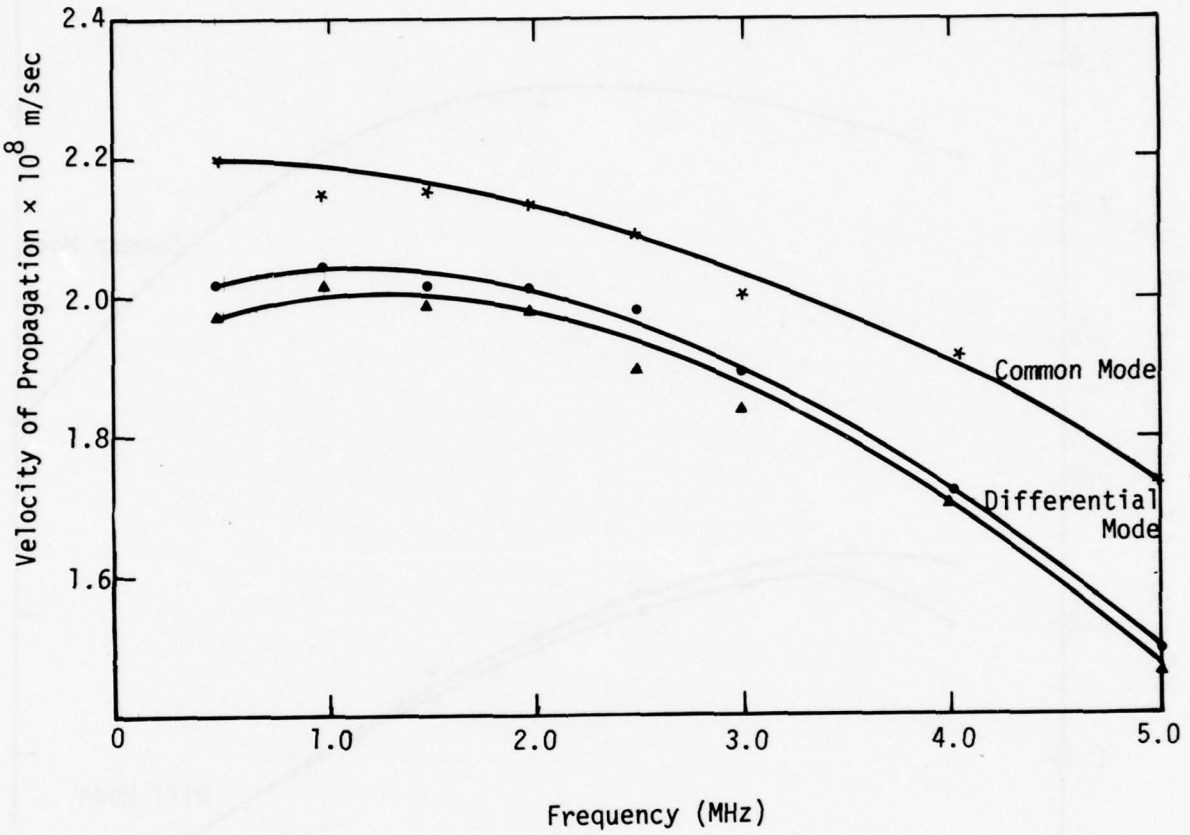

Figure 31b. Velocity of Propagation of Different Modes (Cable over Ribs).

As mentioned earlier, the low-frequency approximation does not seem to hold above 2 MHz and the inductance and capacitance values increase with frequency. This increase in the parameters results in an apparent decrease of propagation velocity for the different modes above 2 MHz.

The following sections discuss the evaluation of the cable parameters at frequencies where the low-frequency approximation is not valid.

2. GENERALIZED ANALYSIS

To obtain the parameters of the multiconductor line at any frequency, the multiconductor transmission-line equations must be used (refs. 6 through 9). In Table 1, some useful formulas are listed, together with corresponding two-wire line equations.

Note that, once the matrices $[Z_{in}^{sc}]$ and $[Y_{in}^{oc}]$ are known, the matrices $[\Gamma]$ and $[Z_o]$ can be determined by equations (3a) and (4a) accordingly. The impedance [Z] and admittance [Y] are then obtained by equations (9a) and (10a). The determination of [L] and [C] follows from equations (6a) and (7a) when [R] and [G] are neglected. Difficulties arise in how to solve the complicated matrix equations (3a) and (4a) for $[\Gamma]$ and $[Z_o]$.

a. Method of Calculations

The calculation can be simplified by using a series of similarity transformations in solving equations (3a) and (4a) of Table 1 for $[\Gamma]$ and $[Z_o]$. This simplification is based on the fact that similar matrices have the same eigenvalues, and that a polynomial matrix function f(A) has eigenvalues $f(\lambda_i)$ when the matrix A has eigenvalues λ_i. A rigorous analysis of the matrix equations is quite complicated (ref.10). Putting aside any discussion of the rigorous justification of the method and assuming it is good in this case, we outline the procedures used in the calculation as follows:

Table 1. LIST OF TRANSMISSION-LINE EQUATIONS

A. N-WIRE LINE		B. TWO-WIRE LINE	
$[Z_{in}^{sc}] = \tanh([\Gamma]\ell)\,[Z_o]$	(1a)	$Z_{in}^{sc} = Z_o \tanh \gamma\ell$	(1b)
$[Y_{in}^{oc}] = [Z_o]^{-1} \tanh([\Gamma]\ell)$	(2a)	$Y_{in}^{oc} = (Z_o)^{-1} \tanh \gamma\ell$	(2b)
$[Z_{in}^{sc}]\,[Y_{in}^{oc}] = [\tanh([\Gamma]\ell)]^2$	(3a)	$Z_{in}^{sc} \cdot Y_{in}^{oc} = \tanh^2 \gamma\ell$	(3b)
$[Z_o] = [\tanh([\Gamma]\ell)]^{-1}[Z_{in}^{sc}]$	(4a)	$Z_o = (\tanh \gamma\ell)^{-1}\, Z_{in}^{sc}$	(4b)
$[Z_o] = ([Y]^{-1}[Z])^{1/2}$	(5a)	$Z_o = (Z/Y)^{1/2}$	(5b)
$[Z] = [R] + j\omega\,[L]$	(6a)	$Z = R + j\omega L$	(6b)
$[Y] = [G] + j\omega\,[C]$	(7a)	$Y = G + j\omega C$	(7b)
$[\Gamma] = ([Z][Y])^{1/2}$	(8a)	$\gamma = (ZY)^{1/2}$	(8b)
$[Z] = [\Gamma][Z_o]$	(9a)	$Z = \gamma Z_o$	(9b)
$[Y] = [Z_o]^{-1}[\Gamma]$	(10a)	$Y = (Z_o)^{-1}\gamma$	(10a)

where,

$[\Gamma]$ is the propagation constant matrix

$[Z_o]$ is the characteristic impedance matrix

$[Z]$ is the series impedance-per-unit-length matrix

$[Y]$ is the shunt admittance-per-unit-length matrix

$[Z_{in}^{sc}]$ is the input impedance matrix for short circuit

$[Y_{in}^{oc}]$ is the input admittance matrix for open circuit.

All matrices are of dimension n×n, where n is the number of wires, excluding the reference wire.

A. Calculate the $[\Gamma]$ matrix using equation (3a)

(1) find $[A] = [Z_{in}^{sc}][Y_{in}^{oc}]$

(2) find the eigenvalues of $[A]$, say $\lambda_1, \lambda_2, \lambda_3$

(3) find the eigenvalues of $[\Gamma]$, namely $\gamma_1, \gamma_2, \gamma_3$, from

$$\begin{bmatrix} \lambda_1 & 0 & 0 \\ 0 & \lambda_2 & 0 \\ 0 & 0 & \lambda_3 \end{bmatrix} = \begin{bmatrix} \tanh^2(\gamma_1 \ell) & 0 & 0 \\ 0 & \tanh^2(\gamma_2 \ell) & 0 \\ 0 & 0 & \tanh^2(\gamma_3 \ell) \end{bmatrix}$$

(4) find the eigen vector matrix $[X]$ of $[A]$

(5) from $[X]$ and its inverse $[X]^{-1}$, find $[\Gamma] = [X][\gamma][X]^{-1}$ where $[\gamma]$ is a diagonal matrix whose elements are γ_1, γ_2 and γ_3.

B. Calculate the Z_o matrix using equation (4a)

(1) find the diagonal matrix D, where

$$D = \begin{bmatrix} \tanh \gamma_1 \ell & 0 & 0 \\ 0 & \tanh \gamma_2 \ell & 0 \\ 0 & 0 & \tanh \gamma_3 \ell \end{bmatrix}$$

(2) find the matrix $\tanh([\Gamma]\ell)$ by $\tanh([\Gamma]\ell) - [X]D[x]^{-1}$ where $[X]$ and $[X]^{-1}$ are the same eigen vector matrices as given in procedure A(5).

(3) Find the inverse $[\tanh([\Gamma]\ell)]^{-1}$

(4) use equation (4a) to find $[Z_o]$, $[Z_o] = [\tanh([\Gamma]\ell)]^{-1}[Z_{in}^{sc}]$

C. Calculate the series impedance matrix [Z] using equation (9a)

D. Calculate the shunt admittance matrix [Y] using equation (10a)

E. Calculate [L] using equation (6a) assuming [R] = 0

F. Calculate [C] using equation (7a) assuming [G] = 0.

b. Results and Conclusions

Figures 32 and 33 show typical self and mutual inductances and capacitances as a function of frequency, which were calculated using N-wire transmission line equations and the procedures outlined above. It is clear that the parameters obtained in this method are fairly constant, whereas the values obtained from the low-frequency approximation increase with frequency. In figure 34, the propagation velocities obtained from the eigenvalues of [Γ] are shown for common and differential modes. Again, the values calculated using the new method are quite constant, as compared to the low-frequency approximations.

The velocities of the differential modes are smaller than the common mode. An equivalent dielectric constant with a value near 2.2 would give the approximate differential velocities. It is interesting to see that this is roughly the same as the dielectric constant of the insulator for the Teledyne wire. The common mode velocity is only about 7% less than that of the velocity of light, indicating that the insulator has less effect on the common mode velocity.

The validity and the accuracy of this new technique are clearly indicated on these figures. It is concluded that using this technique, the multiconductor transmission-line parameters can be obtained quite easily from the simple input impedance measurements.

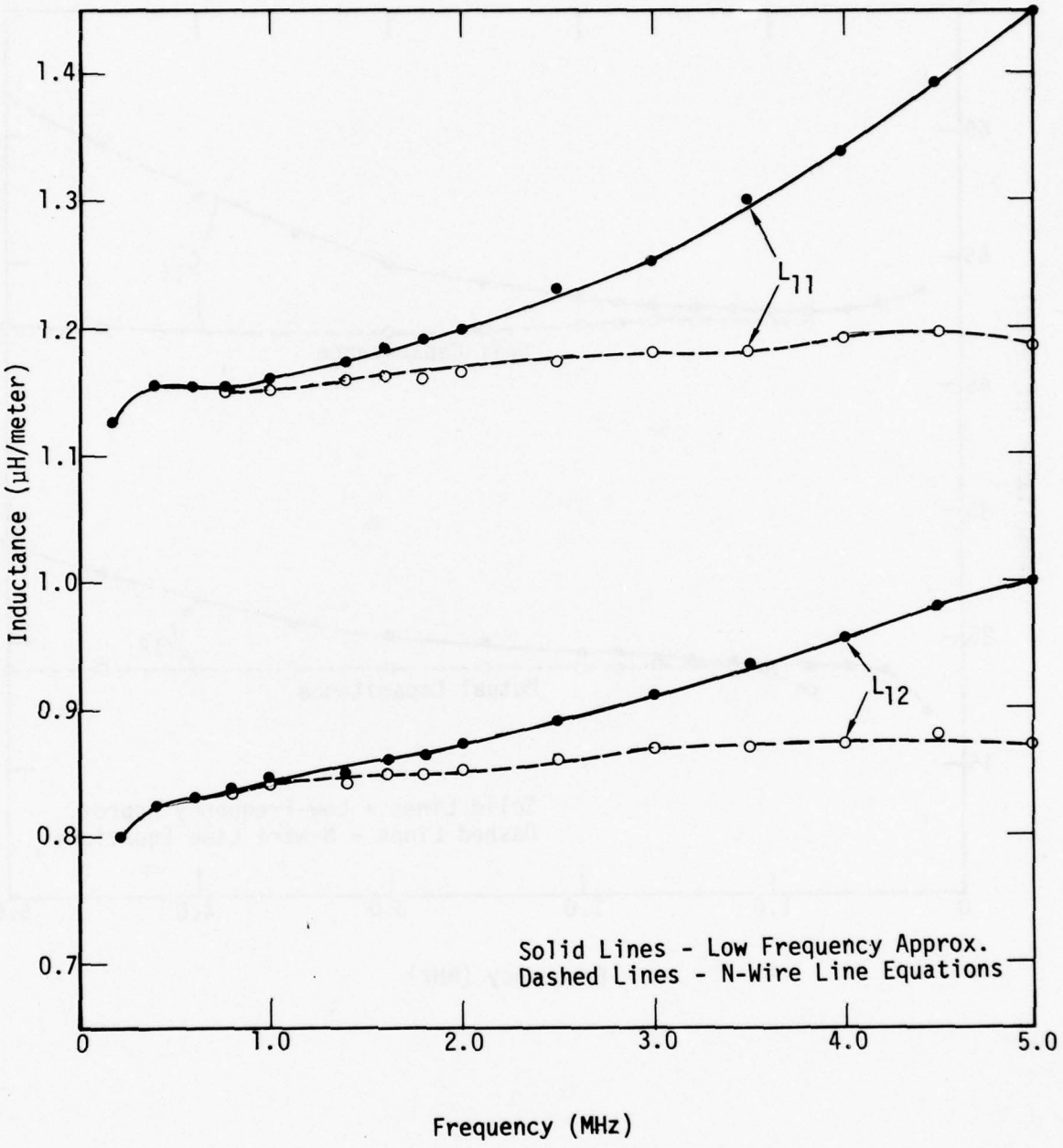

Figure 32. Typical Self and Mutual Inductance as a Function of Frequency

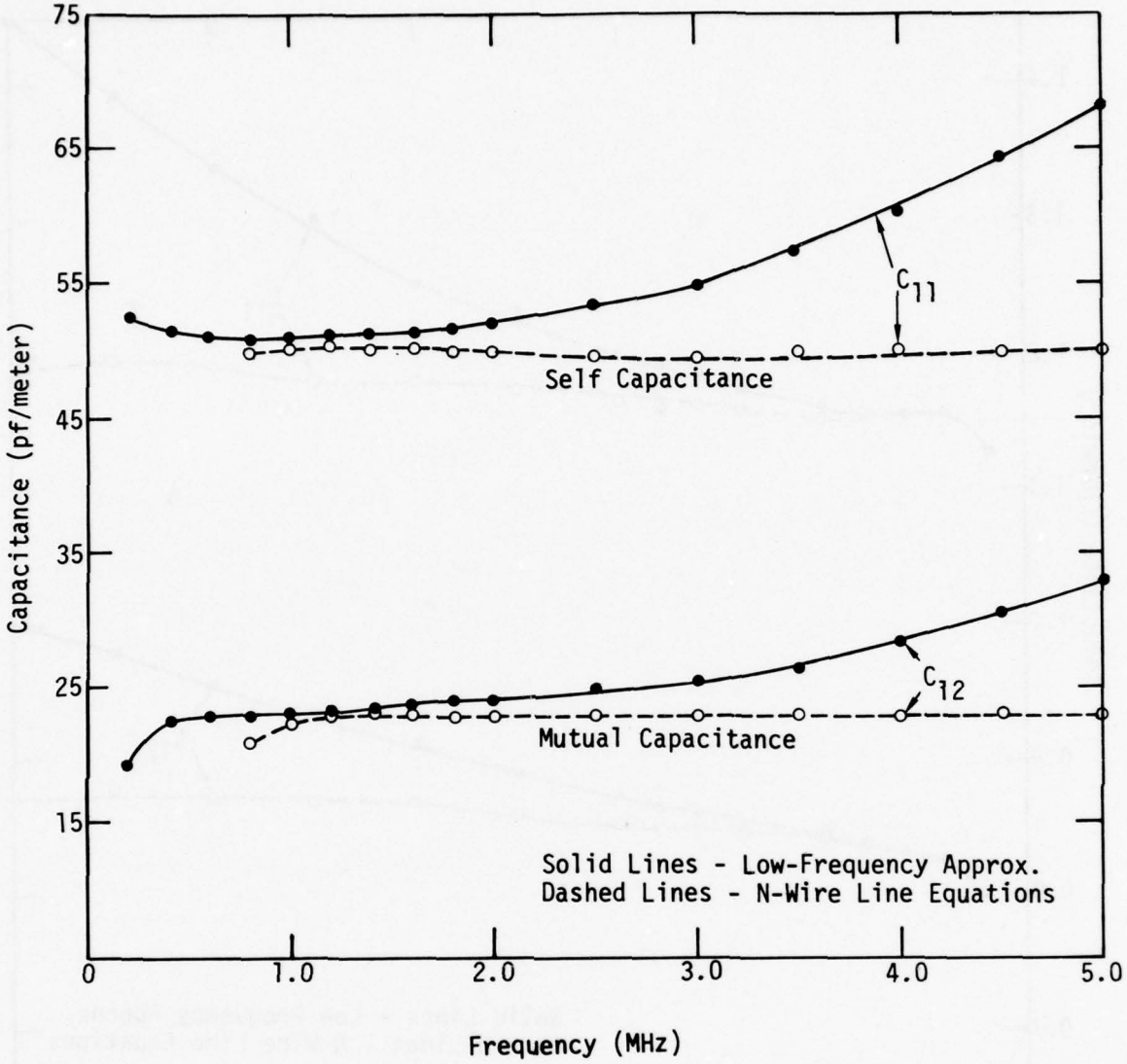

Figure 33. Typical Self and Mutual Capacitance as a Function of Frequency

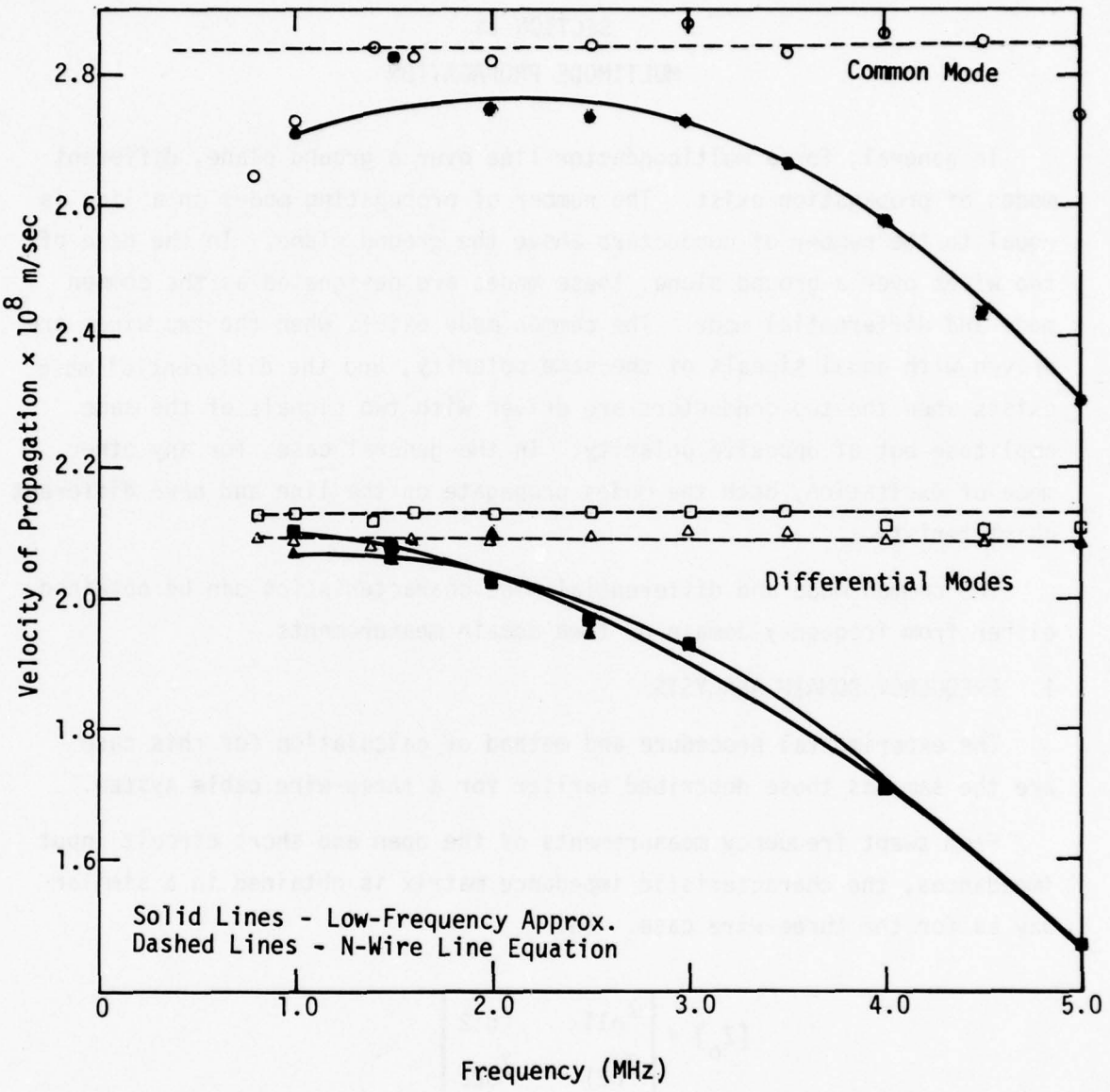

Figure 34. The Propagation Velocities for Different Modes

SECTION IV

MULTIMODE PROPAGATION

In general, for a multiconductor line over a ground plane, different modes of propagation exist. The number of propagating modes on a line is equal to the number of conductors above the ground plane. In the case of two wires over a ground plane, these modes are designated as the common mode and differential mode. The common mode exists when the two wires are driven with equal signals of the same polarity, and the differential mode exists when the two conductors are driven with two signals of the same amplitude but of opposite polarity. In the general case, for any other mode of excitation, both the modes propagate on the line and have different characteristics.

The common mode and differential mode characteristics can be obtained either from frequency domain or time domain measurements.

1. FREQUENCY DOMAIN ANALYSIS

The experimental procedure and method of calculation for this case are the same as those described earlier for a three-wire cable system.

From swept frequency measurements of the open and short circuit input impedances, the characteristic impedance matrix is obtained in a similar way as for the three-wire case. Let

$$[Z_o] = \begin{bmatrix} Z_{o11} & Z_{o12} \\ Z_{o21} & Z_{o22} \end{bmatrix}$$

and

$$[Y_o] = \begin{bmatrix} Y_{o11} & Y_{o12} \\ Y_{o21} & Y_{o22} \end{bmatrix}$$

be the characteristic impedance and admittance matrices.

For waves in the forward direction only, we have

$$[I] = [Y_o][V]$$
$$[V] = [Z_o][I] \tag{62}$$

For a two-wire line over a ground plane these equations reduce to

$$I_1 = Y_{o11}V_1 + Y_{o12}V_2$$
$$I_2 = Y_{o21}V_1 + Y_{o22}V_2 \tag{63}$$

and

$$V_1 = Z_{o11}I_1 + Z_{o12}I_2$$
$$V_2 = Z_{o21}I_1 + Z_{o22}I_2 \tag{64}$$

In the common mode the two conductors are driven by two sources of the same magnitude and phase or, in other words, the two conductors are connected in parallel to one terminal of the source, the other source terminal going to ground.

In that case we have $V_2 = V_1$, and equation (63) yields

$$I_1 = (Y_{o11} + Y_{o12})V_1$$
$$I_2 = (Y_{o21} + Y_{o22})V_1 \tag{65}$$

The common mode characteristic admittance is

$$Y_{oc} = \frac{I_1 + I_2}{V_1} = Y_{o11} + Y_{o22} + 2Y_{o12} \tag{66}$$

and the common mode characteristic impedance is

$$Z_{oc} = \frac{Z_{o11}Z_{o22} - Z_{o12}^2}{Z_{o11} + Z_{o22} - 2Z_{12}} \tag{67}$$

In the differential mode, a two-terminal source is connected between the two line conductors, with no conducting connection to ground. The conductors assume potentials determined by the continuity condition $I_2 + I_1 = 0$. Equation (64) yields

$$\begin{aligned} V_1 &= (Z_{o11} - Z_{o12})\, I_1 \\ V_2 &= (Z_{o21} - Z_{o22})\, I_1 \end{aligned} \tag{68}$$

The differential mode characteristic impedance is

$$Z_{OD} = \frac{V_1 - V_2}{I_1} = Z_{o11} + Z_{o22} - 2Z_{o12} \tag{69}$$

The circuit parameters of each transmission mode can also be obtained directly from the equivalent circuits representing the characteristic impedance or admittance matrix.

Two equivalent circuits are shown in figure 35, a and b.

For the common mode case, from figure 36 a, the reference voltage V_a is applied between ground and the terminals (figure 36a) which are connected together. Then

$$\begin{aligned} Z_{oc} &= \left\{(Z_{11} - Z_{12}) \,\|\, (Z_{22} - Z_{12})\right\} + Z_{12} \\ Z_{oc} &= \frac{Z_{o11}Z_{o22} - Z_{o12}}{Z_{o11} + Z_{o22} - 2Z_{o12}} \end{aligned} \tag{70}$$

For the differential mode, we may assume that the reference mode voltage, V_b, is applied between the terminals 1 and 2 in balance; that is, no current

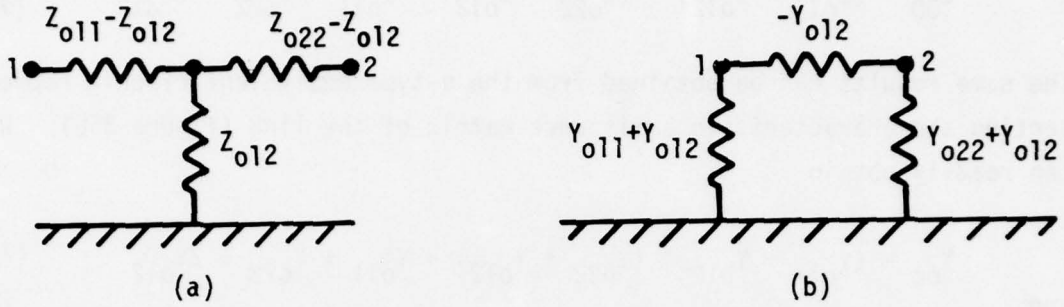

Figure 35. Two-Wire Line Equivalent Circuits

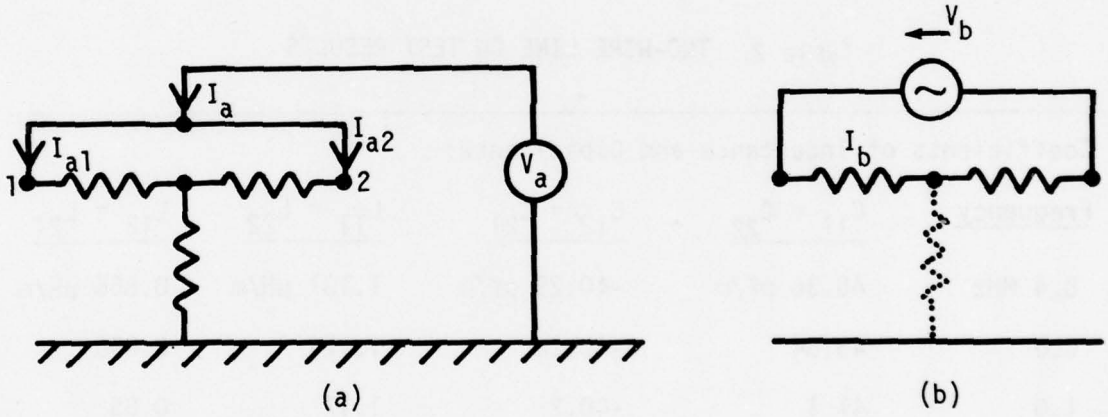

Figure 36. Common Mode (a) and Differential Mode (b) Input Circuits

flows through the impedance Z_{o12}. Consequently the differential mode characteristic impedance is given as

$$Z_{OD} = (Z_{o11} - Z_{o12}) + (Z_{o22} - Z_{o12}) = Z_{o11} + Z_{o22} - 2Z_{o12} \qquad (71)$$

The same results can be obtained from the π-type equivalent circuit representing the characteristic admittance matrix of the line (figure 35b). We can readily obtain

$$Y_{oc} = (Y_{o11} + Y_{o12}) \| (Y_{o22} + Y_{o12}) = Y_{o11} + Y_{o22} + 2Y_{o12} \qquad (72)$$

and

$$Y_{OD} = (-Y_{o12}) \| \{(Y_{o11} + Y_{o12}) + (Y_{o22} + Y_{o12})\} = \frac{Y_{o11}Y_{o22} - Y_{o12}^2}{Y_{o11} + Y_{o22} + 2Y_{o12}} \qquad (73)$$

Figures 37 and 38 show the measured short and open circuit data for the cable geometry of figure 39. From these measurements, the inductance and capacitance matrices are obtained using the technique discussed for a three-wire case. Some of these results are shown in Table 2.

Table 2. TWO-WIRE LINE CW TEST RESULTS

Coefficients of Inductance and Capacitance:

Frequency	$C_{11} = C_{22}$	$C_{12} = C_{21}$	$L_{11} = L_{22}$	$L_{12} = L_{21}$
0.4 MHz	46.36 pF/m	-40.29 pF/m	1.187 μH/m	0.866 μH/m
0.6	46.54	-40.18	1.174	0.856
1.0	47.1	-40.2	1.17	0.85

Impedance and Propagation Velocity:

Frequency	Z_{OC}	Z_{OD}	v_C	v_D
0.4 MHz	290.8 ohms	121.7 ohms	0.943c	0.636c
0.6	282.6	120.7	0.927c	0.637c
1.0	280.5	121.2	0.910c	0.632c

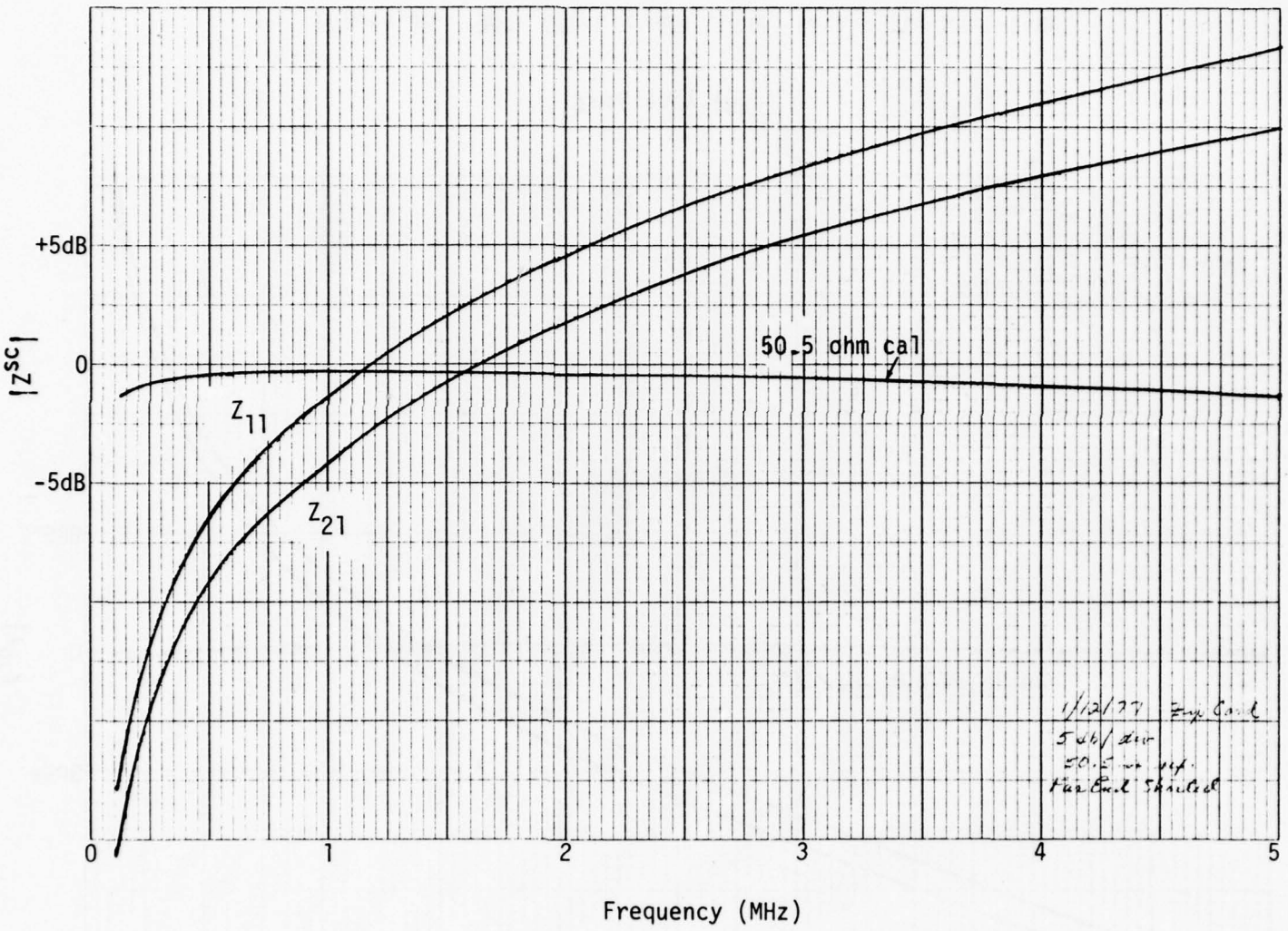

Figure 37. Short Circuit Impedance Data - Two-Wire Line

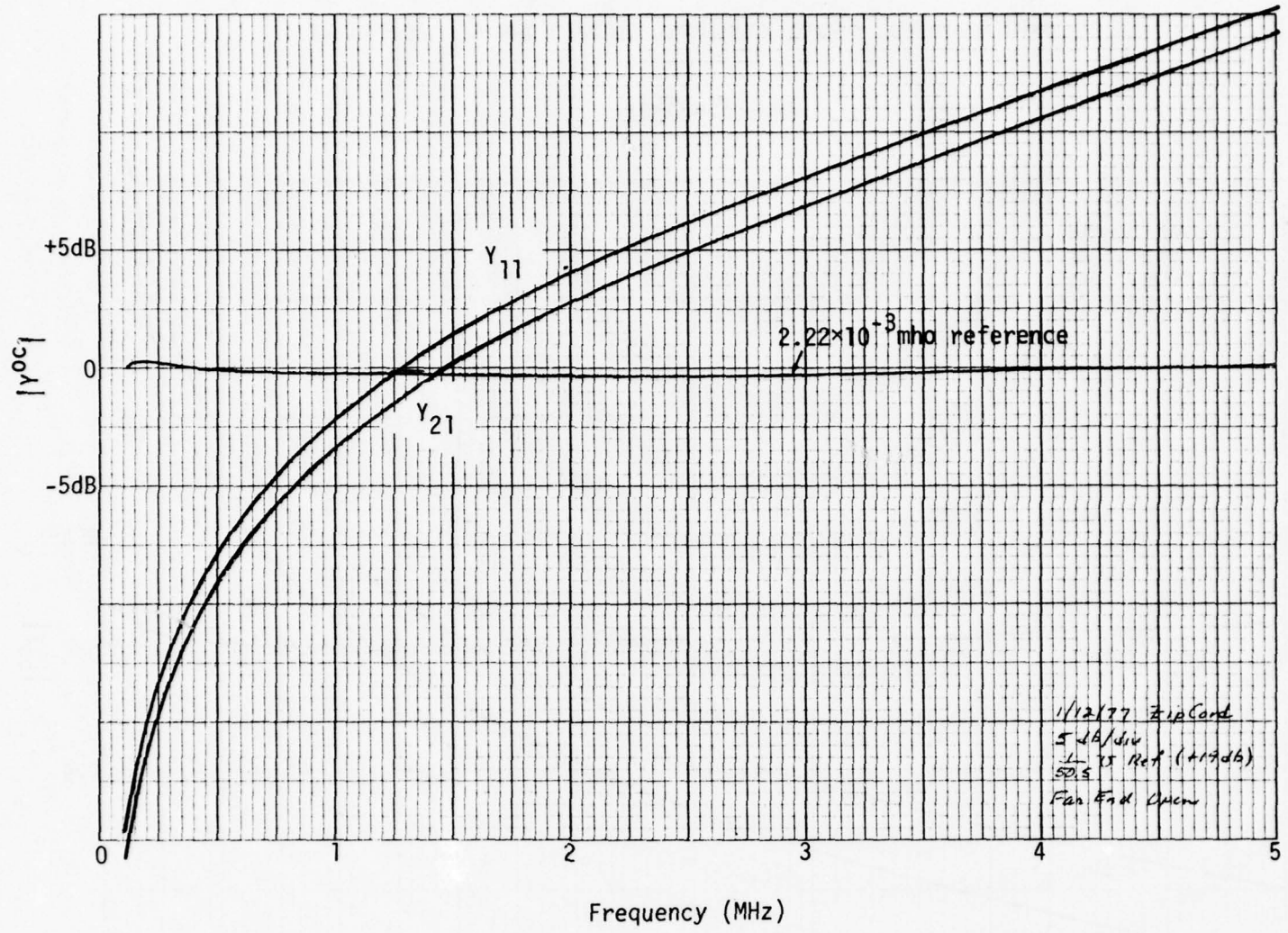

Figure 38. Open Circuit Admittance Data - Two-Wire Line

2. TIME DOMAIN ANALYSIS

Time domain measurements of the cable characteristics were performed using pulse tracing techniques and with time domain reflectometry. The two-wire line test setup is shown in figure 39.

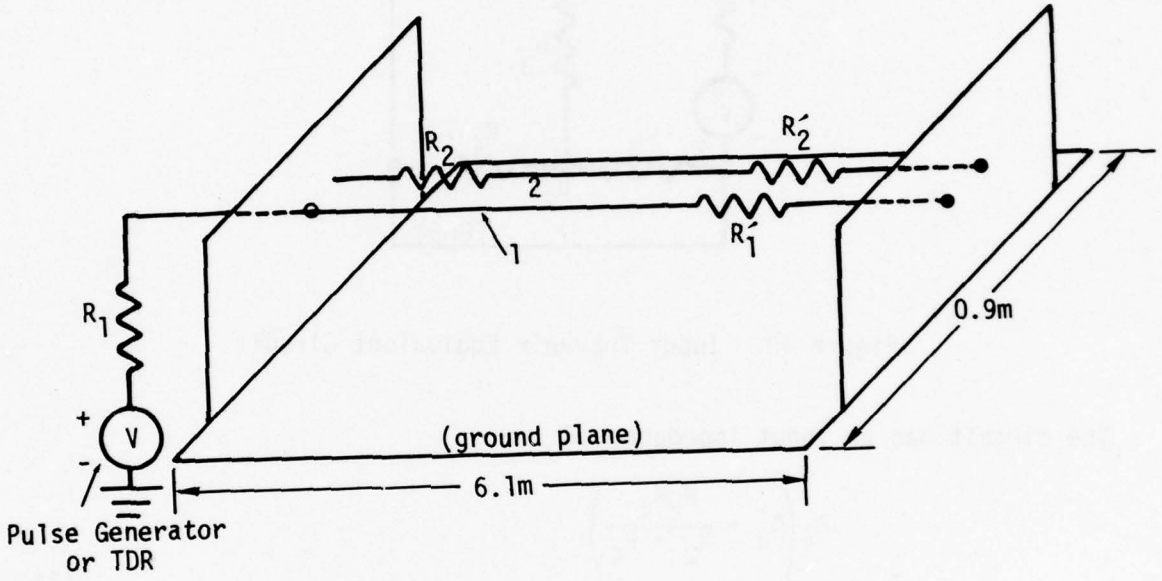

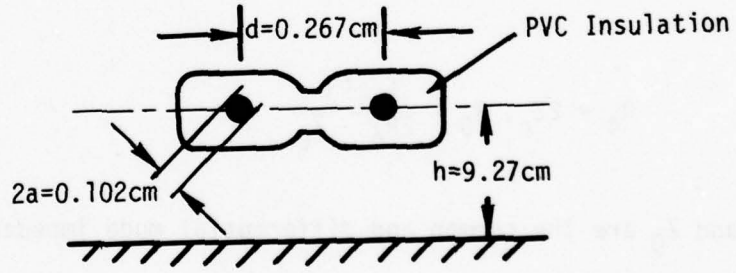

Figure 39. Two-Wire Line Geometry

The input impedance seen by the generator can be derived from the input Thevenin equivalent circuit which is shown in figure 40.

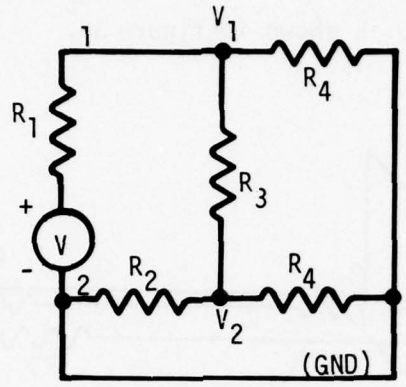

Figure 40. Input Thevenin Equivalent Circuit

The circuit has an input impedance of

$$Z_i = \frac{R_4\left(R_3 + \frac{R_2R_4}{R_2 + R_4}\right)}{R_3 + R_4 + \frac{R_2R_4}{R_2 + R_4}} \tag{74}$$

where

$$R_4 = 2Z_c,\ R_3 = \frac{2R_4Z_D}{2R_4 - Z_D} \tag{75}$$

and Z_c and Z_D are the common and differential mode impedances respectively.

TDR measurements with $R_2 = 0$, $R_2 = \infty$, and with wire no. 2 directly connected to wire no. 1 (common mode) were performed in order to evaluate the common mode and differential mode impedances. For $R_2 = 0, \infty$, the input impedance equation reduces to

$$Z_i(0) = \frac{R_3 R_4}{R_3 + R_4} \quad , \quad Z_i(\infty) = \frac{R_4(R_3 + R_4)}{R_3 + 2R_4} \tag{76}$$

These two equations can be solved for R_4 and R_3 to give the relationships

$$R_4 = Z_i(\infty)\left[1 + \sqrt{1 - \frac{Z_i(0)}{Z_i(\infty)}}\right]$$
$$R_3 = \frac{R_4 Z_i(0)}{R_4 - Z_i(0)} \tag{77}$$

in terms of the measured values of $Z_i(0)$ and $Z_i(\infty)$. The common and differential mode impedances Z_c and Z_D can then be evaluated since

$$Z_c = R_4/2, \quad Z_D = \frac{2R_3 R_4}{2R_4 + R_3} \tag{78}$$

The measurement with wire no. 2 directly connected to wire no. 1 gives the common mode impedance directly.

TDR records for the three cases discussed are shown in figure 41. These records give Z_D = 120 ohms, Z_c = 282 ohms ($R_2 = \infty$), Z_c = 284 ohms (common mode direct) for the two-wire line, in good agreement with the swept frequency results listed in Table 2.

An analysis of the errors in the common and differential mode impedances due to a ±3% error in the reflection coefficient measured with the TDR system was also carried out. The errors are proportional to the impedance levels and it was found that the differential mode impedance was accurate to ±4% for the worst case, while the common mode impedance determined from measurements with $R_2 = \infty$ or by direct measurement was accurate to within 10%.

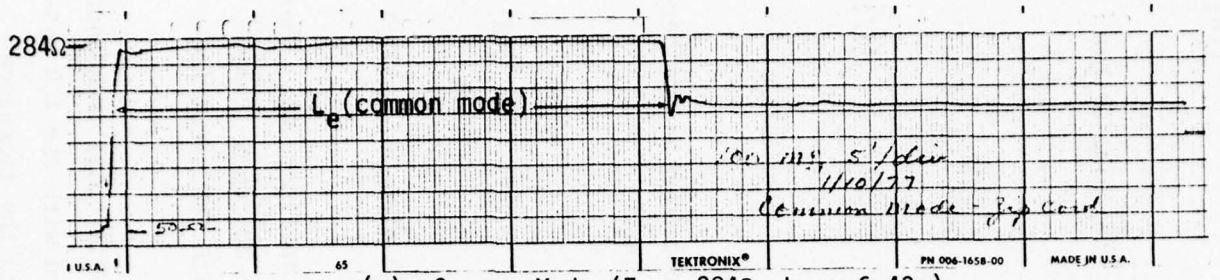

(a) Common Mode (Z_o = 284Ω, L_e = 6.43m)

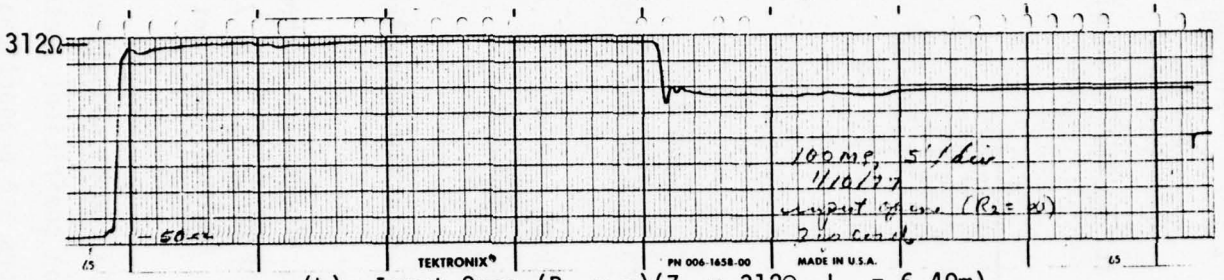

(b) Input Open (R_2 = ∞)(Z_o = 312Ω, L_e = 6.40m)

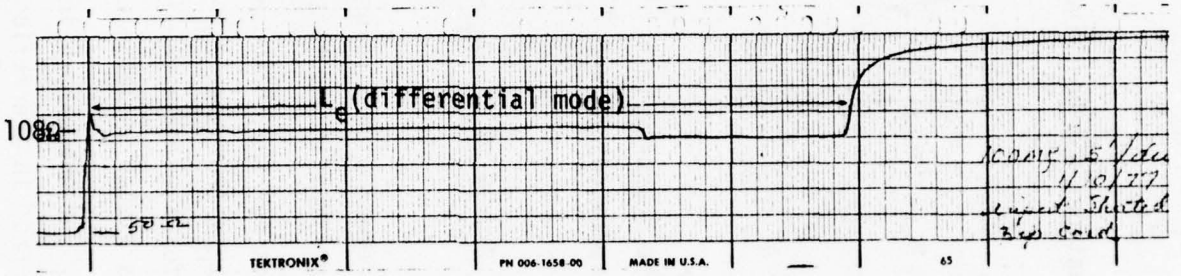

(c) Input Shorted (R_2 = 0)(Z_o = 108Ω, L_e = 9.0m)

Figure 41. Two-Wire Line TDR Records

The TDR records gave a direct measurement of the electrical length of the line for each mode from which the mode propagation velocities and effective dielectric constants could be determined from the relationship

$$L/L_e = v_p/c = 1/\sqrt{\varepsilon'} \tag{79}$$

For the common mode the dielectric is primarily air and the effective dielectric constant would be expected to be close to 1. The insulation between the wires affects the differential mode, and for this case the effective dielectric constant would be expected to approach that of the insulating material. The measured values were found to be 1.12 and 2.34 for the common and differential modes respectively compared with values of 1.0 and approximately 2.8 for air and solid PVC insulation.

Handbook formulas for Z_c and Z_D were evaluated for comparison with the experimentally determined values using the effective dielectric constants of 1.12 and 2.34 for the common and differential modes. The formulas are (ref. 11):

$$Z_c = \frac{60}{\sqrt{\varepsilon'}} \ell n \frac{2h}{\sqrt{ad}} \qquad \textit{(common mode)} \tag{80}$$

$$Z_D = \frac{120}{\sqrt{\varepsilon''}} \ell n \left[\frac{d}{2a} + \sqrt{\left(\frac{d}{2a}\right)^2 - 1} \right] \qquad \text{(differential mode)} \tag{81}$$

In the above formulas, d is the spacing between wire centers, h is the cable height above the ground plane, and a is the wire radius. These formulas evaluate to Z_c = 287 ohms, Z_D = 126 ohms, which are in good agreement with the experimentally determined values.

Table 3 summarizes the test results for the two-wire line.

Table 3. TWO-WIRE LINE PARAMETERS

	Z_c	Z_d	ε' (Common)	ε'' (Differential)
calculated	287 ohms	126 ohms	--	--
TDR	284	120	1.12	2.34
cw	283	121	1.16	2.49

Thevenin equivalent circuits for the common and differential modes were investigated using pulse tracing techniques. This method utilized a pulse generator to drive the cable with both short duration (2ns width) and long duration (40ns width) pulses which were recorded at the input and output ends of the cable with high impedance voltage probes and a Tektronix 485 scope. The long duration pulse width exceeded the round trip travel time on the line and was thus equivalent to the step function response. Various input resistors (R_2 of figure 39) in the 50 to 60 ohm range and load resistors (R_1' and R_2' of figure 39) in the 150 to 300 ohm range were utilized in the tests.

The Thevenin equivalent circuits for the two modes of propagation are shown in figures 42a and 42b.

A typical set of input data for the short duration pulse is presented in figure 43. The corresponding output pulses are shown in figure 44. The recordings of the algebraic sum and difference of the pulses on wires 1 and 2 show twice the common mode (sum) and the differential mode (difference) voltages directly.

Similar data for the long duration pulse are presented in figures 45 and 46.

A summary of computed and measured voltage levels is listed in Table 4.

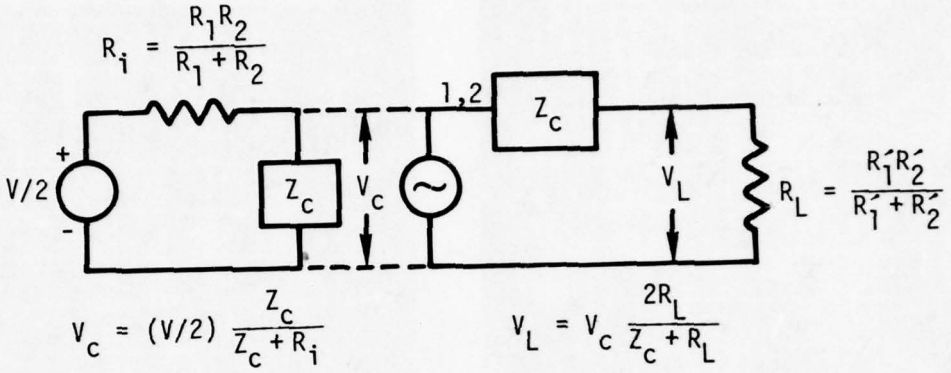

(a) Common Mode Equivalent Circuit

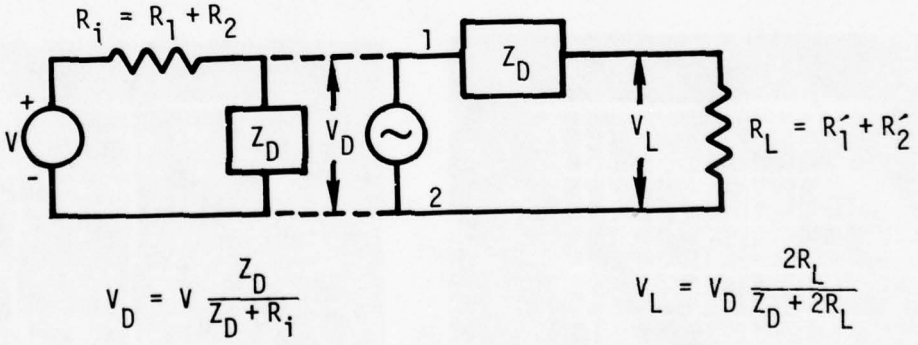

(b) Differential Mode Equivalent Circuit

Figure 42. Thevenin Equivalent Circuits for the Two Modes of Propagation

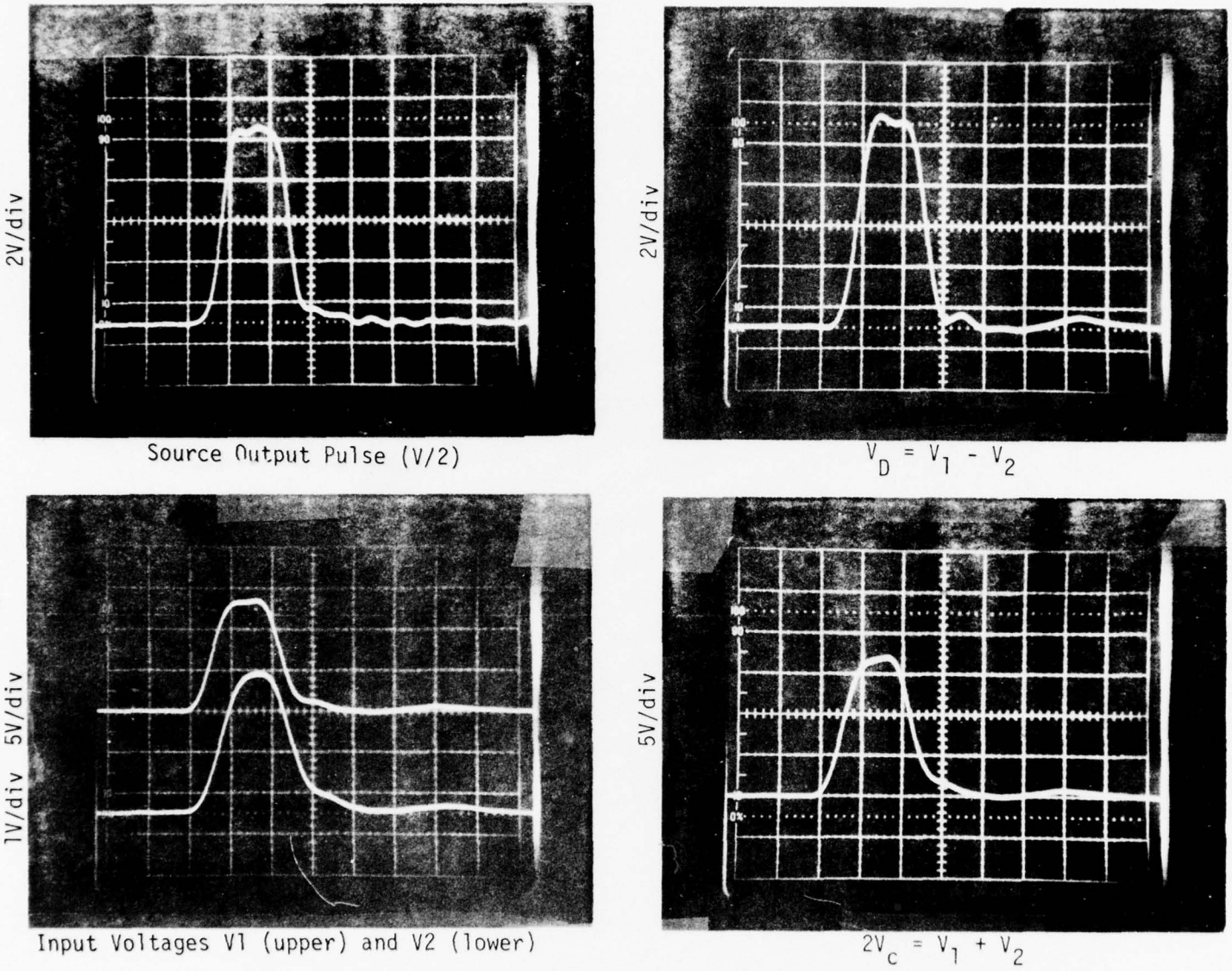

Figure 43. Two-Wire Line Input Data - Short Duration Pulse (2 ns/div)

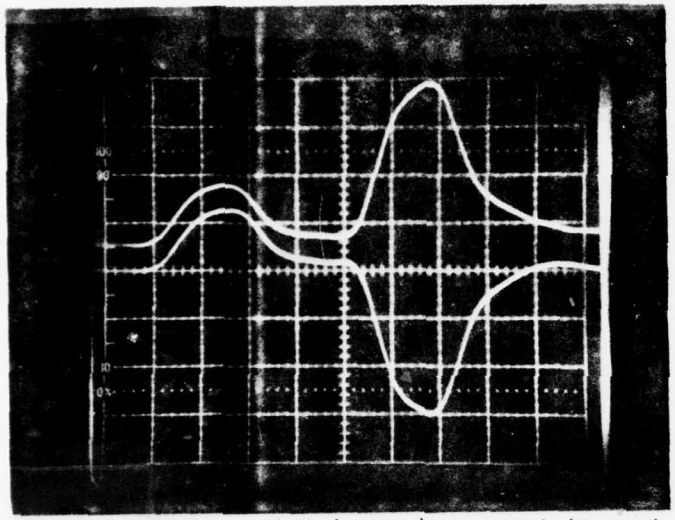

Load Voltages at R1′ (upper) and R2′ (lower)

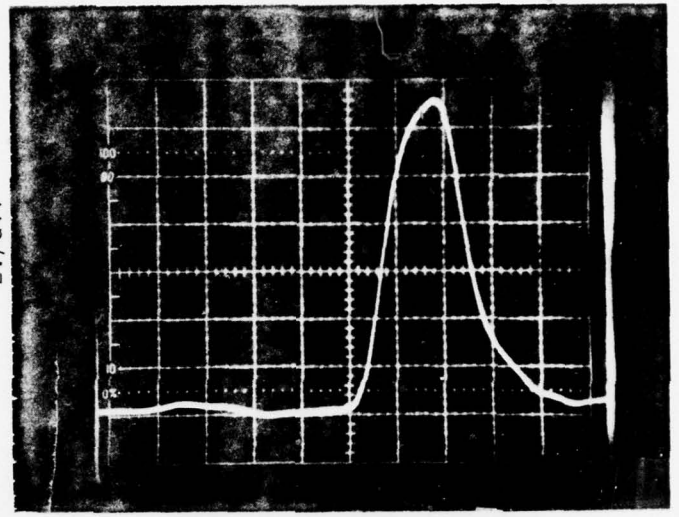

Difference Waveform (Differential Mode)

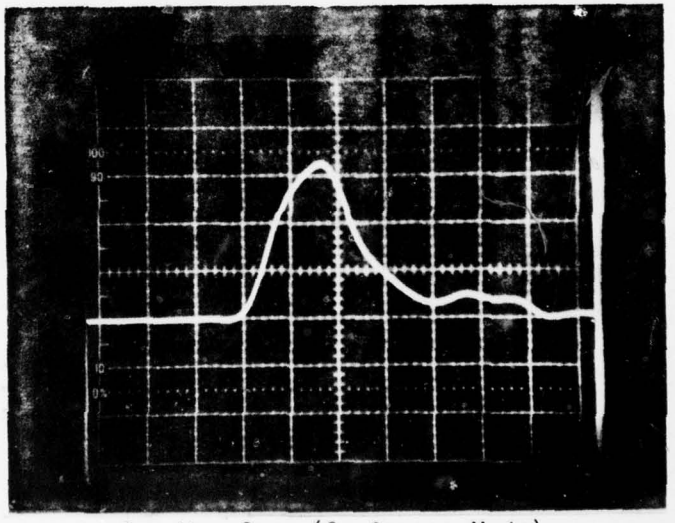

Sum Waveform (2 × Common Mode)

Figure 44. Two-Wire Line Output Data - Short Duration Pulse (2 ns/div)

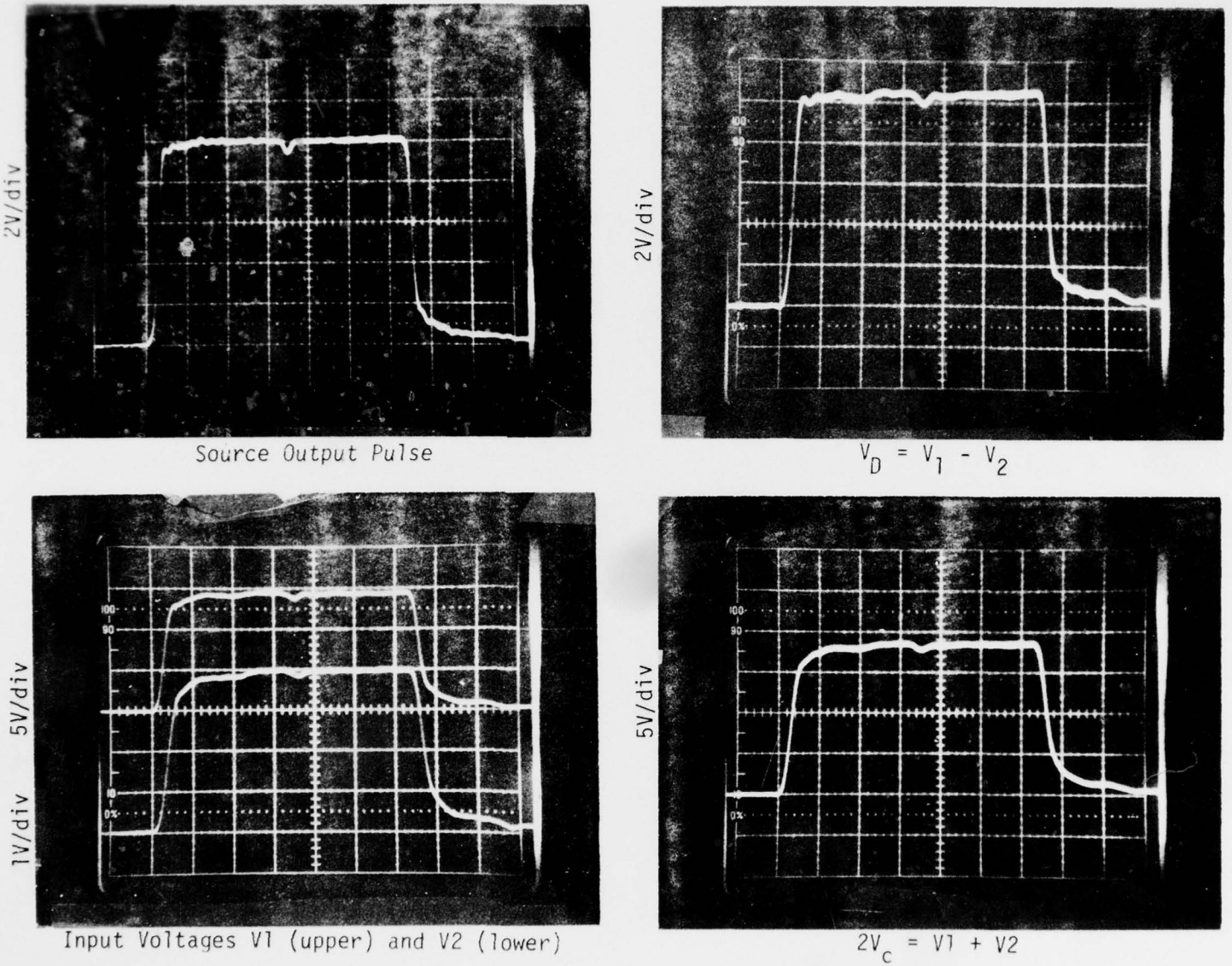

Figure 45. Two-Wire Line Input Data - Long Duration Pulse (5 ns/div)

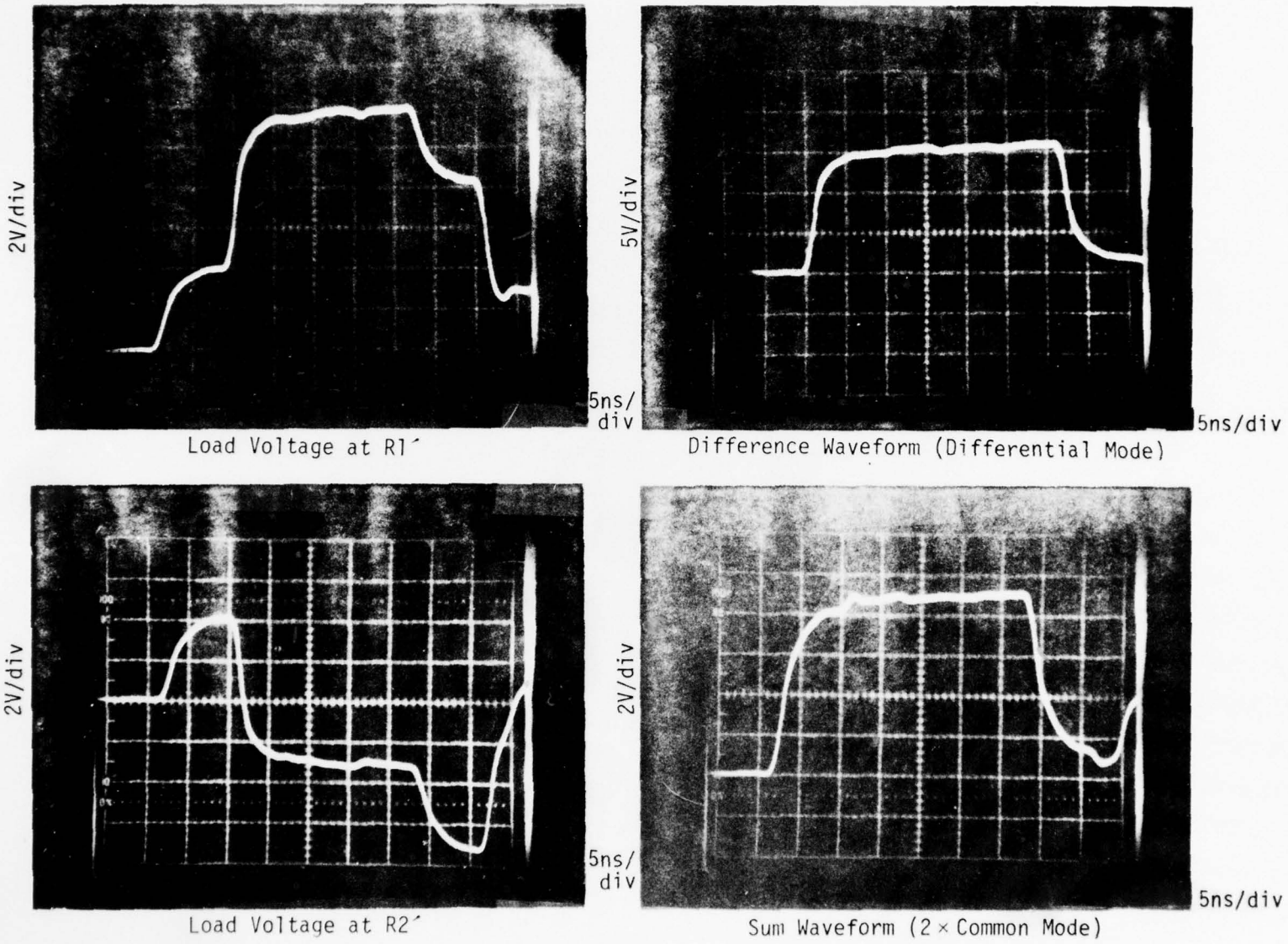

Figure 46. Two-Wire Line Output Data - Long Duration Pulse

Table 4. TWO-WIRE LINE PULSE TRACING TEST RESULTS

	Common Mode		Differential Mode	
	V_C(in)	V_L(out)	V_D(in)	V_L(out)
Short Pulse:				
calculated	8.7v	4.3v	10.2v	15.3v
measured	8.5	3.3	10.1	13.2
% difference	-2.3%	-23%	-0.98%	-14%
Long Pulse:				
calculated	9.2v	4.5v	10.6v	16.1v
measured	9.3	4.0	10.2	16.0
% difference	1.1%	-11%	-3.8%	-0.62%

The results are seen to be in good agreement with the exception of the short pulse load voltages, which show more high frequency attenuation than for the long pulse data. This was not taken into account in the computations.

SECTION V

COMMON MODE PROPAGATION

In the transmission line analysis of aircraft cables the cable/airframe geometry can often be approximated as a single wire equivalent relative to local ground plane. The common mode characteristic impedance and other transmission line parameters can then be estimated from standard handbook equations.

The application of this technique to transmission line configurations similar to those found on aircraft was investigated using bundles of up to 20 wires. The bundles were 6.1 meter lengths of tightly bunched unshielded aircraft wire. The individual wires were of 20 gauge stranded tinned copper insulated with PVC and coated with a thin nylon jacket (Teledyne Thermatics, Inc.). The configurations studied were as follows:

1. Cable near a flat ground plane
2. Cable near a right angle corner
3. Cable in conduit

The common mode characteristic impedance and propagation velocity were measured for each configuration using bundles of 1, 3, 5, 10, 15, and 20 wires.

Time domain reflectometry was used as the principal measurement technique; however, swept frequency (1 MHz to 100 MHz) open and short circuit input impedance measurements were also made for select cases. The cw data are included as figures 1 thru 11 of Appendix B. The swept frequency measurements were generally difficult to interpret at frequencies above approximately 30 MHz due to phase and amplitude perturbations which became more pronounced as the number of wires per bundle was increased. These effects were evidently caused by the nonuniform cable cross section and the random lay of the wires within the bundle. It was noted that fewer perturbations were observed on a 15-wire line when the wires were

combed. Trials with a manufactured vinyl-jacketed 12-wire line showed a further decrease in these effects. The same effects are present on the TDR records. In this case, they appear as multiple reflections of low amplitude over the length of the cables.

The attenuation was not measured directly; however, the TDR pulse reflected from the shorted end of the cable is approximately equal to the step function response over twice the cable length (see Section II). The effects of high frequency attenuation are apparent in the degraded pulse rise time. The attenuation versus frequency is obtainable by Fourier methods.

1. CABLE NEAR A GROUND PLANE

Tests were performed on this geometry with the cable at two heights, 8.9 cm above the ground plane and lying on the ground plane. The TDR records are included as figures 12 through 15 of Appendix B. The test results are summarized in Table 5.

The calculated values of impedance are from the formula (ref. 11)

$$Z_o = \frac{60}{\sqrt{\varepsilon}} \ell n \left(\frac{h}{a} + \sqrt{\left(\frac{h}{a}\right)^2 - 1} \right) \qquad (82)$$

where the radius was taken as the actual cable radius measured to the outside edge of the cable (including the dielectric). A dielectric constant of unity was assumed. Equivalent radii were computed by solving the impedance equation for the radius using measured values of Z_o, ε, and h from the 8.9 cm cable height data. The results are tabulated as a_e for comparison with the actual radii (a).

The ratio h/a_e has been tabulated for the cable lying on the ground plane. The cable was taped down at several points; however, it was not in intimate contact with the ground plane at all points along the cable

Table 5. TEST RESULTS FOR A CABLE NEAR A GROUND PLANE

Above ground plane, $h \simeq 8.9$ cm.

No. Wires	Z_o(CW)	Z_o(TDR)	v/c	a_e	a	Z_o(calc)
1	330 ohms	350 ohms	0.956	0.053 cm	0.051 cm*	352 ohms
3	275	307	0.943	0.109	0.190	273
5	262	283	0.980	0.162	0.272	252
10	235	272	0.990	0.198	0.399	230
15	222	234	0.990	0.381	0.516	216
20	214	227	0.995	0.429	0.533	214

On ground plane, $h \simeq a$.

No. Wires	Z_o	v/c	h/a_e	Z_o(calc)	h/a
1	96.2 ohms	0.788	3.89	75.4 ohms	1.90
3	55.5	0.829	1.69	41.6	1.25
5	45.5	0.808	1.47	34.5	1.17
10	42.4	0.829	1.39	27.8	1.11
15	42.2	0.798	1.41	25.2	1.09
20	34.6	0.769	1.29	23.8	1.08

*The actual conductor radius (without insulation) is listed for the single wire.

run. The actual height of the cable center averaged over the length of the cable would therefore be expected to be somewhat larger than the cable radius, as the test results indicate. This is reflected in the measured impedance levels which show differences of 50% or more when compared with ideal case calculations.

The measured propagation velocities for the 8.9 cm height are approximately equal to the speed of light as would be expected since the dielectric is predominantly air. With the cable lying on the ground plane the velocity was found to be approximately 0.8 c, which is equivalent to an effective dielectric constant of

$$\varepsilon' = (c/v)^2 = 1.6. \tag{83}$$

This value is approximately 60% of that of solid PVC insulation ($\varepsilon = 2.8$). The decrease in impedance that would normally be computed due to the $1/\sqrt{\varepsilon}$ dependence in the impedance formula is more than offset by the uncertainty in the cable height for this case.

2. CABLE NEAR A CORNER

This configuration was studied for two cases with the cable placed along the 45 degree bisector of a right angle corner. The cases studied were with the cable 5 cm from the corner and with the cable placed in the corner. The TDR records are included as figures 16 through 19 of Appendix B. The test results are summarized in Table 6 .

The impedance formula for a single wire placed at a distance d along the bisector is

$$Z_o = \frac{60}{\sqrt{\varepsilon}} \ell n \left(\frac{d}{2a}\right) \quad , \quad d >> a \tag{84}$$

The values of Z_o(calc) listed in Table 6 for the 5 cm distance are from this formula using the actual cable radii and a dielectric constant of unity. The measured and calculated values are seen to be in close agreement. The equation is not valid when the cable is lying very close

to the corner ($d \simeq a\sqrt{2}$), and comparison of measured and claculated values was not possible for this case.

Table 6. TEST RESULTS FOR A CABLE NEAR A CORNER

	Two Inches from Corner			In Corner	
No. Wires	Z_o	v/c	Z_o(calc)	Z_o	v/c
1	263 ohms	0.929	277 ohms	75 ohms	0.775
3	228	0.986	207	46.6	0.801
5	213	0.956	194	43.4	0.825
10	167	0.971	167	32.2	0.821
15	163	0.960	154	33.3	0.794
20	150	0.991	146	26.7	0.757

The propagation velocities of approximately 0.97c and 0.79c correspond to effective dielectric constants of 1.06 and 1.60 and are nearly the same as observed with the cable near a ground plane.

3. CABLE IN CONDUIT

This geometry utilized 1/2 inch and 1 inch standard aluminum conduit with the cables lying against the inside wall.* The wire insulation was in contact with the wall at several points along the cable run; however, as in the case of the cable lying on the ground plane, the average cable height over the length of the conduit exceeded the cable radius. The TDR records are included as figures 20 through 23 of Appendix B. The test results are summarized in Table 7.

The calculated impedances are from the single wire equation (ref. 1)

$$Z_o = \frac{60}{\sqrt{\varepsilon}} \cosh^{-1}\left(\frac{a_1^2 + a_2^2 - b^2}{2a_1a_2}\right) \tag{85}$$

*The inside diameters of standard 1/2 inch and 1 inch conduit are 1.68 cm and 2.66 cm respectively.

with $\varepsilon = 1$, a_1 = actual cable radius, a_2 = conduit radius, and b = distance between cable and conduit centers.

The average propagation velocity of 0.85c is nearly the same in both cases and corresponds to an effective dielectric constant of 1.4. This value is lower than that observed with the cables lying on the ground plane ($\varepsilon' = 1.6$). The difference is due to the fact that in the latter case the cable was taped to the ground plane at several points in an attempt to keep the geometry uniform. This placed more insulation in the region between the cable and ground plane, averaged over the cable length, than for the cable/conduit geometry which could not be controlled.

The measured and calculated impedance levels are in poor agreement due primarily to the uncertainty in the average value of b that should be used in the calculations.

Table 7. TEST RESULTS FOR CABLE IN CONDUIT

	One-Half Inch Concuit			One Inch Conduit		
No. Wires	Z_o	v/c	Z_o(calc)	Z_o	v/c	Z_o(calc)
1	100 ohms	0.816	73.9 ohms	106 ohms	0.815	74.4 ohms
3	65.7	0.851	--	79.0	0.869	--
5	54.4	0.858	37.4	76.9	0.874	39.9
10	41.2	0.870	26.8	49.4	0.878	30.8
15	32.0	0.832	24.4	43.8	0.868	31.0
20	26.2	0.839	14.9	46.2	0.898	19.9

4. MONTE CARLO CALCULATION OF A SINGLE INSULATED WIRE IN A SMALL CONDUIT

For the special case of a single wire in a small conduit, we have found that calculating the average impedance of all possible impedances properly weighted will yield good results. This is done by calculating

the approximate impedance of the wire with its insulating jacket for a large number of random locations within the confines of the conduit outer conductor.

In generating the random locations within the conduit, we assume equal probability for residing at any location inside the outer conductor. The calculation approximates the outer surface of the inner wire insulation to be an equipotential surface. This is exact when the wire is centered but is in error when the wire is close to the outer conductor. Using this model we find for any particular location the characteristic impedance is expressed as

$$Z_t = \frac{Z_1}{\sqrt{\varepsilon_1}} + \frac{Z_2}{\sqrt{\varepsilon_2}} \tag{86}$$

where $Z_1 = 60 \ln \left(a_2/a_1\right)$, the free space coaxial line impedance for inner wire radius a_1 and outer conductor radius a_2. Since we are considering the outer surface of the insulated inner wire as being an equipotential surface then a_2 is just $a_1 + t$, where t is the thickness of the insulation and ε_1 is the relative dielectric constant of that insulation.

Z_2 is found by calculating the free space eccentric coaxial line impedance for an inner conductor having a radius of a_2, an outer conductor radius of a_3 and a distance between centers of b.

Thus

$$Z_2 = \sqrt{\frac{L}{C}} \tag{87}$$

where

$$L = \frac{\mu_o \ln \left(x + \sqrt{x^2 - 1} \right)}{2\pi} \tag{88}$$

and

$$C = \frac{\varepsilon_o 2\pi}{\ln \left(x + \sqrt{x^2 - 1} \right)} \tag{89}$$

and

$$x = \frac{a_3^2 + a_2^2 - b^2}{2a_2a_3} \tag{90}$$

ε_2 is the relative dielectric constant for the medium filling the region between the outer conductor and inner wire (air for our case).

Since these characteristic impedance equations are all in terms of a radii and separation of centers, it is most convenient to randomize the separation distance b using a uniform distribution random number generator and then applying an appropriate weighting function to account for the increased probability of the inner wire residing at the larger separations.

Based on cross-sectional area consideration this weighting function is

$$W = 1 + \frac{2\pi b}{a_3} \tag{91}$$

Thus for our average we have

$$\overline{Z}_t = \frac{\sum_{i=o}^{N} Z_{t_i}(b_i)\left(1 + \frac{2\pi b_i}{a_3}\right)}{\sum_{i=o}^{N}\left(1 + \frac{2\pi b_i}{a_3}\right)} \tag{92}$$

where N is a large number and where the b_i's are generated by a uniform distribution random number generator with $0 \leq b_i < (a_3 - t - a_i)$.

The results of this Monte Carlo calculational procedure converges to an impedance level after sufficient iterations. Table 8 shows the results.

Table 8. MONTE CARLO CALCULATION OF INSULATED WIRE IN CONDUIT

Conduit	Large		Small	
Inner Wire Radius	0.432 cm	0.051 cm	0.432 cm	0.051 cm
Insulation Thickness	0.083	0.051	0.083	0.051
Outer Conductor Radius	1.270	1.270	0.794	0.794
Monte Carlo Z_t	46Ω	132Ω	26Ω	107Ω
Measured Z_t	33Ω	106Ω	25Ω	100Ω
Insulation ε_r	2.3	5	2.3	5

You will note the better agreement for both wire sizes in the smaller conduit, indicating that inner wire's location is randomized throughout its length within the conduit.

For the larger conduit, apparently gravity tends to overcome the randomness to a degree, increasing the probability of the cable lying closer to the outer wall, and hence exhibiting a lower average impedance.

5. RG/213 TRANSMISSION LINE

Tests were also performed by driving the shield of a length of RG/213 transmission line in each of the configurations described. The TDR records are shown in Figures 24 through 26 of Appendix B. The test results are summarized in Table 9.

The results are very similar in most cases to those of the 20 wire bundle. The bundle has an equivalent radius that is approximately the same as the RG/213 shield radius.

The effects of metallic ribs on the characteristic impedance and electrical length of RG/213 cable supported above a ground plane were also studied. The basic geometry of figure 1 was used for the three cable-over-rib configurations shown in figure 47. TDR traces of the shield/ground plane impedance profiles with the far end shorted are shown in figure 48.

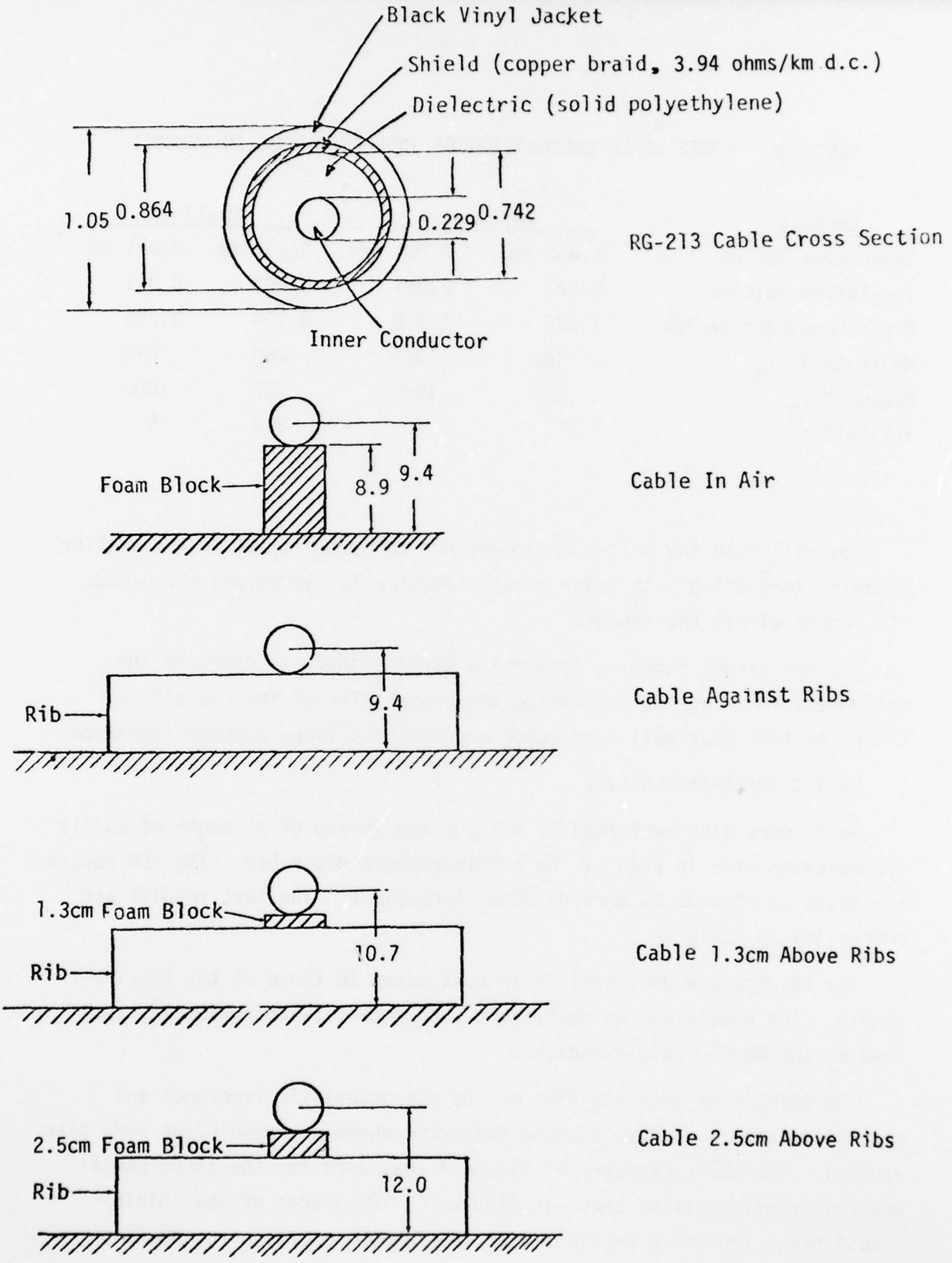

Figure 47. RG/213 Cable Geometries (dimensions in cm)

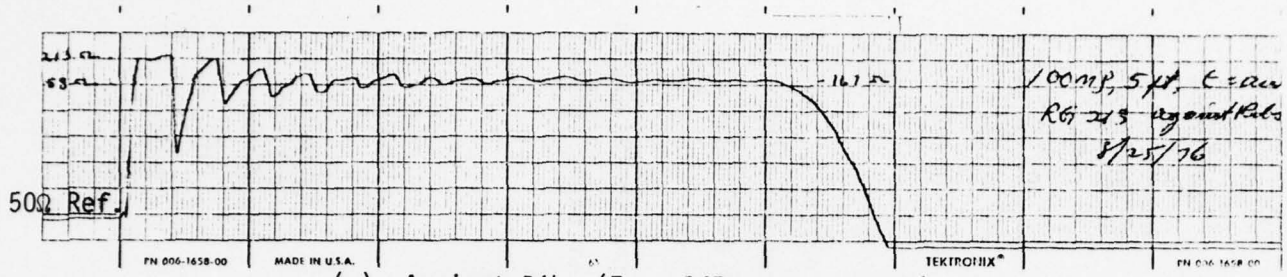

(a) Against Ribs (Z_o = 167Ω, L_e = 7.80m)

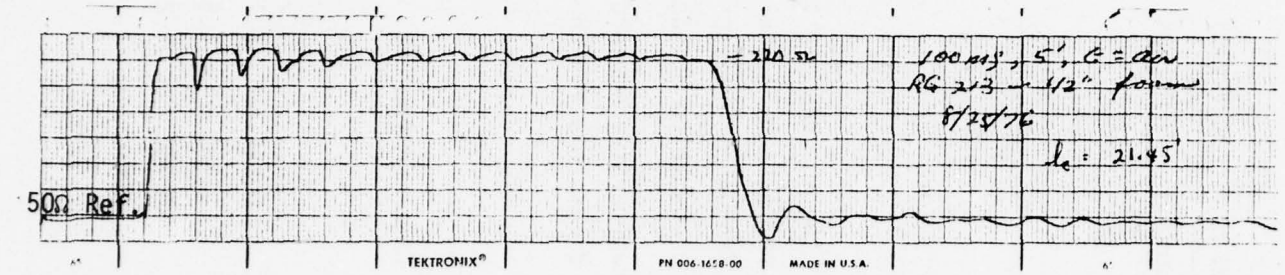

(b) 1.3cm Above Ribs (Z_o = 220Ω, L_e = 6.77m)

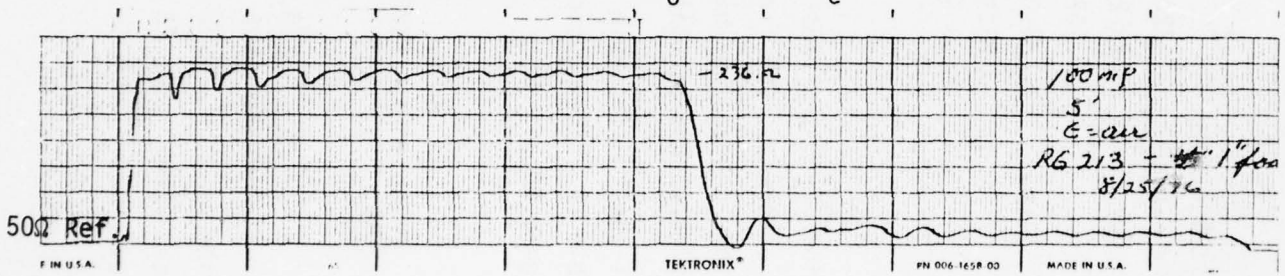

(c) 2.5cm Above Ribs (Z_o = 236Ω, L_e = 6.61m)

Figure 48. RG/213 Cable - Above-Rib TDR Records (L = 6.1m)

AD-A058 267 MISSION RESEARCH CORP ALBUQUERQUE N MEX F/G 17/2
AIRCRAFT CABLE PARAMETER STUDY.(U)
OCT 77 H M FOWLES, L D SCOTT, A K AGRAWAL F29601-76-C-0091
UNCLASSIFIED AMRC-R-92 AFWL-TR-77-107 NL

2 OF 2
AD A058267

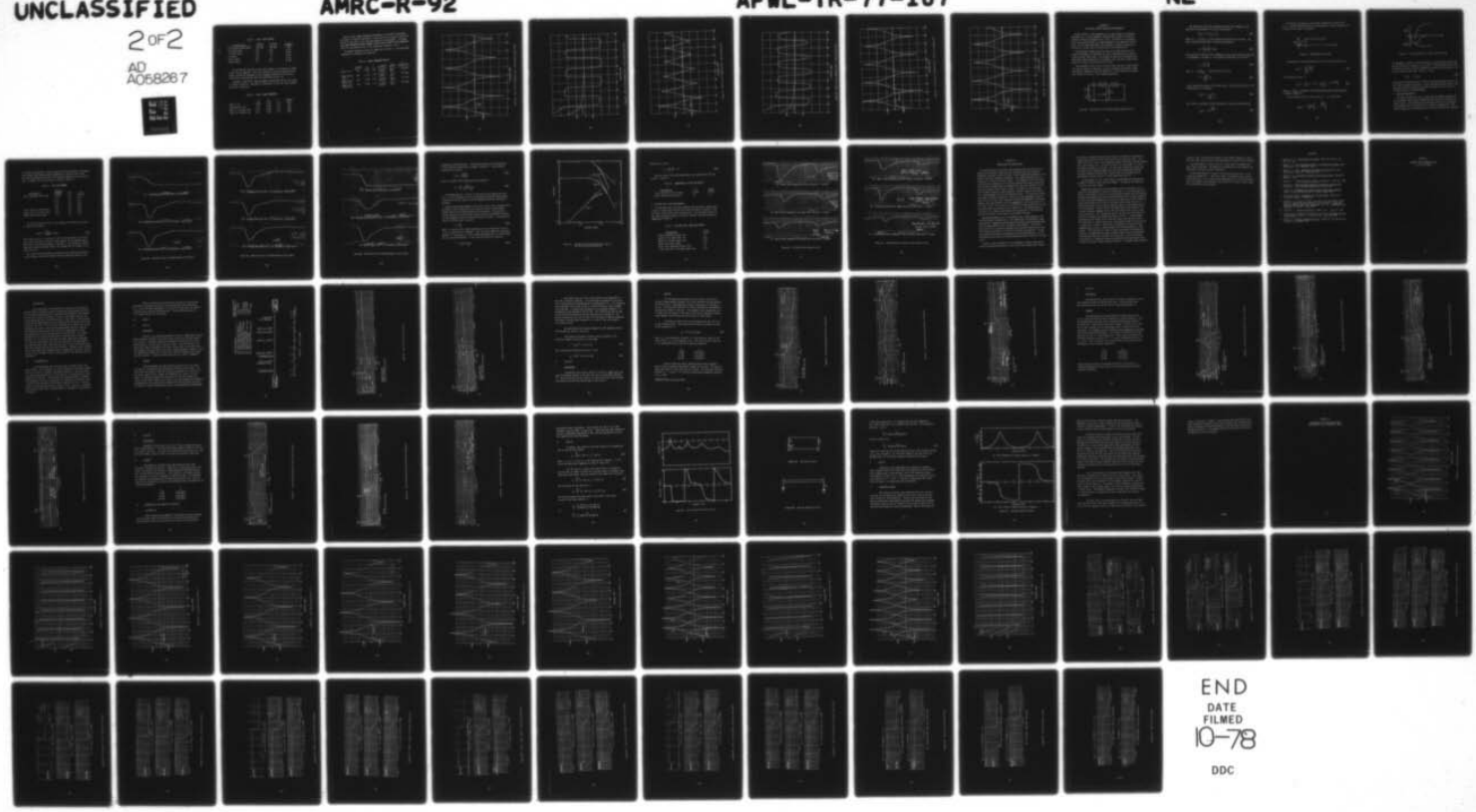

END
DATE FILMED
10-78
DDC

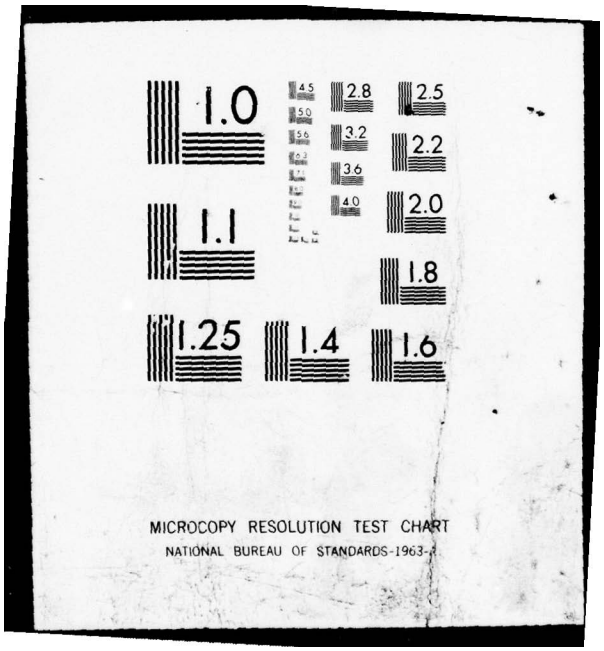
1.0
1.1
1.25
1.4
1.6
1.8
2.0
2.2
2.5
2.8
3.2
3.6
4.0
4.5
5.0
5.6
6.2
MICROCOPY RESOLUTION TEST CHART
NATIONAL BUREAU OF STANDARDS-1963-A

Table 9 . RG/213 TEST RESULTS

Configuration	Z_o(meas)	Z_o(calc)	v/c(meas)
8.9 cm above ground plane	228 ohms	226 ohms	0.941
on ground plane	39.2	38.3	0.775
5 cm from corner	167	154	0.947
in corner	33.0	---	0.763
small conduit	25.3	14.1	0.751
large conduit	33.3	21.3	0.769

The reflections from the ribs and the increase in the electrical length of the line are apparent. The first reflection is the strongest with subsequent reflections degraded by high frequency attenuation as the pulse is partially reflected and partially transmitted at each rib.

A summary of the RG-213 cable parameters determined from the TDR traces is listed in Table 10. The physical dimensions for the four cases studied are given in Figure 47.

Table 10. RG/213 CABLE PARAMETERS

	ℓ_e	v_p	ε'	Z_o(meas)
Cable in air	6.46 m	0.94C	1.12	228Ω
Cable against ribs	7.80	0.78C	1.64	167Ω
Cable 1.3 cm above ribs	6.76	0.90C	1.23	220Ω
Cable 2.5 cm above ribs	6.64	0.92C	1.19	236Ω

Short circuit swept impedance measurements for the RG-213 experiments are shown in figures 49 through 54. Phase plots are included in figures 50 and 52 for the cable in air and cable-against-rib experiments. The phase data were affected by probe loading and are not as useful as the magnitude plots for the determination of the propagation constants α and β.

The swept frequency results are summarized in Table 11. The calculated impedances are included for comparison.

Table 11. SWEPT IMPEDANCE RESULTS

	Z_o(ohms)	v_p	ε'	α_o(nep/m)	f_o(MHz)	Z_o (theory/$\sqrt{\varepsilon'}$)
Cable in air	207	0.96C	1.09	1.2×10^{-3} 5.9×10^{-3}	24.0 94.7	216 ohms
Cable against ribs	166	0.73C	1.90	7.0×10^{-3} 3.2×10^{-3}	17.8 88.3	164 ohms
Cable 1.3 cm above ribs	219	0.90C	1.23	1.3×10^{-3} 4.2×10^{-3}	22.0 89.0	211 ohms
Cable 2.5 cm above ribs	229	0.92C	1.17	1.3×10^{-3} 4.5×10^{-3}	22.8 91.1	222 ohms

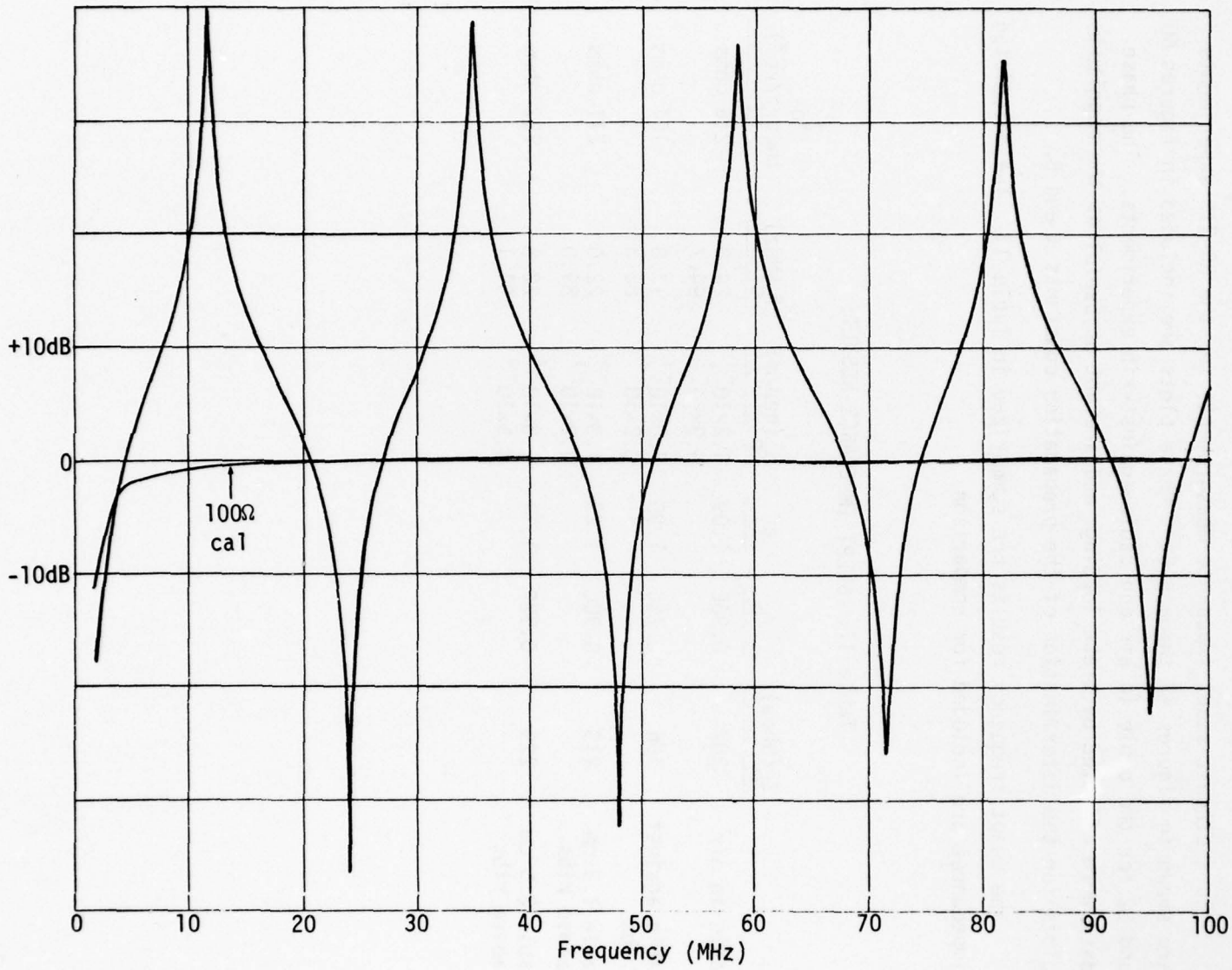

Figure 49. Short Circuit Impedance Data - RG/213 Above Ground Plane

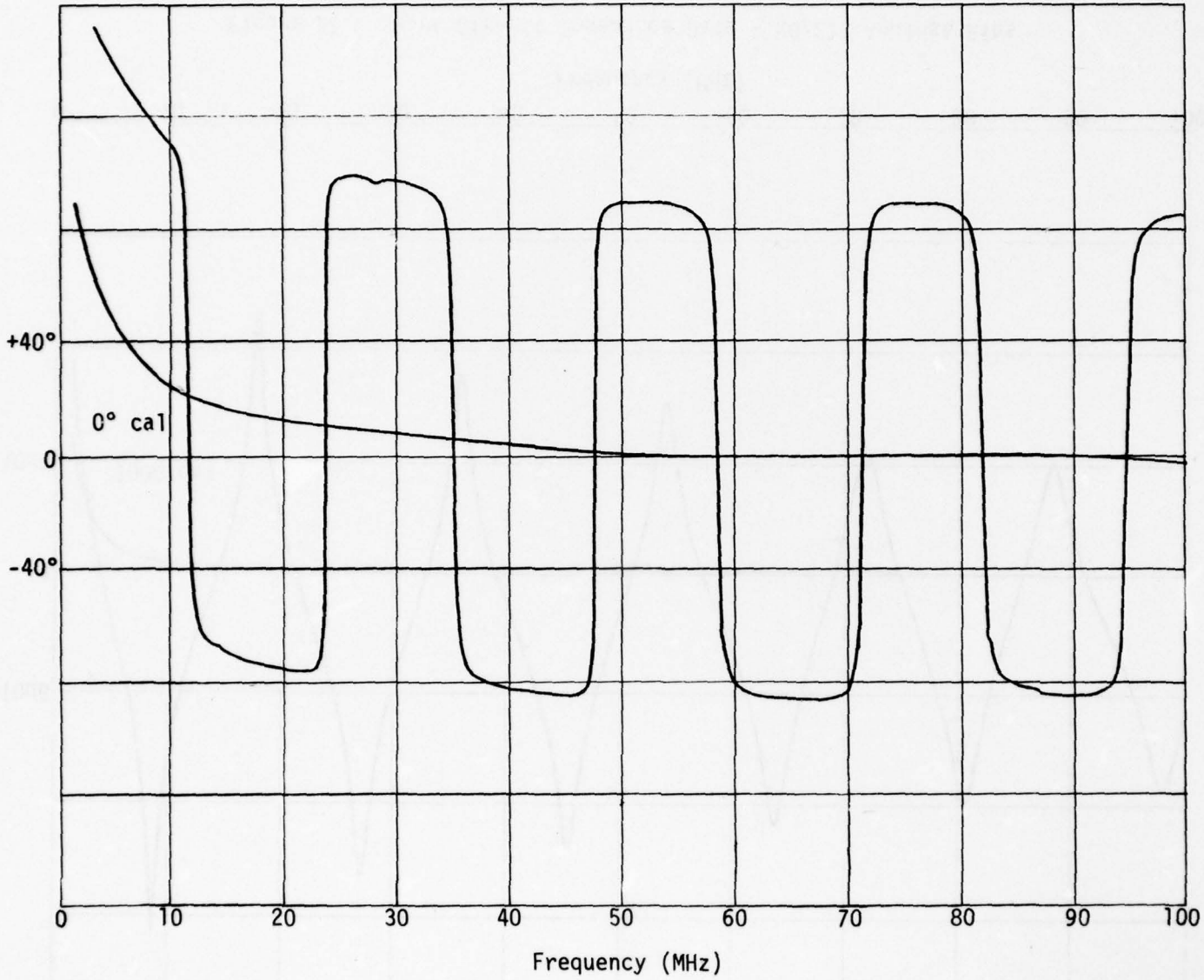

Figure 50. Short Circuit Impedance Data - RG/213 Above Ground Plane

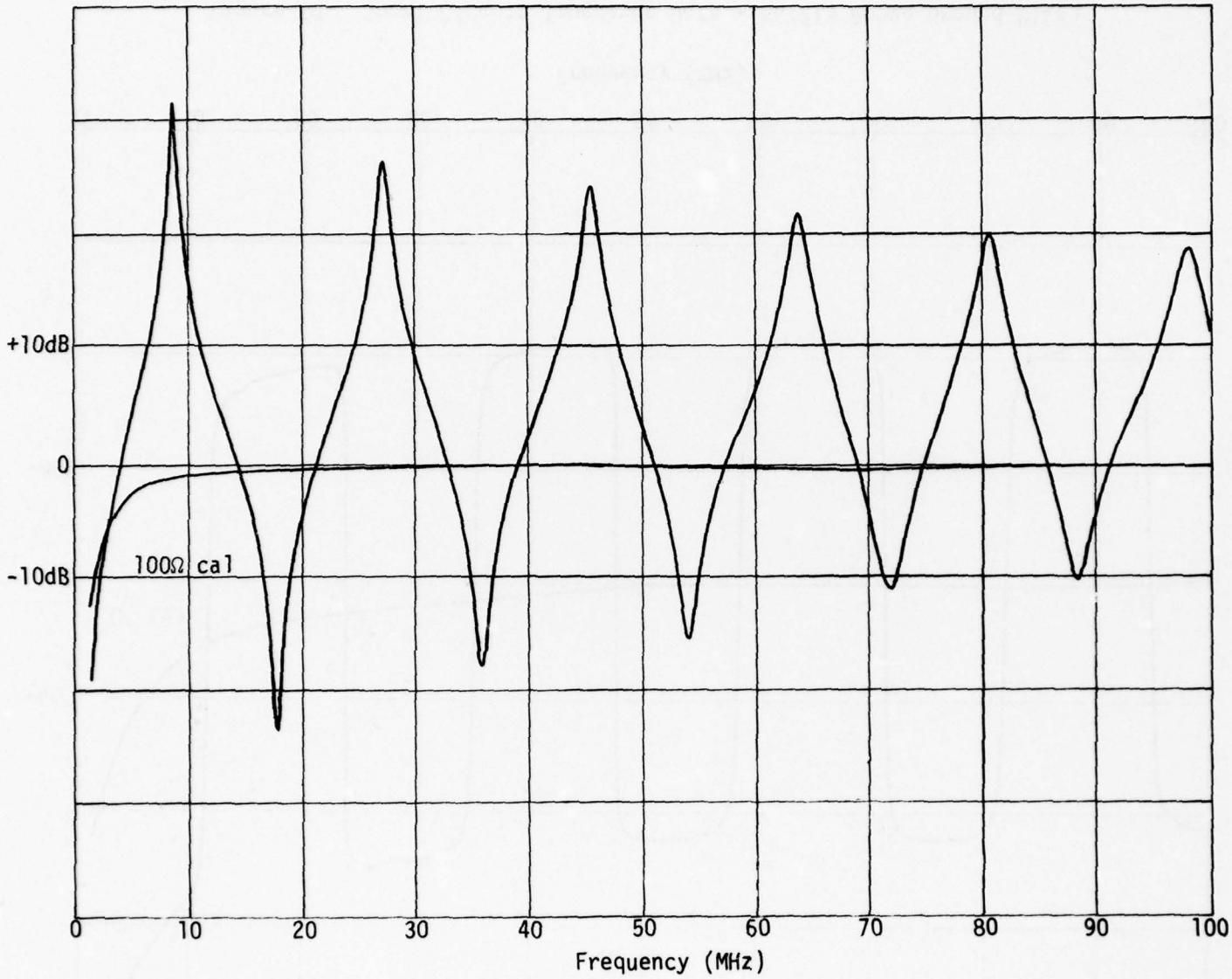

Figure 51. Short Circuit Impedance Data - RG/213 Against Ribs

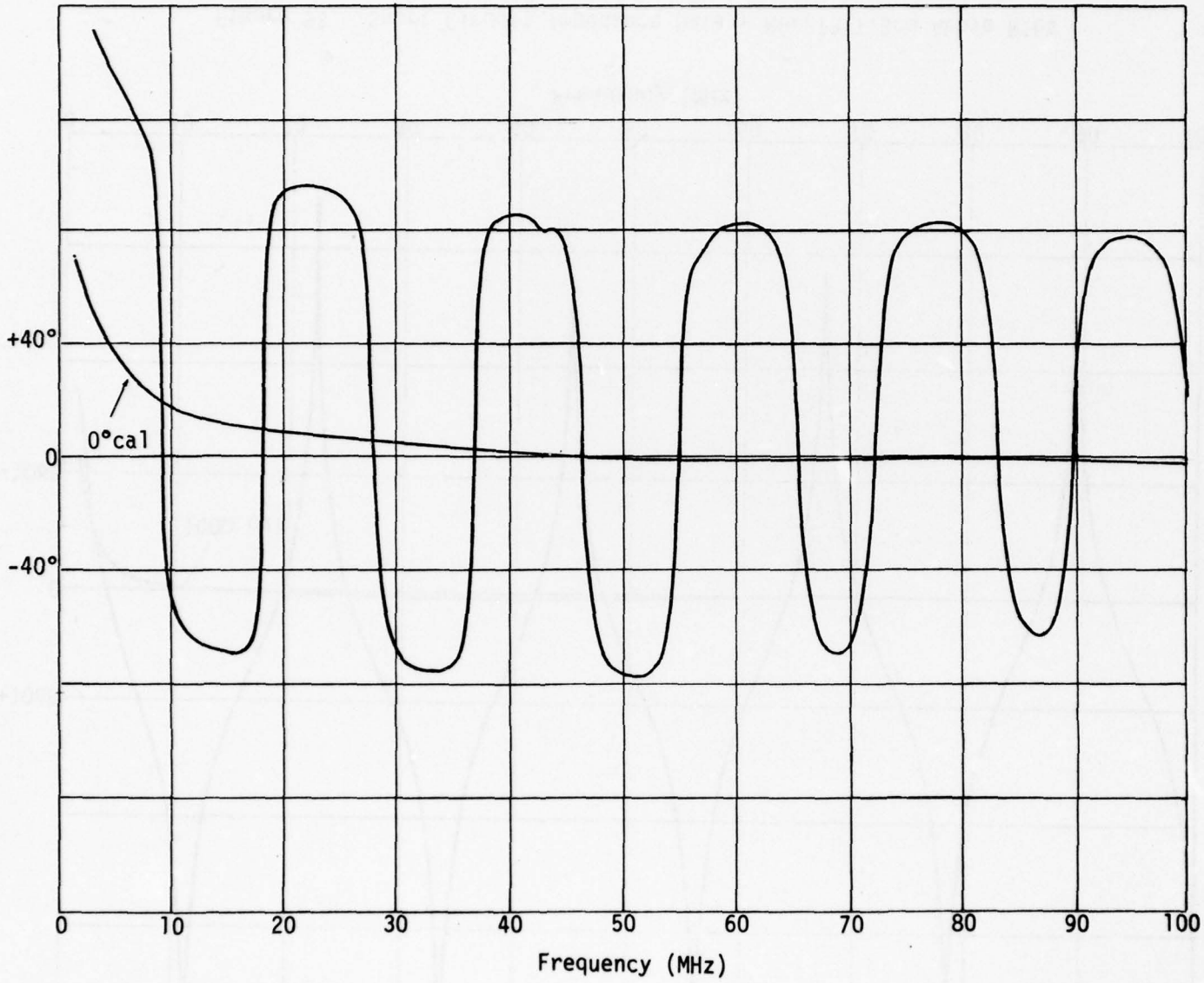

Figure 52. Short Circuit Impedance Data - RG/213 Against Ribs

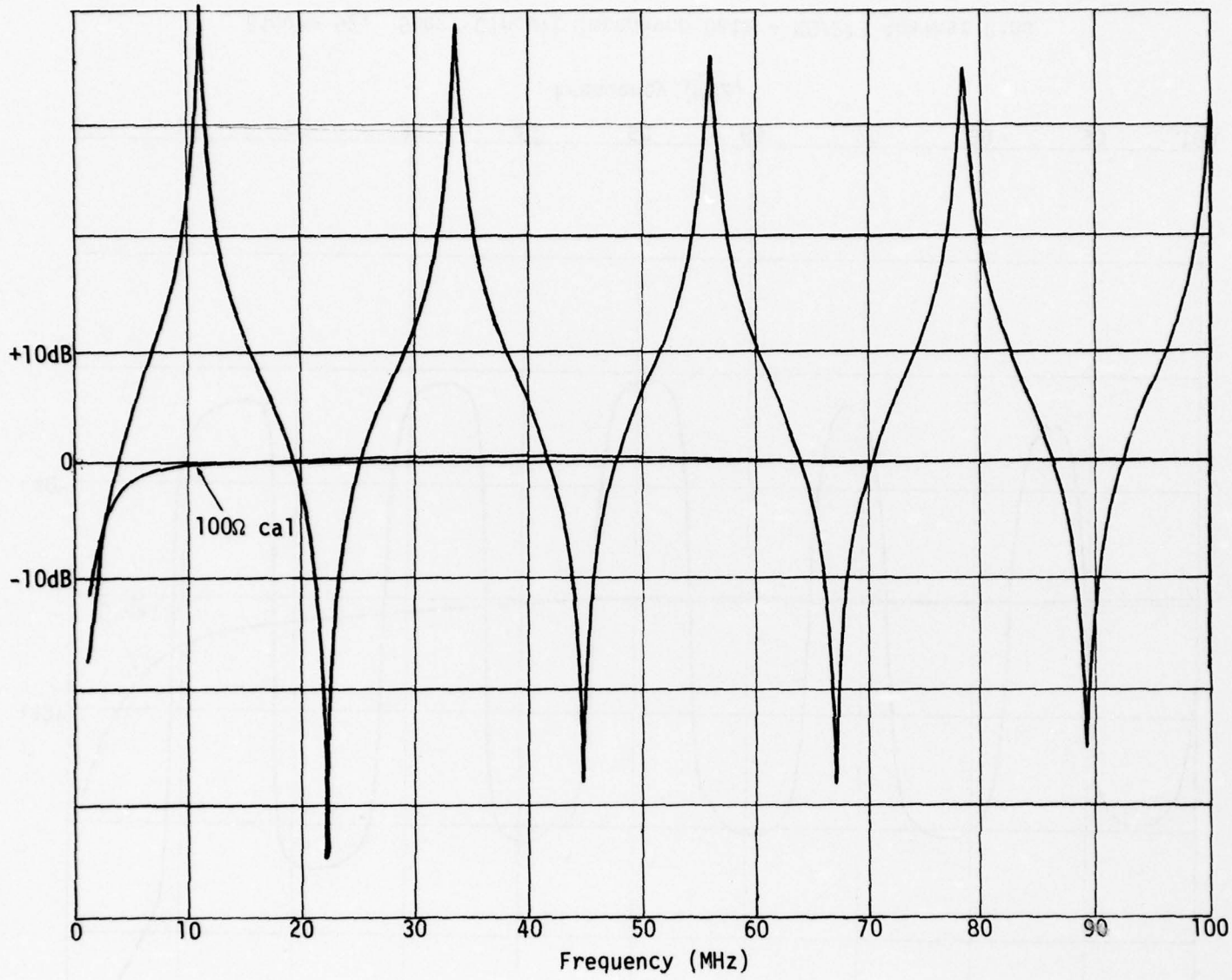

Figure 53. Short Circuit Impedance Data - RG/213 1.3cm Above Ribs

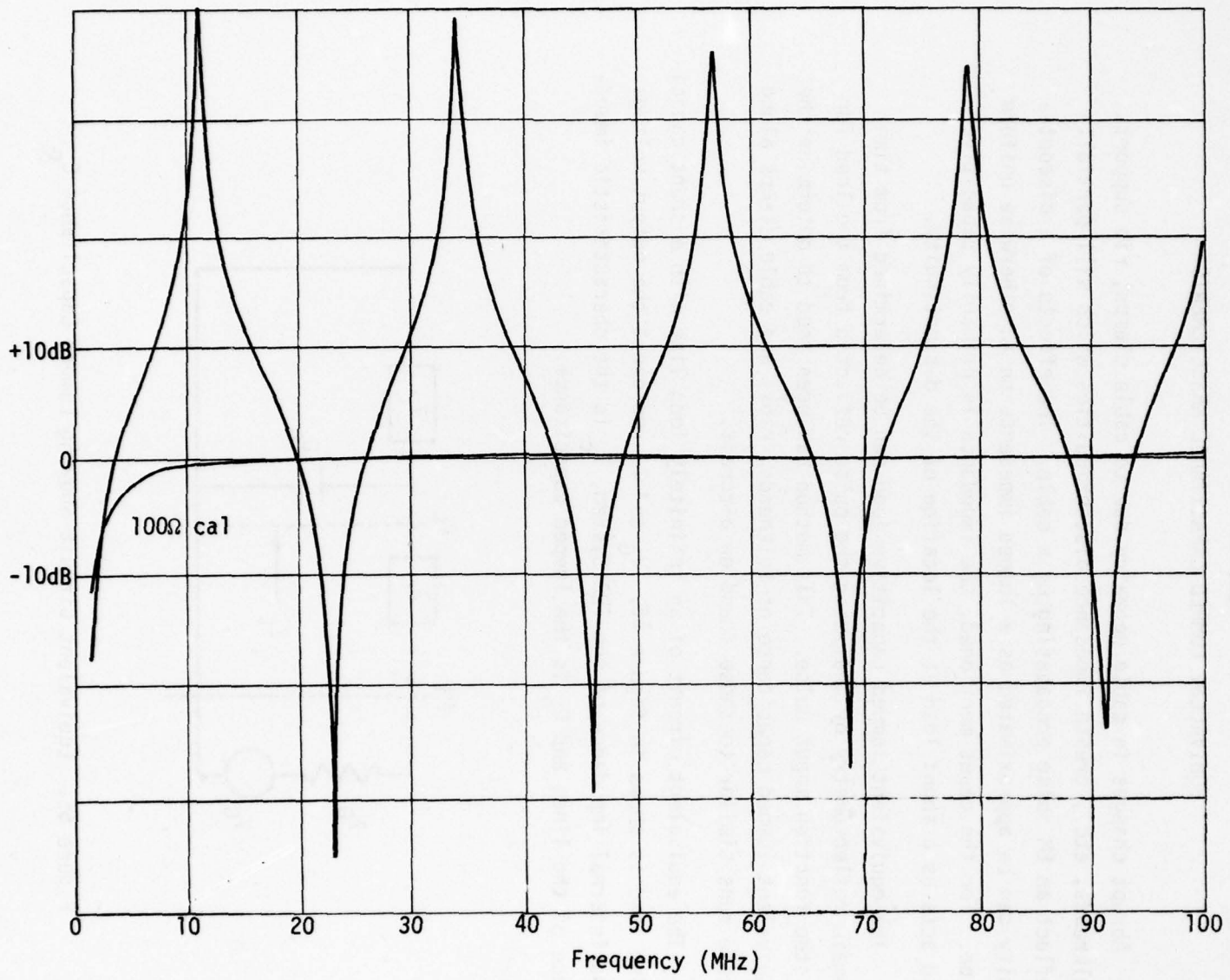

Figure 54. Short Circuit Impedance Data - RG/213 2.5cm Above Ribs

SECTION VI

EQUIVALENT LUMPED CAPACITANCE MEASUREMENTS

Abrupt changes in cable geometry due to cable clamps, rib supports, bulkheads, etc., create impedance discontinuities which will partially reflect an EM pulse propagating on a cable. The effects of a discontinuity can be approximated as a lumped impedance on an otherwise uniform line. For the cases mentioned, the impedance is primarily capacitive and acts as a shunt load at the location of the discontinuity.

The equivalent lumped capacitive load can be determined from time domain reflectometry by analyzing the pulse reflected from the load for a step function input pulse. This method has been used to determine the equivalent lumped capacitance of bulkheads, ribs, and cable clamps along cable runs similar to those found on aircraft.

The equivalent circuit of an infinitely long line with a shunt capacitive load is shown in figure 55. V_G and Z_G represent the output voltage and internal impedance of the TDR System, Z_c is the characteristic impedance of the line, and C_o is the lumped capacitance.

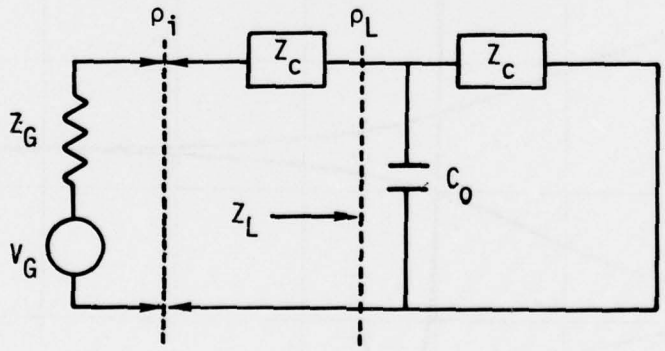

Figure 55. Equivalent Circuit Showing Lumped Capacitance C_o.

The spectrum of the pulse reflected from the load impedance Z_L and observed at the generator is given by the equation

$$V_R(\omega) = A\ \rho_L(\omega)\ V_G\ (\omega) \tag{93}$$

where $A = 1 - \rho_i^2$ and ρ_i is the reflection coefficient at the input. The input reflection coefficient is given by the equation

$$\rho_i = \frac{Z_c - Z_G}{Z_c + Z_G} \tilde{=} \text{const} \tag{94}$$

which except for possible stray impedances at the input interface connection is independent of frequency. The reflection coefficient at the load is

$$\rho_L = \frac{Z_L - Z_c}{Z_L + Z_c} \tag{95}$$

where $Z_L = \dfrac{Z_c}{1 + j\omega C_o Z_c}$. Substituting for Z_L gives

$$\rho_L = \frac{-j\omega}{\frac{2}{C_o Z_c} + j\omega} \tag{96}$$

A unit step input pulse has the spectrum $V_G(\omega) = \dfrac{1}{j\omega}$ and the spectrum of the reflected pulse is therefore

$$V_R(\omega) = -\frac{A}{\frac{2}{C_o Z_c} + j\omega} \tag{97}$$

This function transforms to the time domain to give the reflected pulse

$$v_R(t) = -A\ e^{-\frac{2}{C_o Z_o} t} \tag{98}$$

In practice, the input is not an ideal step but has a finite rise time. A suitable approximation to the input pulse is a step function with a linear rise as shown in figure 56.

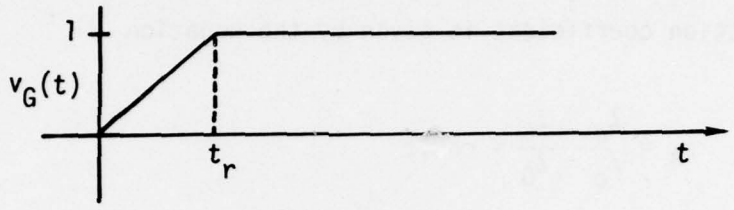

Figure 56. Approximate Input Pulse

The spectrum of the reflected pulse in this case can be written as

$$V_R(\omega) = - \frac{j\omega\ A\ V_G(\omega)}{\frac{2}{C_o Z_c} + j\omega} \tag{99}$$

The transform of $V_R(\omega)$ is

$$v_R(t) = - \frac{A}{\alpha t_r} (1 - e^{-\alpha t}) + \frac{A}{\alpha t_r} \left[1 - e^{- \alpha (t - t_r)} \right] \tag{100}$$

where $\alpha = 2/C_o Z_o$. A sketch of the reflected pulse seen at the generator is shown in figure 57.

The reflected pulse has a peak value at $t = t_r$ of amplitude

$$v_R(max) = - \frac{A\ C_o Z_c}{2 t_r} \left(1 - e^{- \frac{2 t_r}{C_o Z_c}} \right) \tag{101}$$

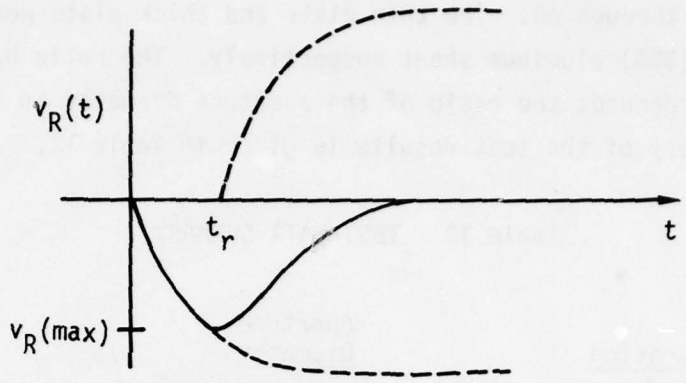

Figure 57. Pulse Reflected by a Shunt Capacitive Load

This equation is solved for the capacitance C_o using measured values from the TDR recording for $V_R(max)$, t_r, Z_c, and A. The amplitude factor A and the pulse rise time t_r are best measured by shorting the transmission line at the location of the load. Then $\rho_L = -1$ and

$$v_R(t) = - A\, v_G(t) \tag{102}$$

from which the amplitude and rise time of the pulse incident on the load can be more accurately measured. In this case the amplitude factor A and any pulse distortion caused by the input interface and line losses are included directly in the measurement.

1. BULKHEAD MEASUREMENTS

The above procedure was used to determine the lumped capacitance of a wire through a metal plate representing the effects of a bulkhead for several cases. The experiments were performed with the wire supported on styrofoam blocks at a height of 8.9 cm above a ground plane. TDR records showing the reflected pulses for the cases studied are presented

in figures 58 through 60. The thin plate and thick plate were of 36 gauge and 16 gauge (B&S) aluminum sheet respectively. The ratio b/a listed for each case denotes the ratio of the aperture diameter to the wire diameter. A summary of the test results is given in Table 12.

Table 12. TEST DATA SUMMARY

Configuration	Aperture Diameter	b/a	C_o
18 ga. bare wire, thin plate	0.58 cm	5.6	0.38 pF
	0.51	5.0	0.39
	0.41	4.0	0.41
	0.31	3.0	0.42
	0.21	2.0	0.44
18 ga. bare wire, thick plate	0.21	2.0	0.49
20 ga. ins. wire, thick plate	0.21	2.0	0.85
RG/213 cable, thick plate	1.11	1.3	1.11

The coaxial capacitance for a wire through an infinitely thick plate is given by the formula

$$C(\text{coax}) = \frac{0.56\varepsilon_r}{\ell n(b/a)} \quad \text{pF/cm} \tag{103}$$

This formula for b/a = 2.0 gives 0.01 pF for the bare wire, 5 mil plate and 0.1 pF for the 50 mil plate as contributions to the measured capacitance due to the finite thickness of the plate. The variation in capacitance with aperture diameter shows a 14% decrease for an increase in b/a from 2.0 to 5.6.

As a check on the TDR analysis procedure, the reflection coefficient in the frequency domain was computed from the amplitude spectra of the

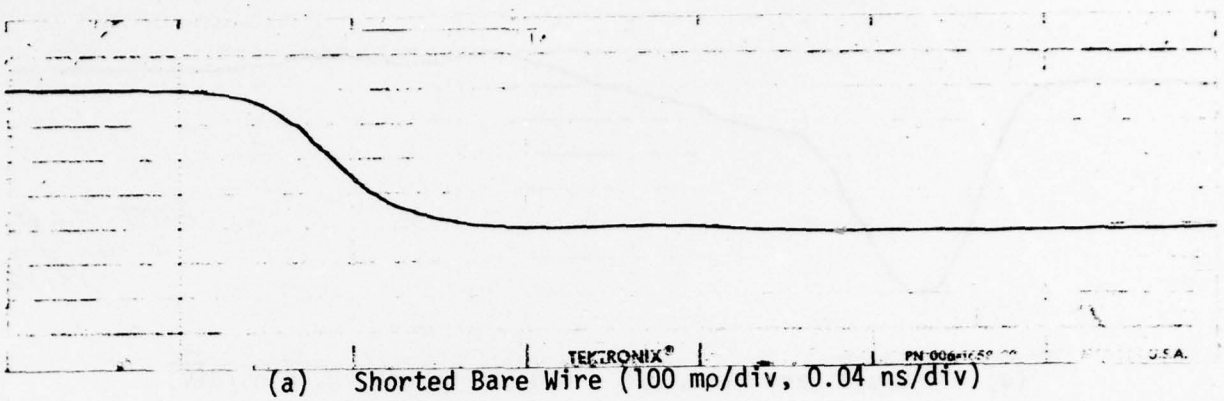

(a) Shorted Bare Wire (100 mρ/div, 0.04 ns/div)

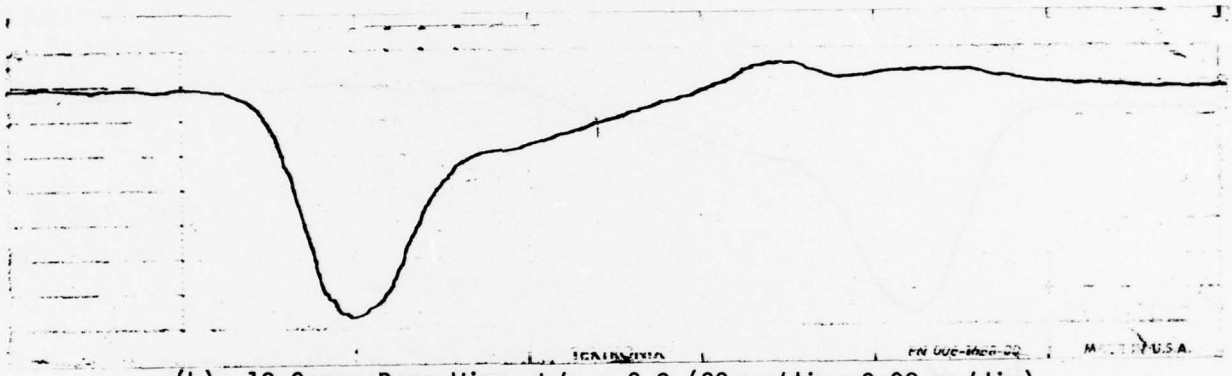

(b) 18-Gauge Bare Wire, b/a = 2.0 (20 mρ/div, 0.08 ns/div)

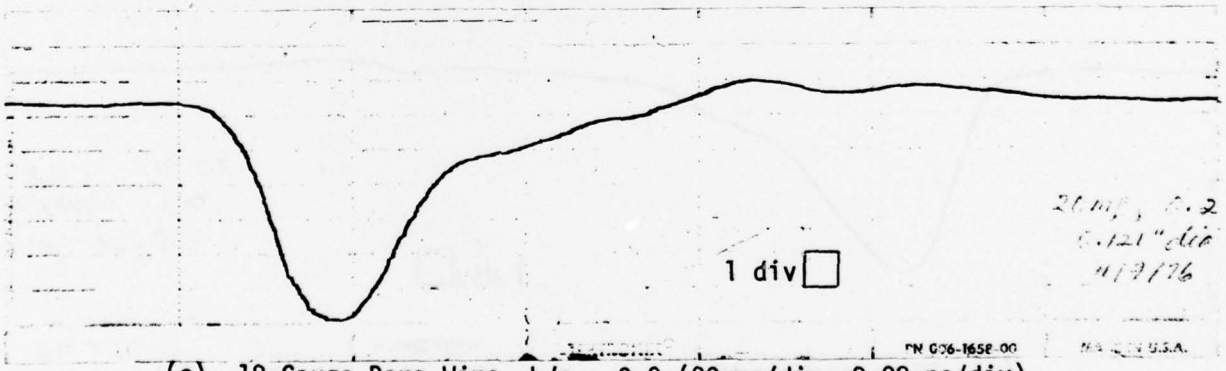

(c) 18-Gauge Bare Wire, b/a - 3.0 (20 mρ/div, 0.08 ns/div)

Figure 58. Reflections from a Bulkhead Mockup (thin plate)

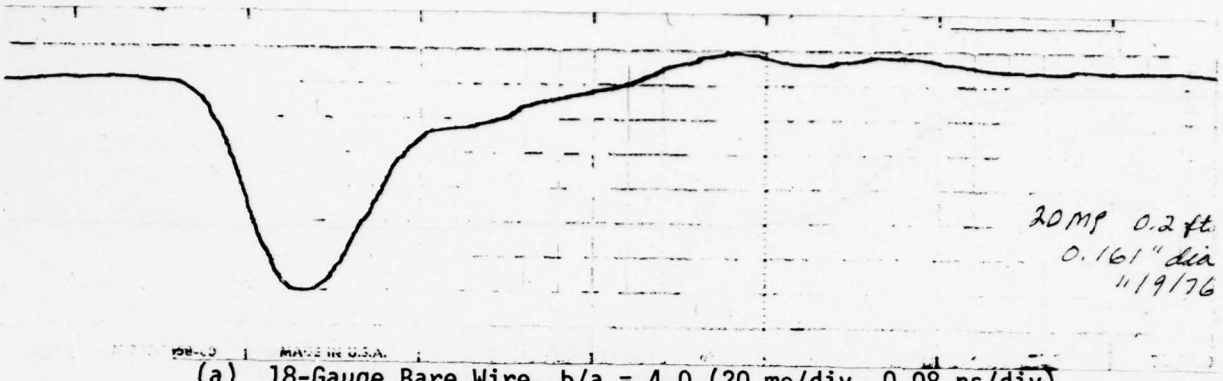

(a) 18-Gauge Bare Wire, b/a = 4.0 (20 mp/div, 0.08 ns/div)

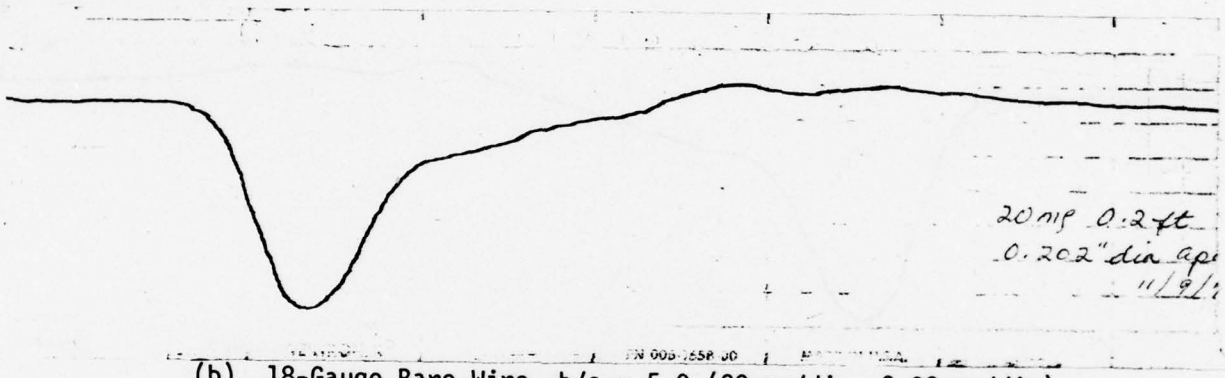

(b) 18-Gauge Bare Wire, b/a = 5.0 (20 mp/div, 0.08 ns/div)

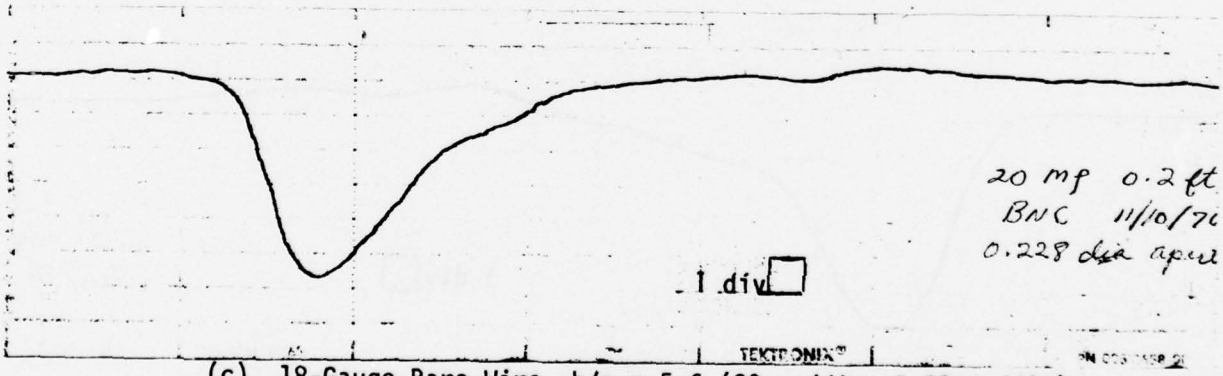

(c) 18-Gauge Bare Wire, b/a = 5.6 (20 mp/div, 0.08 ns/div)

Figure 59. Reflections from a Bulkhead Mockup (thin plate)

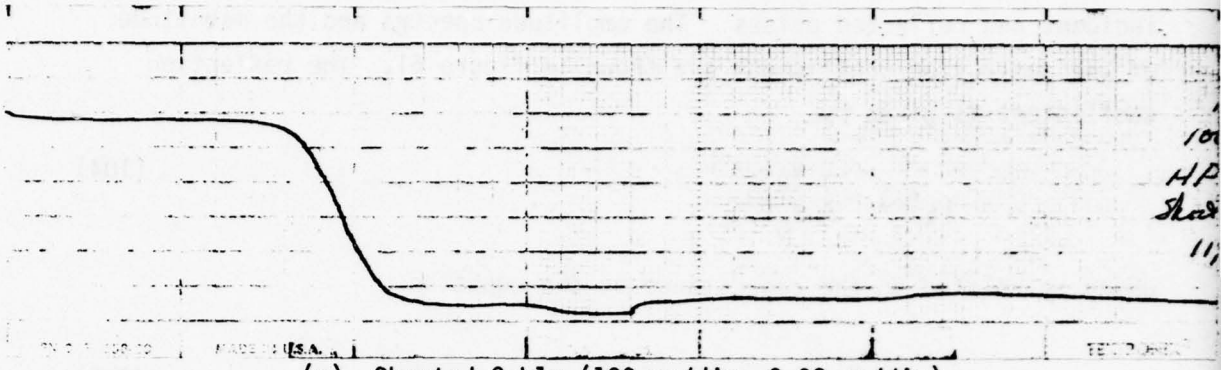

(a) Shorted Cable (100 mρ/div, 0.08 ns/div)

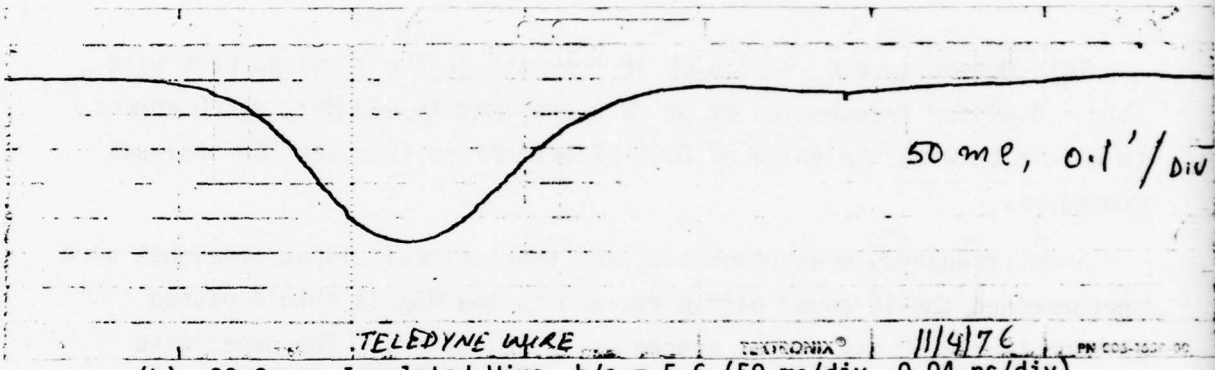

(b) 20-Gauge Insulated Wire, b/a = 5.6 (50 mρ/div, 0.04 ns/div)

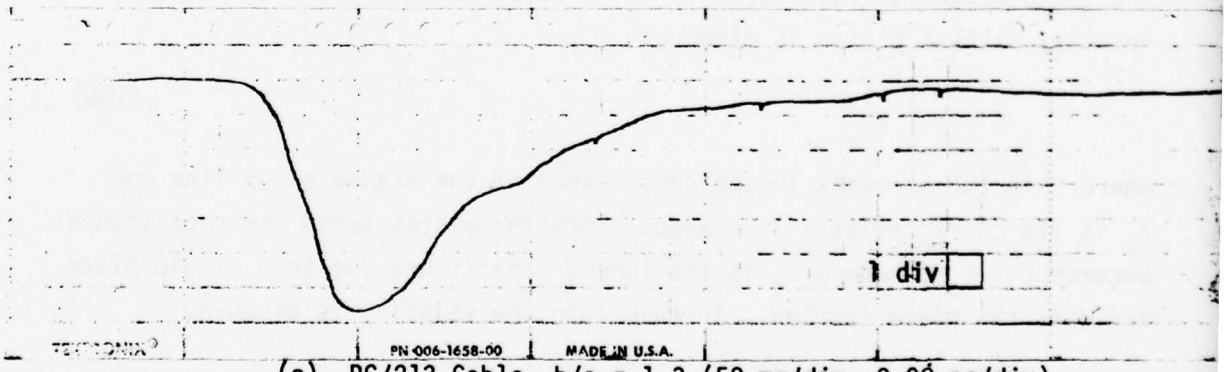

(c) RG/213 Cable, b/a = 1.3 (50 mρ/div, 0.08 ns/div)

Figure 60. Reflections from a Bulkhead Mockup (thick plate)

incident and reflected pulses. The amplitude spectra and the magnitude of the reflection coefficient are shown in figure 61. The reflection coefficient is given by

$$\rho_L(\omega) = \frac{1}{A} \frac{V_R(\omega)}{V_G(\omega)} \tag{104}$$

which is related to the capacitance by the equation

$$C_o = \frac{2}{\omega Z_c} \frac{|\rho_L|}{\sqrt{1 - |\rho_L|^2}} \tag{105}$$

This method gave C_o = 0.35 pF in the case of the 18 gauge bare wire (b/a = 5.6) for frequencies of up to approximately 400 MHz, which agrees to within 8% with the value of 0.38 pF determined from the TDR analysis procedure.

Swept frequency measurements of the short circuit input impedance were performed on the 18 gauge bare wire, and on the RG/213 shield passed through twelve 50 mil plates spaced on 50 cm centers. The capacitive loading caused by the periodically spaced plates was determined by measuring the propagation velocity with and without the plates. The propagation velocity without plates is given by

$$v = \frac{1}{CZ_c} \tag{106}$$

where C is the per unit length capacitance of the transmission line and Z_c is its characteristic impedance. With the plates added the capacitance becomes $C + C_o/d$, where C_o is the lumped capacitance due to a single plate and d is the plate spacing. In this case the velocity is given by

$$v' = \frac{1}{Z_c(C + C_o/d)} \tag{107}$$

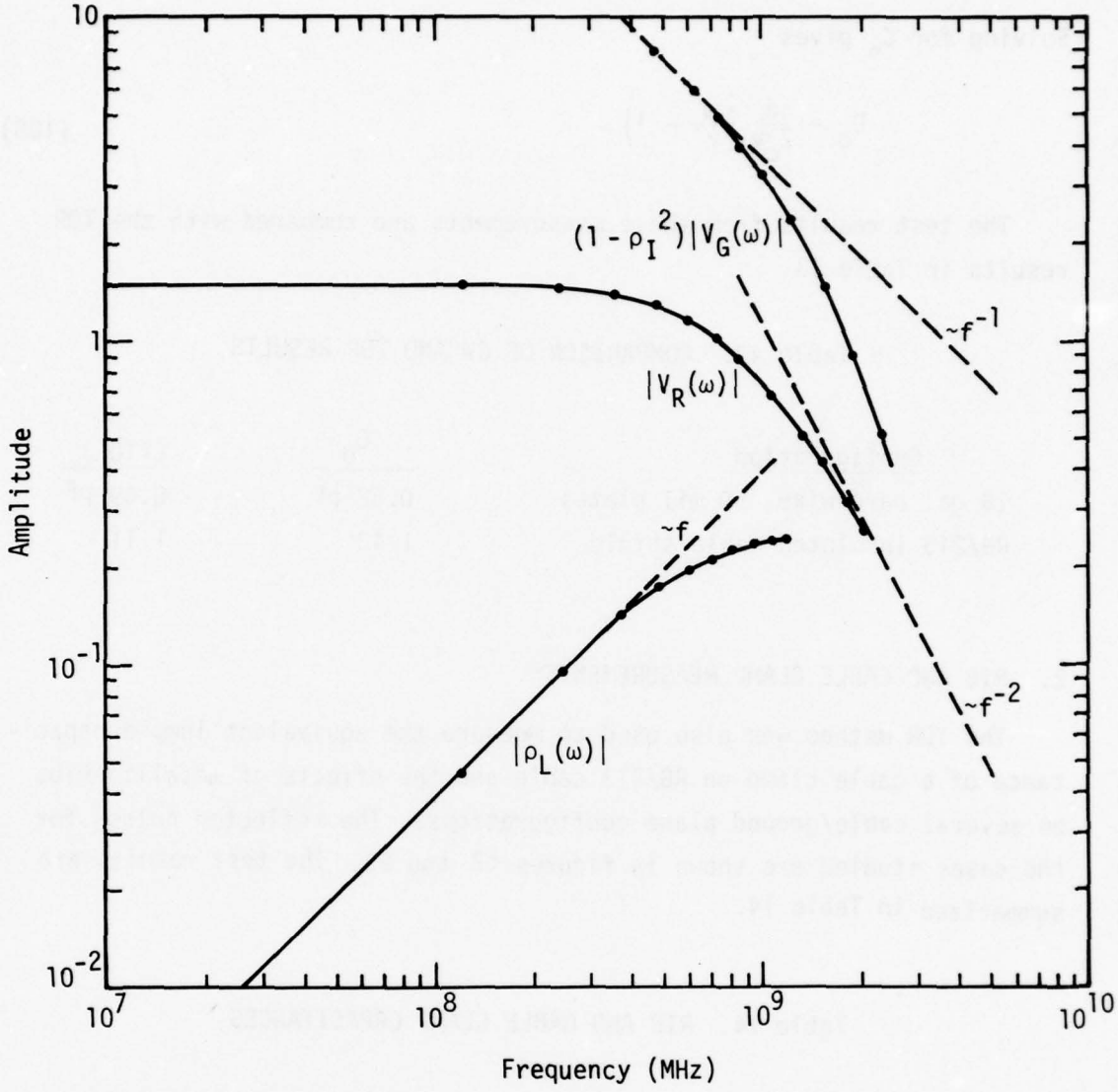

Figure 61. Incident and Reflected Amplitude Spectra and the Reflection Coefficient

Solving for C_o gives

$$C_o = \frac{d}{Z_c v}\left(\frac{v}{v'} - 1\right) \tag{108}$$

The test results from these measurements are compared with the TDR results in Table 13.

Table 13. COMPARISON OF CW AND TDR RESULTS

Configuration	C_o	C(TDR)
18 ga. bare wire, 50 mil plates	0.52 pF	0.49 pF
RG/213 insulated cable shield	1.43	1.11

2. RIB AND CABLE CLAMP MEASUREMENTS

The TDR method was also used to measure the equivalent lumped capacitance of a cable clamp on RG/213 cable and the effects of metallic ribs on several cable/ground plane configurations. The reflected pulses for the cases studied are shown in figures 62 and 63. The test results are summarized in Table 14.

Table 14. RIB AND CABLE CLAMP CAPACITANCES

Configuration	C_o(pF)
RG/213 supported by metal ribs	3.4
RG/213 1.3 cm above metal ribs	0.55
RG/213 2.5 cm above metal ribs	0.39
RG/213 with cable clamps	2.8
20 ga. wire supported by metal ribs	1.4
18 ga. bare wire 1.3 cm above metal ribs	0.27

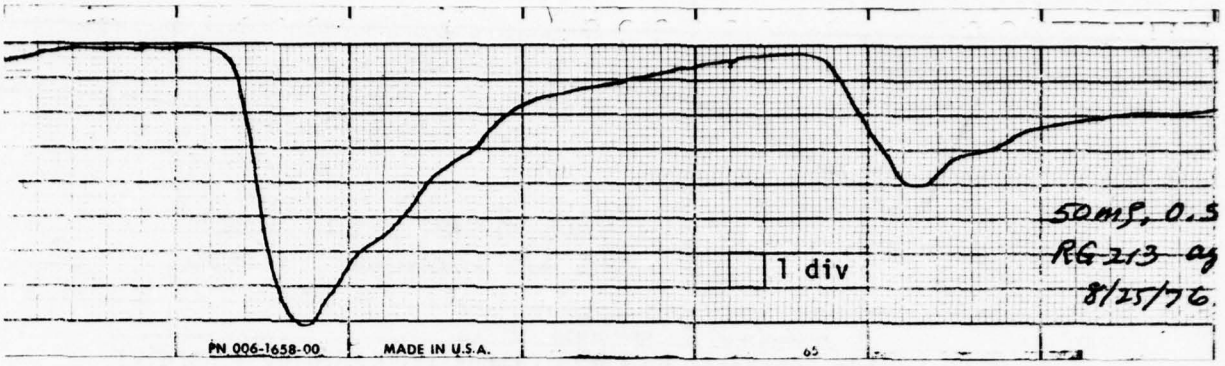

(a) RG/213 Cable Supported by Ribs (50 mρ/div, 1 ns/div)

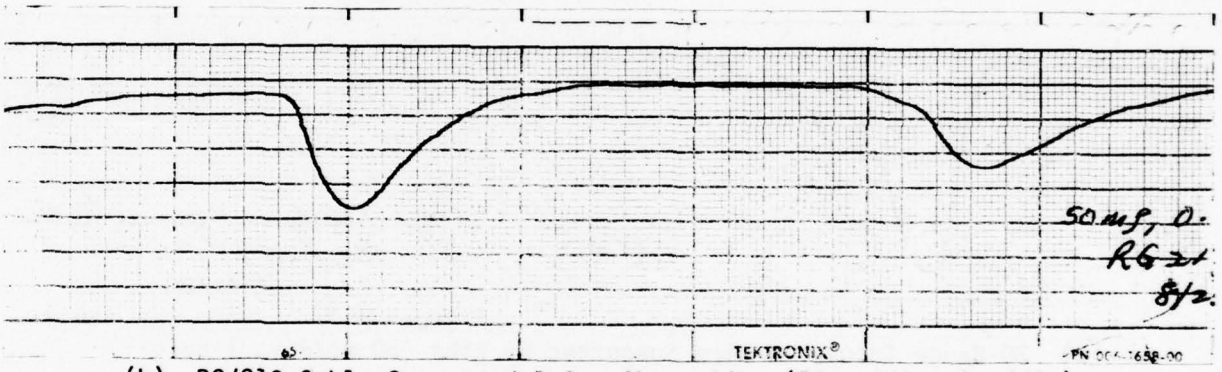

(b) RG/213 Cable Supported 1.3cm Above Ribs (50 mρ/div, 1ns/div)

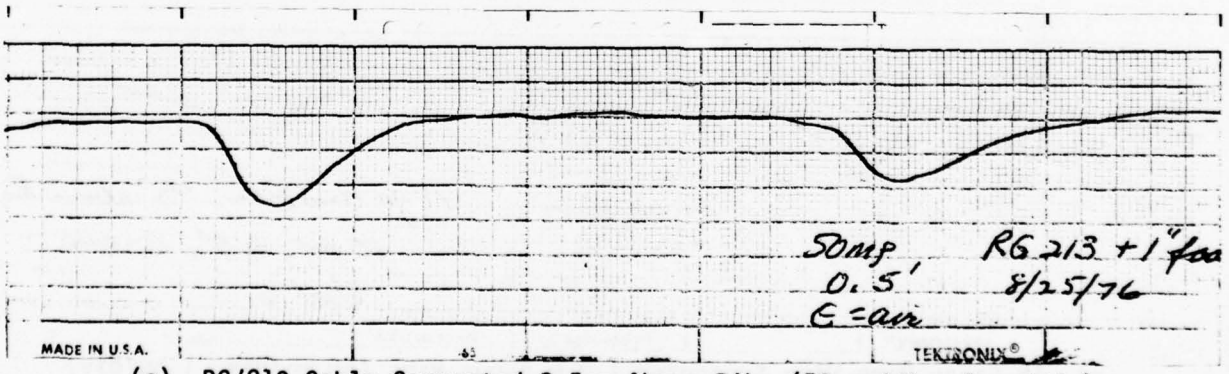

(c) RG/213 Cable Supported 2.5cm Above Ribs (50 mρ/div, 1 ns/div)

Figure 62. TDR Reflections Caused by Ribs

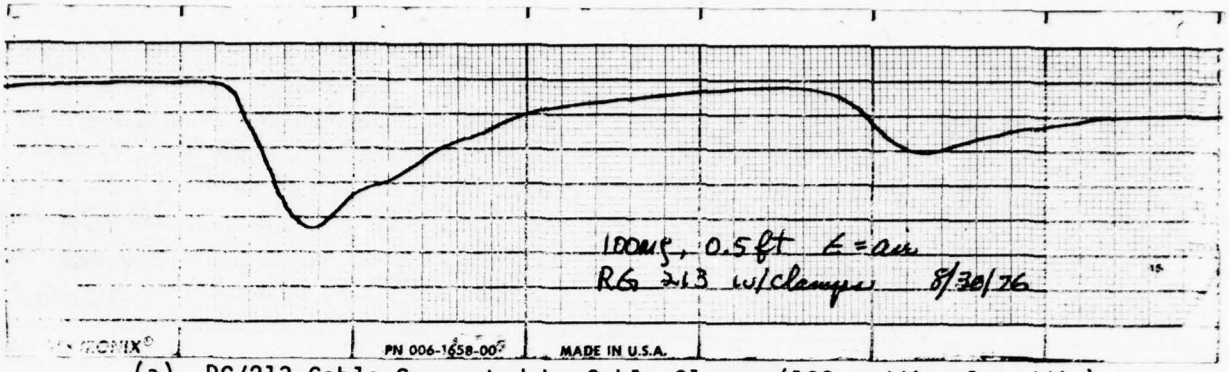

(a) RG/213 Cable Supported by Cable Clamps (100 mρ/div, 1 ns/div)

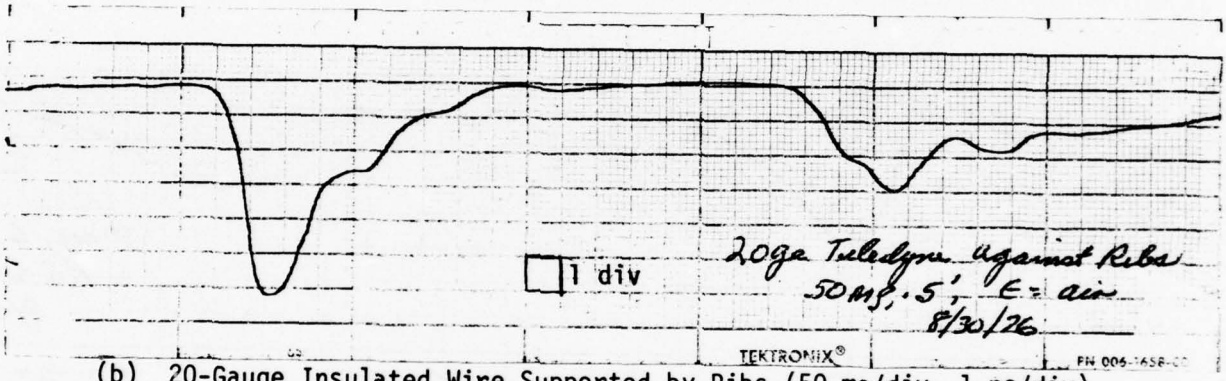

(b) 20-Gauge Insulated Wire Supported by Ribs (50 mρ/div, 1 ns/div)

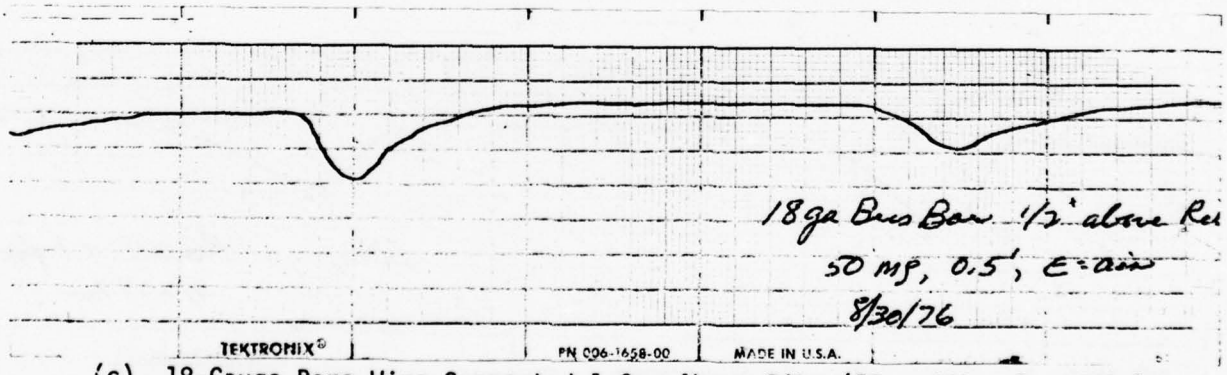

(c) 18-Gauge Bare Wire Supported 1.3cm Above Ribs (50 mρ/div, 1 ns/div)

Figure 63. TDR Reflections Caused by Cable Clamp and Ribs

SECTION VII

CONCLUSIONS AND OBSERVATIONS

The investigation of multiwire cables demonstrated that the per unit length self and mutual capacitance and inductance could be accurately determined from open circuit and short circuit impedance measurements using commonly available laboratory equipment. The methods developed are not restricted to electrically short cables. The propagation velocities associated with the eigenvalues of the [L][C] product were readily identified with the three allowed modes of propagation on the four conductor (3 wire cable above ground plane) model studied. Estimates of the inductance matrix elements based on simple geometric distance formulas were found to be in good agreement (4%) with the measured values. The free space capacitance matrix elements obtained by inversion of the calculated [L] matrix were within 9% of the values obtained from detailed computer calculations; however, the same procedure using the measured [L] matrix gave errors of up to 44% in [C]. This result is due to the ill-conditioned nature of the [L] matrix when inverted and used to compute [C]. The determination of [C] from [L] is further complicated by the uncertainty in the effective dielectric constant of the material surrounding the cable.

Multimode propagation was investigated using a three-conductor line (two wires above a ground plane). The common mode and differential mode characteristic impedances and propagation velocities were determined from swept cw measurements and by time domain reflectometry. The results were found to be in excellent agreement and accurately described by separate Thevenin equivalent circuits for each mode of propagation. It was found that the two modes of propagation could be observed easily in the time domain using the pulse tracing method described in Section II of this report.

Studies of the propagation of electromagnetic signals along cables, which are supported by metallic ribs or which pass through cable clamps

or bulkheads, demonstrated that these effects can generally be modeled as lumped shunt capacitive loads spaced periodically along the cable. This simplification is valid at low frequencies where the periodic spacing between ribs, cable clamps, etc., is a small fraction of a wavelength ($< \lambda/10$) at the highest frequency of interest. For the cases studied the spacing was 50 cm and the low frequency model was valid below approximately 60 MHz. At higher frequencies the periodic loading leads to stop band and pass band behavior and the analysis is more complicated (ref. 12).

The capacitance of ribs, cable clamps, and bulkheads was measured for a number of specific cases using TDR methods. The results are tabulated in Section VI of this report.

Common mode propagation on multiconductor cables containing up to 20 wires was investigated for several configurations. In all cases where the spacing of the cable relative to its local ground reference was well defined, the measured impedance of the bulk cable was found to be in good agreement with the calculated impedance of a single wire equivalent with an effective radius approximately 70% to 80% of the actual cable radius and with an equivalent spacing from the ground reference equal to the average spacing of the conductors. Cables lying on a ground plane, inside conduit, or in a corner exhibited impedance levels that were higher than given by ideal case calculations. The increase was due to the fact that the cables did not lay flat against the conducting surface, and the equivalent height averaged over the length of the cable was larger than the cable radius. The uncertainty in cable position was investigated further for the case of a single wire in conduit. Monte Carlo calculations of the most likely impedance gave results in good agreement with the measurements in small conduit. This technique is useful in those cases where the random wire location is bounded and the proper weighting function can be determined. The effective dielectric constant for those cases in which the cables were laying on a conducting surface was observed to be approximately 60% of that of the solid cable insulation material. The cable losses exhibited

a nearly linear increase with frequency at the higher frequencies, consistent with shunt losses caused by the conductance of the PVC wire insulation.

The measurements on cables lying in a corner were not compared with ideal case calculations. No theoretical formulation for this geometry was found after a review of several references.

Limited measurements of cables on the EC-135 were made early in this program (see Appendix A). These were useful in identifying the problems associated with *in situ* aircraft cable measurements and in defining typical cable environments, both mechanical and electrical, for which simple models were constructed and investigated.

REFERENCES

1. King, R. W. P., Transmission Line Theory, Dover Publications, Inc. New York, 1965.

2. Sunde, E. D., Earth Conduction Effects in Transmission Systems, Dover Publications, Inc. New York, 1968.

3. Weast, R. C. (Ed.), Handbook of Chemistry and Physics (51st ed.), The Chemical Rubber Co. Cleveland, 1970.

4. Papoulis, A., The Fourier Integral and Its Applications, McGraw-Hill. New York, 1962.

5. Terman, F. E., Radio Engineers Handbook, McGraw-Hill. New York, 1943.

6. Frankel, S., Cable and Multiconductor Transmission Line Analysis, HDL-TR-091-1, Harry Diamond Laboratories, 28 June 1974.

7. Uchida, H., Fundamentals of Coupled Lines and Multiwire Antennas, Sasaki Printing and Publishing Co. Sendai, Japan, 1967.

8. The Boeing Company, Parameters for Aircraft Cables, D224-10015-1, The Boeing Company, 19 June 1974.

9. Cretella, J. P. and R. A. Pabst, "Analytical and Experimental Procedures for Determining Multiconductor Line Parameters," Joint EMP Technical Meeting (NEM 1973) Proceedings, Vol. III: Interaction and Coupling, pp. 259-291, 5 June 1975.

10. Lancaster, P., Theory of Matrices, Academic Press. Hew York, 1969.

11. International Telephone and Telegraph Corporation, Reference Data for Radio Engineers (5th Ed.), Stratford Press. New York, 1969.

12. Agrawal, A., Periodic Structure Analysis, AMRC-N-47, Mission Research Corporation, September 1976.

APPENDIX A

AIRCRAFT CABLE PARAMETER STUDY
EC-135 TEST REPORT

I. INTRODUCTION

The transmission line properties of single and multiconductor aircraft cables installed as part of the normal wiring aboard the EC-135 aircraft were investigated using Time Domain Reflectometry (TDR) methods. The work was originally planned for later in the program; however, due to the nonavailability of the EC-135 after 31 July 1976, it was necessary to perform the measurements on short notice during the period from 6 July 1976 to 28 July 1976. The EC-135 was committed for vulnerability testing throughout this period, and the cable measurements had to be made on a noninterference basis during short intervals (approximately 2 hours daily) when the aircraft was accessible to MRC personnel. The rushed schedule did not allow sufficient time to construct cable interface connectors or to disconnect the loads of those cables which terminated in relatively inaccessible locations. The quality of the experimental data obtained under these conditions was not as high as that which could have been attained had more time been available. However, useful information on the common mode impedance levels, propagation velocities, and the losses of four different cable/airframe geometries was obtained from the experiments.

II. INSTRUMENTATION

The measurements were performed with a Tektronix Model 1502 Cable Tester. This instrument is a small portable unit which can operate for up to 5 hours on internal rechargeable batteries. The output pulse is a 225 mV step function with a rise time of 0.1 nanosecond at an impedance level of 50 ohms. The incident and reflected pulses are sampled and displayed on an oscilloscope which is internally calibrated to read in units of the reflection coefficient on the vertical axis. The horizontal axis displays the one way distance in feet. The unit is equipped with a plug-in strip chart recorder module for permanently recording the TDR traces.

Pretest calibration was performed by checking the step voltage amplitude and adjusting the gain to give an amplitude that corresponds to $\rho = 1$ with the output terminated in a precision 50 ohm load. No special calibration was required during operation. The specified accuracy is ±3% in amplitude and ±2% in distance.

III. RESULTS

A. Cable M1

1. Description

Cable M1 is an unshielded bundle 14.4 feet in length which connects Monitor Receiver AN/ARR-71 and Control Panel C-3811/AR in the Radio Operator's Console. The bundle contains approximately 50 wires and is tied to other bundles at various points along its route. From the receiver, the cable runs along the equipment rack frame, crosses over to and runs along the fuselage, then loops back to the rear of Radio Operator's Console. There is a three-wire breakout at 14 inches and a two-wire breakout at 56 inches from the receiver. A diagram of the cable layout is shown in Figure A1.

2. Results

TDR measurements were made from the receiver end of the cable with the far end connected and disconnected from the control panel. The driven end was coupled to the TDR by shorting together all of the pins of the cable connector with a copper disk attached to a length of RG 58/u cable. No shorting connector was available for the 55 pin female connector at the control panel and no short circuit measurements were obtained. Representative strip chart records selected from the available recordings are shown in Figures A2 and A3 with the far end connected and disconnected.

Cable Description		Approximate Ground Plane Distance
A-B	Loop to Receiver Connector	1 to 5 inches
B-C	Tied to Rack Frame (Horizontal)	1 inch
C-D	Tied to Rack Frame (Vertical)	1 inch
D-E	Crosses Between Rack & Fuselage	1 to 20 inches
E-F	Parallel to Fuselage	3 to 10 inches
F-G	Loop From Fuselage to Rack Frame	3 to 20 inches
G-H	Tied to Rack Frame	1 inch
H-I	Loop to Control Panel Connector	1 to 6 inches

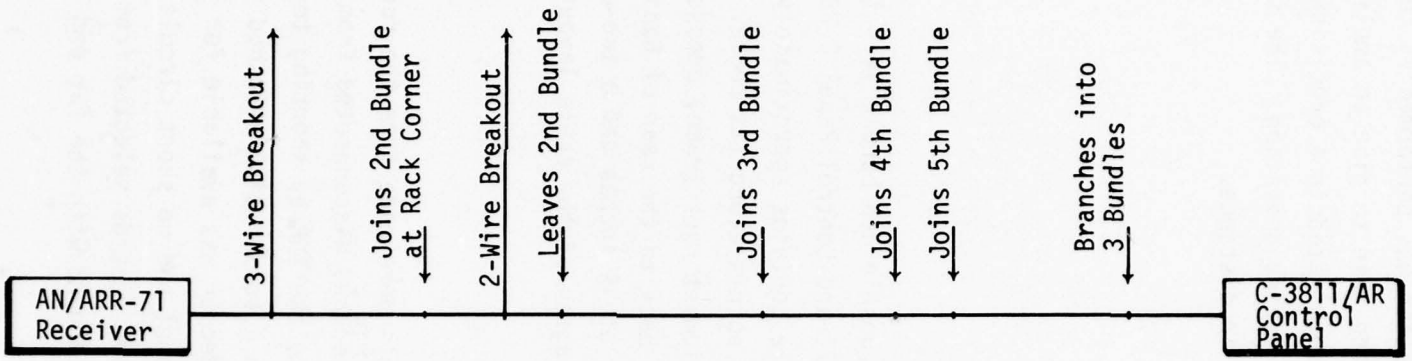

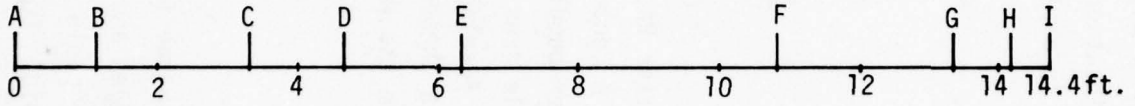

Figure A1. Cable M1 Layout

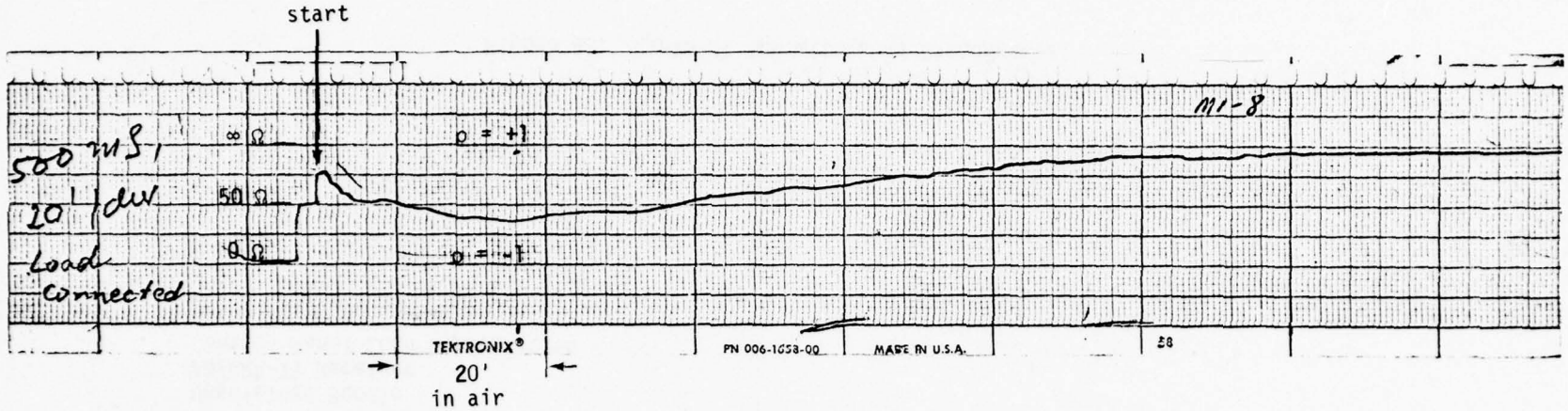

Unshielded Bundle
AN/ARR-71 Receiver
Control Panel Load Connected

Figure A2. Cable M1 TDR with Load Connected

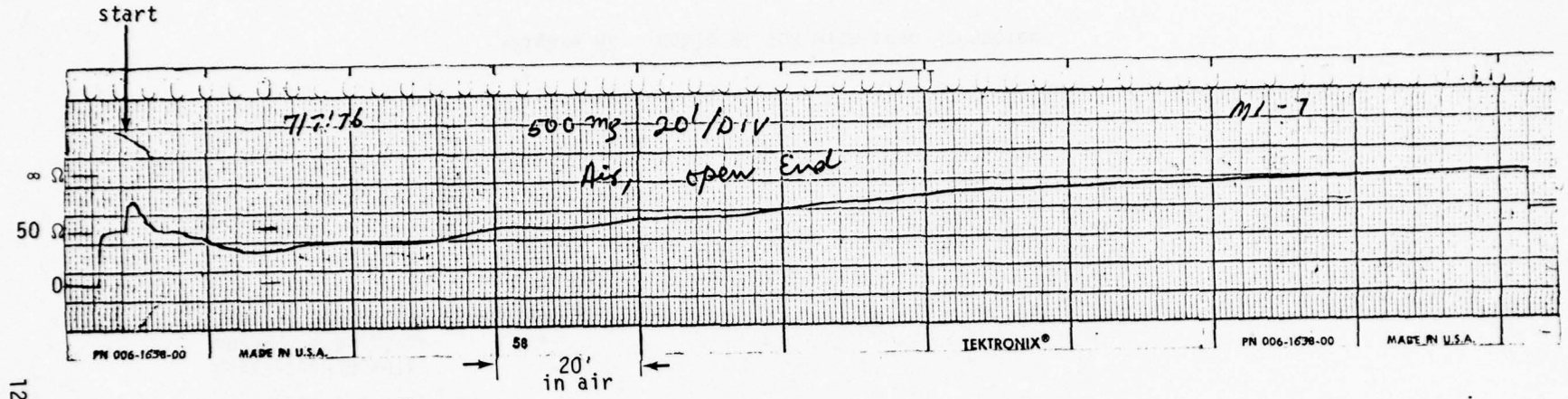

Unshielded Bundle
AN/ARR-71 Receiver
Control Panel Load Disconnected

Figure A3. Cable M1 TDR with Load Disconnected

The records show an initial spike caused by the inductance of the cable interface connection. The spike decays exponentially with time and is negligible after approximately 12 nanoseconds (6 ft.). The impedance level recorded prior to the arrival of the end reflection varies between 20 and 50 ohms. A distinct end reflection is not present; however, it is estimated to occur between 23 and 26 feet. This estimate was made by comparing records obtained with the load connected and disconnected. The records overlay over the first 23 feet or so and begin to depart thereafter. Reflections from the cable breakouts at 1.2 and 4.7 feet are hidden by the inductive spike.

No correlation could be found between the TDR impedance profile and the physical layout of the cable.

The effective dielectric constant that corresponds to the electrical length of the cable is in the range

$$\varepsilon' = (\ell_e/\ell)^2 = 2.6 \text{ to } 3.3. \qquad \text{(A1)}$$

The corresponding propagation velocity is then

$$v_p = c/\sqrt{\varepsilon'} = 0.55c \text{ to } 0.62c. \qquad \text{(A2)}$$

B. Cable M2

1. Description

Shielded RG 115/u coaxial cable is 107 feet in length which connects the antenna coupler in the left wing tip to Liaison Radio Receiver #2. The cable route from the receiver is along the inside of the fuselage and outward along the wing leading edge to the coupler.

2. Results

TDR recordings were obtained on this cable by driving the shield/airframe geometry through a clip lead interface from the Receiver end of the cable. Representative records are presented in Figures A4 and A5. The cable end reflection is clearly observed and corresponds to an electrical length of 163 feet. The impedance varies between 85 and 110 ohms over the length of the cable run due to the changing shield/airframe geometry with distance and the presence of other cables.

The effective cable loss can be estimated from the rise time of the reflected pulse. The formula which relates the 10/90% rise time to the attenuation is*

$$\alpha_o = 2.74\ (f_o t_r)^{\frac{1}{2}}/(2\ell) \qquad \text{(A3)}$$

where α_o is the attenuation in dB/ft., ℓ is the physical length of the cable in feet, f_o is the frequency in Hz. The rise time from Figure A4 is 120 nanoseconds which gives the following attenuation:

f_o	α_o
10 MHz	0.014 dB/ft
50 MHz	0.032 dB/ft
100 MHz	0.045 dB/ft

Figure 6 shows the center conductor/outer shield impedance profile used to determine the physical length of the cable. The physical length was found to be 107 feet from this record. The effective dielectric constant is $\varepsilon' = (\ell_e/\ell)^2 = 2.3$ and the corresponding propagation velocity is $v_p = 0.66c$.

*Tektronix Application Note 25M1.0

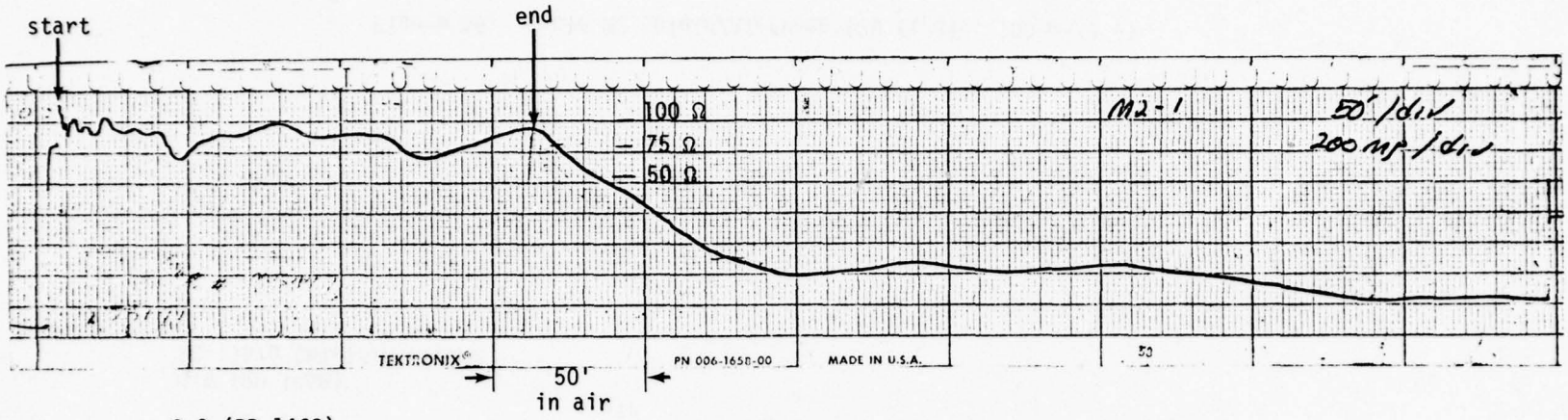

G-9 (RD 1468)
RG-115/u Shield/Airframe

Figure A4. Cable M2 Shield/Airframe (50 ft/div, 200 mp/div)

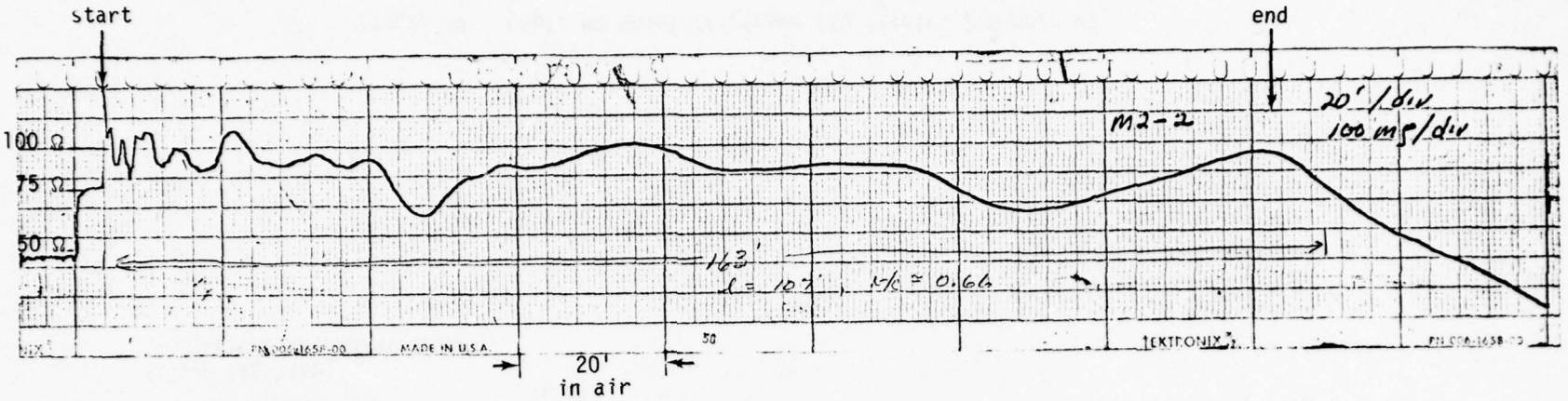

G-9 (RD 1468)
RG-115/u Shield/Airframe

Figure A5. Cable M2 Shield/Airframe (20 ft/div, 100 mμ/div)

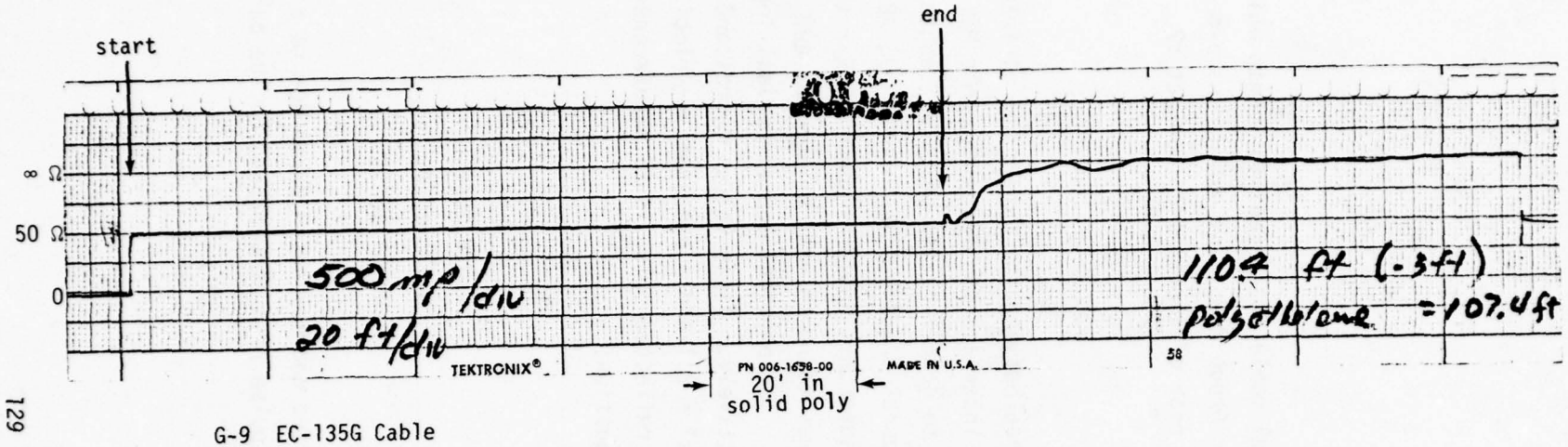

G-9 EC-135G Cable
RG-115/u

Figure A6. Cable M2 Coax Drive TDR (20 ft/div, 500 mρ/div)

C. Cable M3

1. Description

Shielded RG 216/u coaxial cable is 12 feet in length which runs from connector RD 6372 to Receiver Group M-4. The cable runs along the ceiling and loops over to the rear of Electronics Cabinet #2.

2. Results

TDR measurements were made between the shield and airframe of this cable with the same cable interface as used with Cable M2. Coax drive measurements were also made to determine the physical length of the cable run. Representative records are shown in Figures A7, A8, and A9 for short and open circuit measurements and in Figure A10 for the coax drive. The impedance level was found to vary between 68 and 83 ohms along the cable/airframe geometry. The physical and electrical lengths measured 12.0 and 17.2 feet respectively. These values correspond to an effective dielectric constant of $\varepsilon' = 2.1$ and a propagation velocity of $v_p = 0.70c$. The rise time of the reflected pulse is 26 nanoseconds and corresponds to the following attenuation:

f_o	α_o
10 MHz	0.059 dB/ft
50 MHz	0.131 dB/ft
100 MHz	0.185 dB/ft

These values are higher than expected and may be in error due to a possible lengthening of the input pulse rise time caused by the cable interface connection.

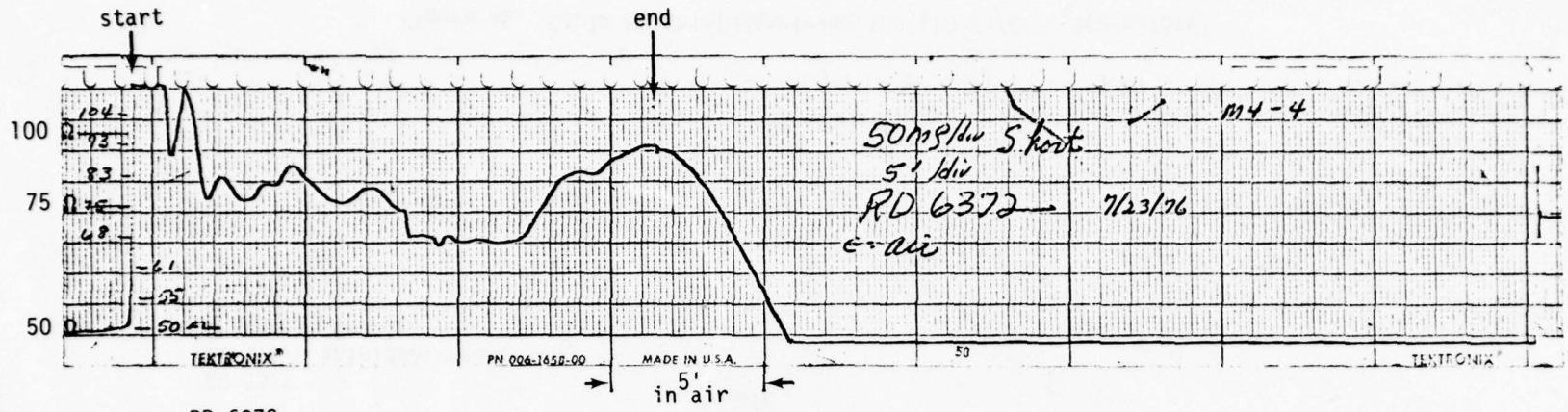

RD 6372
RG 216/u Shield/Airframe
Driven at Coupler

Figure A7. Cable M3 Shield/Airframe TDR (5 ft/div, 50 mρ/div)

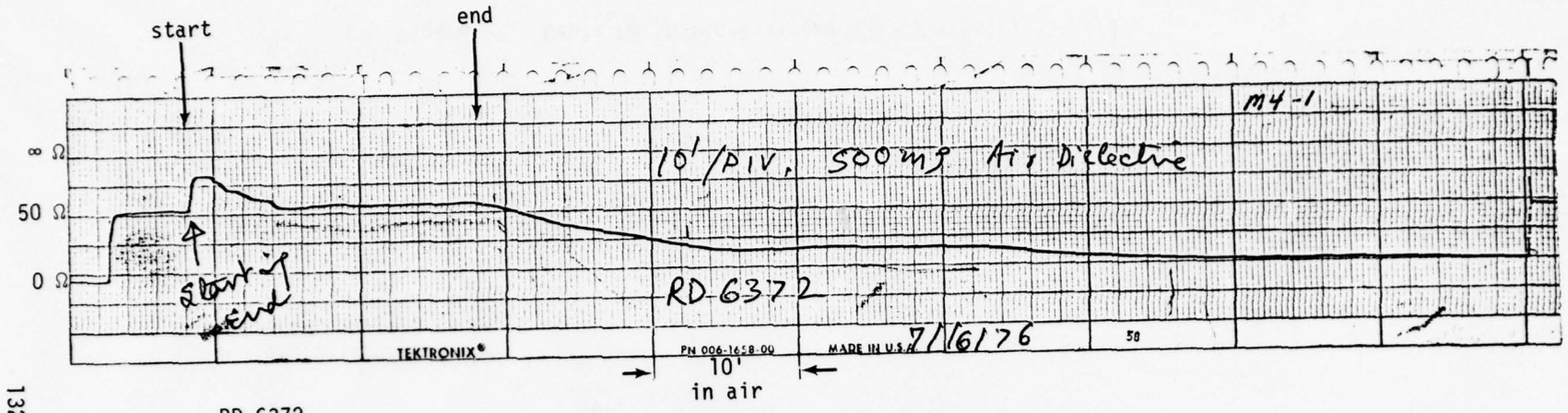

132

RD 6372
RG 216/u Shield/Airframe
Driven at Coupler

Figure A8. Cable M3 Shield/Airframe TDR (10 ft/div, 500 mρ/div)

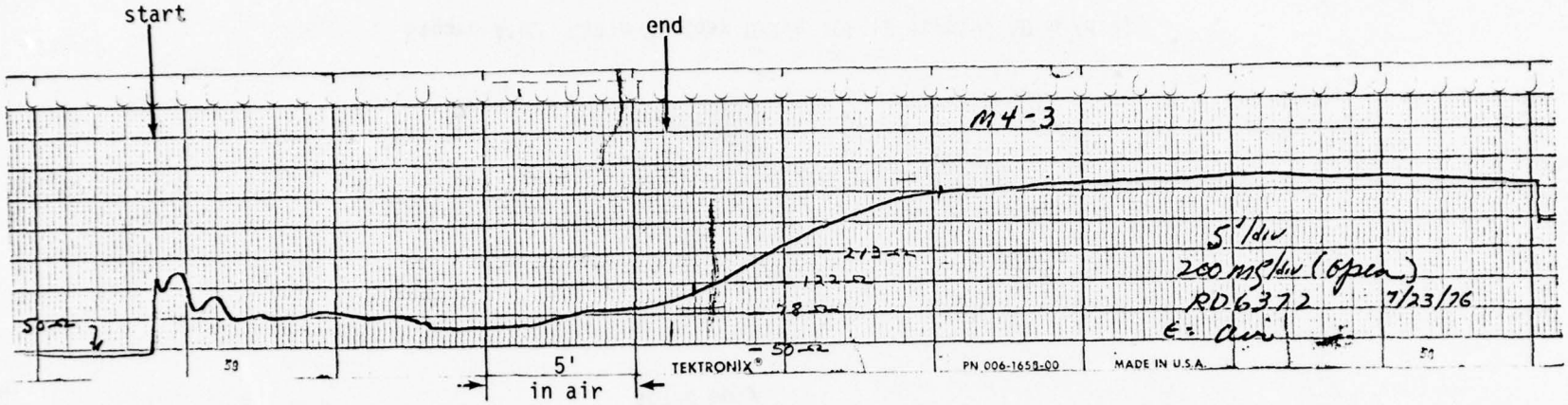

RD 6372
RG 216/u Shield/Airframe
Driven at Coupler

Figure A9. Cable M3 Shield/Airframe TDR (5 ft/div, 200 mp/div)

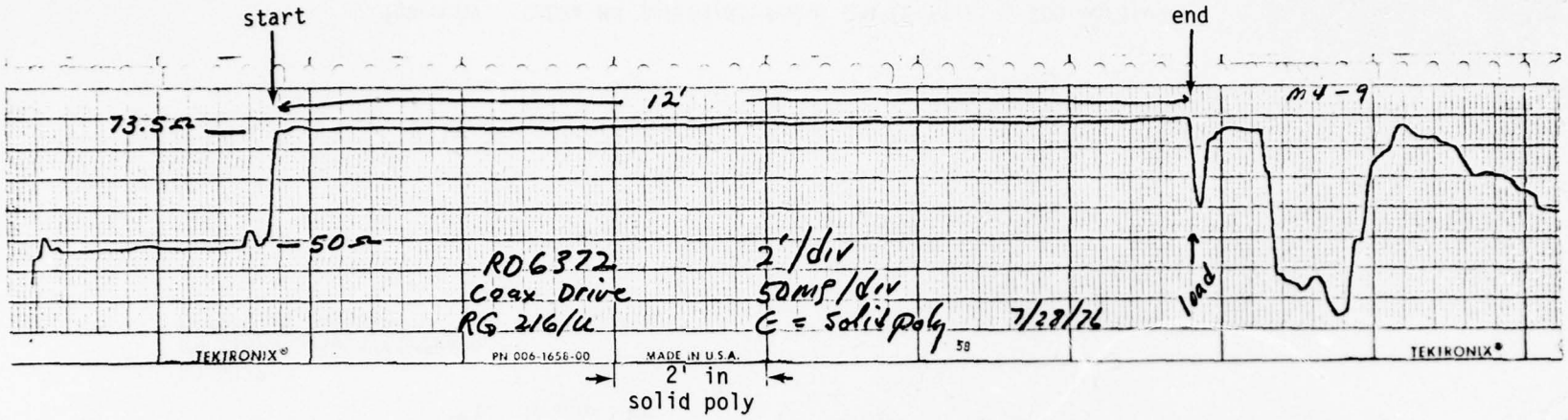

Figure A10. Cable M3 Coax Drive TDR (2 ft/div, 50 mp/div)

D. Cable M4

1. Description

Shielded RG 214/u coaxial cable is 137 feet in length which connects Liaison Receiver #1 and the probe antenna coupler located at the top of the vertical stabilizer. The cable runs along the ceiling to the tail, and up to the antenna coupler located at the top of the vertical stabilizer.

2. Results

Representative shield/airframe TDR records for this cable are shown in Figures A11 and A12. Figure A13 is a TDR trace using a coax drive. The physical and electrical lengths measured from these records give 137 and 194 feet respectively. This results in an effective dielectric constant of 2.0 and a propagation velocity of 0.66c. The impedance was found to vary between 60 and 75 ohms along the cable run. The rise time of the reflected pulse measures 267 nanoseconds and corresponds to the following attenuation:

f_o	α_o
10 MHz	0.016 dB/ft
50 MHz	0.036 dB/ft
100 MHz	0.052 dB/ft

IV. TRANSMISSION LINE ANALYSIS OF CABLE M2

A. Introduction

Swept frequency measurements of the transfer function obtained by driving the shield of this cable with a toroid and monitoring the shield current at the driving point and at the end of the cable were

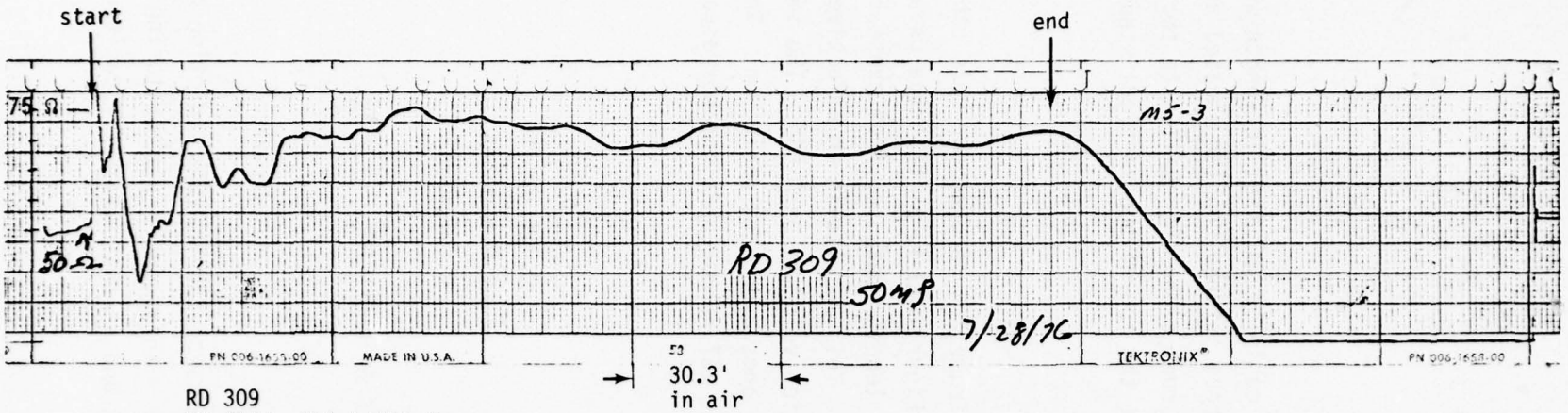

Figure A11. Cable M4 Shield/Airframe TDR (30.3 ft/div, 50 mΩ/div)

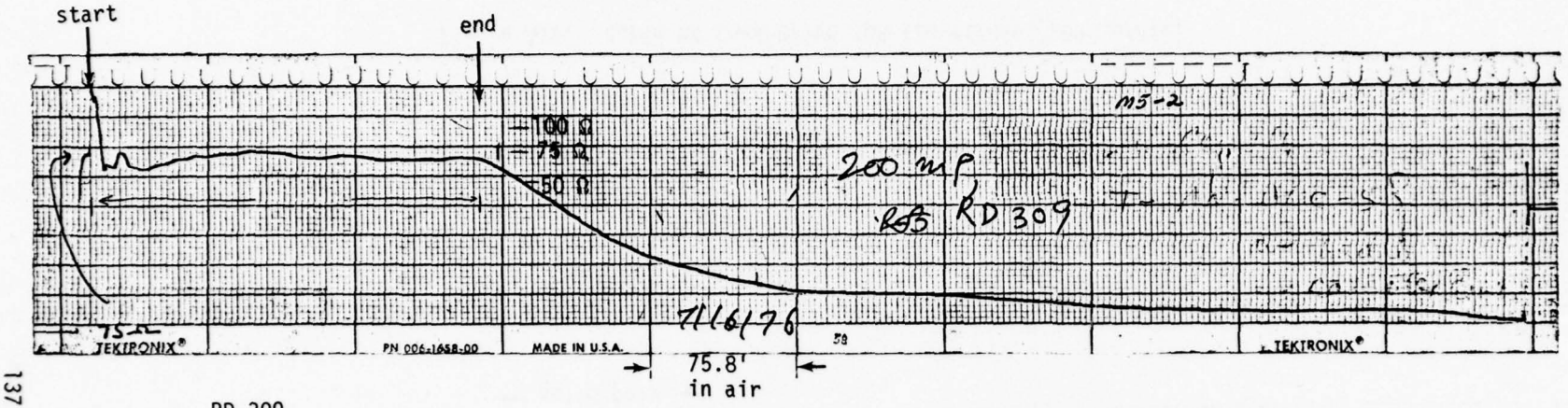

RD 309
RG 214/u Shield/Airframe

Figure A12. Cable M4 Shield/Airframe TDR (75.8 ft/div, 200 mp/div)

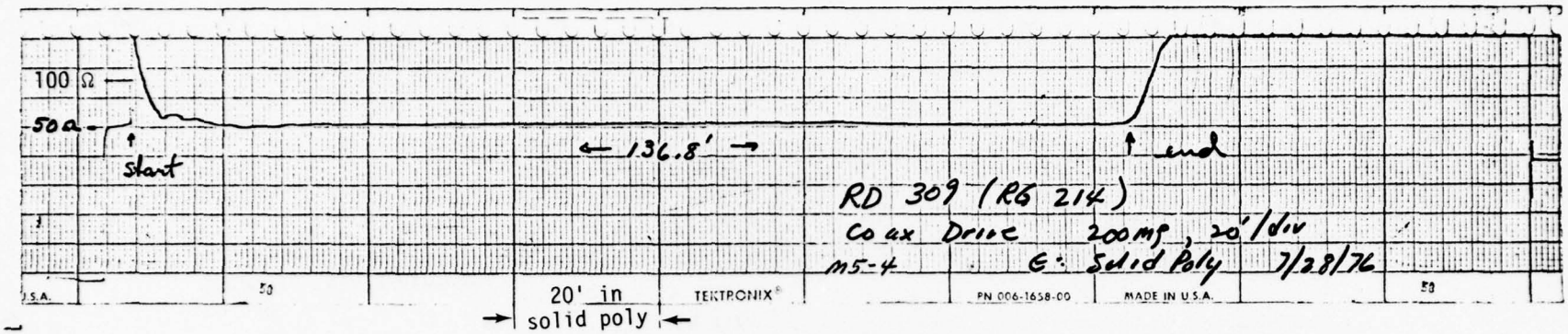

Figure A13. Cable M4 Coax Drive TDR (20 ft/div, 200 mp/div)

performed by other contractors. Their results for the 0.1 to 11 MHz frequency range are shown in Figure A14. These data have been analyzed to obtain an independent measurement of the effective propagation velocity for comparison with the TDR results.

B. Analysis

In general, the current at any cross section of a transmission line is given by the relation

$$I_z = \frac{V_o^e}{D} (Z_s \sinh \gamma\omega + Z_c \cosh \gamma\omega) \tag{A4}$$

where, $\omega = s-z$, $\gamma = \alpha+j\beta$, Z_c is the characteristic impedance. Z_o and Z_s are the termination impedances as shown in Figure A15.

For the case of a coaxial line whose shield is grounded at both the ends, as shown in Figure A16, and the current is induced at the input end of the shield, then the current at the output end is given by

$$I_s = \frac{V_o^e}{D} (Z_s \sinh \gamma\omega_s + Z_c \cosh \gamma\omega_s) \tag{A5}$$

and the current at the input end is

$$I_o = \frac{V_o^e}{D} [Z_s \sinh \gamma\omega_o + Z_c \cosh \gamma\omega_o] \tag{A6}$$

The current transfer function, which is the ratio of the output current to the input current, is

$$\frac{I_s}{I_o} = \frac{Z_s \sinh \gamma\omega_s + Z_c \cosh \gamma\omega_s}{Z_s \sinh \gamma\omega_o + Z_c \cosh \gamma\omega_o}$$

or

$$\frac{I_s}{I_o} = \frac{Z_c}{Z_s \sinh \gamma s + Z_c \cosh \gamma s} \tag{A7}$$

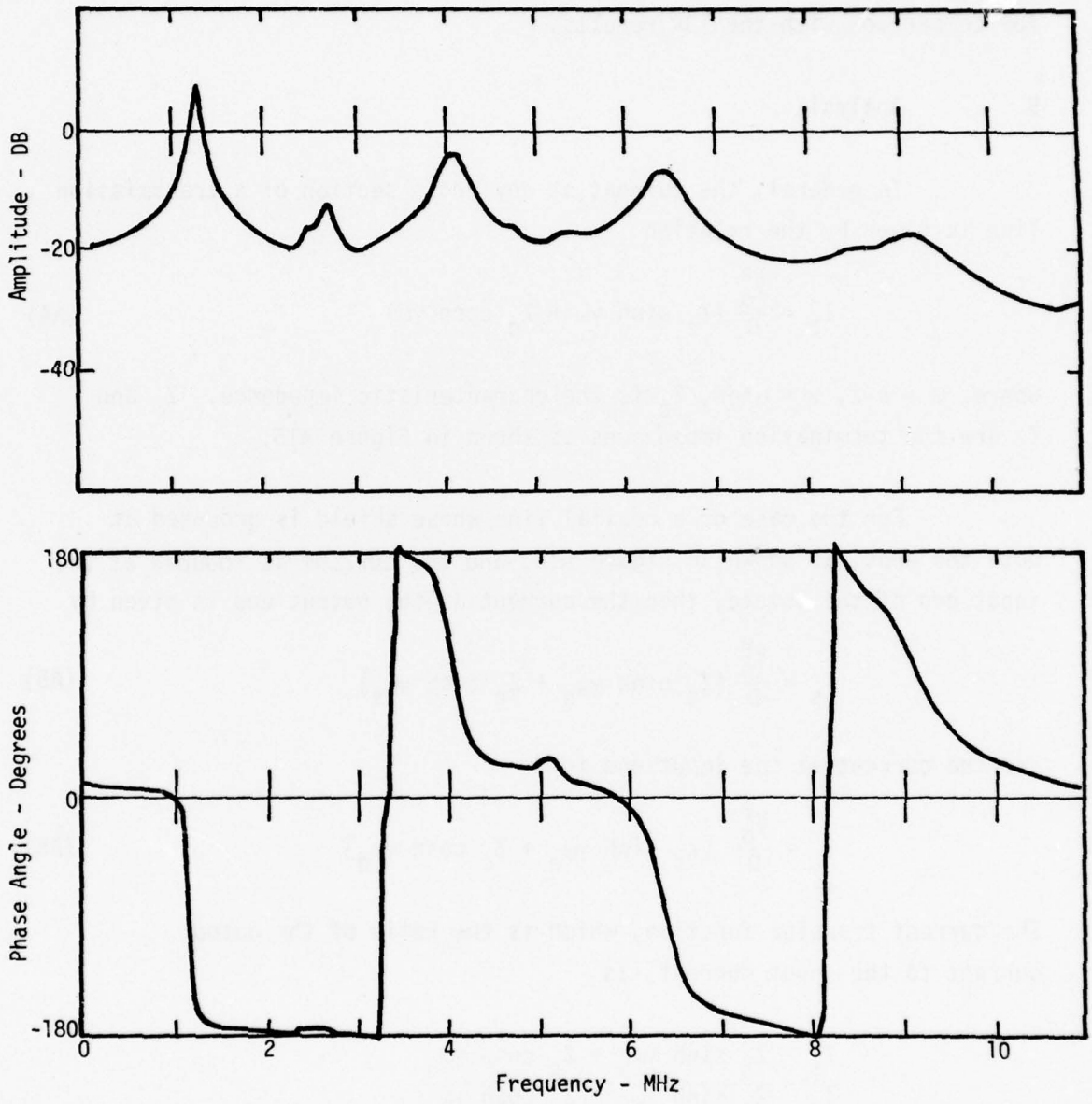

Figure A14. Cable M2 Measured Transfer Function

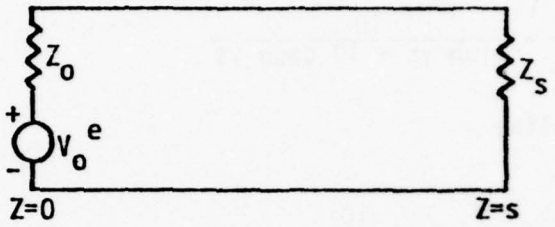

Figure A15. Equivalent Circuit

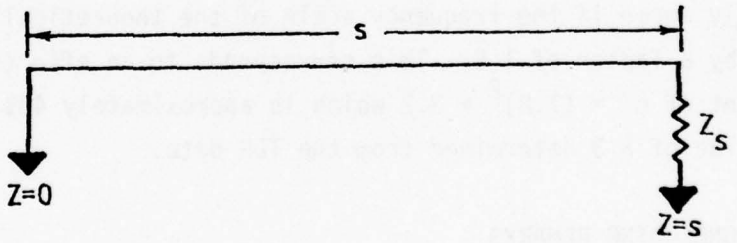

Figure A16. Cable M2 Idealized Circuit

In the above expression, it is assumed that the load impedance Z_s has a small value and is not a perfect short circuit. For the approximation $Z_s = Z_c/10$,

$$\frac{I_s}{I_o} = \frac{10}{\sinh \gamma s + 10 \cosh \gamma s}$$

for the lossless line

$$\frac{I_s}{I_o} = \frac{10}{10 \cos \beta s + j \sin \beta s} \qquad \text{(A8)}$$

Figure A17 shows the plot of magnitude and phase of the transfer function I_s/I_o versus frequency. For the cable length of 105 feet, the first maximum occurs at $\lambda/4$ and the successive maximas are $\lambda/2$ apart.

C. Results

Comparison of the experimental and theoretical frequency plots (Figures A14 and A17) shows that the frequencies at which maxima occur roughly agree if the frequency scale of the theoretical data is divided by a factor of 1.8. This corresponds to an effective dielectric constant of $\varepsilon' = (1.8)^2 = 3.2$ which is approximately 40% larger than the value of 2.3 determined from the TDR data.

V. CONCLUDING REMARKS

This study of aircraft cable characteristics was limited in scope due to the rushed time schedule and the short time period that was available for experimentation. The work was restricted to time domain reflectometry measurements from which the common mode impedance, propagation velocity, and an estimate of the losses of typical EC-135 cable/airframe geometries could be determined. Most of the objectives

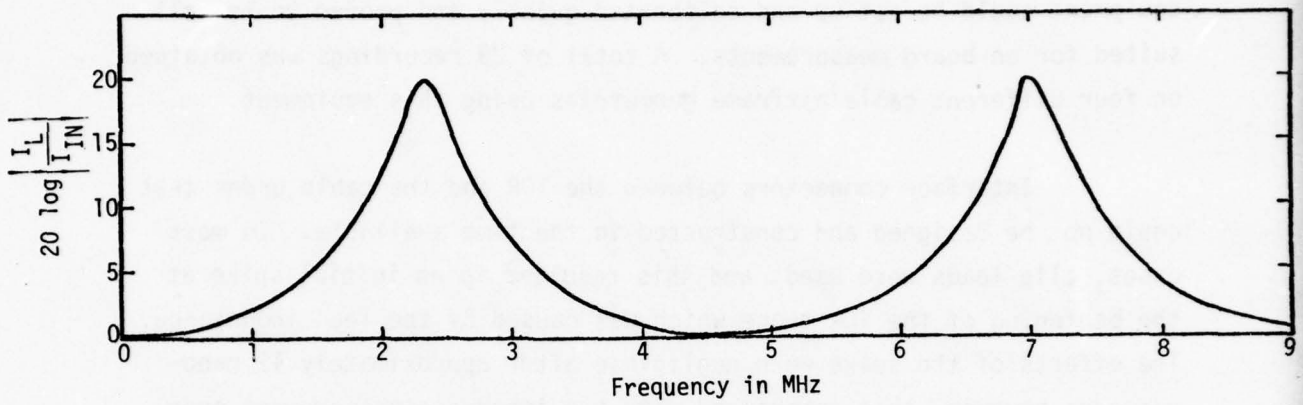

(a) Plot of Magnitude of Transfer Function vs. Frequency

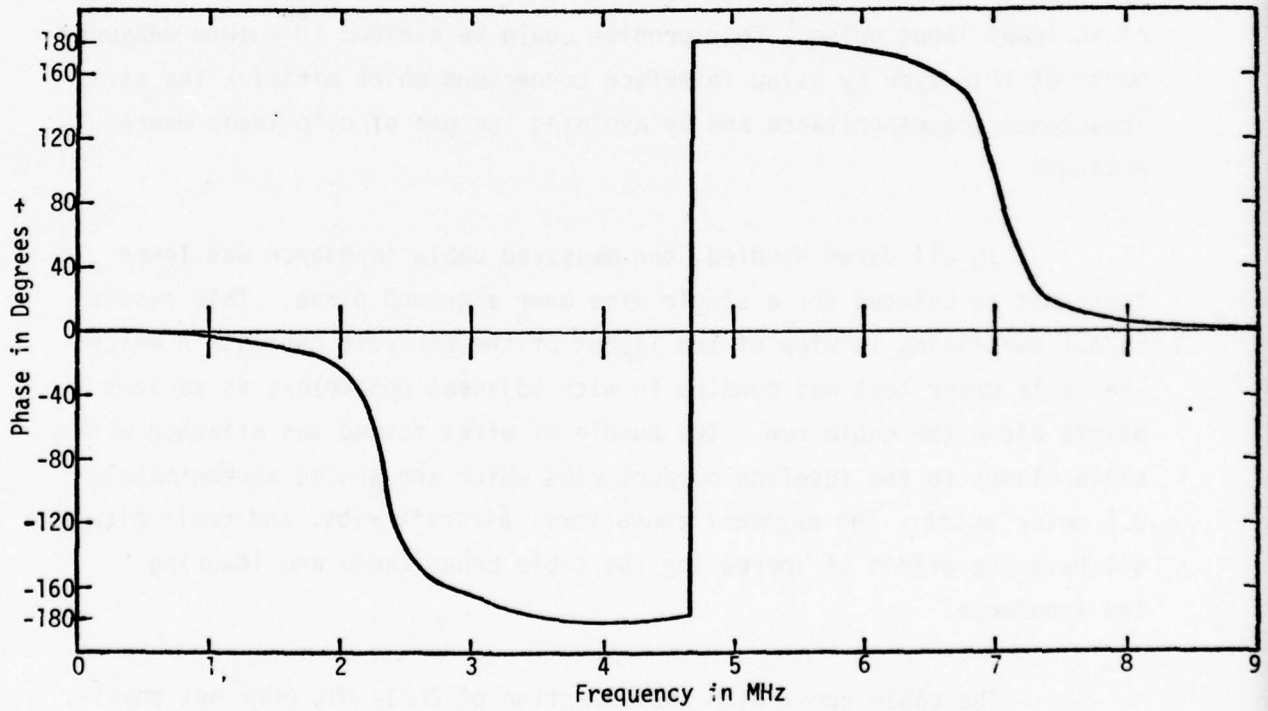

(b) Plot of Phase of Transfer Function vs. Frequency

Figure A17. Calculated Transfer Function

were met by utilizing a Tektronix Model 1502 TDR Cable Tester. This equipment could be set up and calibrated quickly and proved to be well suited for on-board measurements. A total of 29 recordings was obtained on four different cable/airframe geometries using this equipment.

Interface connectors between the TDR and the cable under test could not be designed and constructed in the time available. In most cases, clip leads were used, and this resulted in an initial spike at the beginning of the TDR trace which was caused by the lead inductance. The effects of the spike were negligible after approximately 12 nanoseconds; however, this interfered with the impedance measurement over the first 6 feet of the cable run. The stray inductance also distorted the pulse rise time and this may account for the higher than expected attenuation observed on Cable M3, which was determined under the assumption of an ideal input pulse. This problem could be avoided in future measurements of this type by using interface connectors which minimize the stray inductance and capacitance and by avoiding the use of clip leads where possible.

In all cases studied, the measured cable impedance was lower than that calculated for a single wire over a ground plane. This result is not surprising in view of the layout of the aircraft cables, in which the cable under test was bundled in with adjacent conductors at various points along the cable run. The bundle of wires formed was attached with cable clamps to the fuselage support ribs which are spaced approximately 0.5 meter apart. The adjacent conductors, aircraft ribs, and cable clamps all have the effect of increasing the cable capacitance and lowering the impedance.

The cable runs, with the exception of Cable M1, were not physically accessible over their entire length, and no attempt was made to correlate the TDR impedance profiles of Cables M2, M3, and M4 with the physical

layout of the cables. However, it was observed that the position of a load introduced by touching a cable jacket several feet from the driven end did correlate with the TDR distance to the load when corrected for propagation velocity. The maximum distance at which this effect could be observed was not investigated.

APPENDIX B

EXPERIMENTAL DATA FROM COMMON MODE MEASUREMENTS ON MULTICONDUCTOR CABLES

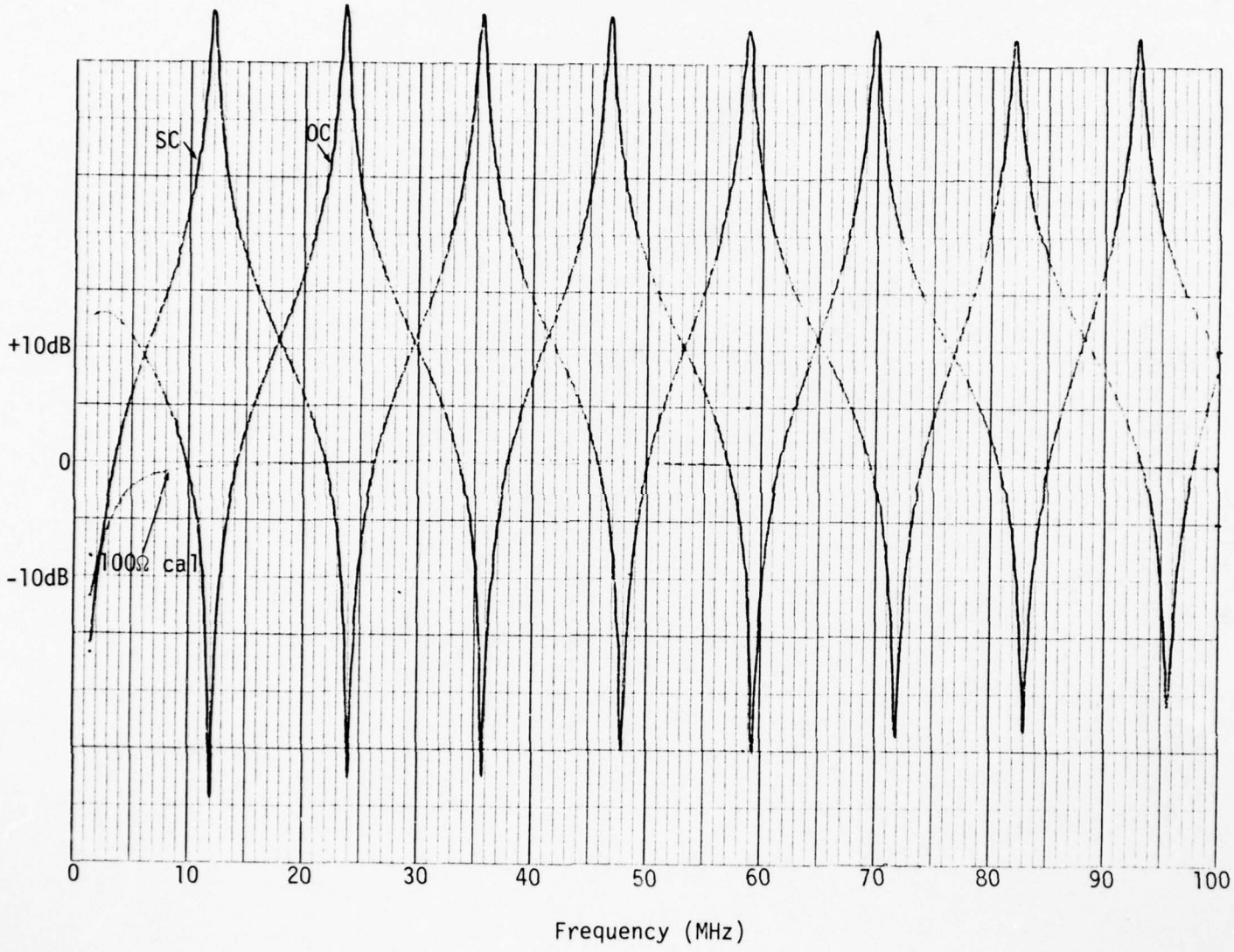

Figure B-1. Cable Above Ground Plane, N = 1

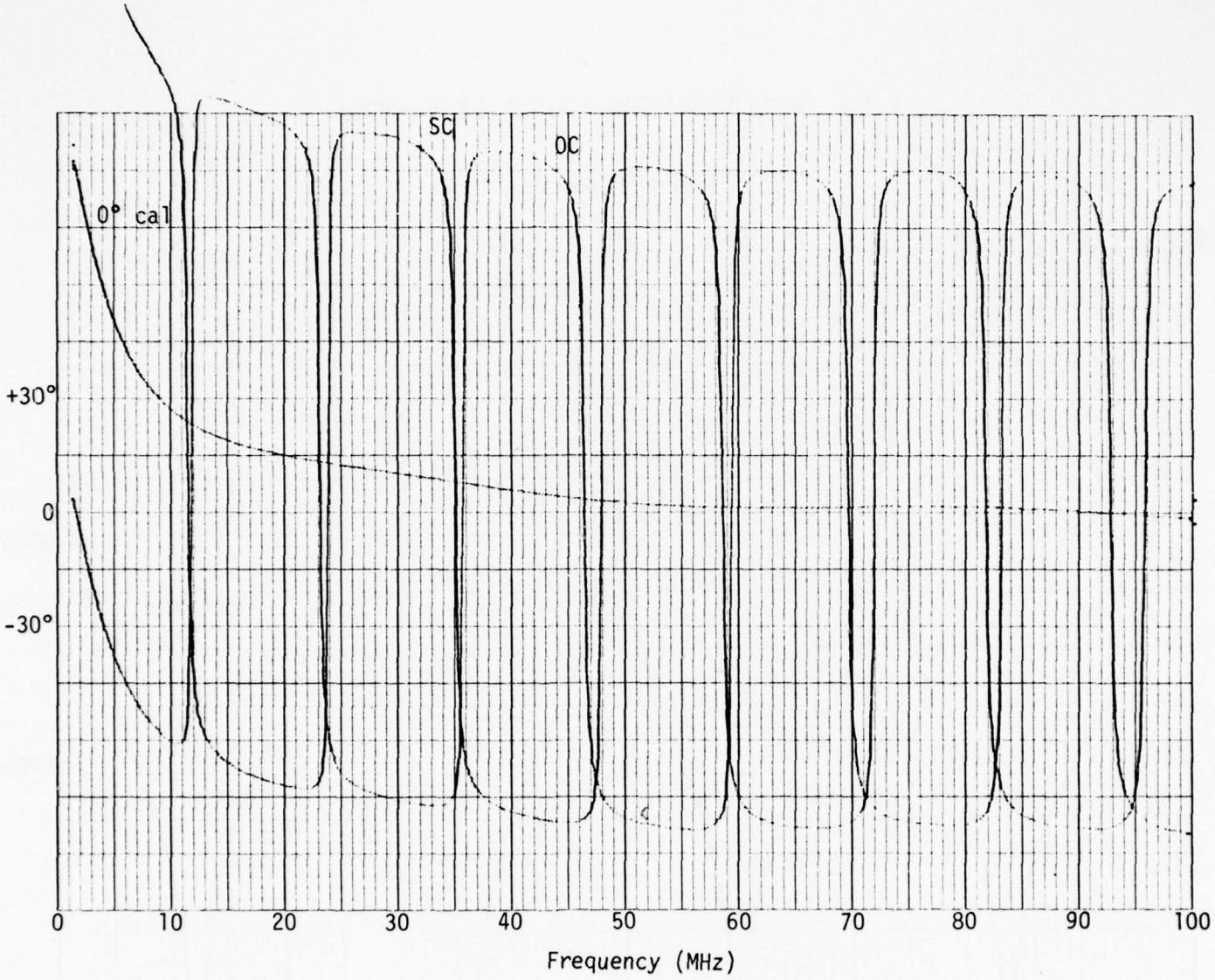

Figure B-2. Cable Above Ground Plane, N = 1

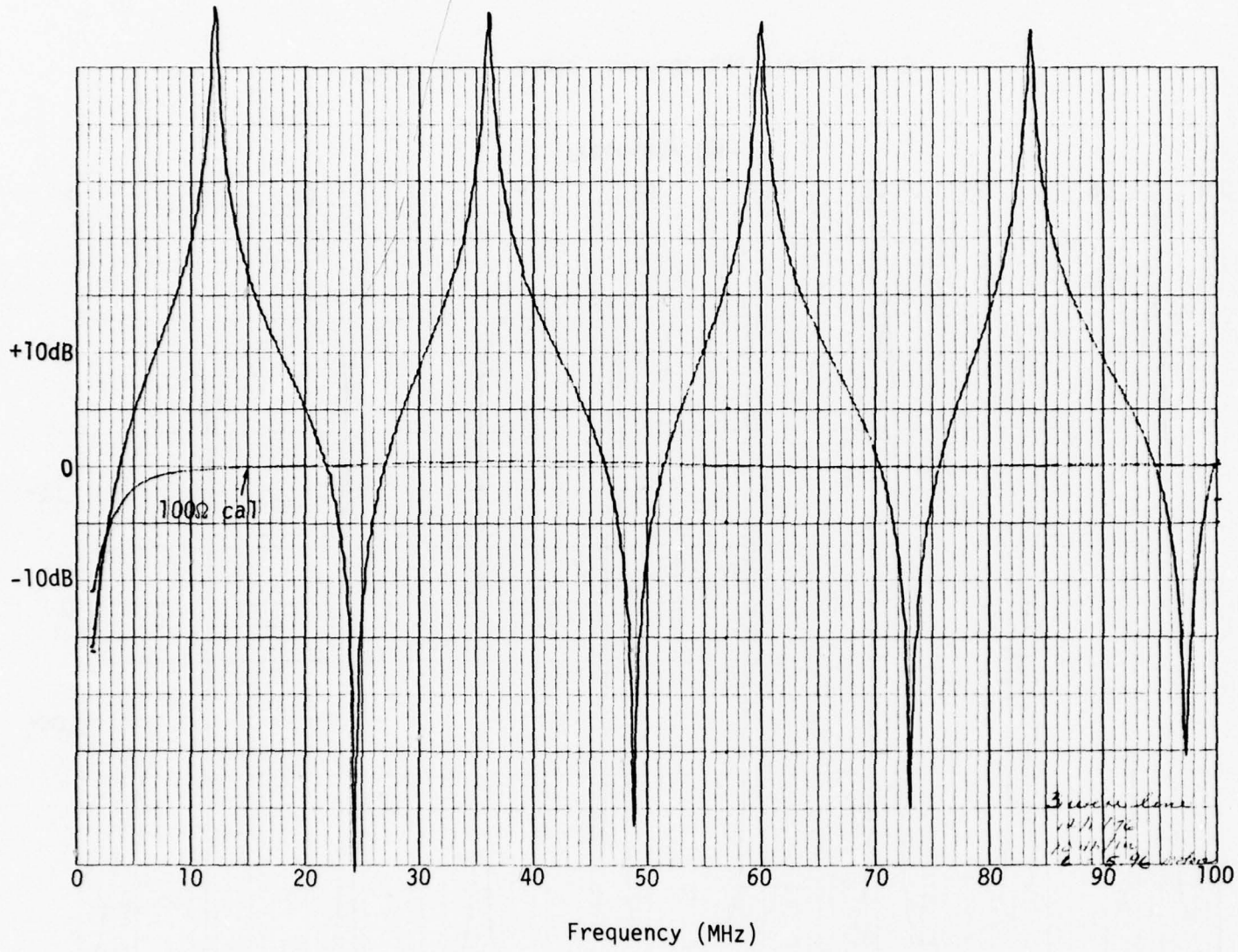

Figure B-3. Cable Above Ground Plane, N = 3

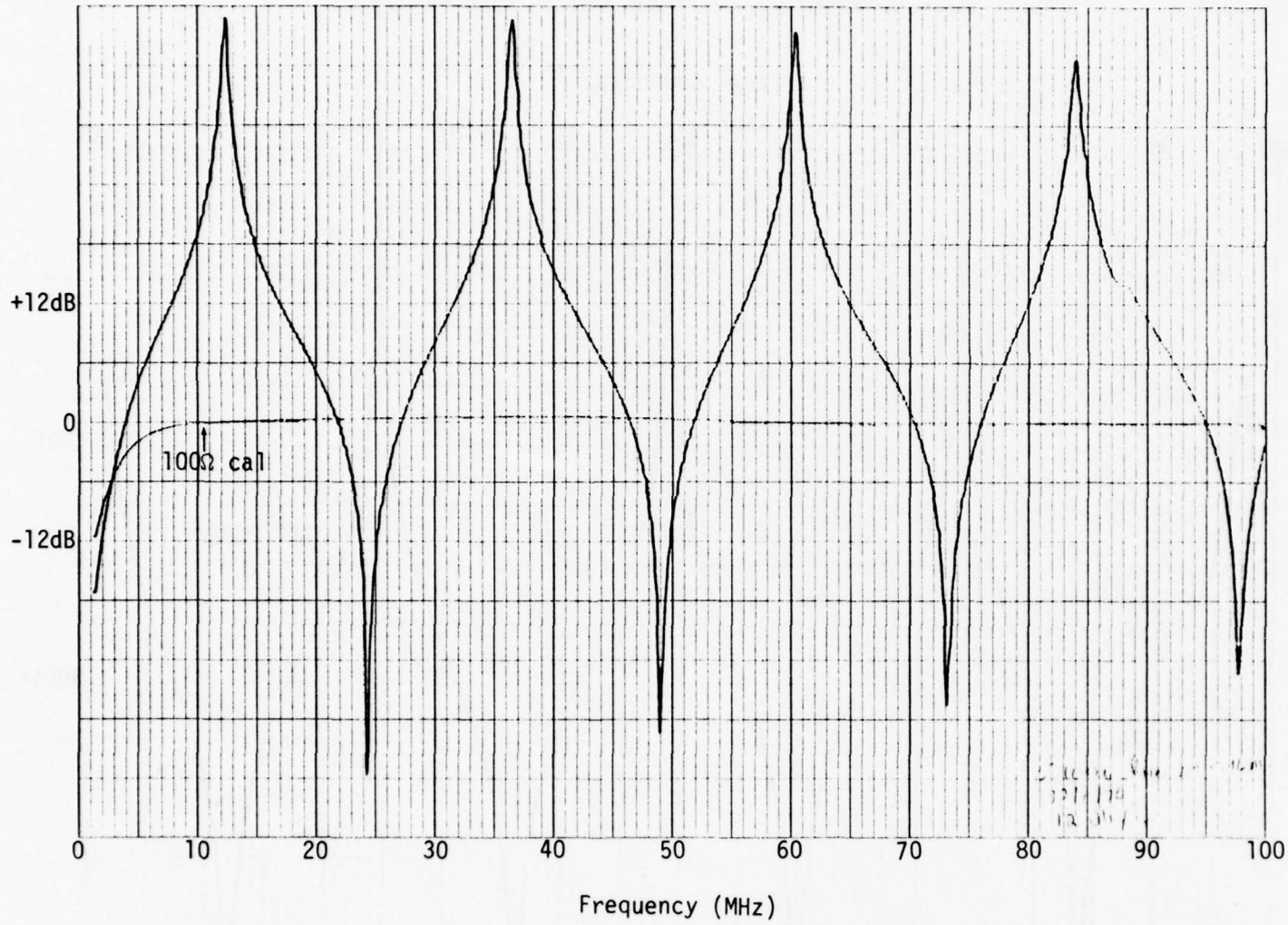

Figure B-4. Cable Above Ground Plane, N = 5

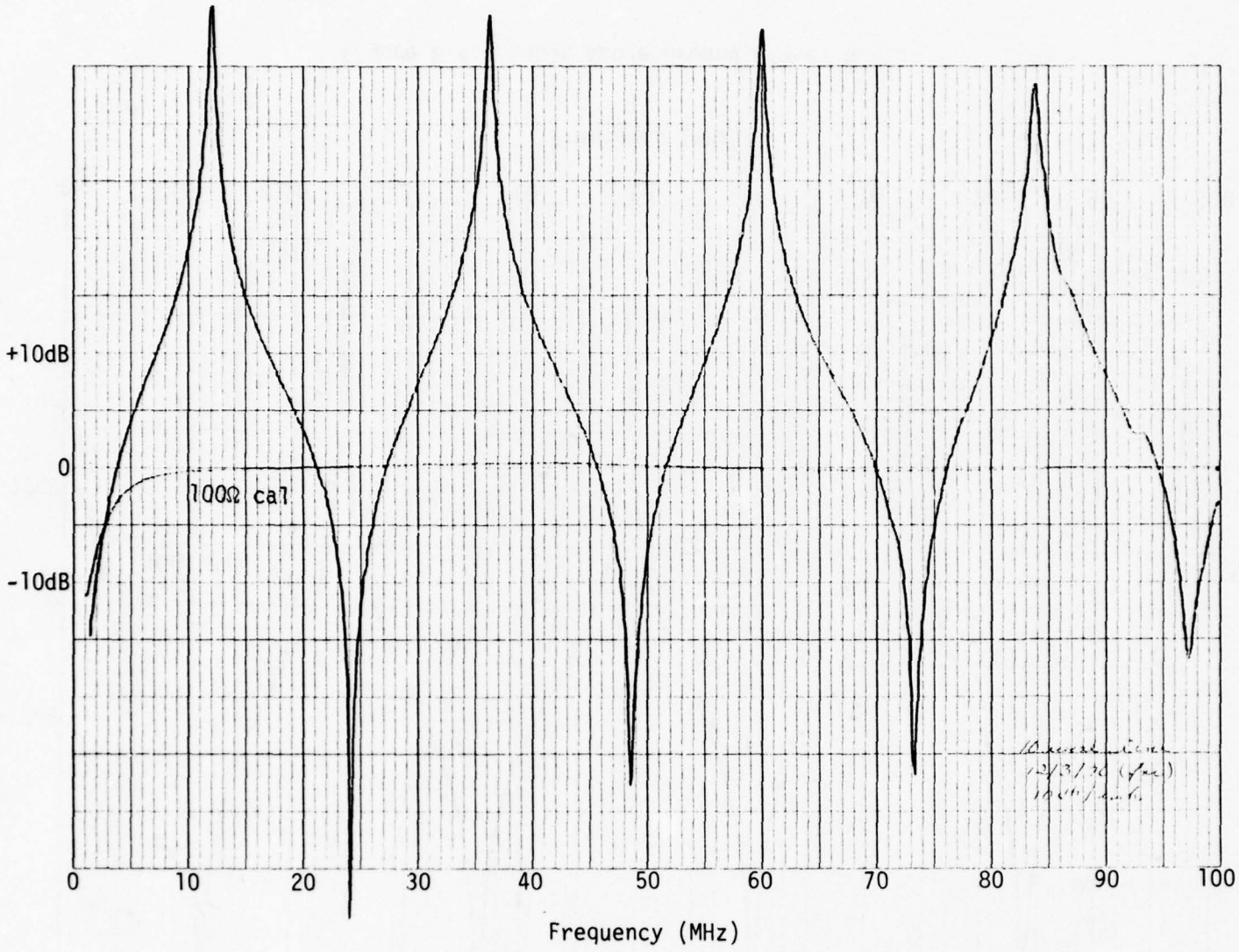

Figure B-5. Cable Above Ground Plane, N = 10

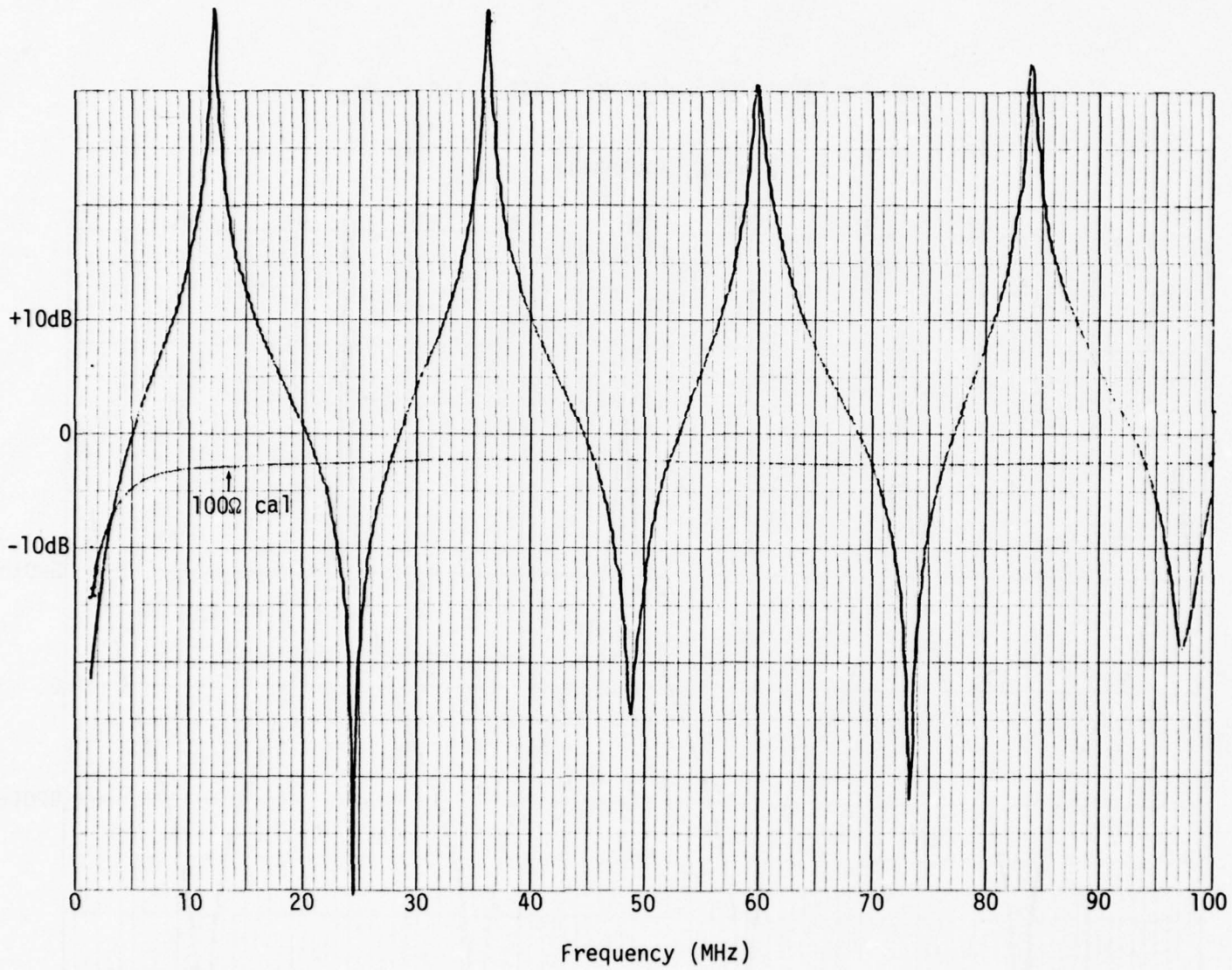

Figure B-6. Cable Above Ground Plane, N = 15

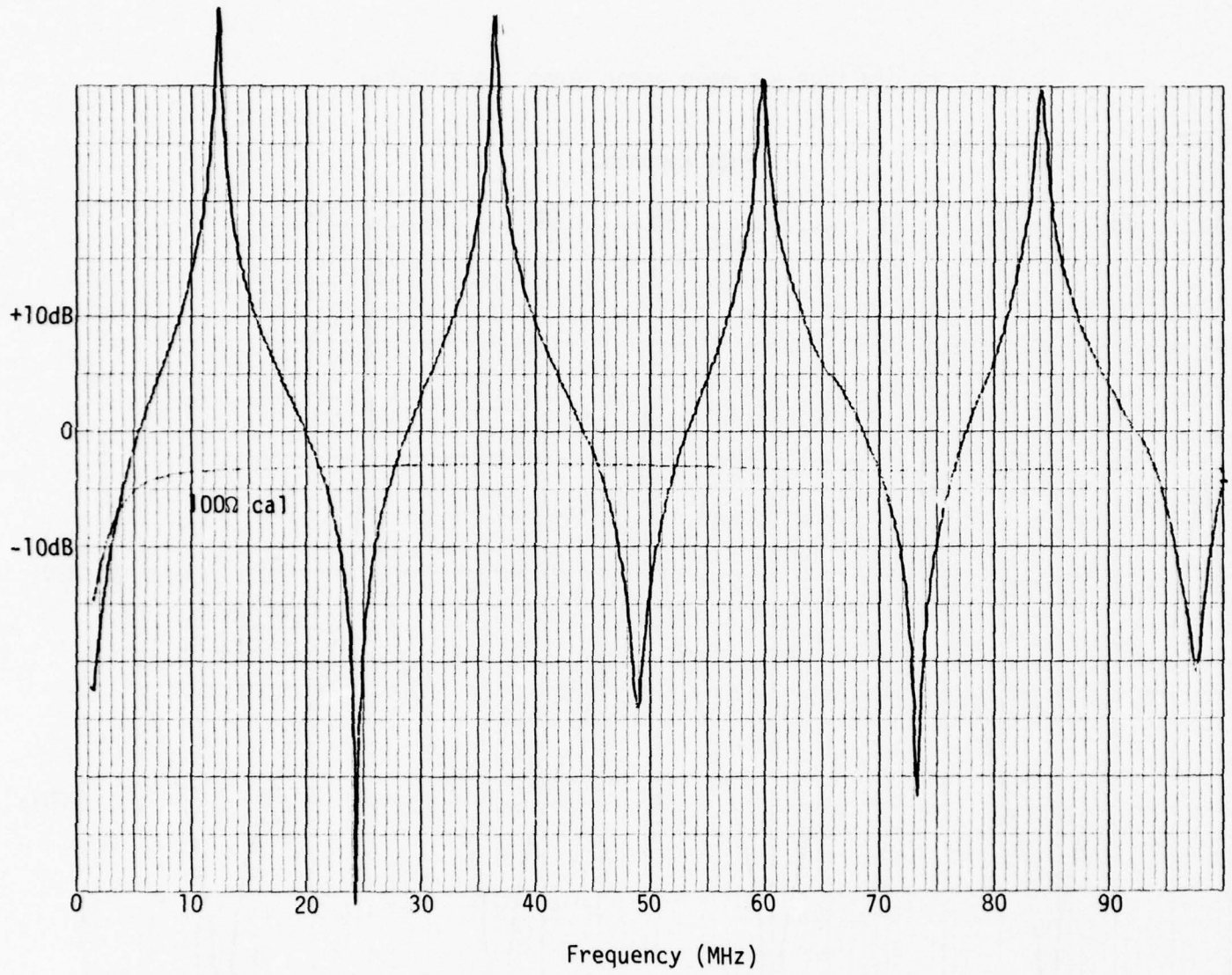

Figure B-7. Cable Above Ground Plane, N = 20

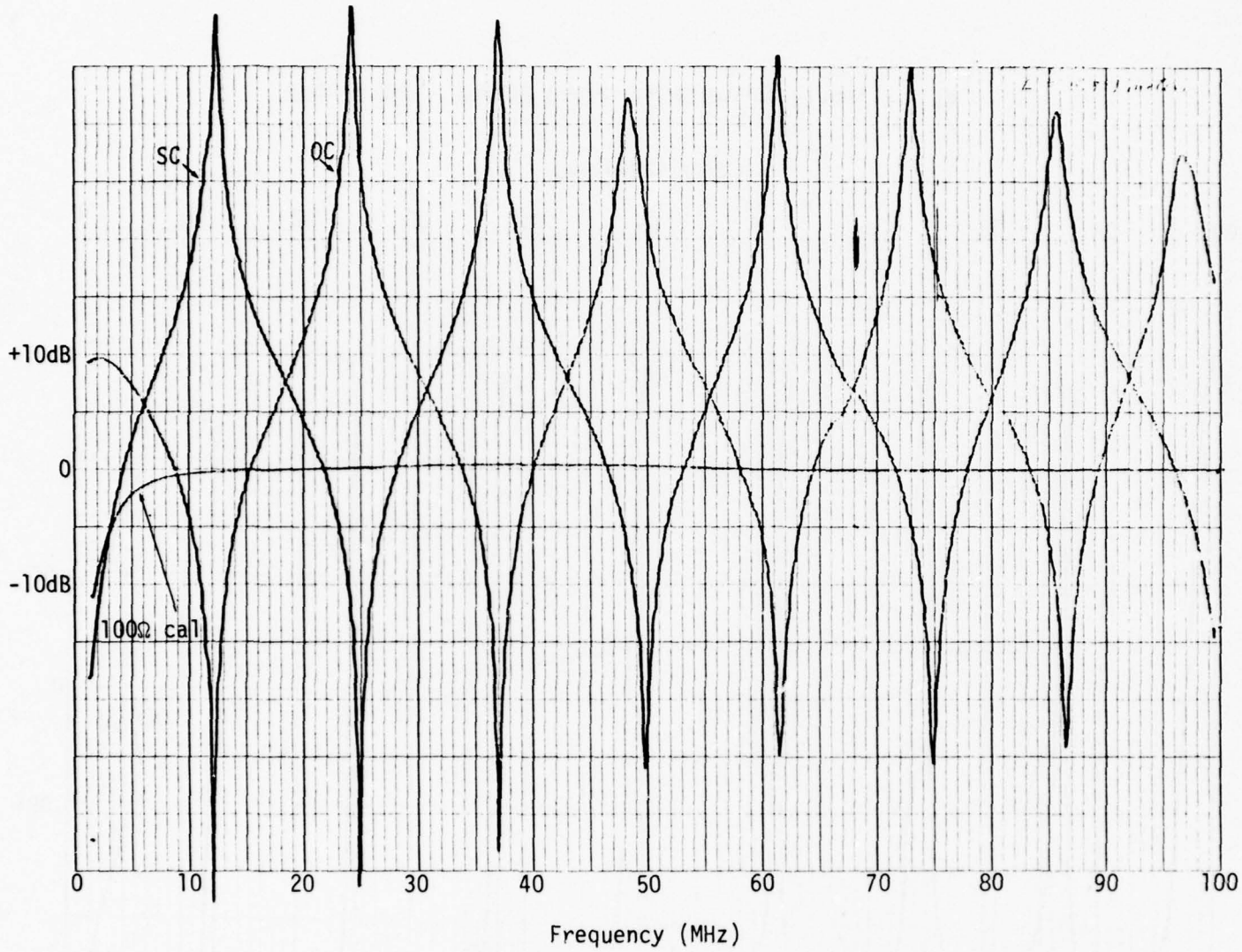

Figure B-8. Combed Cable Above Ground Plane, N = 15

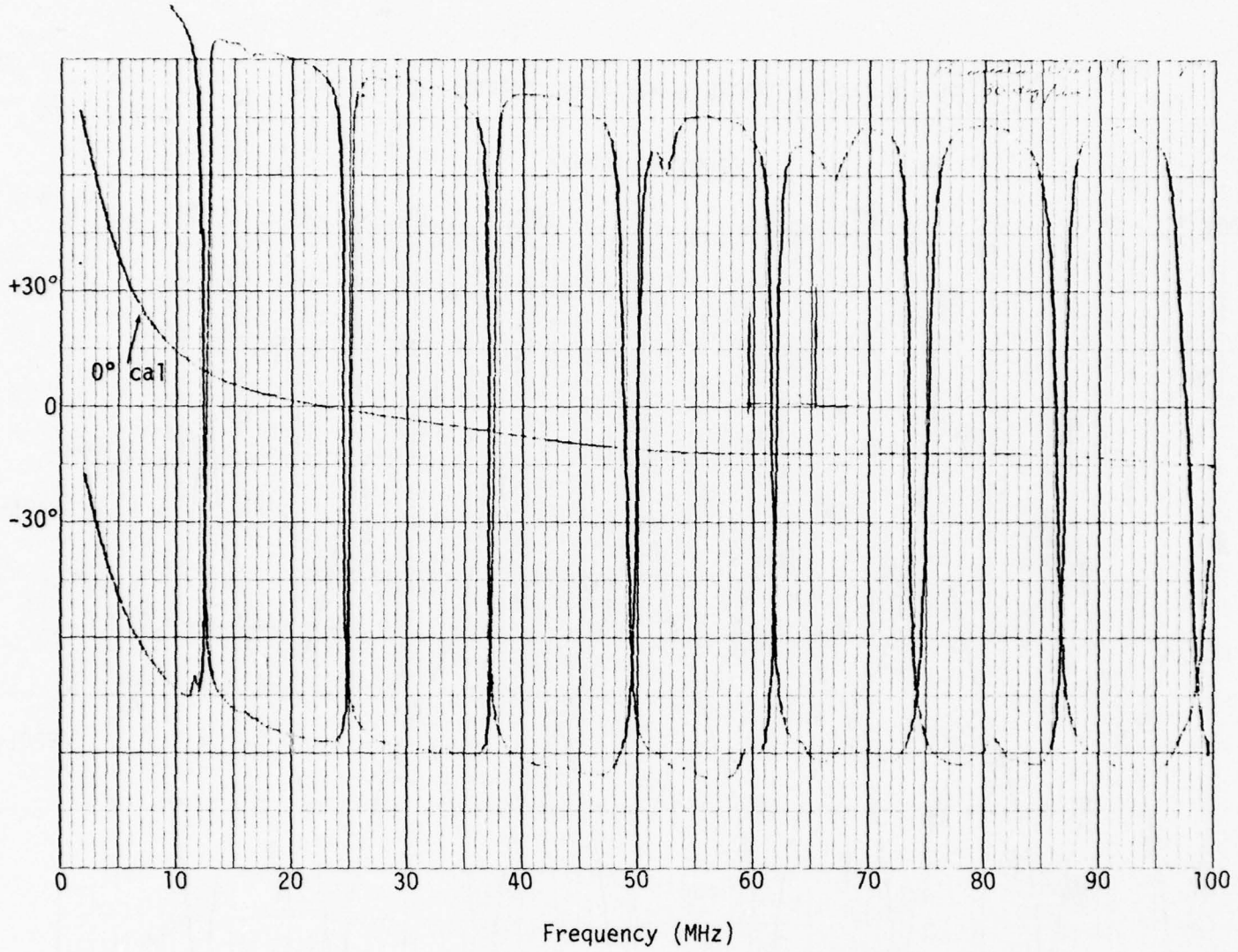

Figure B-9. Combed Cable Above Ground Plane, N = 15

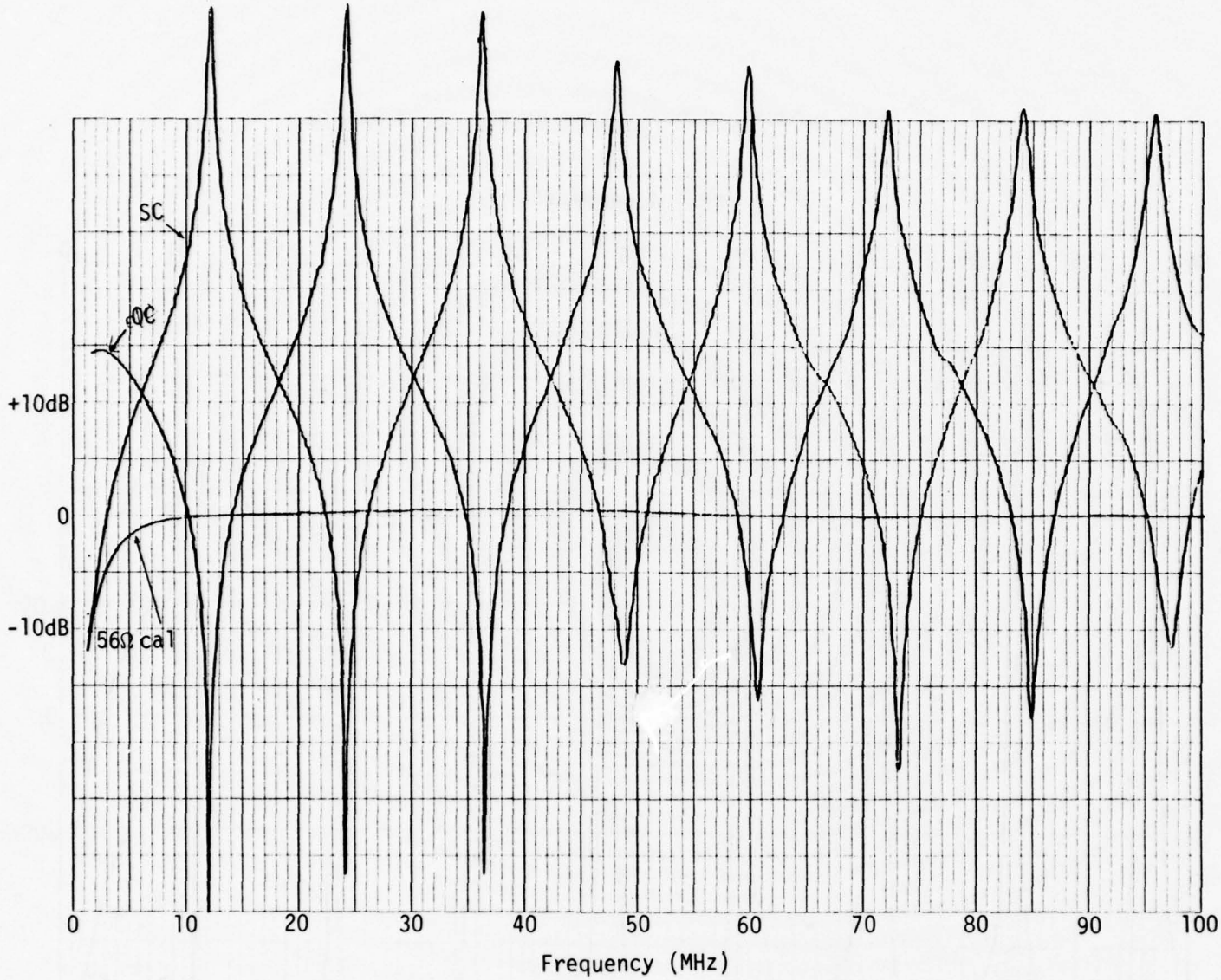

Figure B-10. Cable Above Ground Plane, N = 20

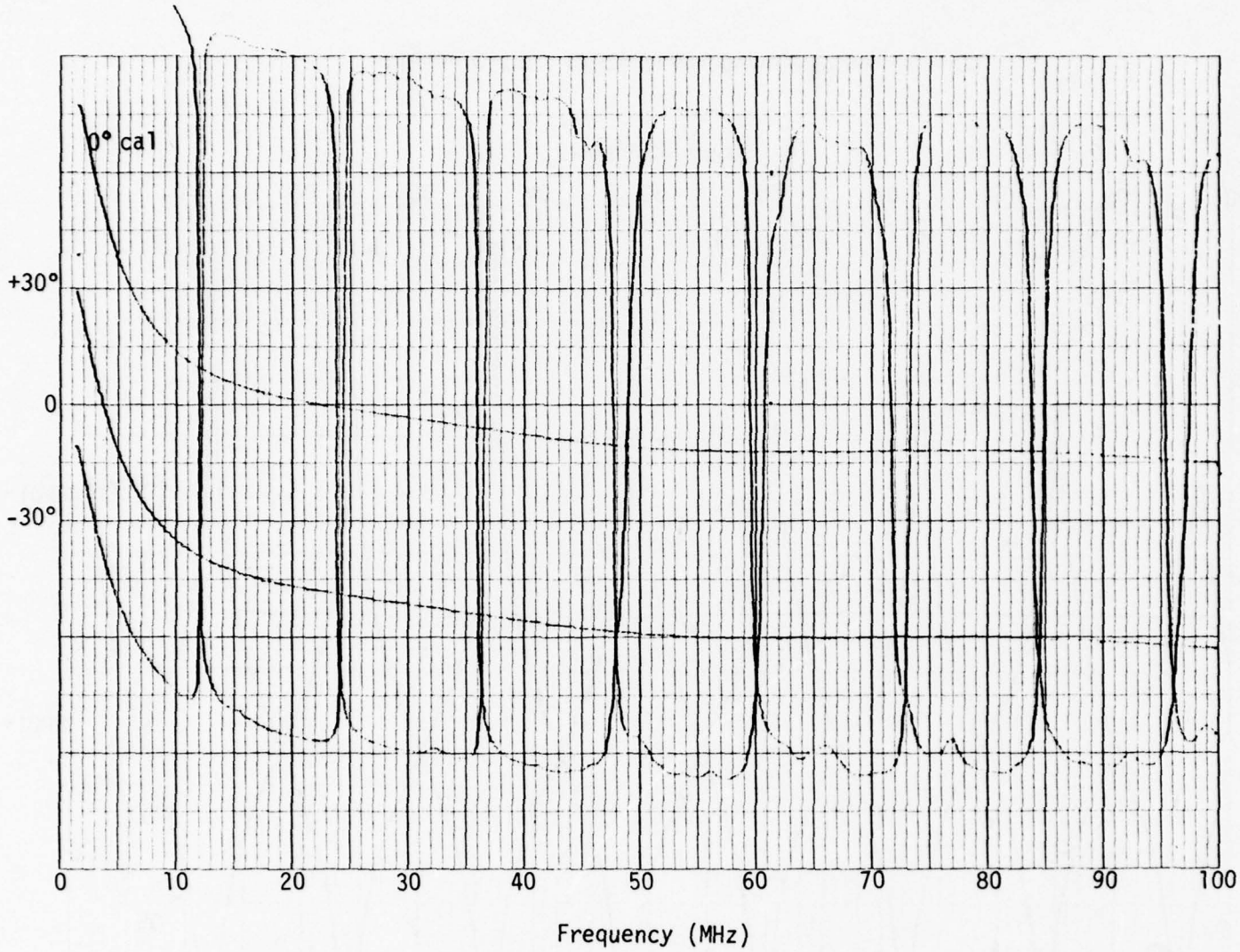

Figure B-11. Cable Above Ground Plane, N = 20

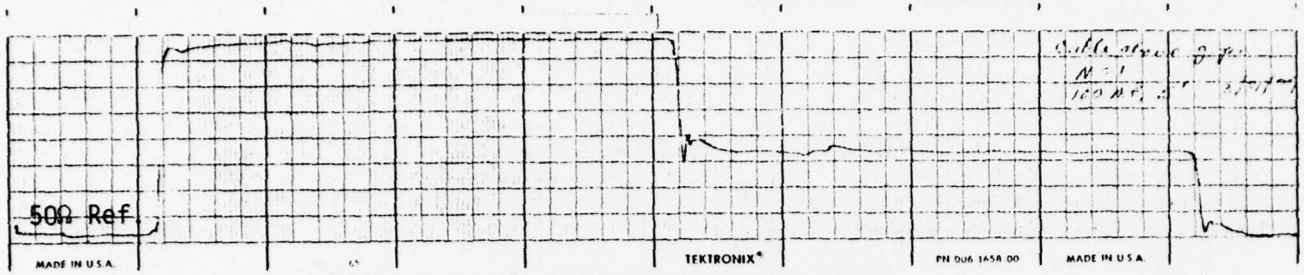

(a) N = 1 ($\bar{Z}_o$ = 350Ω, L_e = 6.04m)

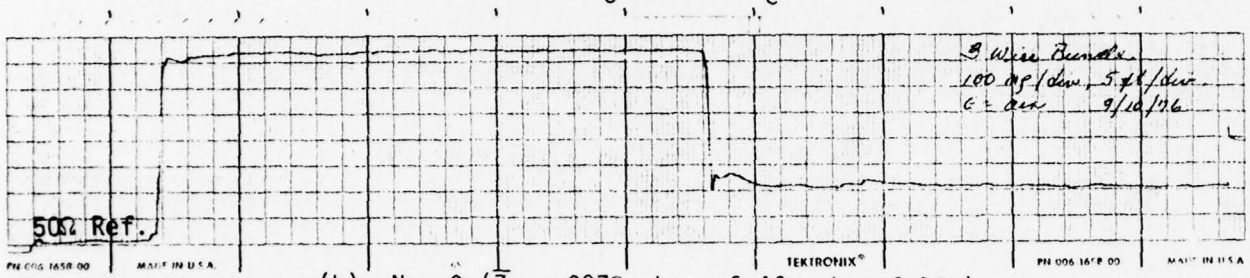

(b) N = 3 ($\bar{Z}_o$ = 307Ω, L_e = 6.46m, L = 6.10m)

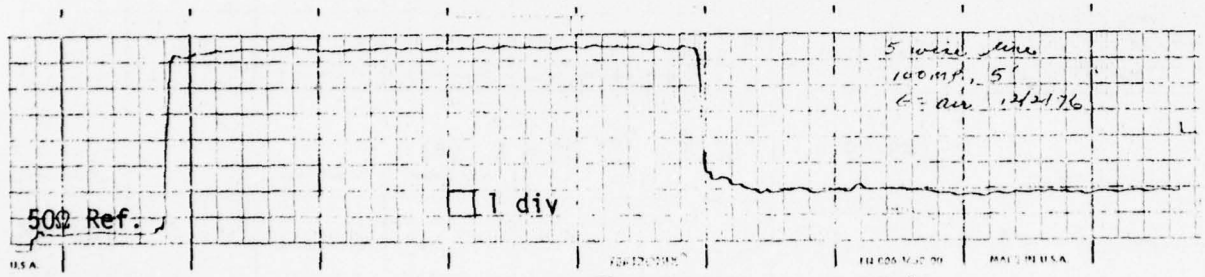

(c) N = 5 ($\bar{Z}_0$ = 283Ω, L_e = 6.22m)

Figure B-12. Cable Above Ground Plane (.305 m/div, 100 mρ/div)

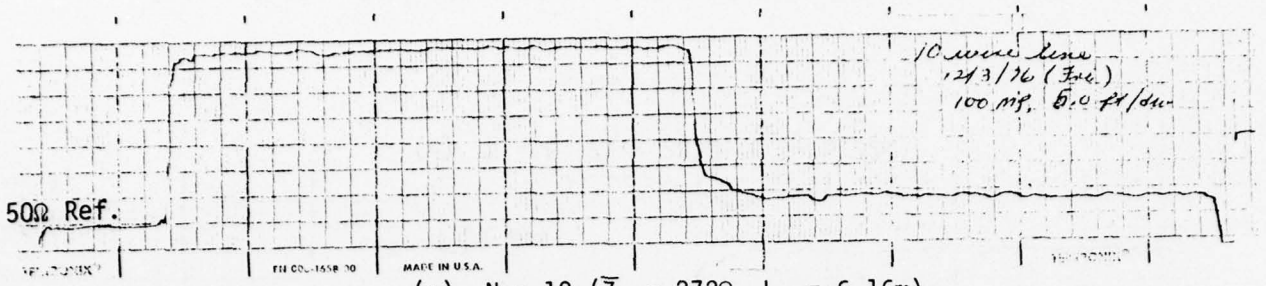

(a) N = 10 ($\bar{Z}_o$ = 272Ω, L_c = 6.16m)

(b) N = 15 ($\bar{Z}_o$ = 234Ω, L_e = 6.16m)

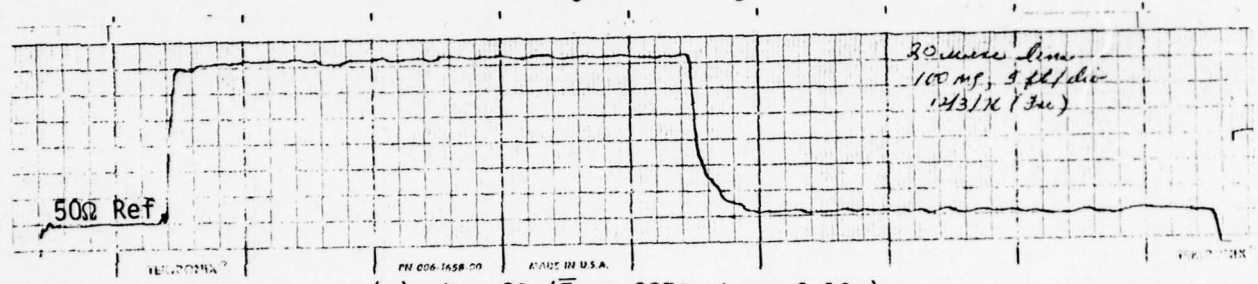

(c) N = 20 ($\bar{Z}_o$ = 227Ω, L_e = 6.13m)

Figure B-13. Cable Above Ground Plane (.305m/div., 100mμ/div.)

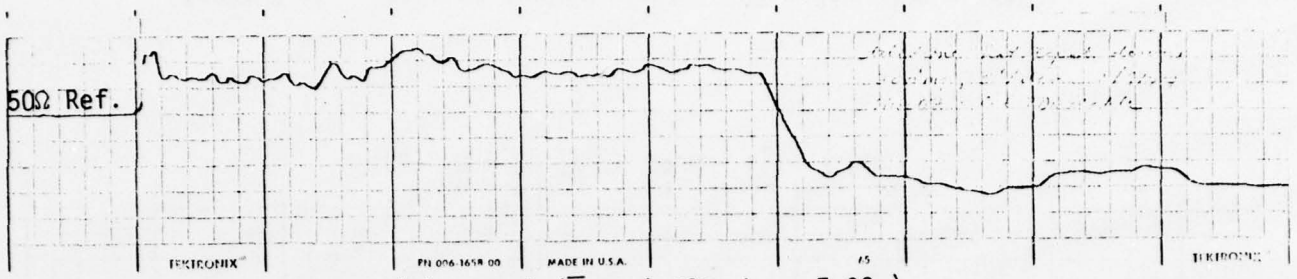

(a) N = 1 ($\overline{Z}_o$ = 9.62Ω, L_e = 7.32m)

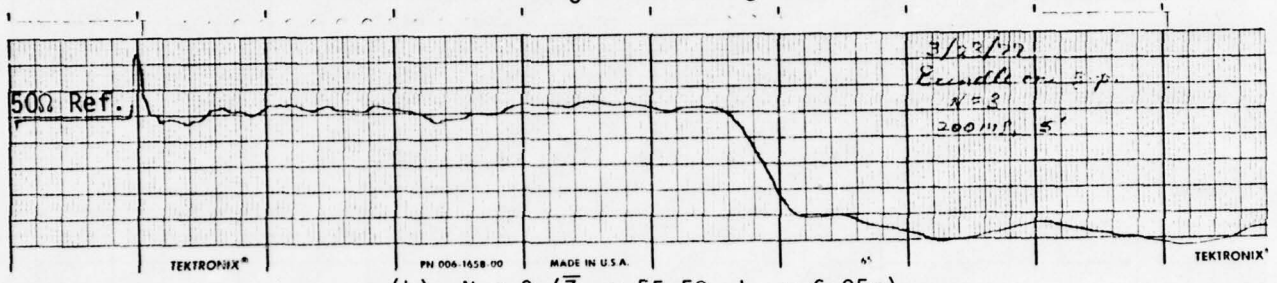

(b) N = 3 ($\overline{Z}_o$ = 55.5Ω, L_e = 6.95m)

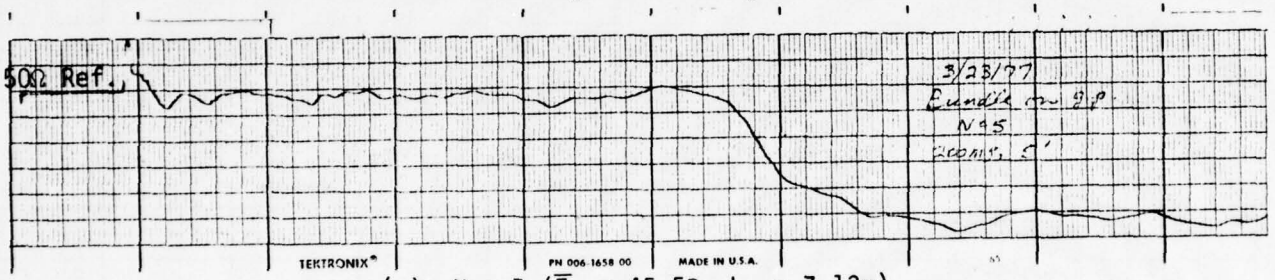

(c) N = 5 ($\overline{Z}_o$ = 45.5Ω, L_e = 7.13m)

Figure B-14. Cable on Ground Plane (.305 m/div, 200 mμ/div)

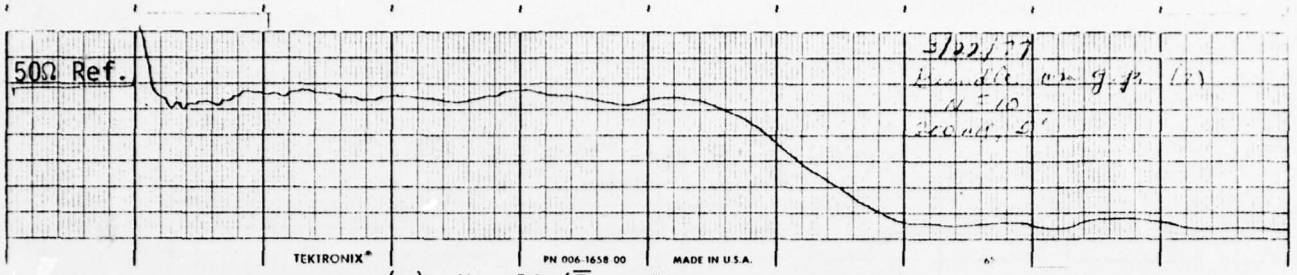

(a) N = 10 ($\overline{Z}_o$ = 42.4Ω, L_e = 6.95m)

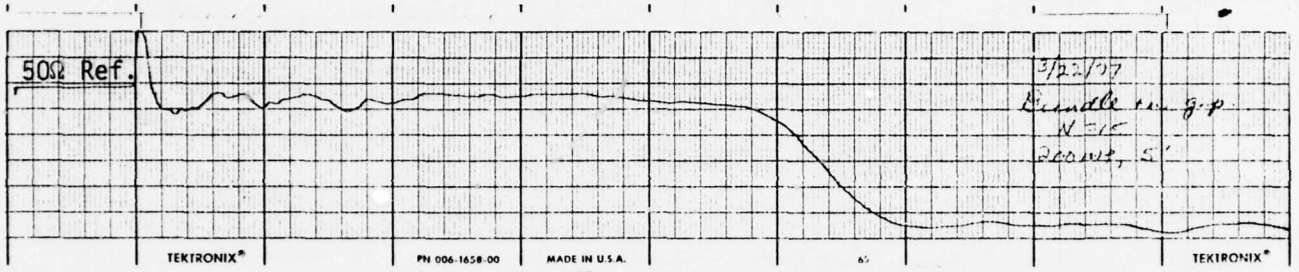

(b) N = 15 ($\overline{Z}_o$ = 42.2Ω, L_e = 7.22m)

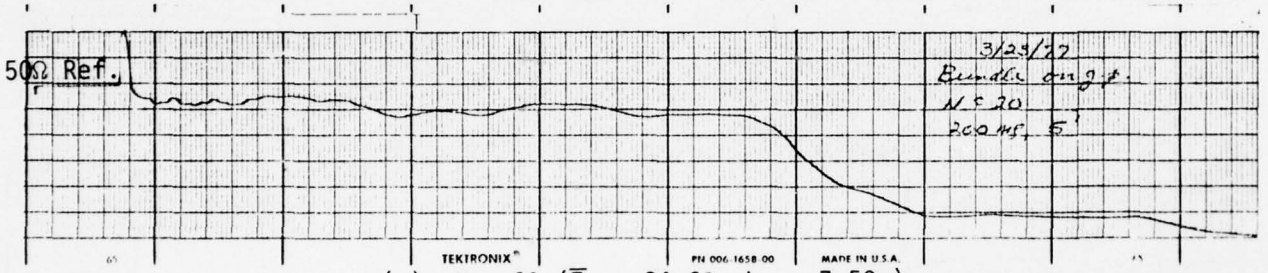

(c) N = 20 ($\overline{Z}_o$ = 34.6Ω, L_e = 7.50m)

Figure B-15. Cable on Ground Plane (.305 m/div, 200 mρ/div)

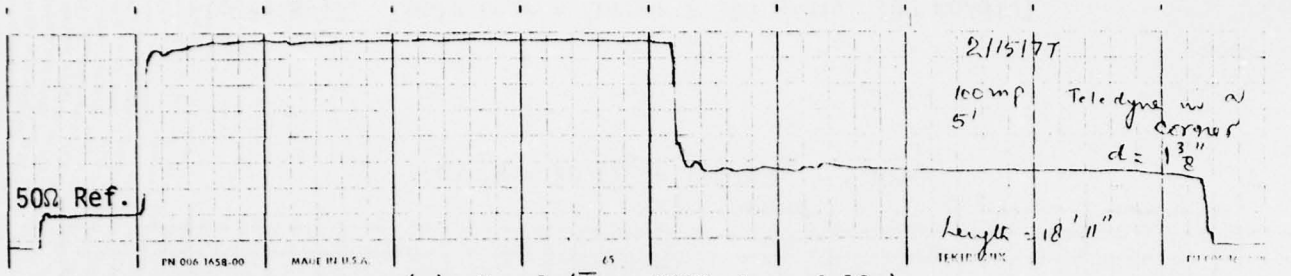

(a) N = 1 ($\overline{Z}_o$ = 263Ω, L_e = 6.19m)

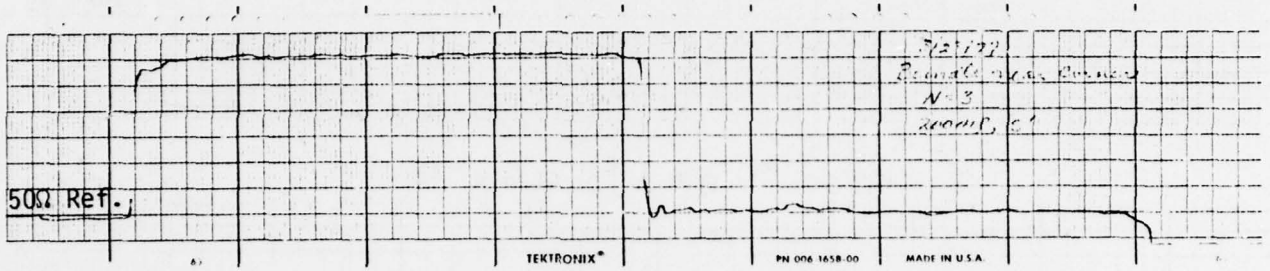

(b) N = 3 ($\overline{Z}_o$ = 228Ω, L_e = 6.04m)

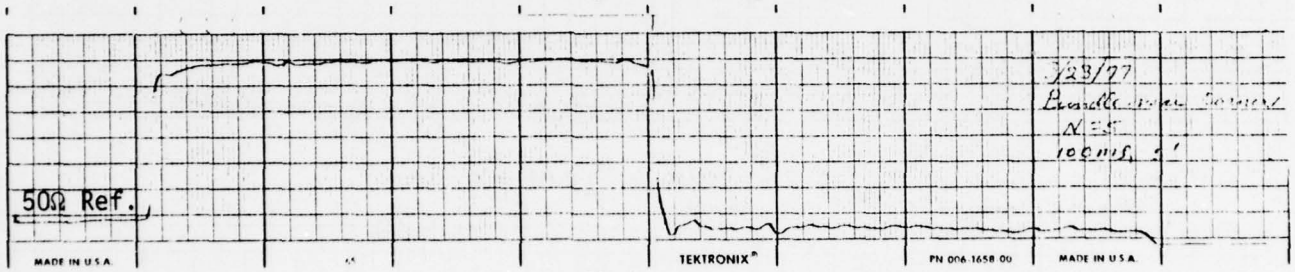

(c) N = 5 ($\overline{Z}_o$ = 213Ω, L_e = 6.00m)

Figure B-16. Cable Near a Corner (.305 m/div, 100 mp/div)

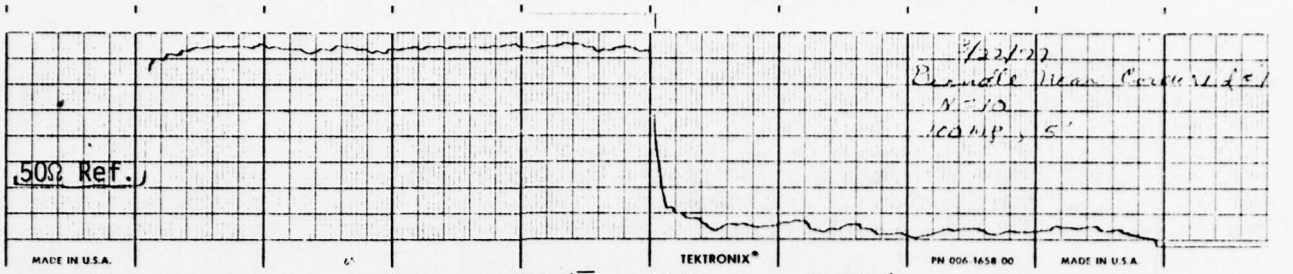

(a) N = 10 ($\overline{Z}_o$ = 167Ω, L_e = 5.94m)

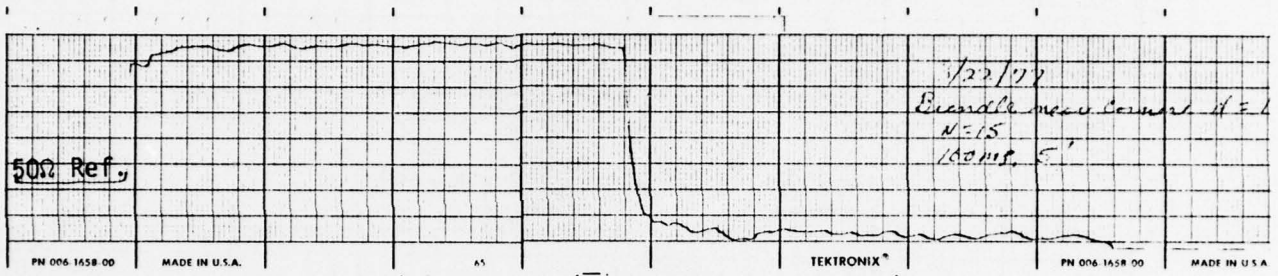

(b) N = 15 ($\overline{Z}_o$ = 163Ω, L_e = 5.85m)

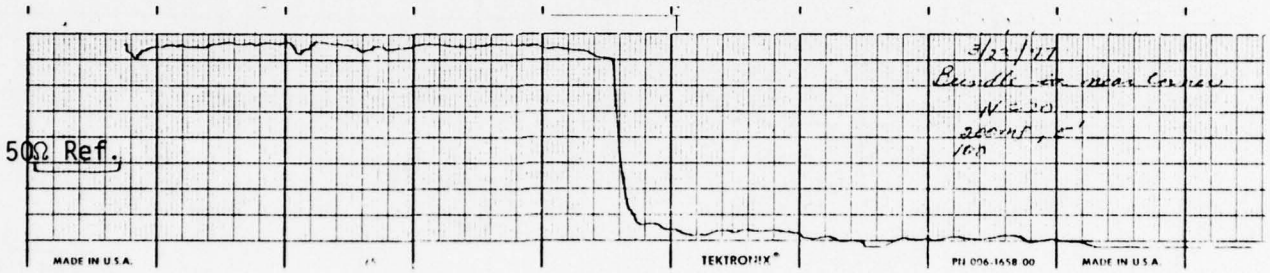

(c) N = 20 ($\overline{Z}_o$ = 150Ω, L_e = 5.82m)

Figure B-17. Cable Near a Corner (.305 m/div, 100 mρ/div)

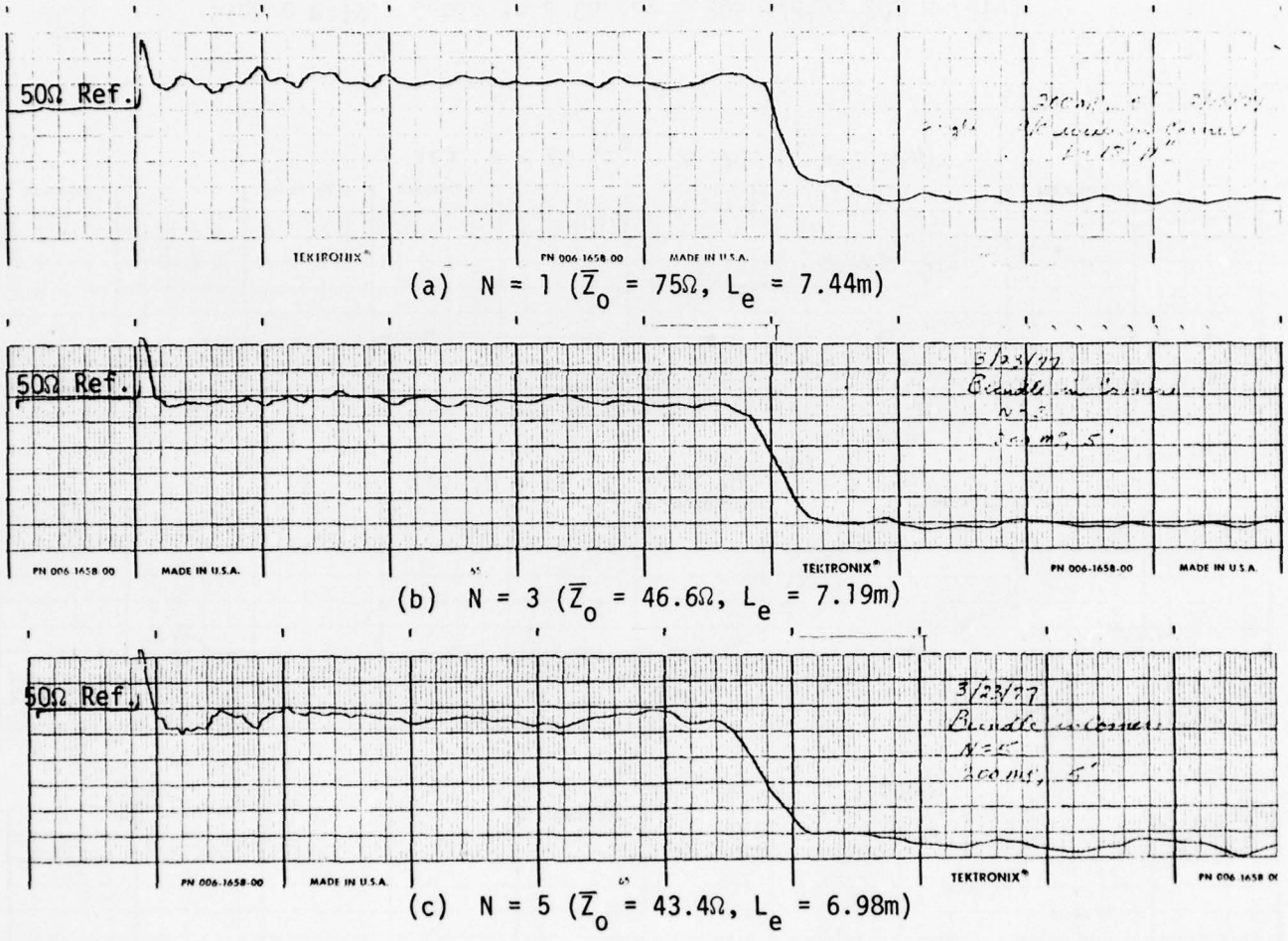

(a) N = 1 ($\overline{Z}_o$ = 75Ω, L_e = 7.44m)

(b) N = 3 ($\overline{Z}_o$ = 46.6Ω, L_e = 7.19m)

(c) N = 5 ($\overline{Z}_o$ = 43.4Ω, L_e = 6.98m)

Figure B-18. Cable in a Corner (.305 m/div, 200 mρ/div)

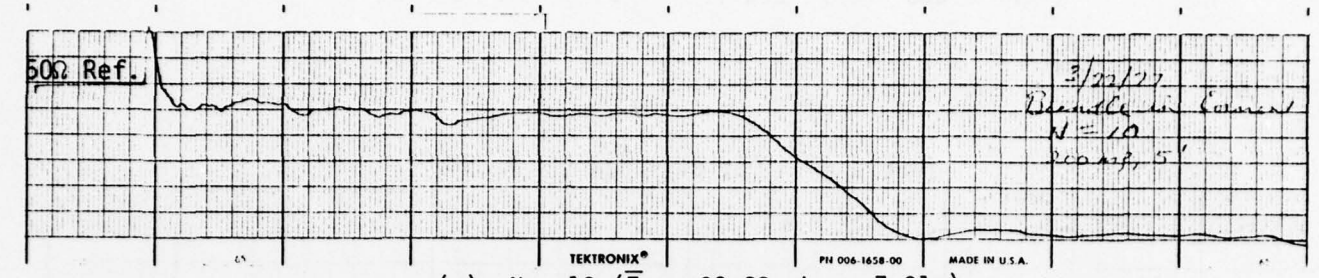

(a) N = 10 ($\overline{Z}_o$ = 32.2Ω, L_e = 7.01m)

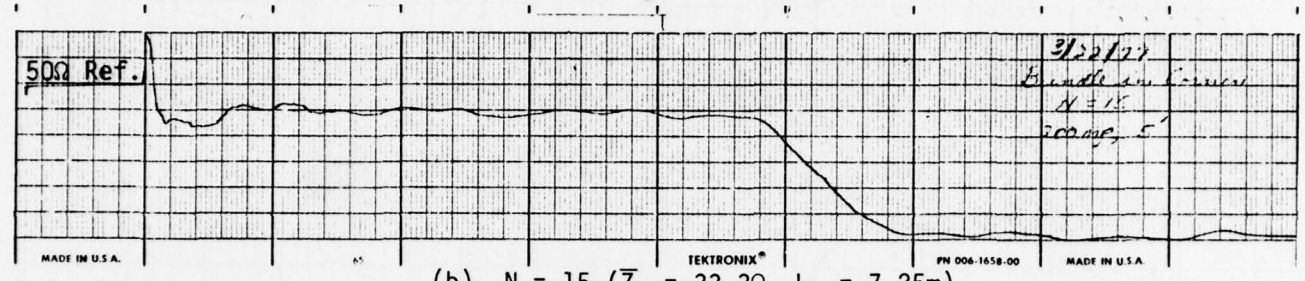

(b) N = 15 ($\overline{Z}_o$ = 33.3Ω, L_e = 7.25m)

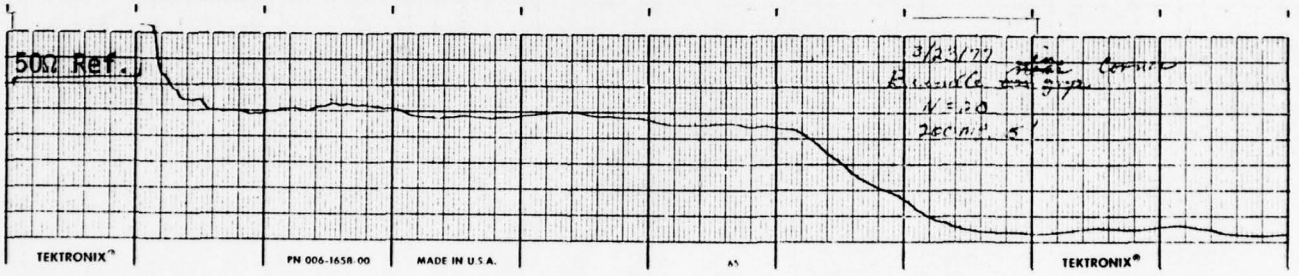

(c) N = 20 ($\overline{Z}_o$ = 26.7Ω, L_e = 7.62m)

Figure B-19. Cable in a Corner (.305 m/div, 200 mρ/div)

(a) N = 1 ($\overline{Z}_o$ = 100Ω, L_e = 7.07m)

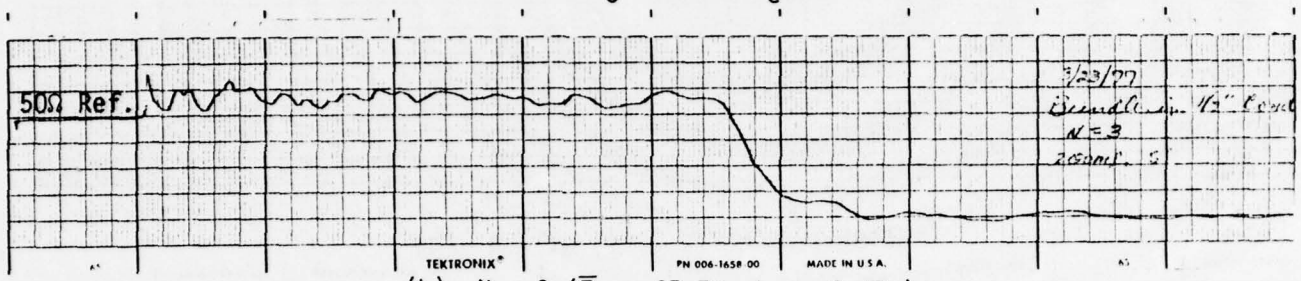

(b) N = 3 ($\overline{Z}_o$ = 65.7Ω, L_e = 6.77m)

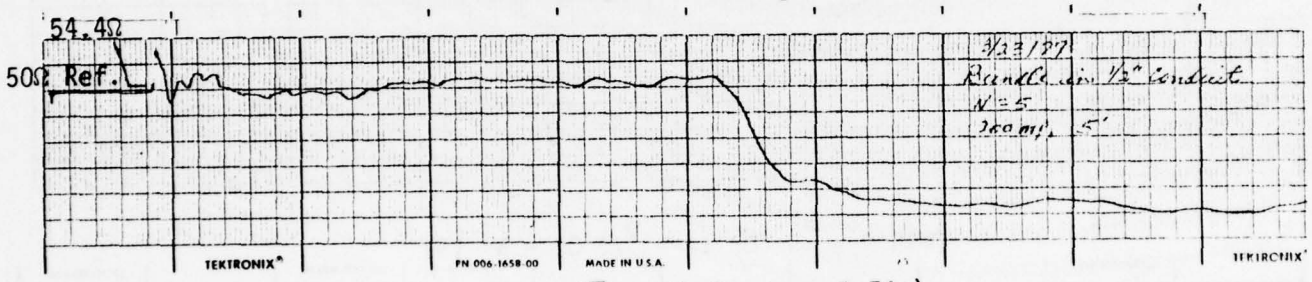

(c) N = 5 ($\overline{Z}_o$ = 54.4Ω, L_e = 6.74m)

Figure B-20. Cable in Small Conduit (.305 m/div, 200 mρ/div)

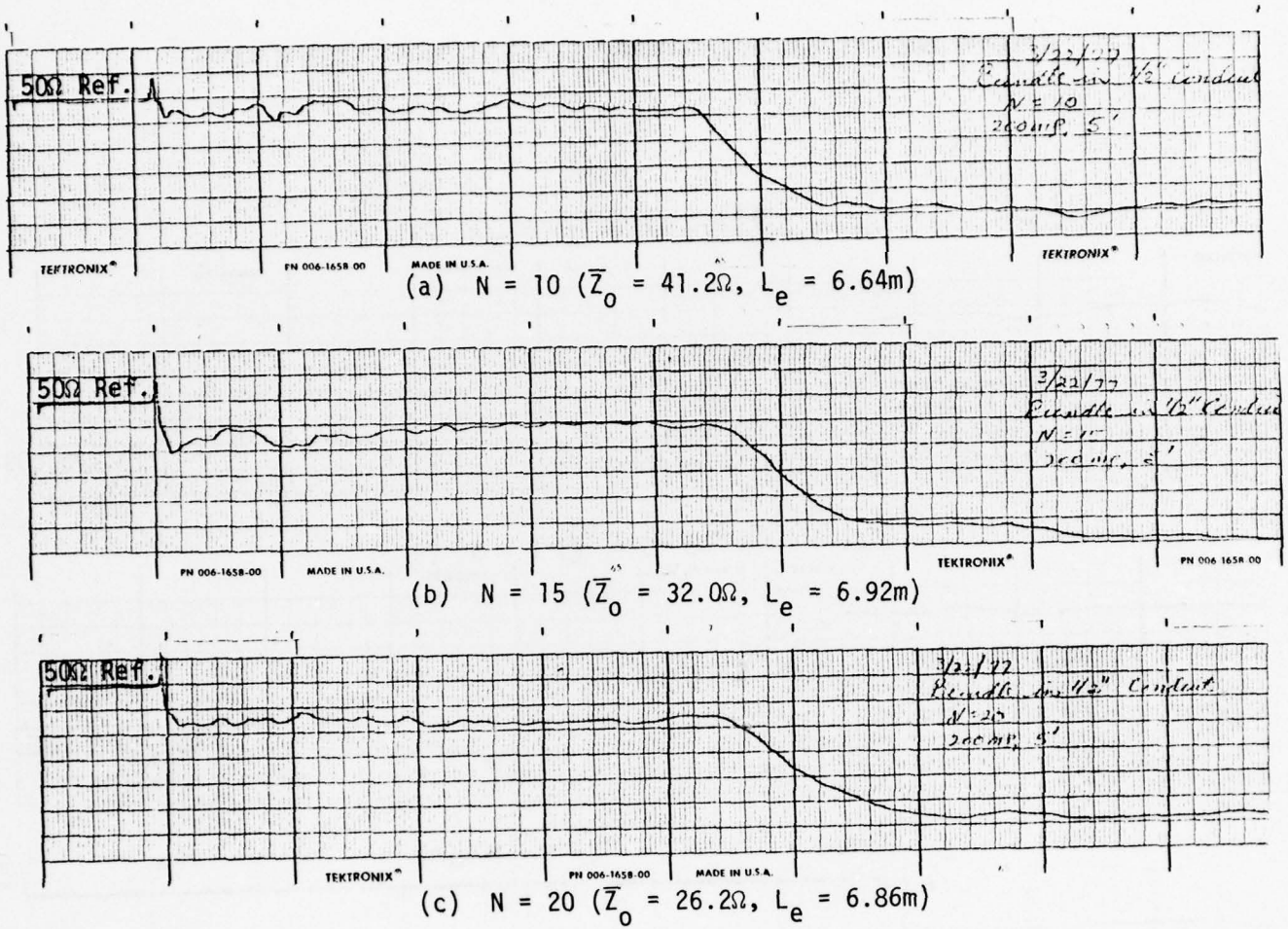

(a) N = 10 ($\overline{Z}_o$ = 41.2Ω, L_e = 6.64m)

(b) N = 15 ($\overline{Z}_o$ = 32.0Ω, L_e = 6.92m)

(c) N = 20 ($\overline{Z}_o$ = 26.2Ω, L_e = 6.86m)

Figure B-21. Cable in Small Conduit (.305 m/div, 200 mρ/div)

(a) N ≈ 1 ($\overline{Z}_o$ = 106Ω, L_e = 7.07m)

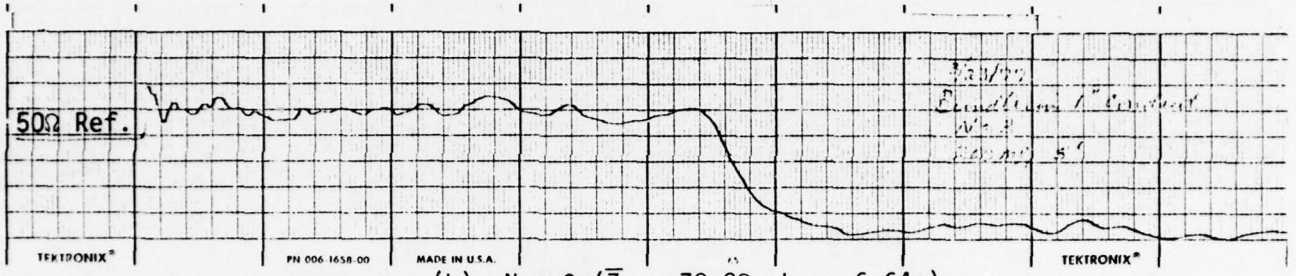

(b) N ≈ 3 ($\overline{Z}_o$ = 78.8Ω, L_e = 6.64m)

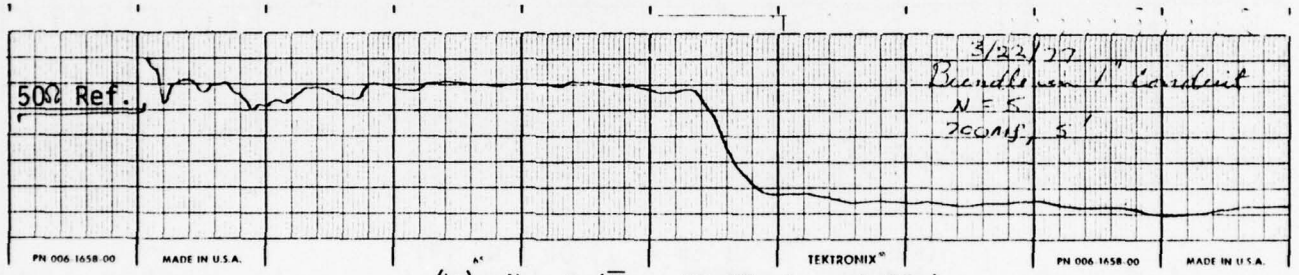

(c) N = 5 ($\overline{Z}_o$ = 76.9Ω, L_e = 6.58m)

Figure B-22. Cable in Large Conduit (.305 m/div, 200 mρ/div)

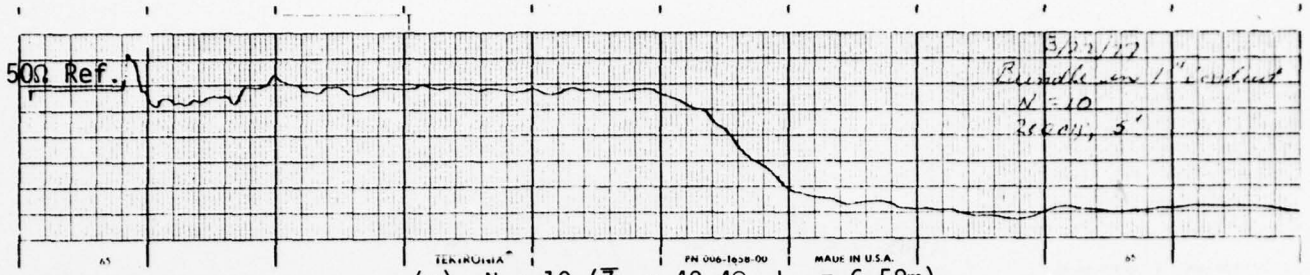

(a) N = 10 ($\overline{Z}_o$ = 49.4Ω, L_e = 6.58m)

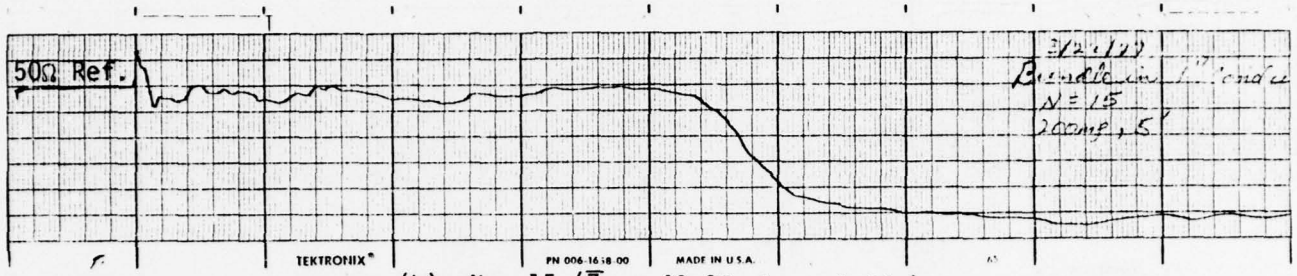

(b) N = 15 ($\overline{Z}_o$ = 43.8Ω, L_e = 6.64m)

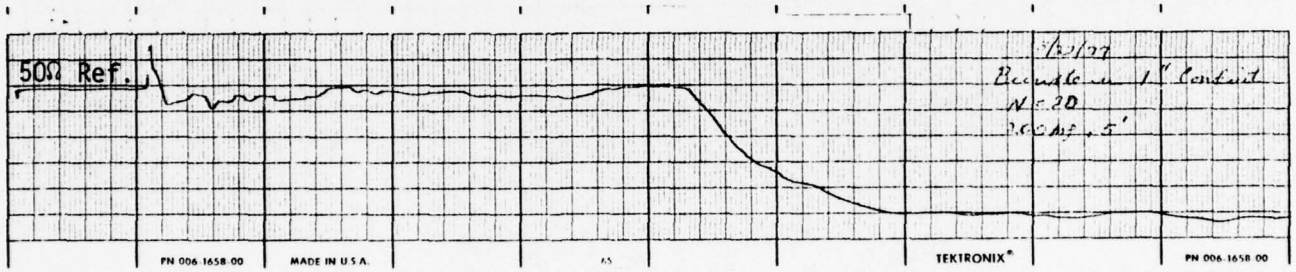

(c) N = 20 ($\overline{Z}_o$ = 46.2Ω, L_e = 6.43m)

Figure B-23. Cable in Large Conduit (.305 m/div, 200 mρ/div)

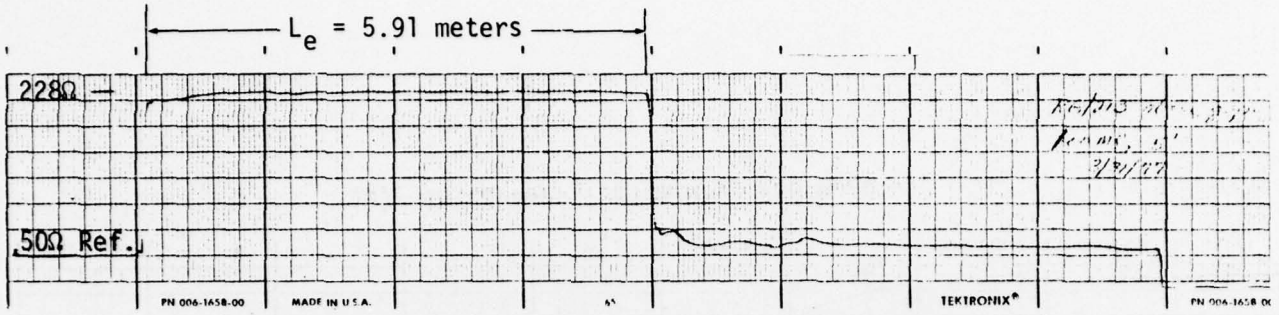

(a) 9.4cm Above Ground Plane (.305 m/div, 100 mρ/div)

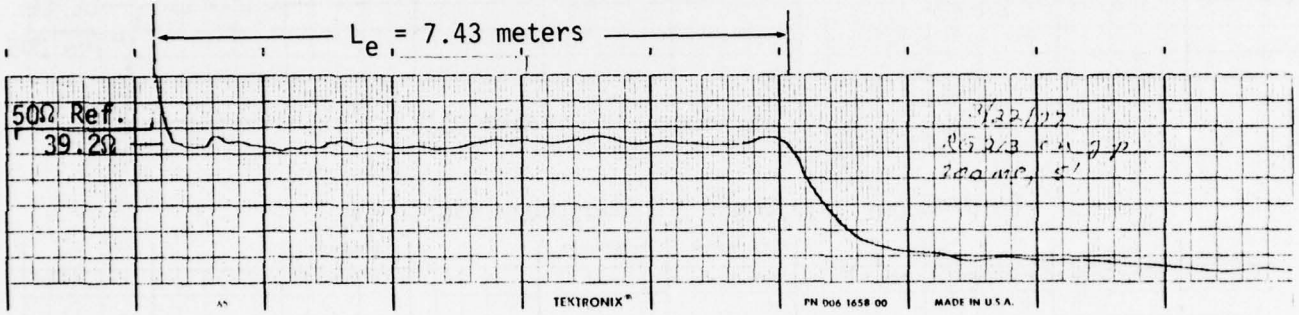

(b) On Ground Plane (.305 m/div, 200 mρ/div)

Figure B-24. RG/213 Cable Near Ground Plane

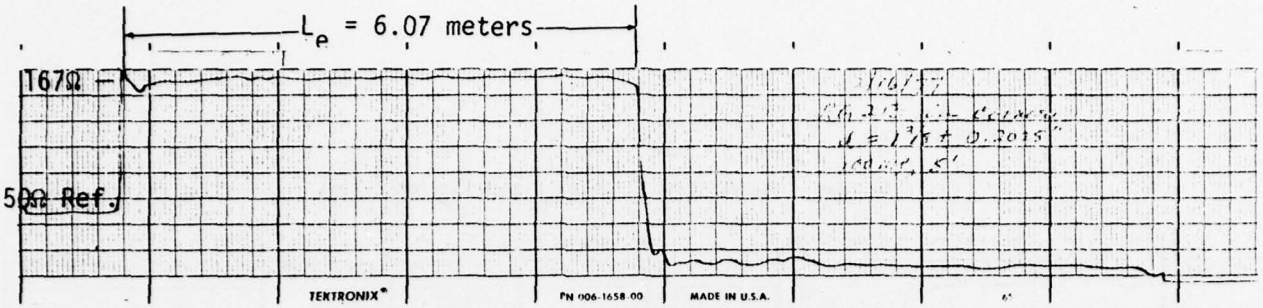

(a) 5.6cm From Corner (.305 m/div, 100 mρ/div)

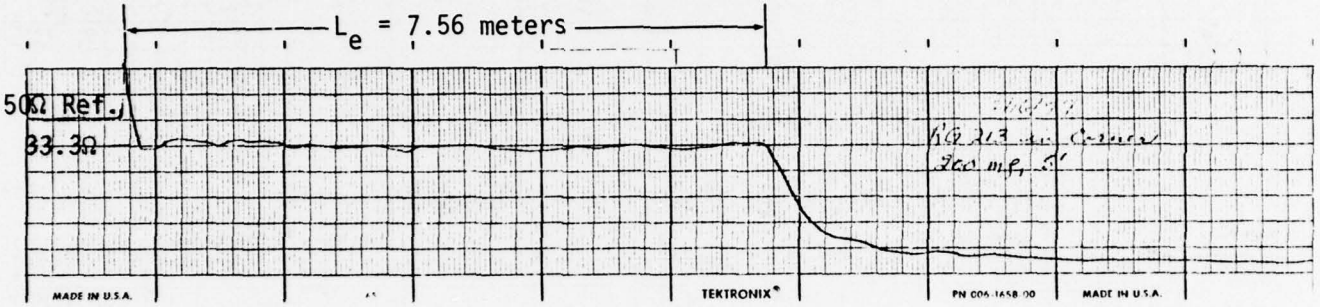

(b) In Corner (.305 m/div, 200 mρ/div)

Figure B-25. RG/213 Cable Near a Corner

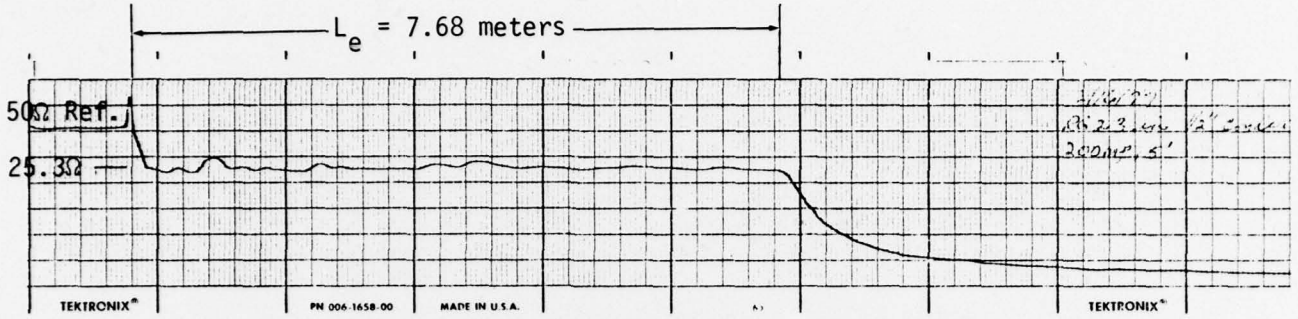

(a) Small Conduit (.305 m/div, 200 mρ/div)

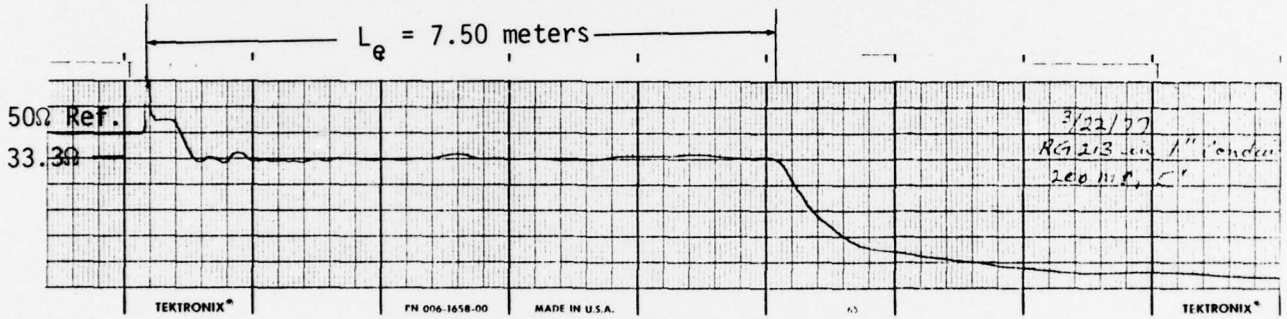

(b) Large Conduit (.305 m/div, 200 mρ/div)

Figure B-26. RG/213 Cable in Conduit